Sea ice and the air-sea exchange of CO_2

Dem Fachbereich 2 - Biologie/Chemie der

Universität Bremen

zur Erlangung des akademischen Grades eines

Dr. rer. nat.

eingereichte Dissertation

von

Michael Fischer

aus

Berlin

Bremen

Januar 2013

Gutachter:

Prof. Dr. Dieter Wolf-Gladrow
Alfred-Wegener-Institut Helmholtz Zentrum für Polar- und Meeresforschung (AWI) und Universität Bremen, Deutschland

Prof. Dr. Hajo Eicken
Geophysical Institute, University of Alaska, Fairbanks, USA

"Hier draußen Auge in Auge der Natur gegenüberzustehen und seinen Scharfsinn an ihren Rätseln zu erproben, das gibt dem Leben einen ganz ungeahnten Inhalt."

Alfred Wegener (25. Dezember 1906)

Vielen Dank an ... / Thanks to ...

An dieser Stelle möchte ich all jenen danken, die durch fachliche und persönliche Unterstützung zum Gelingen dieser Arbeit beigetragen haben.

Dr. Gerhard Dieckmann
für die Begeisterung für das Meereis, das Vertrauen, die wissenschaftliche Freiheiten gewährende Betreuung und ständige Bereitschaft für die uneingeschränkte fachliche und organisatorische Unterstützung.

Prof. Dr. Dieter Wolf-Gladrow
für die wichtigen Gedankenanstöße, die Unterstützung im richtigen Moment und die Bereitschaft, das erste Gutachten zu übernehmen.

Prof. Dr. Hajo Eicken
für die motivierenden und inspirierenden Gespräche und die Bereitschaft, das zweite Gutachten zu übernhemen.

Prof. Dr. Kai Bischof und Mar Fernández Méndez
für die unkomplizierte Übernahme der Aufgaben im Prüfungsausschuss.

Martin "Marty"Bergmann
for sharing your ideas and passion for the Arctic. Although you are no longer with us, your visions continue to inspire me.

Prof. Dr. Jean Louis Tison and Dr. Bruno Delille
for your guidance and contagious curiosity. Thank you for the inspiring discussions and wonderful working atmosphere during our expeditions and experiments. I always enjoyed working with you.

PD. Dr. Sabine Kasten und Dr. Gernot Nehrke
für die konstruktive Kritik und wertvollen Hinweise während der gesamten Arbeit.

Dr. Claudia Sprengel, Dr. Claudia Hanfland und die Helmholtz Graduate School for Polar and Marine Research
für die Organisation der vielen wertvollen Kurse, die Unterstützung für die Auslandsaufenthalte und einfach immer da zu sein.

Die Meereisgruppe
für die Unterstützung, Gespräche auch abseits der Wissenschaft, leckeren Frühstückbuffets und Geburtstagskuchen, Weihnachtsmarktbesuche und besondere Abende beim mongolischen Feuertopf. Insbesondere jedoch meiner Bürokollegin Christiane Uhlig für die Gespräche und die Unterstützung bei den kleinen alltäglichen und nicht-alltäglichen Problemen und Erika Allhusen für die große logistische Unterstützung während jeder Phase meiner Arbeit.

Prof. Søren Rysgaard and the Greenland Climate Research Center
for all the opportunities and support in Greenland and the High Canadian Arctic

Prof. Dr. C. J. Mundy and Prof. Dr. Tim Papakyriakou
for your support and discussion during the fieldwork in Allen Bay, Nunavut. I am grateful for your help and advice in so many things.

Prof. Dr. Stephan Frickenhaus und Prof. Dr. Lars Kaleschke
für die fachliche Unterstützung und die konstruktiven Diskussionen, die mich ein entscheidendes Stück weiter gebracht haben.

Erich Dunker und allen Mitarbeitern der wissenschaftlichen Werkstatt
für die unkomplizierte Unterstützung bei der Anpassung meiner Geräte und Experimente.

All the ship crews of the L'Astrolabe and KISAQ, air support teams, Dumont d'Urville and Polar Continental Shelf Programm field station/base crews and the myriad of other people associated with the logistic support
for making sea ice research possible.

allen Freunden

insbesondere Euch Maja, Flo, Oli und Judith, die mich jederzeit unterstützt haben. Danke einfach fürs Dasein und Zuhören in so manch schwieriger Lebenslage.

Torben Gentz, David Fischer, Till Oehler

ohne Euch und insbesondere Dir Torben, wäre die Arbeit nicht das geworden was sie jetzt ist. Vielen Dank für die gemeinsamen Abende mit vielen wertvollen Hinweisen und ehrlichen Kommentaren.

meine Familie

für die Unterstützung in jeder Lebenslage. Danke, dass Ihr mir dies alles ermöglicht habt!

Abstract

High-latitude oceans in the northern and southern hemisphere are major sinks for CO_2 and sea ice is an essential part of it. The physical barrier itself has a major impact on the gas exchange between atmosphere and ocean, and recently the discussion has been extended to consider how physical and biogeochemical processes within the ice itself can affect diffusion and flux of gases to both atmosphere and ocean. The motivation of this thesis was to improve the state of knowledge concerning the inorganic carbon dynamics, including the precipitation of $CaCO_3$ in sea ice and its significance for the polar carbon cycle as well as to obtain improved estimates of the diurnal and long-term CO_2 flux on small scales during the winter-spring-summer transition.

The first part of the thesis deals with the investigation of the spatial and temporal distribution of $CaCO_3$ in sea ice as well as the biogeochemical parameters, such as salinity, dissolved organic carbon/nitrogen (DOC, DON), inorganic phosphate, and total alkalinity (TA), which might influence the precipitation of calcium carbonate. Sea ice cores and brine samples were collected from pack and land fast sea ice between September and December 2007 during two expeditions, one in the East Antarctic sector and the other off Terre Adélie. Ikaite concentrations in melted sample (sea ice or snow) ranged from 0.01 to 126 mg l^{-1}. The findings indicate that the hydrated polymorph of calcium carbonate is widespread in Antarctic sea ice, albeit highly spatial heterogeneous. Ikaite was found mostly in the uppermost layers of sea ice. The precipitate was also found in the snow on top of the sea ice at some of the sampling locations. No relationship between DOC, DON, TA, inorganic phosphate and $CaCO_3$ precipitation was evident. Ikaite was most likely always the precipitate. Since parameters measured during sample collection do not reflect conditions at the time of precipitation, more work is needed to evaluate the conditions of calcium carbonate precipitation within sea ice and its fate during sea ice melt.

The second study is on the exchange of CO_2 between subarctic sea ice and the atmosphere. For the first time long-term continuous diurnal chamber measurements (24 h) were carried out on both snow free and snow-covered ice. The study was conducted from 10^{th} to 16^{th} March 2010 in Kapisigdlit, Kangerdluat, Southwest Greenland. Diurnal fluxes were highly variable and ranged between -2.2 and 9.5 mmol m^{-2} d^{-1} (where negative values indicate a sink for atmospheric CO_2). Changes from an efflux to an influx within 24 hours show that diurnal long-term measurements are essential. However, a diurnal pattern of the CO_2 fluxes could not be observed. Measurements over snow covered sea ice showed lower fluxes compared to fluxes above bare sea ice. This indicates that snow significantly influences the CO_2 exchange between sea ice and atmosphere.

On the basis of these findings a seasonal sea ice study was performed during the transition from winter conditions into the melting season until sea ice break, which is described in chapter 4. The study was conducted from 3^{rd} May to 26^{th} June 2011. The partial pressure of CO_2 in water, land fast seasonal sea ice, and atmosphere and the related ice-atmosphere flux of CO_2 was examined in Allen Bay, Canadian Arctic Archipelago. The pCO_2 was measured with in situ samplers. The air-ice exchange of CO_2 was examined by using continuous (24 h) long-term chamber measurements. High partial pressures in sea ice of up to ≈ 3900 μatm were observed in the upper layer at the beginning of the study, while low values down to almost ≈ 0 μatm were observed at the ice-water interface during the melting phase. Sea ice is oversaturated in CO_2 until late in the melt season, leading to a net efflux from the sea ice to the atmosphere during May and June. Fluxes of CO_2 between ice and atmosphere were observed during all seasons and ranged between -3.41 to 3.92 mmol m^{-2} d^{-1}. The significance of snow on the flux of CO_2 between sea ice and atmosphere, which was already observed in the second study, was validated. Efflux and influx during the melt season can occur at the same time when gas bubbles from the interior of sea ice become mobile and are subsequently released to the

atmosphere, while melt ponds efficiently take up CO_2 from the atmosphere. In the concluding synthesis the findings of the three studies are discussed in the context of the sea ice driven carbon pump. Based on calculations the efflux from Arctic sea ice to the atmosphere can be expected to result in an annual flux of several Tg C. Melt ponds are considered to be responsible for a potential carbon flux of up to 34 Tg C a^{-1} from the atmosphere into the ocean. At the same time degassing of CO_2 due to the release of bubbles from within sea ice might contribute up to ≈ 5.2 Tg C to the annual carbon flux in the Arctic and Antarctic. Fluxes of CO_2 between sea ice and atmosphere are significant and have to be taken into account when it comes to budgeting the sea ice driven carbon pump. An advanced understanding of each subprocess in the sea ice driven carbon cycle and their translation into potential fluxes of CO_2 is required for an improved budgeting of the polar carbon cycle. The investigation of the components of the sea ice driven carbon cycle over a complete seasonal cycle of sea ice growth and decay is encouraged to provide an optimal data set. However, a priority should be the examination of the biogeochemical processes and resulting fluxes of CO_2 across the air-ice-ocean boundary layer in the ice covered southern ocean. Accepted by the sea-ice-biogeochemical community, the concept of the sea ice driven carbon pump and the presented refinements in this thesis are at the forefront of polar research and needs further propagation outside the community to be incorporated, for example, in model calculations of the global carbon cycle.

Zusammenfassung

Die Ozeane der hohen Breiten in der nördlichen und südlichen Hemisphäre sind bedeutende Senken für CO_2 und Meereis ist ein signifikanter Teil davon. Die physische Barriere selbst hat einen entscheidenden Einfluss auf den Gasaustausch zwischen Ozean und Atmosphäre, während jedoch die aktuelle Forschung erst seit kurzem die physischen und biogeochemischem Prozesse im Meereis untersucht und wie diese die Diffusion und Stofffluss von Gasen zwischen Atmosphäre und Ozean beeinflussen. Die Motivation dieser Arbeit war es, sowohl den Kenntnisstand bezüglich der anorganischen Kohlenstoffdynamik, inklusive der Fällung von $CaCO_3$, im Meereis und deren Bedeutung für den polaren Kohlenstoffkreislauf zu verbessern, als auch verbesserte und genauere Werte für den tageszyklischen Stofffluss von CO_2 zwischen Meereis und Atmosphäre über lange Messzeiträume, während des Überganges vom Winter bis hin zum Sommer, zur Verfügung zu stellen.

Der erste Teil beschäftigt sich mit der Untersuchung der räumlichen und zeitlichen Verteilung von $CaCO_3$ im Meereis. Dabei werden biogeochemische Parametern wie Salzgehalt, gelöster organischer Kohlenstoff/Stickstoff (DOC, DON), Phosphat und Gesamtalkalität (TA) analysiert, die die Fällung von $CaCO_3$ beeinflussen können. Während einer Expedition im östlichen Sektor der Antarktis und einer weiteren vor der Küste von Terre Adélie wurden Eiskerne und Proben der Meereis-Salzlauge von Pack- und Festeis genommen. Die Konzentrationen von Ikait in der geschmolzenen Probe (Meereis oder Schnee) waren zwischen 0.01 und 126 mg l^{-1}. Die Resultate deuten darauf hin, dass diese hydratisierte Form von Kalziumkarbonat, obwohl sehr heterogen verteilt, ubiquitär im antarktischen Meereis ist. Ikait wurde in den obersten Schichten des Meereises gefunden. Das Mineral wurde auch im Schnee auf dem Meereis gefunden. Eine Abhängigkeit zwischen DOC, DON, TA, Phosphat und der Fällung von $CaCO_3$ konnte nicht nachgewiesen werden. Ikait war mit höchster

Wahrscheinlichkeit immer das Fällungsprodukt. Da die Parameter, die während der Beprobung gemessen wurden, nicht die Bedingungen zum Zeitpunkt der Fällung widerspiegeln, ist eine weiterführende Forschung unabdingbar, um die Bedingungen der Kalziumkarobnatfällung im Meereis und dessen folgender Verbleib zu verstehen.

Die zweite Studie befasst sich mit dem Austausch von CO_2 zwischen subarktischen Meereis und der Atmosphäre. Erstmalig wurden kontinuierliche Langzeit-Kammer-Messungen (24 h) über den kompletten Verlauf mehrerer Tageszyklen auf schneefreiem und schneebedeckten Meereis durchgeführt. Die Studie fand zwischen 10. und 16. März in Kapisigdlit, Kangerdluat, Südwestgrönland statt. Die tageszeitlichen Stoffflüsse waren sehr variabel und lagen zwischen -2.2 und 9.5 mmol m^{-2} d^{-1} (negative Werte zeigen dabei eine Senke für CO_2). Der Wechsel von CO_2-Abgabe und Aufnahme innerhalb von 24 Stunden zeigt die Notwendigkeit von Langzeitmessungen über den gesamten Tageszyklus hinweg. Es konnten jedoch keine tageszeitlichen Muster festgestellt werden. Messungen über schneebedecktem Meereis zeigen geringere Stoffflüsse im Vergleich zu schneefreiem Eis. Dies deutet auf einen signifikanten Einfluss von Schnee auf den CO_2-Austausch zwischen Meereis und Atmosphäre hin.

Auf Grundlage dieser Ergebnisse wurde eine Langzeitstudie in Allen Bay, kanadisch-arktisches Archipel, während des Überganges vom Winter bis hin zum Aufbrechen des Meereises im Sommer durchgeführt. Zwischen 3. Mai und 26. Juni 2011 wurden der Partialdruck im Wasser, im Festeis, in der Atmosphäre und der in damit zusammenhängende Stoffffluss von CO_2 zwischen Meereis und Atmosphäre gemessen. Kohlenstoffdioxid wurde in situ gemessen. Der Gasaustausch zwischen Eis und Atmosphäre wurde mit Langzeit-Kammern-Messungen (24 h) analysiert. Die Messungen zeigten in den oberen Schichten des Meereises hohe Partialdrücke von bis zu 3900 μatm zu Beginn der Studie, während extrem niedrige Werte von fast 0 μatm an der Meereis-Wasser Grenzschicht während der Schmelzphase gemessen wurden. Meereis ist bis spät in die Schmelzphase übersättigt mit CO_2. Dies führt zu einem positiven Stoffffluss

vom Meereis zur Atmosphäre. Stoffflüsse wurden während der gesamten Zeit gemessen und lagen zwischen -3.41 und 3.92 mmol m^{-2} d^{-1}. Die Bedeutung des Schnees für den CO_2 Austausch zwischen Meereis und Atmosphäre, der bereits in der vorangegangenen Studie aufgezeigt worden war, konnte in dieser Studie bestätigt werden. Während der Schmelzphase kommt es zu wechselseitigen Stoffflüssen zwischen Eis und Atmosphäre wenn Gasblasen aus dem Inneren des Eises mobil werden und darauf hin in die Atmosphäre entgasen, während zur gleichen Zeit die Schmelztümpel CO_2 effektiv aufnehmen.
In der abschließenden Synthese werden die Ergebnisse der drei Studien im Kontext der meereis-bedingten Kohlenstoffpumpe diskutiert. Berechnungen lassen einen jährlichen Fluss von mehreren Terragramm Kohlenstoff zwischen arktischem Meereis und Atmosphäre erwarten. Schmelztümpel hingegen könnten potentiell für einen Stoffluss von bis zu 34 Tg C von der Atmosphäre in den Ozean verantwortlich sein. Zur gleichen Zeit könnte das Ausgasen von CO_2 aufgrund der Freisetzung von Gasblasen 5,2 Tg C zum jährlichen Kohlenstoffluss in der Arktis und Antarktis beitragen. Infolge der Signifikanz des CO_2 Austausches wischen Meereis und Atmosphäre, muss dieser bei einer Budgetierung der meereis-bedingten Kohlenstoffpumpe berücksichtigt werden. Die einzelnen Prozesse und deren Bedeutung für den Stoffluss von CO_2 müssen im Detail besser verstanden werden, damit eine exakte Budgetierung dieser Kohlenstoffpumpe möglich ist. Die Untersuchung aller zugehörigen Teilprozesse während eines kompletten Zyklus von der Entstehung bis zum Schmelzen des Meereises würden hierfür eine optimale Datengrundlage sein. Dabei sollte jedoch die Analyse der biogeochemischen Prozesse und die daraus resultierenden Stoffflüsse von CO_2 über die Ozean-Meereis-Atmosphären-Grenzschicht im Südozean eine Priorität darstellen. Das Konzept der meereisbedingten Kohlenstoffpumpe, die in der Meereis-Biogeochemie weitgehend akzeptiert ist, und die gewonnen Erkenntnisse in dieser Arbeit sind an der Spitze der internationalen Polarforschung. Sie bedarf jedoch einer Verbreitung in andere Wissenschaftsbereiche, zum Beispiel in der Modellierung des globalen Kohlenstoffkreislaufes.

Contents

Chapter 1

Introduction

Carbon is the element of life. It exists in many forms. Plants, animals, and humans themselves are based on carbon. Carbon is stored in several reservoirs, the lithosphere, the atmosphere, the land biomass, and the ocean. Compared to the very slow turnover of carbon within the lithosphere (millions of years) the exchange between atmosphere, the land biosphere, soils, and the ocean is relatively fast (on a scale between a few and several 1000 years). With regard to climate change and ocean acidification, carbon in the form of the greenhouse gas CO_2 is of special interest. Particularly since human kind has started to burn fossil fuel such as coal, oil and gas and therefore altered the balance between the reservoirs. The anthropogenic release of CO_2 to the atmosphere is responsible for an increase of atmospheric CO_2 concentrations from preindustrial $\approx$ 280ppm (Etheridge et al., 1996) to 394 ppm at its maximum in 2011 (Thoning et al., 2012, and Fig. 1.1). In some remote observatories in Alert, Nunavut, Canada and Barrow, USA in the Arctic, maximum values in 2012 for the first time exceeded the threshold of 400 ppm (according to NOAA measurements). Looking at the most active parts of the carbon cycle and observing our planet from an ocean's perspective reveals impressive numbers. Compared to the atmosphere and the land biomass, the ocean is the giant of these carbon reservoirs. The ocean stores 38000 Pg C, which is

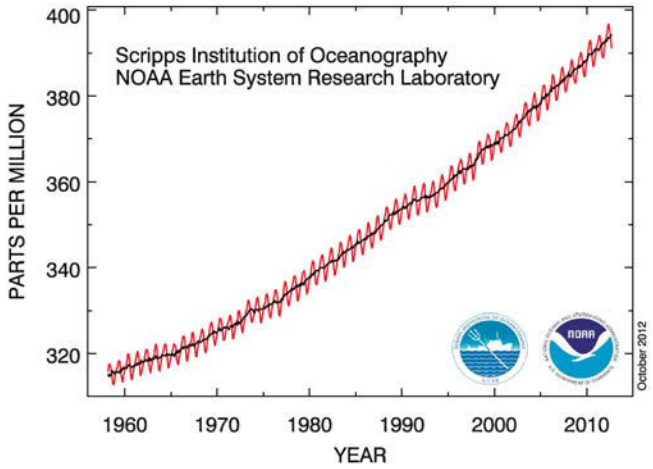

Figure 1.1: Atmospheric CO_2 (red curve), measured as the mole fraction in dry air, on Mauna Loa Observatory starting from March 1958 until October 2012. The black curve represents the annual mean values. Data and figure provided by NOAA/ESRL (www.esrl.noaa.gov/gmd/ccgg/trends/) and Scripps Institution of Oceanography (scrippsco2.ucsd.edu/).

fifty times the amount in the atmosphere and about twenty times more than the land biomass reservoir (Sundquist, 1993). The ocean has a large impact on the global carbon cycle by driving the changes of atmospheric CO_2 concentration (Zeebe and Wolf-Gladrow, 2001; Sigman et al., 2010). According to Sabine et al. (2004), 48% of the total fossil-fuel and cement-manufacturing CO_2-emissions have been taken up by the ocean. Therefore the ocean plays a crucial part in the uptake of anthropogenic CO_2. The present net global ocean CO_2 uptake corresponds to about 25% of the industrial emissions of about 7 Pg C a^{-1} (Takahashi et al., 2009, and references therein). Takahashi et al. (2009) shows that the high-latitude oceans in the northern and southern hemisphere are major sinks for CO_2, and sea ice, especially in the Arctic, is an essential part of it (Halloran, 2012). Sea ice covers up to 7% of the total surface area of the oceans at its maximum extent (Comiso, 2010). The physical barrier itself has a major impact on the gas exchange between atmosphere and

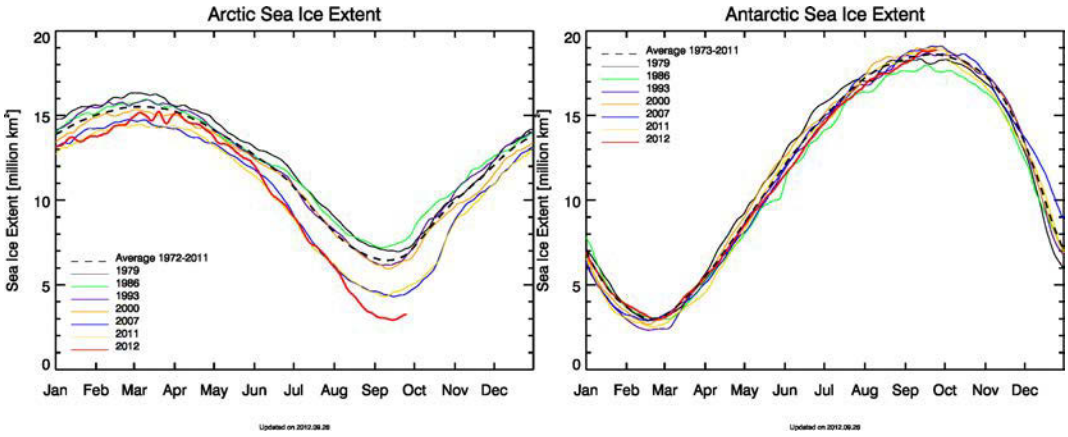

Figure 1.2: Seasonal Arctic and Antarctic sea ice extent (total area of at least 15% ice concentration) for selected years since 1979, http:// www.iup.uni-bremen.de:8084/ssmis/index.html

ocean, and recently the discussion has been extended to consider how physical and biogeochemical processes within the ice itself can affect diffusion and flux of gases to both atmosphere and ocean (Tison et al., 2002; Delille, 2006; Rysgaard et al., 2007, 2009, 2011; Miller et al., 2011b; Loose et al., 2011a).

1.1 Introduction to sea ice

The frozen ocean is one of the largest biomes on earth. It provides a unique habitat for organisms ranging from bacteria to whales. At the same time sea ice influences biogeochemical processes on small scales in the ocean up to large scales in the deep sea and the atmosphere and subsequently the global climate. Ignored by models in the past (i.e. Sun and Matsumoto 2010), it has become apparent during the last decade, that sea ice cannot be left out of future climate predictions (Dieckmann and Hellmer, 2010). Polar regions are experiencing the largest changes with respect to climate change. For example warming in the Arctic is 1.5 to 4.5 times more intensive than the overall global warming (Holland and Bitz, 2003). This is consistent with values of the IPCC

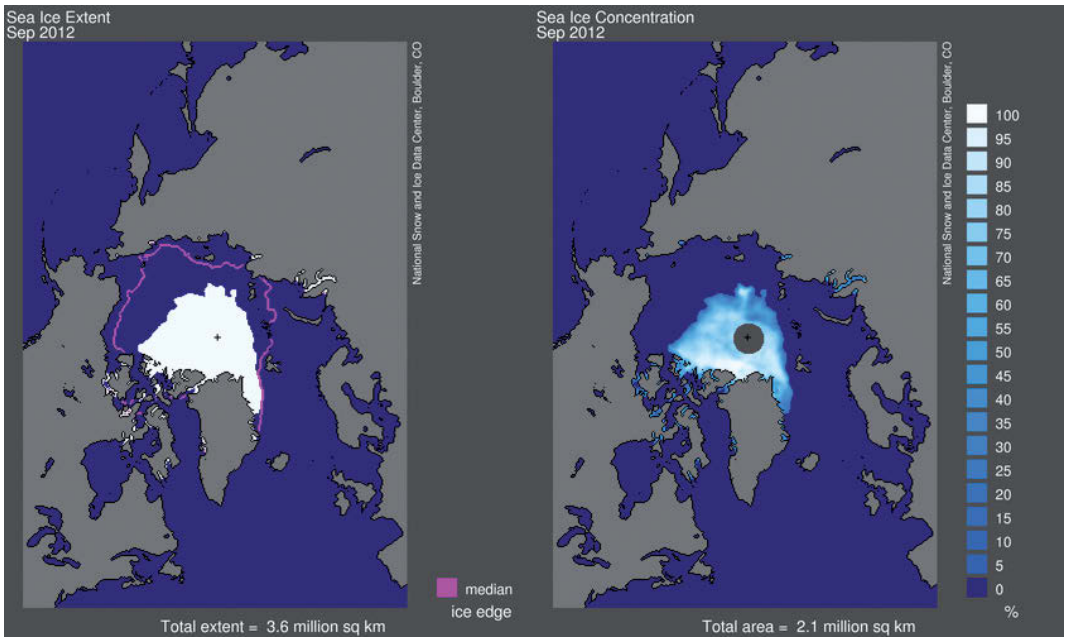

Figure 1.3: Record sea ice minimum and concentration in September 2012 in the Arctic, (National Snow and Ice Data Center, Boulder, CO, USA)

report (IPCC, 2007). While the overall sea ice cover around the Antarctic continent seems to remain stable or is in fact slightly increasing (0.9% per decade, ±0.6%, according to NSIDC September extent trend for 1979 to 2012), with the exception of the Antarctic Peninsula (Dieckmann and Hellmer, 2010), the Arctic is changing more rapidly (see Fig. 1.2). Regular observations of sea ice extent showed a record minimum in the Arctic in September 2012 (3.4 million km^2). This is only half of the sea ice coverage observed since the first satellite records were obtained in 1979. Sea ice coverage is the most obvious change. In addition a rapid thinning of Arctic sea ice has been observed (Rothrock et al., 1999; Liu et al., 2004; Maslanik et al., 2007; Lindsay et al., 2008). This results in a reduction of multi-year ice in favour of more seasonal sea ice (Kwok et al. 2009 and Fig. 1.3). Although the Antarctic seems to remain stable, sea ice conditions when looking at overall numbers, show regional trends. The West-Antarctic suffers from increasing temperatures and resulting loss of sea

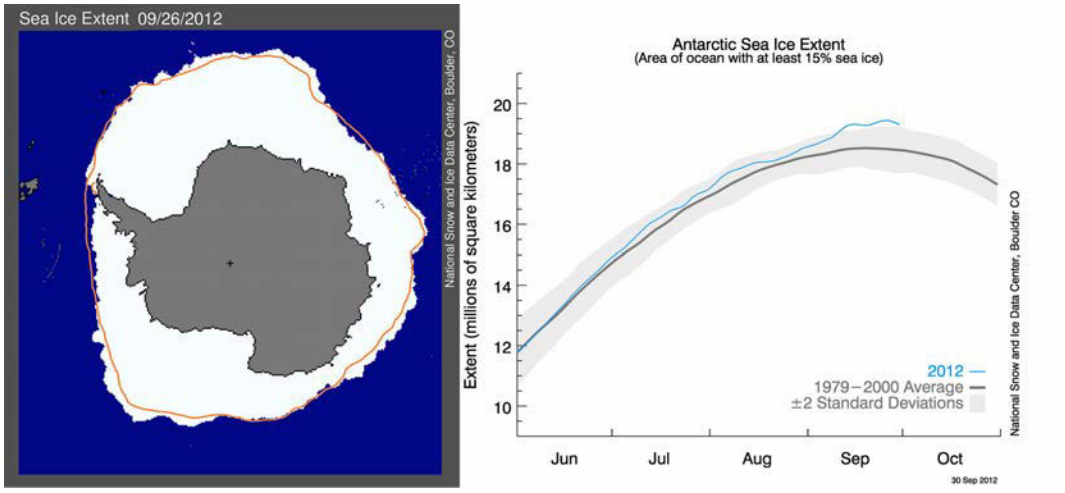

Figure 1.4: Antarctic sea ice extent in September 2012 with 19.44 million square kilometers, (National Snow and Ice Data Center, Boulder, CO, USA)

ice (Turner et al., 2012). In contrast, other regions such as the Ross Sea sector (Turner et al., 2009) show an increase in sea ice coverage (Fig. 1.5). These changes affect the entire ecosystem in many ways. Though a lot of research is conducted in this fragile environment, little is still known about all consequences on polar regions and consequently the processes in the sea ice itself.

Sea ice is a complex substratum and environment, which has a major impact on the gas exchange between atmosphere and ocean (Delille, 2006; Rysgaard et al., 2011; Loose et al., 2011a). During the last decades, major efforts have been undertaken to study the biogeochemical processes, which occur within the sea ice (i.e. Gleitz et al. 1995; Delille 2006; Delille et al. 2007; Rysgaard et al. 2007; Fransson et al. 2011; Papadimitriou et al. 2012; Geilfus et al. 2012b). During sea ice formation and decay salinity and temperature within the ice undergo dramatic shifts. The dissolved salts in the parent seawater mass are quantitatively expelled from the ice crystal matrix and become concentrated in the residual brine which is trapped in channels and pockets. The brine is rejected in large parts from the growing ice column into the underlying water column due to gravity drainage, with the remaining brine residing in pockets

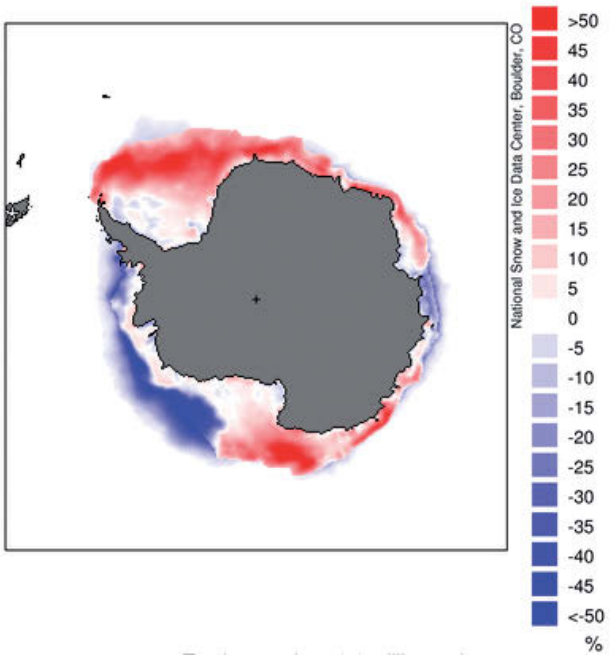

Figure 1.5: Sea ice concentration anomalies in the Antarctic in April 2012, (National Snow and Ice Data Center, Boulder, CO, USA)

and channels within the sea ice (Eicken, 2003). This hyper-saline solution undergoes substantial changes with respect to thermodynamic equilibrium, which is influenced by salinity and temperature of the sea ice system (Thomas et al., 2010a) and which is described in more detail in the following section. Readers with an interest in more detail on sea ice and techniques of sea ice sampling are referred to Thomas and Dieckmann (2010) and Eicken et al. (2010).

1.2 Carbonate chemistry within sea ice

The marine carbon cycle in the open ocean is a well-studied environment (Zeebe and Wolf-Gladrow, 2001; Sarmiento and Gruber, 2006; Emerson and Hedges, 2008). In contrast, the chemical environment in sea ice has only been studied in any comprehensive way since the 1990s (Thomas et al., 2010a, and references therein). The biogeochemical parameters within sea ice brine ex-

perience a strong seasonality driven by a large variability in temperature and salinity ranging from the freezing point of sea water (-1.86°C at S = 34, Petrich and Eicken 2010) to temperatures well below -10°C (Miller et al., 2011b; Geilfus et al., 2012b). At these subzero temperatures salinity can easily reach values beyond 100 (Perovich and Richter-Menge, 1994). The temperature-driven increase of salinity in brines is accompanied by a decrease in brine volume and increases in the concentrations of other dissolved components, including dissolved inorganic carbon (DIC) and total alkalinity (TA). The chemical environment in sea ice is highly dynamic. Different processes occur within the ice altering this environment and especially the carbonate system, which is modified by photosynthetic production, respiration, $CaCO_3$ precipitation and dissolution as well as CO_2 degassing and uptake. A comprehensive overview is given by Thomas et al. (2010b) and Papadimitriou et al. (2012). Recently sea ice is being considered as a significant boundary layer in the air-sea CO_2 flux in polar seas (Delille, 2006; Loose et al., 2011a; Rysgaard et al., 2011). For determining and understanding the fluxes of CO_2 between sea ice and atmosphere throughout the season, measurements of the gradients of pCO_2 (partial pressure of CO_2) between the ocean, sea ice, and the atmosphere are inevitable.

The measurement of CO_2 in sea ice is difficult. Most studies determine two out of the four measurable variables of the carbonate system. Usually DIC, TA, and/or pH are measured in bulk sea ice (Rysgaard et al., 2007, 2009, 2012; Fransson et al., 2011; Geilfus et al., 2012b) or brine samples (Gleitz et al., 1995; Papadimitriou et al., 2004; Delille, 2006; Papadimitriou et al., 2007; Delille et al., 2007; Papadimitriou et al., 2009; Nomura et al., 2010a; Geilfus et al., 2012b; Papadimitriou et al., 2012) and used for the calculation of pCO_2 (Zeebe and Wolf-Gladrow, 2001). Delille (2006); Delille et al. (2007) and Geilfus et al. (2012b) were, to the best of my knowledge, the only ones to measure pCO_2 directly in sea ice brine. However, as has been pointed out by Papadimitriou et al. (2012), averaging out bulk samples potentially yields

inaccurate estimates in the carbonate system.

As mentioned above the carbonate system in sea ice brine is driven by changes in salinity and temperature. Brine temperature (T_b) and brine salinity (S_b) are related by the freezing point relation $T_b = T_f(S_b)$. Thus we can assume that brine temperature is always at the freezing point, $T_f(S)$. The brine salinity for temperatures above $-23°C$ is given by Petrich and Eicken (2010):

$$S_b = \left(1 - \frac{54.11}{T}\right)^{-1} * 1000 \tag{1.1}$$

which results in values that lie slightly above the values given by Feistel (2008, Table 6). However, these differences are very small and can therefore be neglected in the current context. The solubility of CO_2 increases with decreasing temperature and in contrast decreases with increasing salinity (Thomas et al., 2010b). If any two (i.e. DIC, TA) of the six variables in the carbonate system are given together with S_b and T_b, one can calculate the partial pressure of CO_2 in brine channels (Zeebe and Wolf-Gladrow, 2001). The increase of pCO_2 is mainly due to the strong variation of the equilibrium constants of the carbonate system with salinity ('salinity effect') with a smaller contribution by the higher concentrations of DIC and TA. Increase of TA and decrease of temperature both lead to smaller pCO_2 values. The salinity effect is demonstrated by the following calculations (for simplicity the effect of gas-exchange, precipitation of minerals, and biological processes are neglected): Dissolved inorganic carbon and total alkalinity are conservative variables (Zeebe and Wolf-Gladrow, 2001) and can be multiplied by the degree of salt enrichment of the brines relatively to the initial sea water salinity of 35 (Papadimitriou et al., 2007).

$$DIC_{S_b} = DIC_i \frac{S_b}{35} \tag{1.2}$$

$$TA_{S_b} = TA_i \frac{S_b}{35} \tag{1.3}$$

Taking values for $S_b = 70$ derived from relationships of DIC and TA with sea ice brine as presented for Arctic sea ice (Geilfus et al., 2012b) results in $DIC_{S_b} = 4455.7$ μmol kg^{-1}, $TA_{S_b} = 4835.6$ μmol kg^{-1}, and subsequently for $S_i = 35$ in $DIC_i = 2227.9$ μmol kg^{-1} and $TA_i = 2417.8$ μmol kg^{-1} according to equations 1.2 and 1.3. Using the dissociation constants pK_1 and pK_2 for carbonic acid from Mehrbach et al. (1973) as refitted by Dickson and Millero (1987) results in $pCO_{2_{S_b}} = 785$ μatm for the brine. For $S_i = 35$ this would result in $pCO_{2_i} = 241.4$ μatm. Doubling brine salinity to $S_b = 140$ and using equations 1.1, 1.2, and 1.3 gives a pCO_2 of 4451.2 μatm. This difference in pCO_2 is huge. If we would do the same calculation by doubling only salinity while keeping temperature constant we would even obtain a pCO_2 of 5624.2 μatm. However, the increase of pCO_2 from 785 μatm (for $S_b = 70$) to 4451.2 μatm (for $S_b = 140$), when doubling salinity and cooling brine to the freezing point corresponding to this salinity (see Equation 1.1), is only slightly smaller than when doubling salinity only. Thus high pCO_2 values are mainly caused by the variation of equilibrium constants with salinity and to a lesser extent by the decrease of temperature (Thomas et al., 2010b).

Moreover, if we use other dissociation constants of i.e. Roy et al. (1993) or Millero et al. (2006) we would get 693.6 μatm and 1170.8 μatm respectively, for $S_b = 70$. This displays discrepancies when applying existing dissociation constants for the carbonate chemistry within sea ice brine. Dissociation constants, which are available at present for the calculation of pCO_2, are only valid for a salinity range up to 50 (Mehrbach et al., 1973; Dickson and Millero, 1987; Roy et al., 1993; Delille, 2006; Millero et al., 2006). Though Delille (2006) showed that their validity might be stretched a bit beyond their estimated salinity range and calculations at lower brine salinities ($S_b < 44$) as observed by Fransson et al. (2011) are possible, calculations at very low sub-zero temperatures and resulting high salinities ($S_b > 50$) might result in incorrect values of pCO_2. In addition calculations of pCO_2 using TA and DIC at high pCO_2 have been shown to result in inconsistencies in carbonate chemistry measurements

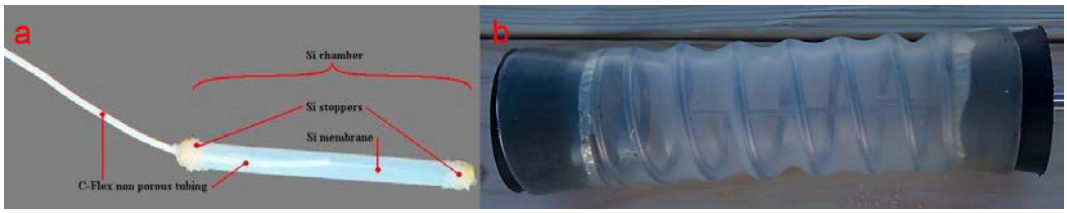

Figure 1.6: a) Peeper - silicone exchange chamber as deployed by Owens (2008) and Miller et al. (2011b), b) improved peeper with in-port and out-port as deployed by Miller et al. (2011a) and Brown et al. (in prep.)

(Hoppe et al., 2012). Therefore the direct measurement of pCO_2 should be preferred.

Recently there have been new attempts to measure CO_2 directly in sea ice (Owens 2008; Miller et al. 2011a,b, and Brown et al. in prep.) or with a direct non-destructive sampling method (Geilfus et al., 2012a). While the latter provides high-resolution measurements it is not suitable for observing sea ice CO_2 over a long period at the same location. Since fluxes of CO_2 above sea ice are also observed during winter (Heinesch et al., 2010; Miller et al., 2011b) a long-term observation is needed to track the CO_2 in the water, sea ice, and in the atmosphere from winter conditions into the melting season allowing to connect CO_2 gradients and resulting fluxes between ice and atmosphere.

The new in situ method for measuring pCO_2 in sea ice of Owens (2008) and Miller et al. (2011b) is adapted from soil research. Their techniques is based on silicone exchange chambers to form an isolated chamber from which a sample can be withdrawn (Fig. 1.6). Silicon chambers are more robust in harsh conditions such as sea ice compared to diffusion bags, which are also used in soil sciences (Owens, 2008; Miller et al., 2011b, and references therein). The used Si membrane is impermeable for fluids, but porous for gas molecules, which allows a passive diffusion along a concentration gradient between the interior and the exterior of the chamber until a equilibrium level with its surrounding is reached (Owens, 2008, and references therein). The time to reach

equilibrium depends on the particular gas. Carbon dioxide equilibrates much faster than other gases. Owens (2008) and (Miller et al., 2011b) report that an equilibration time of 1-2 days should be sufficient, even at subzero temperatures. Two methods are used to sample the peepers. Owens (2008) and (Miller et al., 2011b) sampled the peepers using a syringe, which is immediately injected into evacuated 10 ml vials for analysis on a gas chromatograph. Miller et al. (2011a) and Brown et al. (in prep.) improved the peepers by providing an in-port and out-port (Fig. 1.6b) while at same time applying a stainless tubing as suggested by Miller et al. (2011b). The in-port and out-port of the peeper are connected to a portable infrared gas analyzer (LI-COR 820) in a closed loop. This method avoids biases such as negative pressure inside the chambers due to evacuation as reported by Miller et al. (2011b). Problems such as the silicone photo reaction, which produces CO_2, have been shown to be insignificant for the applied measurements (Owens, 2008).

In addition, on the basis of thermodynamic equilibrium calculations, the precipitation of $CaCO_3$ was predicted to occur during natural sea ice formation (Gitterman, 1937; Jones and Coote, 1981; Anderson and Jones, 1985) and it was proposed to precipitate as calcite (Marion, 2001). However, actual evidence was, for a long time, only indirect (Killawee et al., 1998; Papadimitriou et al., 2004; Tison et al., 2002; Papadimitriou et al., 2012) until Dieckmann et al. (2008) found calcium carbonate as ikaite $CaCO_3 \cdot 6H_2O$ in Antarctic sea ice, and more recently in Arctic sea ice (Dieckmann et al., 2010; Rysgaard et al., 2012). Rysgaard et al. (2007, 2009) showed that with brine, dissolved organic carbon (DIC) is rejected from growing sea ice to the underlying waters. They ascribe the high pCO_2 levels found below sea ice to calcium carbonate precipitation. Rysgaard et al. (2007) proposed that $CaCO_3$ precipitation in sea ice could result in a significant CO_2 uptake by the ocean. The generated CO_2 during $CaCO_3$ precipitation (Eq: 1.4) may escape together with the rejected brine from the sea ice system to the underlying water column leading to high TA:DIC ratios in sea ice and high pCO_2 levels below sea ice (Rysgaard et al.,

2009). The formed $CaCO_3$ is trapped in the sea ice matrix. Thus, CO_2 and $CaCO_3$ are separated. As springs arrives calcium carbonate will most likely dissolve (Rysgaard et al., 2012). The dissolution of the mineral consumes CO_2 and therefore contributes to a polar carbon pump (Rysgaard et al. 2011, Section 1.3).

$$Ca^{2+} + 2HCO_3^- <> CaCO_3 + CO_2 + H_2O \tag{1.4}$$

There is a lack of knowledge on the exact conditions leading to ikaite precipitation as well as on the amount and fate of ikaite. One assumption is that phosphate and dissolved organic matter (DOM) may reduce the precipitation of calcium carbonate (Bischoff et al., 1993; Zullig and Morse, 1988). Both dissolved inorganic phosphate and DOM can be present in sea ice in very high concentrations (Thomas et al., 1998, 2001), thus it can be hypothesized that where these substances are present in high concentrations that precipitation of some polymorphs of calcium carbonate will be inhibited.

Besides the function of calcium carbonate in sea ice as a component in the carbon cycle, the mineral is also thought to have a key role in tropospheric ozone depletion events (ODEs) at high latitudes (Sander et al., 2006; Sander and Morin, 2010). Simulations of the chemistry occurring in polar regions over newly-formed sea ice relate the ODE to the transformation of inert sea-salt bromide to reactive bromine monoxide (BrO) when precipitation of calcium carbonate from freezing sea water is taken into account. The discovery of ikaite in firn ice of the Antarctic continent, which appears to be derived from sea ice 300 km away, may also have implications for its use as a sea ice proxy (Sala et al., 2008). However, to date most studies of calcium carbonate in sea ice have been mainly qualitative and little is known about the spatial and temporal distribution of $CaCO_3$ within sea ice, which would be highly valuable to assess its significance to the polar and subsequently the global carbon cycle.

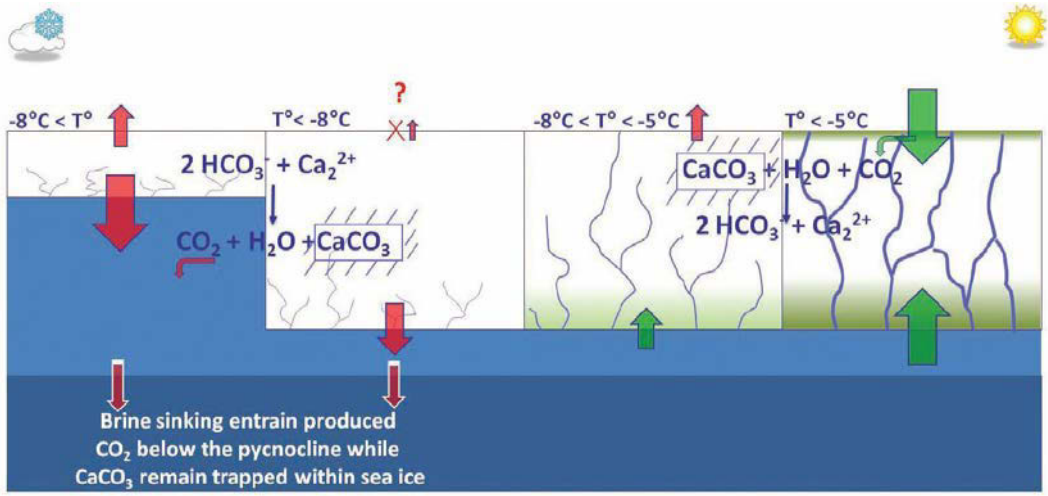

Figure 1.7: Schematic of the current understanding of CO_2 dynamics within sea ice and related air-ice-ocean CO_2 exchange during all phases of the ice growth and decay cycle (Delille, 2010)

1.3 Polar carbon pump

Permeable for gases and hosting a very active biogeochemical system - sea ice is crucial for the exchange of CO_2 between atmosphere and ocean. Sea ice was and is in some cases still thought to impede fluxes of gases such as CO_2 between ocean and atmosphere (Gibson and Trull, 1999; Bates, 2006). However, recent research shows the importance of sea ice and its role as polar carbon pump (Delille, 2010; Rysgaard et al., 2011; Loose et al., 2011a). A schematic of the current understanding of the polar carbon pump by Delille (2010) is shown in Figure 1.7.

Proposed for more than 100 years (Nansen, 1906), revived in the mid 80's (Aagaard et al., 1985; Midttun, 1985), the formation of deep water masses due to brine rejection from growing sea ice is now a widely accepted crucial process for the global ocean circulation and climate (Rudels et al., 2000; Årthun et al., 2011). Recently implications of the rejection of DIC together with the brine for the air-sea flux of CO_2 has received increasing attention. Killawee et al.

(1998); Anderson et al. (2004), and Rysgaard et al. (2007) show that during sea ice growth, large volumes of DIC and $CO_{2\ (aq)}$ are rejected to the underlying water column together with sea ice brine, subsequently increasing the partial pressure of CO_2 below the ice (Gibson and Trull, 1999; Semiletov et al., 2004). This CO_2-rich water is incorporated into intermediate and deeper layers and is sequestered when passing below the pycnocline (Delille, 2010). Sea ice is supersaturated with CO_2 with respect to atmospheric values, since a decrease in temperature and thus an increase of salinity leads to higher pCO_2 values (Section 1.2). Therefore and as long as sea ice is permeable (above -5 to -11°C Golden et al. 1998; Delille 2010; Geilfus et al. 2012b), CO_2 is released to the atmosphere (Nomura et al., 2006; Miller et al., 2011b). In addition $CaCO_3$ precipitation in sea ice (Dieckmann et al., 2008, 2010) is thought to contribute significantly to the high pCO_2 levels below sea ice and subsequently to the pCO_2 uptake by the ocean (Rysgaard et al., 2007).

High DIC concentrations below sea ice have been observed during winter by Anderson et al. (2004) and Rysgaard et al. (2007), indicating an ongoing rejection of DIC during continuous sea ice growth. Reduced air temperatures lead to lower sea ice temperatures, which result in lower brine volumes and subsequently a decrease in permeability. Although, this process is thought to impede the ice-atmosphere gas exchange (Rysgaard et al., 2011; Loose et al., 2011a), recent studies report winter-time fluxes above cold sea ice (Heinesch et al., 2010; Papakyriakou and Miller, 2011; Miller et al., 2011b). However, these fluxes in winter remain elusive, and coupled measurement of time-dependent sea-ice pCO_2 and CO_2 fluxes are needed to confirm these observations (Papakyriakou and Miller, 2011).

As spring arrives, increasing temperatures and permeability lead to an efflux of CO_2 from the ice toward the atmosphere as long as brine is supersaturated with respect to atmospheric CO_2 values (Rysgaard et al., 2011). With further increasing temperature and enhanced sea ice melting, brine becomes undersaturated in CO_2 due to dilution and reduction of salinity (Section 1.2, Delille

2010) turning sea ice into a sink for CO_2. Moreover dissolution of $CaCO_3$ and photosynthetic activity by ice algae also reduces the CO_2. Together, these processes may lead to an extensive reduction of pCO_2 values down to 0 μatm (Geilfus et al., 2012b). Stratification of the surface water column due to sea ice melt and low pCO_2 values within this layer as described above, enhances air-sea CO_2 fluxes (Rysgaard et al., 2011, and references therein). Though it is difficult to estimate, the sea ice driven carbon pump is potentially of equal size to the pelagic productivity-driven air-sea exchange on a large scale (Rysgaard et al., 2009). Budgeting the carbon cycle in the polar oceans in both hemispheres (North of 62°N and south of 50°S) shows that the sea ice driven carbon pump is equivalent to 17-42% of the air-sea CO_2 flux in open oceanic waters at high latitudes (Rysgaard et al., 2011; Papadimitriou et al., 2012). Therefore, sea ice cannot longer be seen as a lid on the ocean and has to be considered as an essential part of the global carbon cycle (Delille, 2010; Rysgaard et al., 2011; Loose et al., 2011a; Halloran, 2012).

1.4 Sea ice - atmosphere gas exhange

For a long time sea ice was considered to impede gas exchange between ocean and atmosphere (Gibson and Trull, 1999). In particular, when modelling the carbon cycle in polar regions, the gas exchange between sea ice and atmosphere has been neglected (Sun and Matsumoto, 2010). Though Miyake and Matsuo (1963), and Kelley and Gosink (1979) already considered sea ice as permeable for gases, measurements of fluxes of CO_2 between ice and atmosphere were first conducted during the last decade (Semiletov et al., 2004; Delille, 2006). Resulting from these and other studies (i.e. Zemmelink et al. 2006; Nomura et al. 2006; Semiletov et al. 2007) there is growing evidence, that sea ice is permeable for gas exchange between ocean and atmosphere. The gas exchange from consolidated sea ice across its interfaces with the atmosphere and the ocean is controlled by the connectivity of brine inclusions with its surround-

ings. The connectivity of brine inclusions within the ice, with the atmosphere above, and the underlying water column is determined by the brine volume (Papadimitriou et al., 2012). The brine volume in turn is determined by sea ice temperature and bulk salinity (S_{si}) (Cox and Weeks, 1986; Leppäranta and Manninen, 1988). Hence, the brine volume fraction can be calculated from:

$$\frac{V_b}{V} = \left(1 - \frac{V_a}{V}\right) \frac{(p_i/1000)S_{si}}{F_1(T) - (p_i/1000)S_{si}F_2(T)} \tag{1.5}$$

where V_a/V is the air volume fraction, which is usually neglected since its volume is much smaller than the brine volume fraction. However, it might become substantial in multiyear or deteriorated ice (Timco and Frederking, 1996; Petrich and Eicken, 2010). The density of pure ice (ρ_i) can be calculated from:

$$\rho_i = 917 - 0.1403T \tag{1.6}$$

The empirical polynomial functions $F_1(T)$ and $F_2(T)$ are based on the phase relations (Petrich and Eicken, 2010):

$$F_i(T) = a_i + b_iT + c_iT^2 + d_iT^3 \tag{1.7}$$

The coefficients for different temperature intervals are listed in Table 1.1. If first year sea ice formed from ocean water reaches a temperature of -5°C it most likely has a bulk salinity of 5, which would result in the porosity of 5% according to the equations 1.1 and 1.5. These values are also known as the rules of fives (Golden et al., 1998, 2007; Petrich and Eicken, 2010). Any change in sea ice temperature affects the brine volume, salinity, and the chemical composition of the brine and thus the gas fluxes between sea ice and atmosphere of i.e. CO_2 due to the resulting change in connectivity and change in pCO_2 (see section 1.2). Two methods are applied for CO_2 flux measurements above sea ice. For measuring turbulent fluxes the eddy covariance (EC) method is applied (Zemmelink et al., 2006; Miller et al., 2011b; Papakyriakou and Miller, 2011), while for higher spatial resolution and determining fluxes on small scales

Table 1.1: Coefficients for functions $F_1(T)$ and $F_2(T)$ for different temperature intervals. From Petrich and Eicken (2010) according to Cox and Weeks (1986); Leppäranta and Manninen (1988).

T, (°C)	a_1	b_1	c_1	d_1
$0 \geq T > -2$	-0.041221	-18.407	0.58402	0.21454
$-2 \geq T > -22.9$	-4.732	-22.45	-0.6397	-0.01074
$-22.9 \geq T > -30$	9899	1309	55.27	0.7160
T, (°C)	a_2	b_2	c_2	d_2
$0 \geq T > -2$	0.090312	-0.016111	$1.2291\text{x}10^{-4}$	$1.3603\text{x}10^{-4}$
$-2 \geq T > -22.9$	0.08903	-0.01763	$-5.330\text{x}10^{-4}$	$8.801\text{x}10^{-6}$
$-22.9 \geq T > -30$	8.547	1.089	0.04518	$5.819\text{x}10^{-4}$

the chamber technique is used (Semiletov et al., 2004; Delille et al., 2007; Nomura et al., 2010b; Geilfus et al., 2012b).

The eddy covariance is a direct and non-destructive method for measuring fluxes of CO_2 above large areas (Burba and Anderson, 2007). The use of micrometeorological techniques has increased in various studies since their first use in the 70's (Baldocchi et al., 1988; Baldocchi, 2003). The movement of air can be conceptualized as individual parcels of air in random motion, which are sometimes called the "turbulent element" or "eddy" (Fig. 1.8). These eddies transport properties such as their content of heat, water vapour, kinetic energy, and carbon dioxide. All these properties move with them in any direction in which they are transported across the boundary layer (Geiger et al., 2009). The exchange rate of CO_2 between the atmosphere and the surface can be measured by determining the covariance between fluctuations in vertical wind velocity and CO_2 mixing ratio (Baldocchi, 2003). This technique underlies several assumptions and requires high-frequency sensor response, high sensor sensitivity to the fluctuating components and the adequate spatial or temporal averaging (Geilfus, 2011, and references therein). Moreover, eddy

Figure 1.8: Schematic of an air flow above a canopy, consisting numerous rotating eddies of various sizes (Burba and Anderson, 2007).

covariance requires a suite of mathematical calculations and corrections leading to a complex data processing. In addition a careful error treatment has to be conducted, since errors (i.e. frequency response, density fluctuations) may combine to over 100% of the flux (Burba and Anderson, 2007). A comprehensive overview on eddy covariance measurements is given by Burba and Anderson (2007) and Baldocchi (2003). Although applied on sea ice (i.e. Zemmelink et al. 2006; Miller et al. 2011b), there is, to the best of my knowledge, no overview on the application of EC in polar regions.

In contrast, the chamber technique is easy to set up and is not as expensive as eddy covariance measurements. The chamber technique was applied first in soil sciences (de Jong et al., 1979). Semiletov et al. (2004) and Delille (2006) were the first to apply the chamber technique on Arctic and Antarctic sea ice, respectively. To measure the flux of CO_2, a chamber, which is closed at the top and connected in a closed loop to a gas analyzer, is placed onto the ice (Fig. 1.9). The rate at which CO_2 diffuses into the air from the ice interface or vice versa is determined by measuring the rate of increase/decrease of CO_2

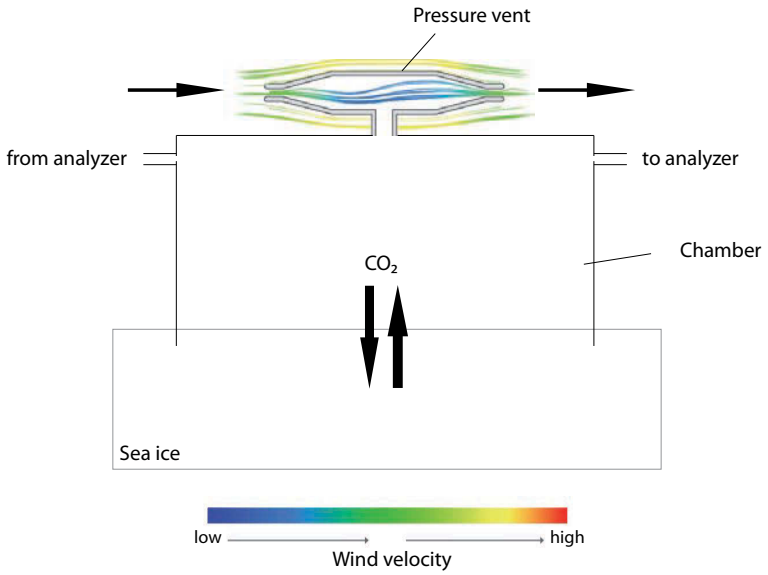

Figure 1.9: Schematic of air-ice CO_2 flux measurement using the chamber technique. The chamber is installed above the sea ice and equipped with a patented pressure vent that maintains pressure equilibrium inside the chamber and the ambient air under calm and windy conditions (Xu et al., 2006). Air from inside the chamber is pumped in a closed loop to an infrared gas analyzer and back to the chamber. The rate at which CO_2 diffuses into the air from the ice interface or vice versa is determined by measuring the rate of increase/decrease of CO_2 within the chamber over a designated time interval.

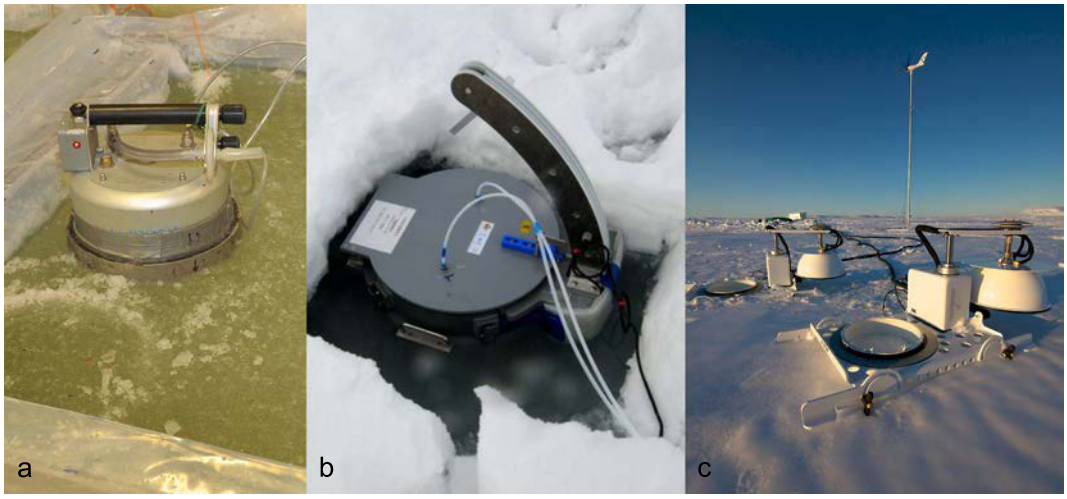

Figure 1.10: Ice-atmosphere flux measurement of CO_2 using the chamber technique. a) Accumulation chamber by West Systems, Italy (Delille, 2006), b) Self made chamber system (Nomura et al. 2010b, Photo: D. Nomura) c) Long-term chamber with pressure vent by LI-COR Biosciences, USA (Chapter 3 and 4)

within the chamber over a designated time interval (Geilfus, 2011). Self made systems (Semiletov et al., 2004; Nomura et al., 2010b) or the commercial system from West Systems S.r.l., Italy (Delille et al., 2007; Geilfus et al., 2012b) are applied on sea ice (Fig. 1.10). Measurements were limited only to a few measurements per day during the experiments and were not conducted over night. Thus, a possible diurnal cycle could not be observed and interpretations of the measurements might be misleading when it comes to quantification of fluxes above sea ice. The small temporal (minutes to hours) extent from these studies may not be representative (Geilfus, 2011) and potentially miss important events of efflux or influx. Continuous measurements, as provided by the eddy covariance method, are missing for the chamber method and are therefore required to fully asses the ice-atmosphere CO_2 flux.

As pointed out by Geilfus (2011) EC and chamber technique are applied at different spatial and temporal scales. The values obtained from one method may not be quantitatively similar to the values derived from the other. Each

method has been ascribed several advantages and disadvantages (Oechel et al., 1998). While there is debate whether open or closed path eddy covariance is the most suitable method for flux measurements between sea ice and atmosphere (Papakyriakou and Miller, 2011), EC has proven to be applicable over flat and homogeneous surfaces under stable atmospheric conditions. Eddy covariance measurements provide data on a large-scale resolution. However, data processing needs a suite of corrections and over extremely variable surfaces such as ridges and pack ice, the spatial resolution of the eddy covariance technique is not high enough (Loose et al., 2011a). In contrast chamber measurements are able to resolve a high spatial variability. They are easy to deploy and inexpensive. However, Oechel et al. (1998) ascribes the chamber method a potential bias from pressure gradients. Hence, a system is needed which tracks the ambient atmospheric pressure during the measurement.
Chamber measurements are mostly conducted on bare sea ice (Delille et al., 2007; Semiletov et al., 2004). Only a few studies investigated the influence of snow cover on sea ice on the CO_2 flux between atmosphere and ice with the chamber technique (Nomura et al., 2010b; Geilfus et al., 2012b). Moreover, none of these studies provide continuous long-term measurements above different surfaces.

1.5 Objective and outline of the thesis

As described in the sections above, large gaps still exist in our understanding of the components of the polar carbon cycle. Climate change, which is more intense in the polar regions (Section 1.1), and its implication for the seasonal sea ice cover has consequences for example on the exchange of CO_2 between the ocean-sea ice-atmosphere-boundary layer (Barber et al., 2012). In order to predict future changes in the air-sea CO_2 fluxes in polar regions, a comprehensive understanding of the role of sea ice in the air-sea exchange of CO_2 is a priority (Geilfus et al., 2012b).

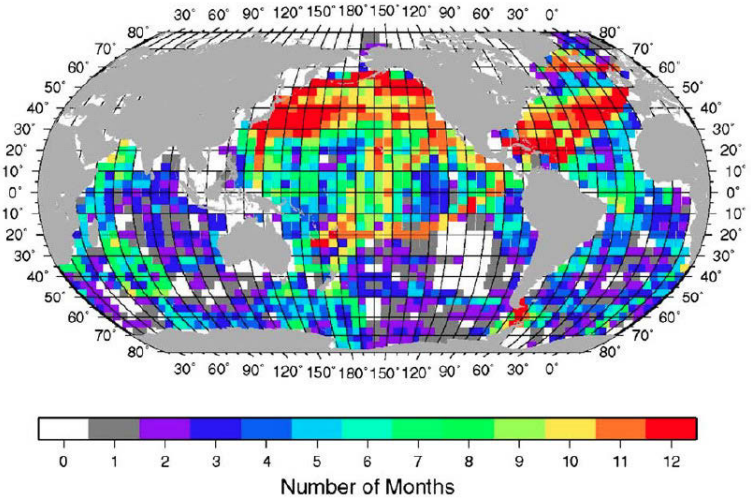

Figure 1.11: Number of months in each 4 x 5° box area where at least one surface water pCO2 measurement has been made since they early 1970's. White areas have no measurements (Takahashi et al., 2009).

Important questions remain about the significance of calcium carbonate in sea ice on the polar carbon cycle (Barber et al., 2012; Rysgaard et al., 2012). Moreover, in situ pCO_2 and relating flux measurements on small scales are missing in polar regions (Fig. 1.11, Section 1.4). Hence, my intention with this project was to improve the state of knowledge concerning the inorganic carbon dynamics, including the precipitation of $CaCO_3$ in sea ice and it significance for the polar carbon cycle as well as to obtain improved estimates of the diurnal and long-term CO_2 flux on small scales during the winter-spring-summer transition.

Chapter 2 deals with the spatial and temporal distribution of $CaCO_3$ as ikaite in Antarctic sea ice. Biogeochemical parameters, such as dissolved organic carbon, inorganic phosphate, and total alkalinity were analyzed for their possible influence on the precipitation of ikaite. Moreover, potential conditions promoting or leading to calcium carbonate precipitation and the likely significance of ikaite in sea ice for the polar carbon cycle are discussed.

Chapter 3 examines the fluxes of CO_2 between the atmosphere and subarctic sea ice with and without snow cover using for the first time long-term continuous (24 hours) chamber measurements as usually applied in soil sciences. Diurnal fluxes are analyzed and fluxes are compared to existing observations above sea ice and snow. Moreover, variables which may influence the flux of CO_2 between sea ice and atmosphere are investigated.

Chapter 4 is on investigations of the pCO_2 in water, sea ice, and atmosphere and the resulting fluxes between ice and atmosphere in the Canadian Arctic Archipelago from winter conditions into the melting season until sea ice break-up. Diurnal long-term continuous (24 hours) chamber measurements as described in chapter 3, atmospheric profiling of pCO_2, measurements of pCO_2 in melt ponds, in situ in sea ice, and water column were carried out. The effect of melt ponds and snow on the fluxes of CO_2 are analyzed. Further, the implications of the findings for the Arctic carbon cycle are discussed.

Chapter 5 provides a synthesis of the major findings in the context of the sea ice driven carbon pump. The significance of $CaCO_3$ precipitation, CO_2 degassing, and the formation of bubbles within sea ice for the polar carbon cycle is discussed. Before perspectives for future research are given, an improved understanding of the sea ice driven carbon pump is presented.

1.6 List of publications

This doctoral thesis is based on the following manuscripts:

Chapter 2: Fischer, M., Thomas, D.N., Krell, A., Nehrke, G., Göttlicher, J. Norman, L., Meiners, K.M., Riaux-Gobin, C., and Dieckmann, G.S. 2013: Quantification of ikaite in Antarctic sea ice, Antarctic Science, in press

The experiments were planned by myself and Gerhard Dieckmann. Field work, laboratory analyzes and data acquisition were realized by me with support of

Andreas Krell, Louiza Norman, Gernot Nehrke, Jörg Göttlicher, and Gerhard Dieckmann. I interpreted the data and wrote the manuscript with contributions by the co-authors.

Chapter 3: Fischer, M., Tison, J.-L., Dieckmann, G.S., and Rysgaard, S., Delille, B.: Longterm chamber measurements of CO_2 fluxes on subarctic sea ice, Manuscript draft

The experiment was planned by myself and Bruno Delille. Field work and data acquisition were realized by me with support of Bruno Delille, Jean-Louis Tison, David Thomas and Søren Rysgaard. I interpreted the data and wrote the manuscript draft.

Chapter 4: Fischer, M., Brown, K., Papakyriakou, T., Tison, J.L., Delille, B., Mundy, C.J., Haas, C., Kaleschke, L., Miller, L., and Wolf-Gladrow, D.A.: Surface based flux measurements and the evolution of CO_2 in Arctic sea ice, melt ponds, seawater, and atmosphere during winter-spring-summer transition, Manuscript draft

The experiments were planned by myself and Kristina Brown. Field work and data acquisition was realized by me with support of C.J. Mundy, Bruce Johnson, and Christian Haas. I interpreted the data and wrote the manuscript with contributions by the co-authors.

Photo Credits: C. Fresser, C. Qillfeldt, K. Pierre

Chapter 2

Quantification of ikaite in Antarctic sea ice

Fischer, M.[1], Thomas, D.N.[2,3,4], Krell, A.[1], Nehrke, G.[1], Göttlicher, J.[5], Norman, L.[2], Meiners, K.M.[6,7], Riaux-Gobin, C.[8], and Dieckmann, G.S.[1] (2013): Quantification of ikaite in Antarctic sea ice, Antarctic Science, doi:10.1017 / S0954102012001150

[1]Alfred Wegener Institute for Polar and Marine Research, Bremerhaven, Germany

[2]Ocean Sciences, College of Natural Sciences, Bangor University, Menai Bridge, UK

[3]Marine Centre, Finnish Environment Institute (SYKE), Helsinki, Finland

[4]Arctic Research Centre, Aarhus University, Aarhus, Denmark

[5]Institute of Synchrotron Radiation (ISS), Synchrotron Radiation Source ANKA, Karlsruhe Institute of Technology, Eggenstein-Leopoldshafen, Germany

[6]Australian Antarctic Division, Department of Sustainability, Environment, Water, Population and Communities, Kingston, Tasmania, Australia

[7]Antarctic Climate and Ecosystems Cooperative Research Centre,Hobart, Tasmania, Australia

[8]USR3278, CRIOBE, CNRS-EPHE, Perpignan, France

Abstract. $CaCO_3$ precipitation in sea ice is thought to potentially drive significant CO_2 uptake by the ocean. However, little is known about the quantitative spatial and temporal distribution of $CaCO_3$ within sea ice, although it is hypothesized that high quantities of dissolved organic matter and/or phosphate (common in sea ice) may inhibit its formation. In this quantitative study of hydrous calcium carbonate as ikaite, sea ice cores and brine samples were collected from pack and land fast sea ice between September and December 2007 during two expeditions, one in the East Antarctic sector and the other off Terre Adélie. Samples were analyzed for $CaCO_3$, salinity, dissolved organic carbon/nitrogen (DOC, DON), inorganic phosphate, and total alkalinity. No relationship between these parameters and $CaCO_3$ precipitation was evident. Ikaite was found mostly in the uppermost layers of sea ice with maximum concentrations of up to 126 mg ikaite per liter melted sea ice being measured, although both the temporal and horizontal spatial distributions of ikaite were highly heterogeneous. The precipitate was also found in the snow on top of the sea ice at some of the sampling locations.

Keywords Antarctica, Southern Ocean, Sea ice, ikaite, calcium carbonate precipitation, biogeochemistry

2.1 Introduction

Sea ice covers up to seven per cent of the total surface area of the oceans at its maximum extent (Comiso, 2010). The physical barrier itself has a major impact on the gas exchange between atmosphere and ocean, and recently the discussion has extended to considering how physical and biogeochemical processes within the ice itself can affect diffusion and flux of gases to both atmosphere and ocean (Tison et al., 2002; Rysgaard et al., 2007, 2009, 2011; Miller et al., 2011b; Loose et al., 2011a). On the basis of thermodynamic equilibrium calculations, the precipitation of $CaCO_3$ was predicted to occur

during natural sea ice formation (Jones and Coote, 1981; Anderson and Jones, 1985) and it was proposed to precipitate as calcite (Marion, 2001). However, actual evidence was, for a long time, only indirect (Killawee et al., 1998; Papadimitriou et al., 2004; Tison et al., 2002; Papadimitriou et al., 2012) until Dieckmann et al. (2008) found calcium carbonate as ikaite $CaCO_3 \cdot 6H_2O$ in Antarctic sea ice, and more recently in Arctic sea ice (Dieckmann et al., 2010; Rysgaard et al., 2012). Rysgaard et al. (2007, 2009) showed that with brine, dissolved inorganic carbon (DIC) is rejected from growing sea ice to the underlying waters. They ascribe the high pCO_2 (partial pressure of CO_2) levels found below sea ice to calcium carbonate precipitation. Rysgaard et al. (2007) proposed that $CaCO_3$ precipitation in sea ice could result in a significant CO_2 uptake by the ocean and therefore contribute to a polar carbon pump.

Besides its function as a component in the carbon cycle, the mineral is also thought to have a key role in tropospheric ozone depletion events (ODEs) at high latitudes (Sander et al., 2006; Sander and Morin, 2010). Simulations of the chemistry occurring in Polar Regions over newly formed sea ice relate the ODE to the transformation of inert sea-salt bromide to reactive bromine monoxide (BrO) when precipitation of calcium carbonate from freezing seawater is taken into account. The discovery of ikaite in firn ice of the Antarctic continent, which appears to be derived from sea ice 300 km away, may also have implications for its use as a sea ice proxy (Sala et al., 2008). However, to date most studies of calcium carbonate in sea ice have been mainly qualitative and little is known about the spatial and temporal distribution of $CaCO_3$ within sea ice.

There is also a lack of knowledge on the exact conditions leading to ikaite precipitation as well as on the amount and fate of ikaite: e.g. one assumption is that phosphate and dissolved organic matter (DOM) may reduce the precipitation of calcium carbonate (Bischoff et al., 1993; Zullig and Morse, 1988). Both dissolved inorganic phosphate and DOM can be present in sea ice in very high concentrations (Thomas et al., 2001), and it can be hypothesized that

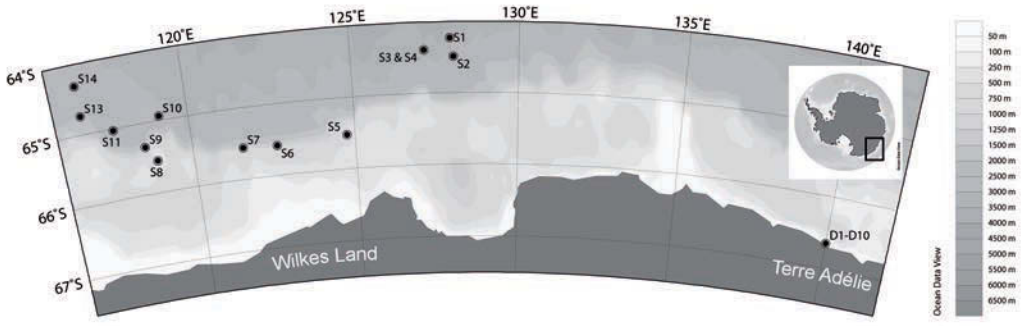

Figure 2.1: Locations of ice stations sampled during SIPEX and DDU campaign

where these parameters are present in high concentrations that precipitation of some polymorphs of calcium carbonate will be inhibited. The objective of this study therefore was to: (1) Provide the first systematic observation and quantification of $CaCO_3$ precipitation in Antarctic sea ice on a spatial and temporal scale and (2) to investigate relationships between calcium carbonate and alkalinity, phosphate, and dissolved organic matter.

2.2 Methods

2.2.1 Study Area and sea ice sampling

Two campaigns were performed between September and December 2007. During the first campaign (Sea Ice Physics and Ecosystem eXperiment (SIPEX) onboard RSV Aurora Australis from September to October 2007) fourteen ice cores (S1 to S14) were taken at different locations between S64° and S66° and E116° and E128° (Fig. 2.1). The cores were cut into 10 cm sections within a few minutes after sampling and stored in plastic containers. Ice cores from station S1 to S4 and S6 to S14 represent pack ice with different degrees of deformation (Table 2.1). The ice core from station S5 was taken from fast ice between grounded icebergs. Details on ice types, bulk salinity, ice temperature,

and brine volume, see Table 2.1, Fig. 2, and Fig. 3, and Meiners et al. (2011). A general description of the ice conditions during the expedition can be found in (Worby et al., 2011). Brine from sackholes from 10 out of 14 stations (Table 2.2) was collected for nutrient and DOM analyzes (Norman et al., 2011).
During the second campaign (from November to December 2007) sea ice samples were collected close to the French base Dumont d'Urville (DDU), S66° 39' 13" E140° 00'5" near station C described in Delille et al. (2007). Six complete ice cores (D1 to D6) were taken from young fast ice (age: $\approx$ 3 months, Anne Jacquet, pers. comm.), which had formed in August. This area was predominantly free of snow with only isolated patches of snow being present. The cores were also cut into 10 cm sections and stored as described above. In order to determine small-scale vertical distribution of ikaite, we also collected four surface cores (D7 to D10) between 10 and 15 cm length (Table 2.1). Cores D7 and D9 were taken from the main sampling site without any snow on top, while D8 was taken next to it and included snow. Ice sample D10 was taken from older fast ice approximately 200 m away from the main sampling site. Ice core D10 was taken from sea ice, which had formed in autumn and had remained intact since its formation, in contrast to cores D1-D9, which were from younger sea ice. Ice cores D7 to D10 were cut into 2 cm sections. In addition, to determine horizontal spatial variability of calcium carbonate, we chose an area 50 m away from the first sampling site. On this site the first top 10 cm of fast ice were sampled every 5 m (x and y direction) in a grid of 20 m by 20 m (D-SP1 to D-SP25, Table 2.1). The partial ice cores obtained were stored in clean plastic containers. At the main sampling site, sackholes (D-SH1 to D-SH7) of 30 cm were cored every two or three days for a temporal analysis of brine and ice. All samples were collected within an area of 10 m x 10 m to minimize bias due to spatial heterogeneity. The partial ice core obtained from these sackholes was also stored in clean plastic containers. Brine was allowed to accumulate in the sackholes and sampled with a vacuum pump and transferred into different vials for total alkalinity (TA), dissolved organic

carbon (DOC), dissolved organic nitrogen (DON), and phosphate analyses. Samples for DOM and nutrients were collected as described by Norman et al. (2011) and kept frozen until analyses within 6 months. The TA samples were measured directly in the base laboratory.

Two sediment traps MST6 (HYDRO-BIOS, 0.005 m^2 surface) and a current-meter RCM7 (ANDERRA) were deployed under the sea ice at Dumont d'Urville from 13/11/07 to 04/12/07 immediately adjacent to the temporal study site. The first sediment trap at 5 m under the ice and the second one at 25 m. Water depth at the site was 53 m. Mercuric chloride was used for fixation of the samples. Sediment trap samples were immediately analyzed under the binocular microscope after the traps were retrieved.

We also sampled glacial firn ice 6 kilometres away from the ice shelf at Cape Prud'homme to test if calcium carbonates are found on the ice shelf in this region. One surface core (1m) was collected and cut into three equal sections. The sections were stored in plastic containers and brought to the laboratory.

2.2.2 Analytical techniques

All sea ice samples were slowly melted in a climate controlled room where the temperatures never exceeded 4°C to avoid decomposition of the mineral ikaite. Regular monitoring (several times a day) guaranteed a processing of the samples as soon as the cores, or sections were melted. This ensured that the temperature of the melt water never rose above 0°C. The melt water was filtered through 0.2 μm polycarbonate filters using a vacuum pump and the volume of filtrate measured. The filters with crystals were placed in plastic vials (Safe-Lock Tubes 2 ml, Eppendorf, Germany) and subsequently filled with 75% v/v ethanol and frozen at −18°C for later mineralogical phase identification and quantitative measurements. In several instances crystals were collected after swirling the melted samples and allowing crystals to settle in the resulting vortex. The crystals were transferred from the vortex to a petri dish

using a glass pipette Dieckmann et al. (2008). These were briefly inspected under the binocular microscope and photographed to check the morphology and subsequently also filtered as described above. Mineral phase identification was conducted by micro X-ray diffraction (μ-XRD) under cryogenic conditions on selected samples at the Synchrotron Laboratory for Environmental Studies SUL-X at the synchrotron radiation source ANKA, Forschungszentrum Karlsruhe (now Karlsruhe Institute of Technology) as described by Dieckmann et al. (2008). To quantify the calcium carbonate within a sample, the quantity of calcium ions were determined using Inductively-Coupled Plasma Optical Emission Spectrometry (ICP OES). The Safe-Lock tubes containing the filters were rinsed with concentrated ethanol and the content was transferred to larger vials. The transferred samples were dried at 60°C until all the ethanol had evaporated, leaving only the calcium carbonate crystals. Five ml concentrated HNO_3 was added to dissociate all molecules according to equation 2.1 before the samples were analyzed in the ICP OES. The amount of ikaite was calculated using a molar calcium/ikaite ratio of one.

$$[CaCO_3 \cdot 6H_2O] = [Ca^{2+}] + [CO_3^{2-}] + 6[H_2O] \tag{2.1}$$

Brines from sackholes (D-SH1 to D-SH7 and from 10 ice stations during the SIPEX campaign) were analyzed for in situ concentrations of phosphate, DON, DOC and alkalinity (Table 2.2). Analysis for the major dissolved inorganic nutrients, nitrate (NO_3^-), nitrite (NO_2^-), and of dissolved inorganic phosphorus (DIP) was done using standard colorimetric methodology (Hanson and Koroleff, 1983) as adapted for flow injection analysis (FIA) on a LACHAT Instruments Quick-Chem 8000 autoanalyzer (Hales et al., 2004). Dissolved organic carbon was analyzed by high temperature combustion on an MQ1000 TOC analyser according to Qian and Mopper (1996). Dissolved organic nitrogen was determined by subtraction of NO_3^-, and NH_4^+ from the total dissolved nitrogen (TDN) analyzed using on-line peroxodisulfate oxidation coupled with ultraviolet radiation at pH 9.0 and 100°C (Kroon, 1993).

Table 2.1: Sample types and thickness of sea ice during SIPEX and DDU campaign

Sample	Cruise	Date of Sampling	Time (UTC)	T_{Air} [°C]	T_{ice} [°C] at 5 cm below surface	Sample type	Sample thickness in cm
S1	SIPEX	11.09.2007	04:00	-15.9	-8.7	Pack ice, Brine from sackhole	51
S2	SIPEX	12.09.2007	06:00	-18.6	-9.6	Pack ice, Brine from sackhole	98
S3	SIPEX	14.09.2007	06:00	-20.1	-11.7	Pack ice, Brine from sackhole	49
S4	SIPEX	17.09.2007	08:00	-19	N/A	Pack ice, Brine from sackhole	55
S5	SIPEX	18.09.2007	08:00	-18	-10.2	fast ice between grounded icebergs, brine from sackhole	85
S6	SIPEX	21.09.2007	03:00	-11.7	-9.1	heavily rafted ice floes, brine from sackhole	81
S7	SIPEX	22.09.2007	02:30	-12.3	-7.2	Pack ice, brine from sackhole	53
S8	SIPEX	25.09.2007	10:00	-7	-4.9	large level floe, brine from sackhole	37
S9	SIPEX	28.09.2007	03:00	-11.1	-4.9	heavily rafted and deformed ice, brine from sackhole	98

Sample	Cruise	Date of Sampling	Time [UTC]	T_{Air} [°C]	T_{ice} [°C] at 5 cm below surface	Sample type	Sample thickness in cm
S10	SIPEX	30.09.2007	04:00	-14.8	-4	large level floe,coring site on an adjecent rafted area, probably an old chunk catched by new ice, brine from sackhole	133
S11	SIPEX	03.10.2007	02:00	-7.3	-6.8	rafted floe, ice surface very rough probably crushed together pancakes at an earlier stage, brine from sackhole	101
S12	SIPEX	05.10.2007	07:00	-6.9	-6.5	rafted ice floes, brine from sackhole	109
S13	SIPEX	06.10.2007	02:00	-7.8	-5.3	rafted floes, ice surface very rough probably consisting of thin rafted ice chunks, brine from sackhole	78
S14	SIPEX	07.10.2007	01:00	-10	-5.5	Pack ice, brine from sackhole	64
D1	DDU	14.11.2007	N/A	-6.6	-5.2	young (approx. 3 month) fast ice, 10 cm sections	65
D2	DDU	17.11.2007	N/A	-3.2	-4.1	young (approx. 3 month) fast ice, 10 cm sections	65

Sample	Cruise	Date of Sampling	Time [UTC]	T_{Air} [°C]	T_{ice} [°C] at 5 cm below surface	Sample type	Sample thickness in cm
D3	DDU	23.11.2007	N/A	-5.9	-5.2	young (approx. 3 month) fast ice, 10 cm sections	60
D4	DDU	24.11.2007	N/A	-2.6	N/A	young (approx. 3 month) fast ice, 10 cm sections	60
D5	DDU	27.11.2007	N/A	-2.9	-5.1	young (approx. 3 month) fast ice, 10 cm sections	60
D6	DDU	03.12.2007	N/A	-4.6	-2.9	young (approx. 3 month) fast ice, 10 cm sections	60
D7	DDU	23.11.2007	N/A	-5.9	-5.2	young (approx. 3 month) fast ice, 2 cm sections	10
D8	DDU	24.11.2007	N/A	-2.6	N/A	young (approx. 3 month) fast ice, 2 cm sections, snow on top	16
D9	DDU	24.11.2007	N/A	-2.6	N/A	young (approx. 3 month) fast ice, 2 cm sections	14
D10	DDU	05.12.2007	N/A	-2	-5.4	fast ice (age = 1 year), 2 cm sections	16
D-SH1	DDU	14.11.2007	N/A	-6.6	-5.2	ice and brine samples from sackholes in fast ice	30
D-SH2	DDU	17.11.2007	N/A	-3.2	-4.1	ice and brine samples from sackholes in fast ice	30

Sample	Cruise	Date of Sampling	Time [UTC]	T_{Air} [°C]	T_{ice} [°C] at 5 cm below surface	Sample type	Sample thickness in cm
D-SH3	DDU	18.11.2007	N/A	-3.5	-4.2	ice and brine samples from sackholes in fast ice	30
D-SH4	DDU	23.11.2007	N/A	-5.9	-5.2	ice and brine samples from sackholes in fast ice	30
D-SH5	DDU	25.11.2007	N/A	-0.2	-2.65	ice and brine samples from sackholes in fast ice	30
D-SH6	DDU	27.11.2007	N/A	-2.9	-5.1	ice and brine samples from sackholes in fast ice	30
D-SP1 - D-SP25	DDU	02.12.2007	N/A	-2	N/A	top layer of fast ice	10

Total alkalinity (D-SH1 to D-SH7) was measured at the station laboratory within one day after sampling as described by Nomura et al. (2010b).
For the spatial analysis of the horizontal distribution of $CaCO_3 \cdot 6H_2O$ a conventional geostatistical spatial interpolation was applied by using the simple kriging method (Sarma, 2009).

2.3 Results

2.3.1 Ikaite precipitation

Calcium carbonate crystals were found in all samples analyzed, including snow, sea ice and glacial ice. Mineral phase identification of selected samples confirmed that ikaite was the precipitate present. Since all crystals extracted from the ice cores showed the same morphological features, it is most likely that the XRD identification as ikaite is representative for all crystals found in this study (Fig. 2.4). Ikaite concentrations in melted sample (sea ice or snow) ranged from 0.01 to 126 mg l^{-1} (Fig. 2.7 and 2.8) and 0.07 to 0.12 mg l^{-1} in glacial ice. The maximum amount of ikaite was found in older fast ice (D10). Data from 14 ice cores of the SIPEX campaign show the highest concentrations of the ikaite crystals in the upper layers of ice (Fig. 2.5). Although the highest concentration of ikaite in melted sea ice in the pack ice samples was 9.5 mg ikaite l^{-1}, most of the values in the uppermost 10 cm did not exceed 2 mg ikaite l^{-1}. Below a depth of 20 cm (with the exception of two ice cores (S3 and S6)) in the pack ice, ikaite concentrations ranged between 0.02 and 0.3 mg l^{-1}. Ice texture analyses of cores S3 and S6 showed it to be rafted sea ice (Meiners et al., 2011).

The ikaite concentrations in land fast ice off Terre Adélie were of a similar magnitude, but generally higher than the pack ice cores (Fig. 2.6): Most were between 2 and 5 mg l^{-1} in the top layer. A higher resolution sampling (2 cm) over the first 10 to 15 cm showed that the highest concentrations of the min-

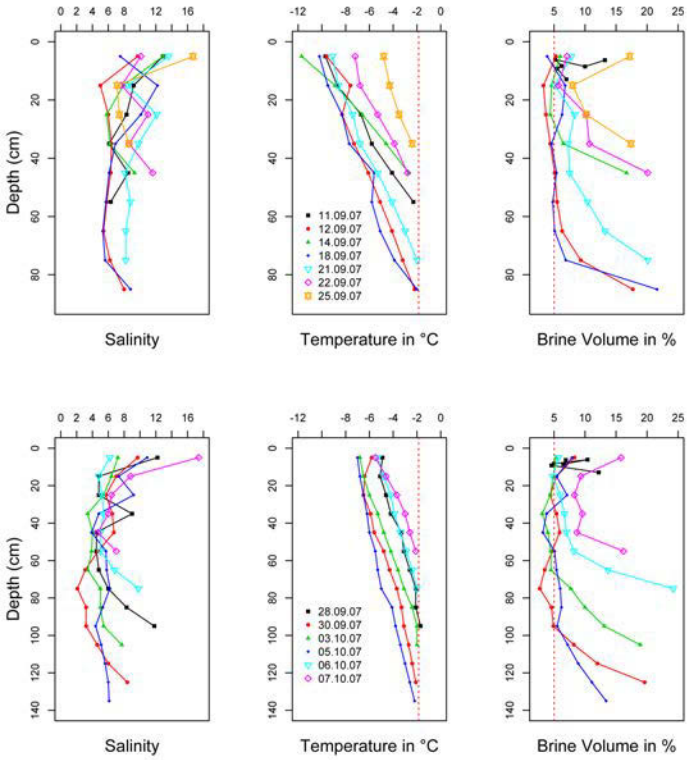

Figure 2.2: Bulk salinity, sea ice temperature, and calculated (Cox and Weeks, 1986) brine volume in different ice cores taken between September and October 2007 in East Antarctic during SIPEX campaign

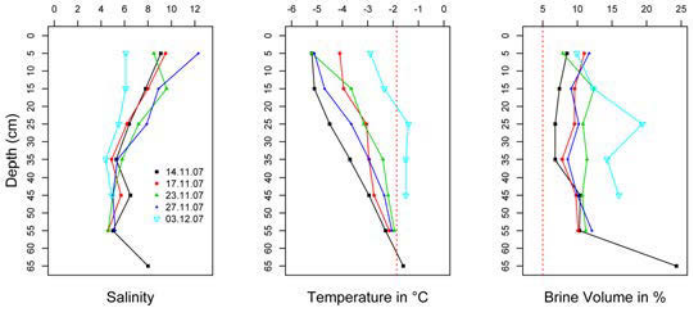

Figure 2.3: Bulk salinity (S), sea ice temperature, and calculated (Cox and Weeks, 1986) brine volume in land fast sea ice cores taken between November and December 2007 in East Antarctic during DDU campaign

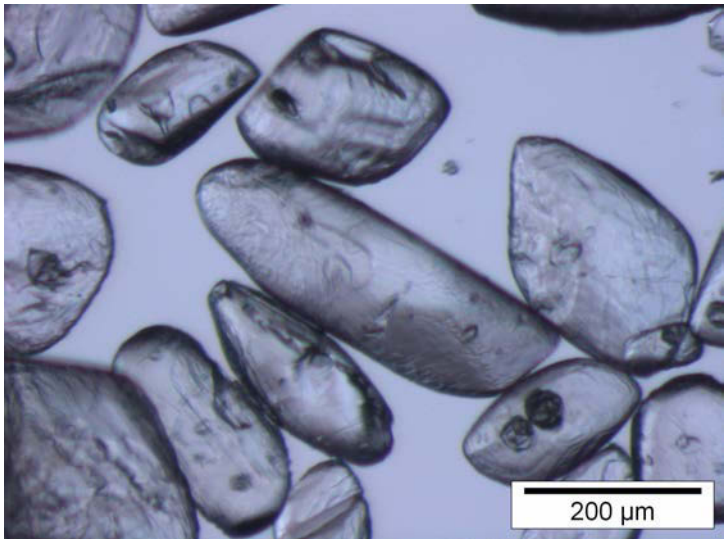

Figure 2.4: Light microscopy image of ikaite crystals taken from a single bulk sea ice sample from land fast ice off Terre Adélie

eral were in the top 2 to 4 cm of the cores (Fig. 2.7). Ice core D10 (Fig. 2.8) was sampled from a separate older fast ice (ice thickness 133 cm) location, 200 m away from the initial sampling site. This core had higher mineral concentrations than those from the younger sea ice. Ice core D8 from snow covered ice (Fig. 2.9) had ikaite crystals throughout the sample and even in the snow itself. The highest concentration (38.77 mg l^{-1}) was measured at the snow/ice interface. The shapes of salinity profiles were similar to those of the amount of ikaite in core D8 (Fig. 2.9).

A temporal change in ikaite concentration was not observed during the sampling between 14 and 27 November 2007 at DDU. Values measured in the temporal and spatial experiment were in the same range (0.06 and 3.93 mg l^{-1}, Fig. 2.10 and 2.11, Table 2.2). Hence, we could not differ temporal from spatial heterogeneity. The spatial experiment showed that the distribution of ikaite in sea ice can be highly heterogeneous. No $CaCO_3$ crystals were found in the sediment traps.

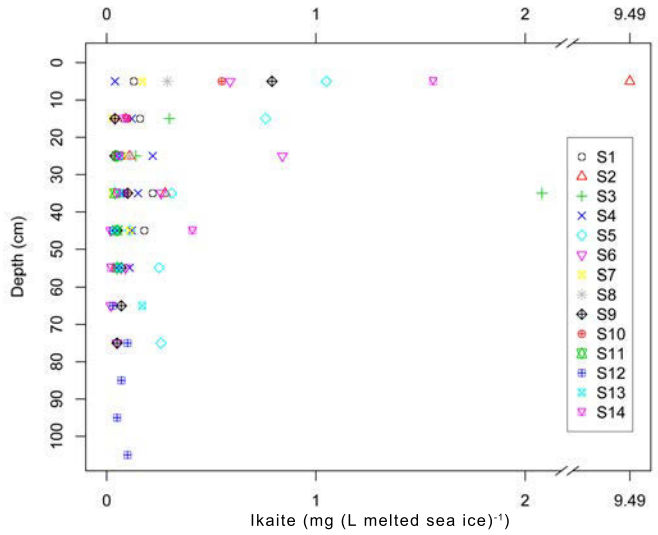

Figure 2.5: Distribution of ikaite in sea ice during SIPEX cruise in different ice cores taken between September and October 2007 in East Antarctic

2.3.2 Biogeochemical parameters

When brine concentrations are normalized to a salinity of 35, DON_{35} and DOC_{35} concentrations increased non-linearly over a period of time. During the DDU campaign, DIP_{35} (normalized to S=35) shows the same trend as DON_{35} and DOC_{35} at the beginning, it did not increase over time and remained low. Only NO_3^- showed a trend, which might indicate biological activity, although no biological parameters were measured in these samples. TA fell from almost 2600 to approximately 2200 μmol l^{-1} and did not show a linear trend, similar to the other measured chemical parameters. Neither DIC, DON, DOC concentrations (from SIPEX and DDU campaign) nor TA (DDU campaign) correlated significantly with the amount of ikaite present in the ice horizons from where the brines were collected from. Comparison of theoretical values of brine salinity (calculated according Petrich and Eicken (2010)) versus measured values (Table 2.2) showed no significant differences. Thus, brine volumes, although being above 5%, most likely were low enough to prevent influences by seawater.

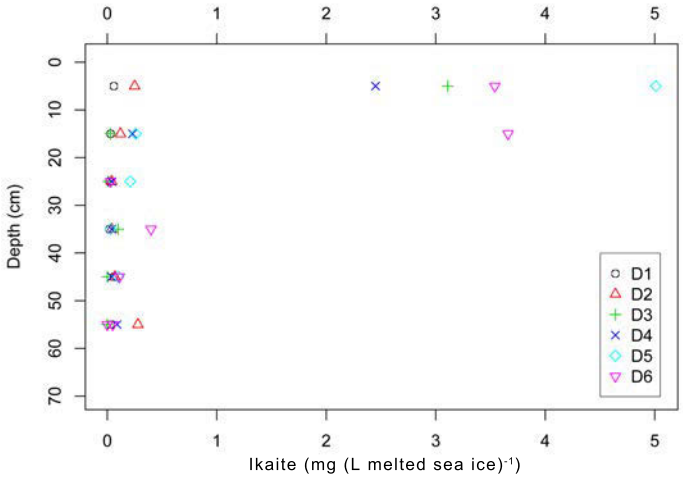

Figure 2.6: Distribution of ikaite in sea ice during DDU campaign in land fast sea ice off Terre Adélie sampled in November 2007

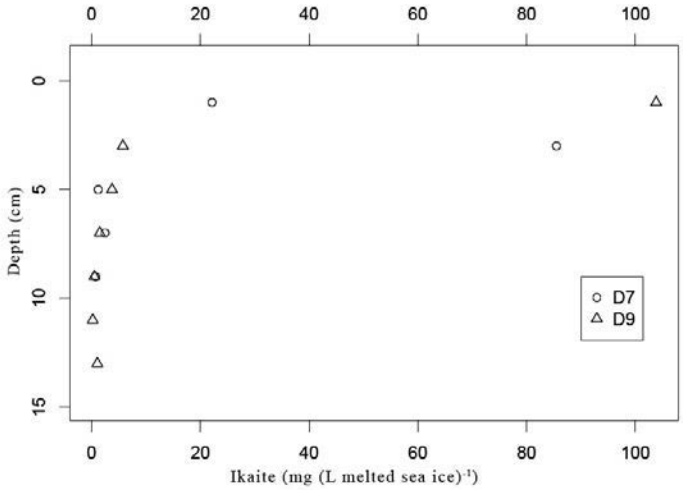

Figure 2.7: Distribution of ikaite in the surface layer of young ($\approx$ 3 month) land fast sea ice off Terre Adélie (DDU)

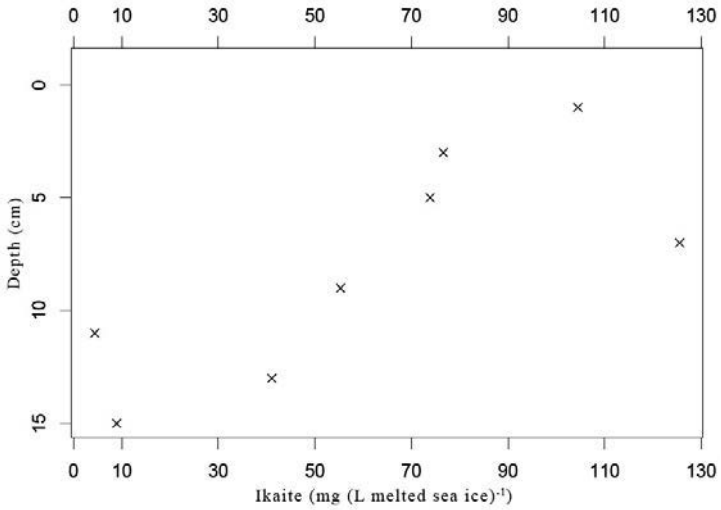

Figure 2.8: Distribution of ikaite in the top layer of older ($\approx$ 1 year) land fast sea ice, off Terre Adélie (DDU) in November 2007 core D10

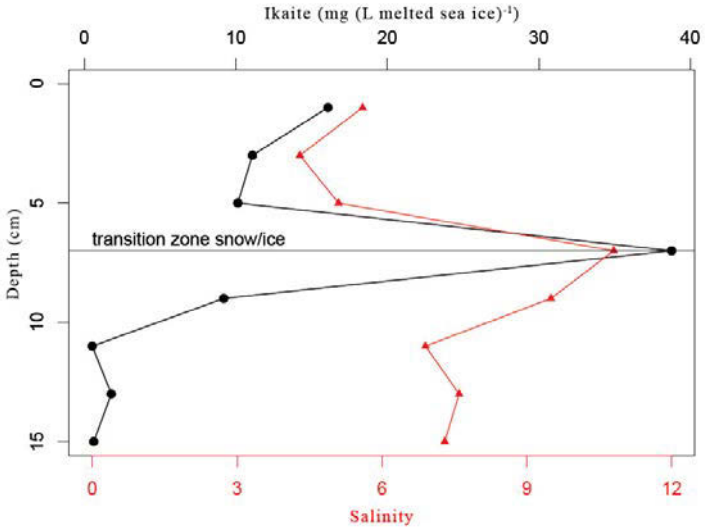

Figure 2.9: Distribution of ikaite across the snow-ice interface from top layer of land fast sea ice off Terre Adélie (DDU) in November 2007, core D8, Black line = amount of ikaite, red line = bulk salinity, in contrast to the general use the 0 cm for the snow/ice interface, it here indicates the top of the snow

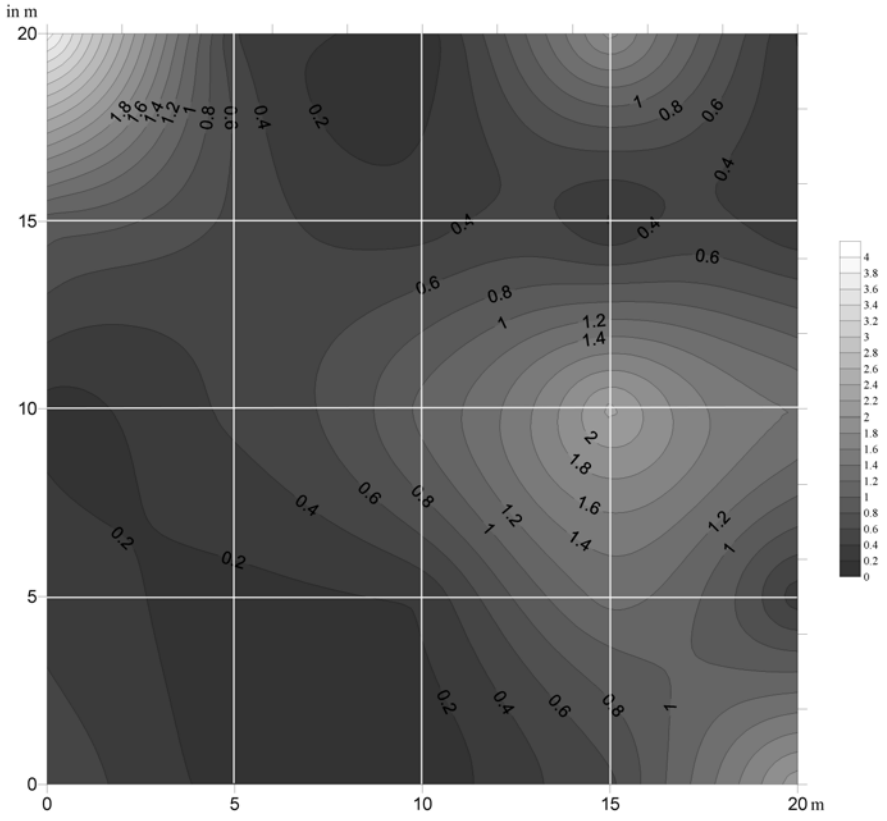

Figure 2.10: Contour plot of the spatial distribution of ikaite in the upper 10 cm of land fast sea ice off Terre Adélie (DDU) in November 2007 on a 20 m x 20 m grid with sample points every 5 m by 5 m (shown by intersections of the white lines and at the edges). Values are in mg ikaite l^{-1} melted sea ice.

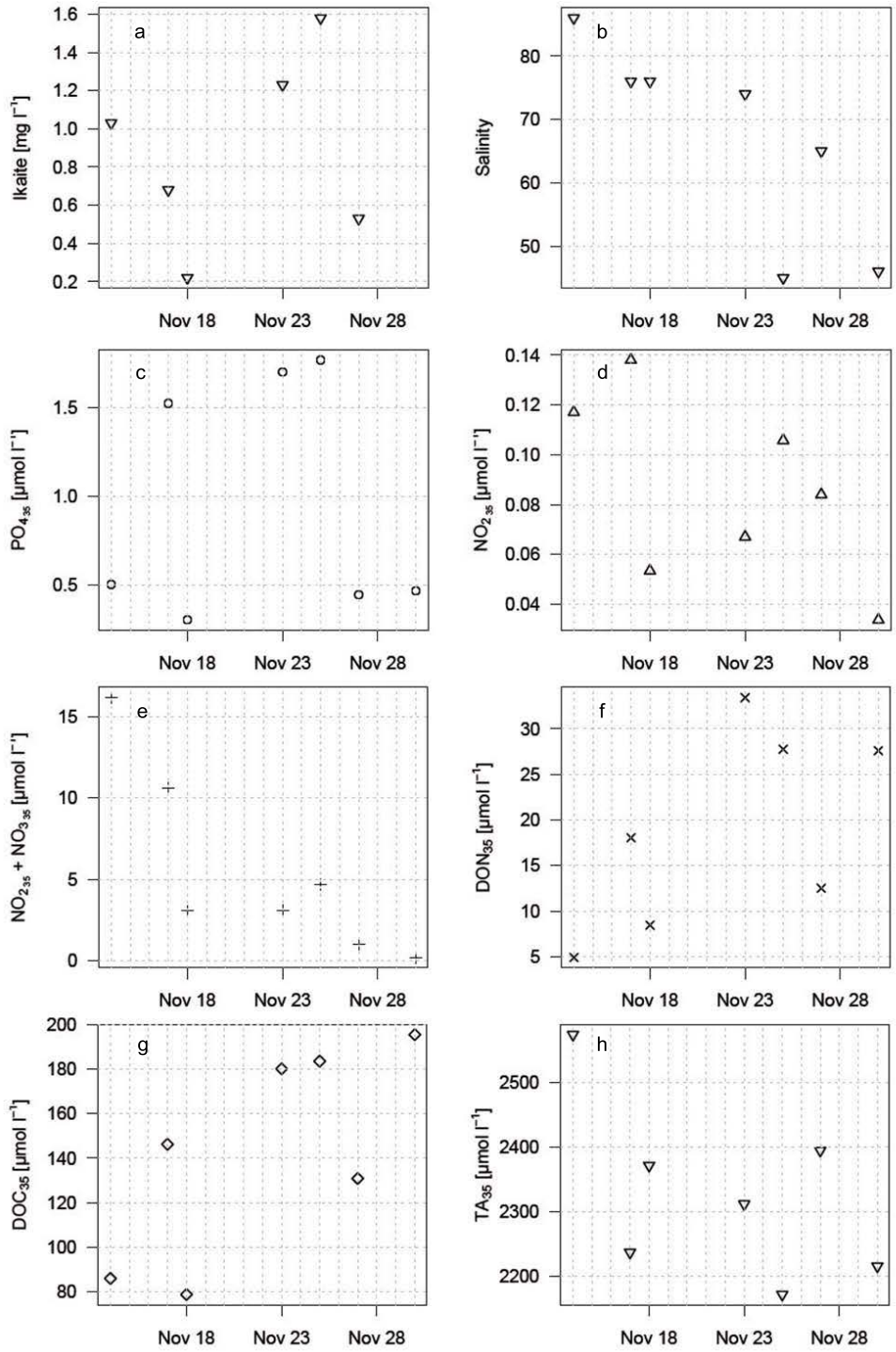

Figure 2.11: Temporal observation of ikaite in ice cores (30cm) obtained from sackholes D-SH1 to D-SH7 (DDU campaign) (a) Salinity (b) Salinity-normalized PO_4^{2-} (c) NO_2^- (d) NO_3^- (e) DON (f) DOC (g) and total alkalinity (h) in Antarctic land fast sea ice, off Terre Adélie (DDU) in November 2007

Table 2.2: Physico-chemical properties of brine collected from sackholes from land fast ice off Terre Adélie (DDU) in November 2007 (D-SH1 to D-SH7) and from sea ice in East Antarctica (see map) between September and October 2007 (S1 to S14). TA, DON, DOC, and nutrients are normalized to S=35. Ikaite values are from ice cores (30cm) obtained from the sackholes (D-SH1 to D-SH7, DDU campaign) and ice cores adjacent to the sackholes (S1 to S14, SIPEX cruise, sum of the first three 10 cm sections) and presented in mg l^{-1} melted sea ice.

Sample	Date	T_{brine}	S_{brine}	$[PO_4^{2-}]_{35}$	$[Si]_{35}$	$[NO_2]_{35}$	$[NO_2]+[NO_3^-]_{35}$	$[SNH_4]_{35}$	DON_{35}	DOC_{35}	Ikaite	TA_{35}
D-SH 1	14.11.07	-4.8	86	0.50	50.30	0.12	16.17	0.37	4.91	85.99	1.03	2573.79
D-SH 2	17.11.07	-4	76	1.53	41.39	0.14	10.63	2.04	17.50	146.17	0.68	2236.36
D-SH 3	18.11.07	-3.9	76	0.30	62.18	0.05	3.06	0.45	8.45	78.80	0.22	2370.92
D-SH 4	23.11.07	-4	74	1.33	53.12	0.07	3.11	0.91	33.41	180.04	1.23	2311.20
D-SH 5	25.11.07	-2.5	45	1.77	68.80	0.11	4.71	1.47	27.75	183.44	1.58	2171.08
D-SH 6	27.11.07	-3.6	65	0.45	49.83	0.08	0.98	0.32	12.51	130.84	0.53	2394.29

Sample	Date	T_{brine}	S_{brine}	$[PO_4^{2-}]_{35}$	$[Si]_{35}$	$[NO_2]_{35}$	$[NO_2]+[NO_3^-]_{35}$	$[SNH_4]_{35}$	DON_{35}	DOC_{35}	Ikaite	TA_{35}
D-SH	03.12.07	-2.6	46	0.47	55.53	0.03	0.20	0.77	27.59	195.34	N/A	2215.04
7												
S1	11.09.07	-5.1	88	1.75	36.37	0.14	28.48	N/A	2.40	41.52	0.34	N/A
S2	12.09.07	-12.4	179	0.92	52.21	0.36	32.07	N/A	2.35	68.24	9.69	N/A
S3	14.09.11	-8.3	138	1.17	40.07	0.25	28.15	N/A	4.06	49.46	N/A	N/A
S5	18.09.11	-9.3	153	0.64	45.91	0.18	28.18	N/A	1.59	55.68	5.89	N/A
S6	21.09.07	-7.8	132	1.57	45.52	0.25	28.64	N/A	0.98	67.31	1.47	N/A
S7	22.09.07	N/A	N/A	N/A	N/A	N/A	N/A	N/A	N/A	N/A	0.28	N/A
S8	25.09.07	-3.9	73	1.93	52.25	0.13	29.93	N/A	3.55	61.38	0.49	N/A
S9	28.09.07	N/A	N/A	N/A	N/A	N/A	N/A	N/A	N/A	N/A	0.87	N/A
S10	30.09.07	-5.0	97	2.78	55.56	0.16	33.89	N/A	3.89	43.33	0.7	N/A
S11	03.10.07	-5.1	98	0.07	54.95	0.04	3.15	N/A	4.90	73.15	N/A	N/A
S13	06.10.07	-3.7	78	1.44	42.63	0.10	23.78	N/A	4.94	73.14	N/A	N/A
S14	07.10.07	-5.2	78	0.27	46.92	0.13	10.00	N/A	5.00	67.31	1.71	N/A

2.4 Discussion

These results together with previous observations (Dieckmann et al., 2008) indicate, that calcium carbonate precipitation is widespread in Antarctic sea ice, albeit highly spatial heterogeneous, as is the case for many other biogeochemical parameters in sea ice (Thomas and Dieckmann, 2010). Although we were not able to verify the $CaCO_3$ polymorph for each sample collected, the visual characterisation by light microscopy confirmed that the morphology of all crystals was identical to those analyzed by X-ray diffraction. We are therefore convinced that ikaite was always the precipitate. Higher brine salinities in the uppermost layers, resulting from lower temperatures at the sea ice surface, and correspondingly high Ω_{ikaite} (ikaite saturation state of seawater) values, resulted in a more likely precipitation of ikaite near the ice surface than in lower parts in sea ice where temperatures are higher and brine salinity can drop to seawater values. However, it is still not clear at what point in time ikaite precipitation occurs, and our interpretation is confounded because the various biogeochemical parameters measured during sample collection do not reflect conditions at the time of precipitation. For example the question arises why a TA decrease by 400 μmol did not result in a correlation with the precipitation of ikaite. As discussed above, the measurements reflect only a small time frame in the seasonal carbon cycle within sea ice and not necessarily the conditions at time of precipitation. Observations of higher values of ikaite in older land fast ice (Fig. 2.8) also raise the question of whether or not precipitation can take place during subsequent sea ice growth, or if ikaite, after it has formed in young sea ice remains stable under various conditions until the sea ice melts thereby not altering TA or the carbonate system itself.

Based on a thermo-molecular pressure gradient as described by Wettlaufer and Worster (1995), brine, as unfrozen liquid, can be transported from the ice interior toward the relatively colder surface (Rankin and Wolff, 2002). The accumulated brine at the surface has a salinity of about 100 (Perovich and

Richter-Menge, 1994) and favours the precipitation of salts. Under those conditions frost flowers may start to grow (Perovich and Richter-Menge, 1994; Rankin and Wolff, 2002) and in turn can initiate $CaCO_3$ precipitation. However, conditions not necessarily leading to frost flower formation, may also lead to $CaCO_3$ precipitation if the temperature is low and salinity is high. The occurrence of calcium carbonate in the snow cover can most likely also be explained by the thermo-molecular pressure gradient and capillary transport. Brine is transported due to these processes into the snow where subsequently the precipitation of ikaite occurs. This is supported by the maximum concentrations of ikaite at the snow ice interface (Fig. 2.9). It is plausible that ikaite was there before snow accumulation, but this would not explain the different values in different snow layers.

Higher values of calcium carbonate in some middle layers of sea ice (S3 in Fig. 2.5) were attributable to rafting of floes subsequent to sea ice formation (see Meiners et al. 2011). Pack ice may be subject to deformation and floes may raft over each other resulting in the translocation of surface layers into interior layers of the newly established ice floe. It is not possible to determine the temporal development of $CaCO_3$ in the sea ice investigated during the DDU campaign. This is due to the large variability in $CaCO_3$ concentrations even on small spatial scales. The reason for this heterogeneity might be due to the inherent variability in many sea ice properties ranging from temperature, salinity, texture, chemistry and lastly as well as biological activity. The spatial heterogeneity is already apparent on small scales as shown by the spatial study during the DDU campaign. Thus, it is difficult to draw conclusions on the temporal evolution of the precipitation of ikaite. Although $CaCO_3$ concentrations were in the same order of magnitude in pack ice and land fast ice there appear to be differences in the amount of precipitated calcium carbonate indicating a potential temporal evolution. The highest values were recorded in approximately one-year-old land fast sea ice, followed by high amounts in land fast ice and the lowest concentrations in pack ice. The processes respon-

sible for the observed differences in ikaite concentrations in the different types of sea ice observed remain unclear. One explanation could be, that $CaCO_3$ is also precipitating during subsequent sea ice growth. Another reason could be, that sea ice is experiencing different growth conditions i.e. such as higher temperatures resulting in lower salinities and saturation states and thus lower values of ikaite.

The high concentrations of DOC and DON found in fast ice off Terre Adélie were expected to inhibit $CaCO_3$ precipitation (Bischoff et al., 1993). Zullig and Morse (1988) and Berner et al. (1978) have shown that DOM influences the precipitation of some polymorphs of calcium carbonate. However, these studies refer only to the inhibition for anhydrous polymorphs of $CaCO_3$. Besides the repression by polyphosphate and magnesium ions on the precipitation of anhydrous calcium carbonate in favour of hydrated forms, Dickens and Brown (1970) postulate that hydrated salts may play an important part in biological mineralization. Taking this into account, additionally to the elevated Ω_{ikaite}, microbial biomass, such as cell surfaces and/or extracellular polymeric substances, could catalyse the precipitation of calcium carbonate (Kandianis et al., 2008). This also coincides with findings of elevated abundance of bacteria and exopolymers in frost flowers (Bowman and Deming, 2010) and the top layer of experimentally formed sea ice (Aslam et al., 2012), which supports the hypothesis of $CaCO_3$ precipitation during frost flower and initial sea ice formation as discussed above.

The reasons why we did not find $CaCO_3$ in the sediment trap are not clear and the absence can at this stage only be attributed to several factors, which cannot be verified. These include the dissolution of crystals during ice melt, which means crystals do not leave the sea ice as temperatures increase (Rysgaard et al., 2012). The dissolution occurred in the sediment trap itself before the trap was retrieved, but this would mean that crystals, which dropped out of the ice a day before retrieval would also have dissolved.

Previous studies have pointed out the importance of sea ice for the carbon

uptake in polar oceans due to i.e. $CaCO_3$ precipitation (Tison et al., 2002; Delille, 2006; Nedashkovsky et al., 2009; Rysgaard et al., 2009, 2011). An estimation of the contribution of calcium carbonate precipitation to the polar carbon cycle would be useful. However, the large heterogeneity observed in the distribution of ikaite will make such an estimate highly uncertain. Yet, based on our observations we propose a first estimate of the possible contribution of calcium carbonate precipitation to the carbon cycle. For simplicity we take into account only the top 10 cm of sea ice, since the amount in the lower part was negligible. Absolute values of ikaite found in the top 10 cm of sea ice ranged between 0.1 and 6.5 g m^{-2}. Based on the total seasonal ice cover in the Antarctic (Comiso, 2010) we calculate that $CaCO_3$ formation in sea ice potentially could represent a contribution of between 0.1 and 6 Tg C to the carbon flux in the Southern Ocean. Assuming the same distribution in Arctic sea ice together with the ice cover from (Comiso and Nishio, 2008) then the precipitation of $CaCO_3$ would be responsible for a flux between 0.04 and 3 Tg C. For both the Arctic and Antarctic this would be between 0.1% and 4.5% of the air-sea CO_2 flux in open oceanic water at high latitudes (Takahashi et al., 2009; Rysgaard et al., 2011) or up to 13% for the Southern Ocean south of 50° (Takahashi et al., 2009). Though there is a large amount of ikaite in the snow, the amount of $CaCO_3$ therein was not taken into account for the calculation, since the distribution of $CaCO_3$ crystals in the snow remains elusive. However, of widespread this would be a significant addition to the polar carbon flux.
In addition, considering polynyas with new sea ice forming during the winter and assuming, that $CaCO_3$ precipitation mainly occurs during young sea ice and frost flower formation, this phenomenon might then contribute even to a larger extent to the air-sea flux. However, this would only be the case if CO_2, which is released during $CaCO_3$ precipitation, is rejected to the underlying water column. Yet, polynyas are still poorly understood with respect to gas fluxes (Else et al., 2011). Therefore it is essential to determine and quantify the CO_2 pathways during sea ice formation to fully quantify the contribution

of calcium carbonate precipitation to the air-sea CO_2 flux. The fact that ikaite is mainly formed at the surface of sea ice add support to the work of Sander et al. (2006) and Sander and Morin (2010) which describes the contribution of $CaCO_3$ precipitation to ozone depletion events. It also supports the work of Sala et al. (2008), since ikaite crystals at the snow-ice interface and in the snow are more likely exposed to aeolian transport and could therefore serve as sea ice proxy.

2.5 Conclusion

This study is providing an investigation of the spatial and temporal distribution of $CaCO_3$ in sea ice. We showed the heterogeneous occurrence of $CaCO_3$ in sea ice. Large scale quantification of $CaCO_3$ precipitation in different types of sea ice and during the entire season in both the Arctic and Antarctic is necessary to validate these findings and to provide a quality data set to estimate its contribution to the polar carbon cycle. Since parameters measured during sample collection do not reflect conditions at the time of precipitation, much work is needed to evaluate the conditions of calcium carbonate precipitation within sea ice and its fate during sea ice melt.

Acknowledgements. We thank the EPONTA (EPONTic micro-algae adapted to sea-ice) program for funding and Institut Polaire Francais, Paul-Émile Victor (IPEV) for the logistic assistance during the DDU campaign. We thank Harald Zöller, Thomas Spangenberg, Michael Wünsch, and Karlheinz Cerff (all at Forschungszentrum Karslruhe) for technical and computing support before and during the measurements, as well as Christiane Uhlig for preparing the samples for mineralogy and synthetic ikaite. We also thank Frank Gérard, all the scientists, and technicians from the French research station Dumont d'Urville, Antarctica as well as the captain and crew of the polar vessel Astrolabe and the pilots of the Australian Antarctic Division for all their

help and support. Andreas Krell, Louiza Norman, and Klaus Meiners are particularly grateful to the support of the SIPEX team and crew of Aurora Australis, especially the expedition leader Tony Worby. David Thomas and Louiza Norman thank NERC (UK) and the Leverhulme Trust for funding. We thank the DFG for financial support through grant NE 1564/2-1 (SPP1158). This project was supported by the Australian Government Cooperative Research Centre Program through the Antarctic Climate and Ecosystems Cooperative Research Centre (ACE CRC) and through Australian Antarctic Science grant #2767.

2.6 Supplemental material

Table 2.3: Ikaite values in ice cores from sea ice in East Antarctica (SIPEX Cruise, September-October 2007) and land fast ice off Terre Adélie (DDU, November-December 2007).

Sample	Cruise	Date	Depth (cm)	Ikaite (mg l^{-1})
S1	SIPEX	11.09.07	0-11	0.13
S1	SIPEX	11.09.07	11-21	0.16
S1	SIPEX	11.09.07	21-31	0.07
S1	SIPEX	11.09.07	31-41	0.22
S1	SIPEX	11.09.07	41-51	N/A
S2	SIPEX	12.09.07	0-10	9.49
S2	SIPEX	12.09.07	10-20	0.09
S2	SIPEX	12.09.07	20-30	0.11
S2	SIPEX	12.09.07	30-40	0.28
S3	SIPEX	14.09.07	0-10	N/A
S3	SIPEX	14.09.07	10-20	0.3
S3	SIPEX	14.09.07	20-30	0.14

Sample	Cruise	Date	Depth (cm)	Ikaite (mg l^{-1})
S3	SIPEX	14.09.07	30-40	2.08
S4	SIPEX	14.09.07	0-10	0.04
S4	SIPEX	14.09.07	10-19	0.12
S4	SIPEX	14.09.07	19-29	0.22
S4	SIPEX	14.09.07	29-37	0.15
S4	SIPEX	14.09.07	37-47	0.12
S4	SIPEX	14.09.07	47-55	0.11
S5	SIPEX	18.09.07	0-10	1.05
S5	SIPEX	18.09.07	10-20	0.76
S5	SIPEX	18.09.07	20-30	4.08
S5	SIPEX	18.09.07	30-40	0.31
S5	SIPEX	18.09.07	40-50	0.11
S5	SIPEX	18.09.07	50-60	0.25
S5	SIPEX	18.09.07	60-70	N/A
S5	SIPEX	18.09.07	70-80	0.26
S6	SIPEX	21.09.07	0-10	0.59
S6	SIPEX	21.09.07	10-20	0.04
S6	SIPEX	21.09.07	20-30	0.84
S6	SIPEX	21.09.07	30-40	0.26
S6	SIPEX	21.09.07	40-50	0.02
S6	SIPEX	21.09.07	50-60	0.09
S6	SIPEX	21.09.07	60-70	0.02
S6	SIPEX	21.09.07	70-81	0.05
S7	SIPEX	22.09.07	0-10	0.17
S7	SIPEX	22.09.07	10-20	0.03
S7	SIPEX	22.09.07	20-30	0.08
S7	SIPEX	22.09.07	30-40	0.03

Sample	Cruise	Date	Depth (cm)	Ikaite (mg l^{-1})
S7	SIPEX	22.09.07	40-50	0.11
S8	SIPEX	25.09.07	0-10	0.29
S8	SIPEX	25.09.07	10-20	0.09
S8	SIPEX	25.09.07	20-30	0.11
S8	SIPEX	25.09.07	30-37	0.08
S9	SIPEX	28.09.07	0-10	0.79
S9	SIPEX	28.09.07	10-20	0.04
S9	SIPEX	28.09.07	20-30	0.04
S9	SIPEX	28.09.07	30-40	0.1
S9	SIPEX	28.09.07	40-50	0.05
S9	SIPEX	28.09.07	50-60	0.07
S9	SIPEX	28.09.07	60-70	0.07
S9	SIPEX	28.09.07	70-80	0.05
S9	SIPEX	28.09.07	80-90	N/A
S9	SIPEX	28.09.07	90-98	N/A
S10	SIPEX	30.09.07	0-10	0.55
S10	SIPEX	30.09.07	10-20	0.1
S10	SIPEX	30.09.07	20-30	0.05
S10	SIPEX	30.09.07	30-40	0.09
S10	SIPEX	30.09.07	40-50	0.03
S10	SIPEX	30.09.07	50-60	0.04
S11	SIPEX	03.10.07	0-10	N/A
S11	SIPEX	03.10.07	10-20	N/A
S11	SIPEX	03.10.07	20-30	0.05
S11	SIPEX	03.10.07	30-40	0.04
S11	SIPEX	03.10.07	40-50	0.05
S11	SIPEX	03.10.07	50-60	0.05

Sample	Cruise	Date	Depth (cm)	Ikaite (mg l^{-1})
S12	SIPEX	05.10.07	0-10	N/A
S12	SIPEX	05.10.07	10-20	N/A
S12	SIPEX	05.10.07	20-30	0.06
S12	SIPEX	05.10.07	30-40	0.08
S12	SIPEX	05.10.07	40-50	0.03
S12	SIPEX	05.10.07	50-60	0.06
S12	SIPEX	05.10.07	60-70	0.03
S12	SIPEX	05.10.07	70-80	0.1
S12	SIPEX	05.10.07	80-90	0.07
S12	SIPEX	05.10.07	90-100	0.05
S12	SIPEX	05.10.07	100-109	0.1
S13	SIPEX	06.10.07	0-10	N/A
S13	SIPEX	06.10.07	10-20	N/A
S13	SIPEX	06.10.07	20-30	0.06
S13	SIPEX	06.10.07	30-40	0.06
S13	SIPEX	06.10.07	40-50	0.04
S13	SIPEX	06.10.07	50-60	0.06
S13	SIPEX	06.10.07	60-70	0.17
S14	SIPEX	07.10.07	0-10	1.56
S14	SIPEX	07.10.07	10-20	0.09
S14	SIPEX	07.10.07	20-30	0.06
S14	SIPEX	07.10.07	30-40	0.05
S14	SIPEX	07.10.07	40-50	0.41
S14	SIPEX	07.10.07	50-60	0.02
D1	DDU	14.11.07	0-10	0.06
D1	DDU	14.11.07	10-20	0.03
D1	DDU	14.11.07	20-30	0.02

Sample	Cruise	Date	Depth (cm)	Ikaite (mg l^{-1})
D1	DDU	14.11.07	30-40	0.02
D1	DDU	14.11.07	40-50	0.06
D1	DDU	14.11.07	50-60	0.03
D1	DDU	14.11.07	60-65	0.08
D2	DDU	17.11.07	0-10	0.25
D2	DDU	17.11.07	10-20	0.12
D2	DDU	17.11.07	20-30	0.04
D2	DDU	17.11.07	30-40	0.04
D2	DDU	17.11.07	40-50	0.07
D2	DDU	17.11.07	50-60	0.28
D2	DDU	17.11.07	60-65	0.5
D3	DDU	23.11.07	0-10	3.11
D3	DDU	23.11.07	10-20	0.03
D3	DDU	23.11.07	20-30	0.18
D3	DDU	23.11.07	30-40	0.01
D3	DDU	23.11.07	40-50	0.1
D3	DDU	23.11.07	50-60	0.05
D4	DDU	24.11.07	0-10	2.45
D4	DDU	24.11.07	10-20	0.23
D4	DDU	24.11.07	20-30	0.04
D4	DDU	24.11.07	30-40	0.04
D4	DDU	24.11.07	40-50	0.04
D4	DDU	24.11.07	50-60	0.09
D5	DDU	27.11.07	0-10	5.01
D5	DDU	27.11.07	10-20	0.26
D5	DDU	27.11.07	20-30	0.21
D5	DDU	27.11.07	30-40	0.03

Sample	Cruise	Date	Depth (cm)	Ikaite (mg l^{-1})
D5	DDU	27.11.07	40-50	0.1
D5	DDU	27.11.07	50-60	0.05
D6	DDU	03.12.07	0-10	3.54
D6	DDU	03.12.07	10-20	3.66
D6	DDU	03.12.07	20-30	0.03
D6	DDU	03.12.07	30-40	0.4
D6	DDU	03.12.07	40-50	0.11
D7	DDU	23.11.07	0-2	22.15
D7	DDU	23.11.07	2-4	85.49
D7	DDU	23.11.07	4-6	1.22
D7	DDU	23.11.07	6-8	2.47
D7	DDU	23.11.07	8-10	0.72
D8	DDU	24.11.07	0-2 / snow	16.09
D8	DDU	24.11.07	2-4 / snow	11.1
D8	DDU	24.11.07	4-6 / snow	10.14
D8	DDU	24.11.07	6-8	38.77
D8	DDU	24.11.07	8-10	9.21
D8	DDU	24.11.07	10-12	0.53
D8	DDU	24.11.07	12-14	1.79
D8	DDU	24.11.07	14-16	0.63
D9	DDU	24.11.07	0-2	103.82
D9	DDU	24.11.07	2-4	5.76
D9	DDU	24.11.07	4-6	3.76
D9	DDU	24.11.07	6-8	1.51
D9	DDU	24.11.07	8-10	0.52
D9	DDU	24.11.07	10-12	0.21
D9	DDU	24.11.07	12-14	1.06

Sample	Cruise	Date	Depth (cm)	Ikaite (mg l^{-1})
D10	DDU	05.12.07	0-2	104.47
D10	DDU	05.12.07	2-4	76.60
D10	DDU	05.12.07	4-6	73.87
D10	DDU	05.12.07	6-8	125.56
D10	DDU	05.12.07	8-10	55.31
D10	DDU	05.12.07	10-12	4.41
D10	DDU	05.12.07	12-14	41.08
D10	DDU	05.12.07	14-16	8.95

Chapter 3

Longterm chamber measurements of CO_2 fluxes on subarctic sea ice

Fischer, M.[1], Tison, J.-L.[2], Dieckmann, G.S.[1], Rysgaard, S.[3,4,5], and Delille, B.[6], Long-term chamber measurements of CO_2 fluxes on Subarctic sea ice, Manuscript draft

[1]Alfred Wegener Institute for Polar and Marine Reserach, Bremerhaven, Germany

[2]Glaciology Unit, Department of Earth and Environmental Science, Université Libre de Bruxelles, Belgium

[3]Greenland Climate Research Centre, Greenland Institute of Natural Resources, Nuuk, Greenland

[4]Centre for Earth Observation Science, CHR Faculty of Environment Earth and Resources, University of Manitoba, Winnipeg, Canada

[5]Arctic Research Centre, Aarhus University, Aarhus, Denmark

[6]Unité d'Oceanographie Chimique, Astrophysics, Geophysics and Oceanography department, University of Liège, Belgium

Abstract. The exchange of CO_2 between Subarctic sea ice, with and without snow cover, and the atmosphere was examined from 10 March to 16 March 2010 in Kapisigdlit, Kangerdluat, Southwest Greenland using for the first time long-term diurnal chamber measurements. Fluxes ranged between -2.2 and 9.5 mmol m^{-2} d^{-1} (where negative values indicate a sink for atmospheric CO_2). Within 24 hours fluxes can shift from an efflux to an uptake. This shows that fluxes are highly variable on a diurnal cycle and continuous (24 h) measurements over sea ice are essential. However, a diurnal pattern of the CO_2 fluxes could not be observed. Measurements over snow-covered sea ice showed reduced fluxes compared to bare sea ice. This suggest that snow significantly influences the CO_2 exchange between sea ice and atmosphere.

3.1 Introduction

The oceans cover 70% of the surface of the earth. They store more than 60 times the amount of CO_2 compared to the atmosphere. The recent net global ocean CO_2 uptake is 1.5-2.0 Pg C y^{-1}, which corresponds to about 25% of the industrial emissions (Takahashi et al., 2009) and shows the important role of the ocean in the global carbon cycle. The atmospheric concentration of CO_2 at Mauna Loa increased from about 315 ppm in 1958 to 394 ppm at its maximum in 2011 (Thoning et al., 2012). At remote observatories in Alert, Nunavut, Canada and in Barrow, USA in the Arctic, maximum values in 2012 exceeded for the first time the threshold of 400 ppm (according to NOAA measurements). Takahashi et al. (2009) shows that the high-latitude oceans in the northern and southern hemisphere are major sinks for CO_2 and sea ice, especially in the Arctic, is a crucial part of it (Halloran, 2012).

The role of ice-covered oceans in the global CO_2 balance shifted into the focus of recent research (Papadimitriou et al., 2004; Delille, 2006; Rysgaard et al., 2007, 2009, 2011; Miller et al., 2011b,a; Papakyriakou and Miller, 2011; Fischer et al., 2013; Geilfus et al., 2012b). For a long time sea ice was thought

to impede gas exchange between ocean and atmosphere and to act as a barrier (Gibson and Trull, 1999) though Miyake and Matsuo (1963); Gosink et al. (1976) and Kelley and Gosink (1979) already considered sea ice as permeable for gases. However, recent studies show, that fluxes of gases such as CO_2 between atmosphere and ice are evident (Tison et al., 2002; Nomura et al., 2006; Loose et al., 2009, 2011b).

There are two main methods assessing the CO_2 flux between sea ice and atmosphere, the eddy covariance (EC) and the chamber method. An overview off the conducted measurements with different methods in the Polar Oceans and relating fluxes is provided in Table 3.1. For measuring turbulent fluxes the eddy covariance technique is applied (Semiletov et al., 2004, 2007; Zemmelink et al., 2006; Papakyriakou and Miller, 2011). While there is debate wether open or closed path eddy covariance is the most suitable method for flux measurements between sea ice and atmosphere, EC has proven to be applicable over flat and homogeneous surfaces under stable atmospheric conditions. Eddy covariance measurements provide data on a large scale resolution. However, data processing needs a suite of corrections and the spatial resolution of the eddy covariance technique is not high enough over extremely variable surface such as ridges and pack ice (Loose et al., 2011a). In contrast chamber measurements are able to resolve a high spatial variability. They are easy to deploy and inexpensive. The chamber method was applied in the Arctic (Semiletov et al., 2004; Nomura et al., 2010a,b; Geilfus, 2011; Geilfus et al., 2012b) and Antarctic (Delille, 2006; Delille et al., 2007). All chamber measurements were done by using permanently closed chambers. Thus, besides anomalous chamber heating, Oechel et al. (1998) ascribes the chamber method a potential bias from pressure gradients. Hence, a system is needed which tracks the ambient atmospheric pressure during the measurement. Flux measurement with chambers is a novel method which has been applied for only one decade on sea ice. Pioneers in the Arctic (Semiletov et al., 2004) and Antarctic (Delille, 2006) provided valuable insights in the processes of CO_2 fluxes between ice and

Table 3.1: Overview of flux measurements on sea ice, EC=Eddy covariance, negative values = influx, positive = efflux

Publication	Date	Location	Method	Type of sea ice	Range of CO_2 flux [mmol m^{-2} d^{-1}]
(Semiletov et al., 2004)	June 2002	Arctic, near Barrow, Alaska, Lapetv Sea and East Siberian Sea	EC closed path	fast ice	approx. -60 to 50
(Semiletov et al., 2004)	June 2002	Arctic, near Barrow, Alaska, Lapetv Sea and East Siberian Sea	Chamber	fast ice	-51.1 to -3.93
(Delille, 2006)	Oct. 2003 & Dec. 2004	Antarctic, Southern Ocean & Weddell Sea	Chamber	first and multi year pack ice	-5.2 to 1.9
(Nomura et al., 2006)	NA	Laboratory Experiment	Lab	artificial	0.4 to 1.0
(Zemmelink et al., 2006)	Dec. 2004	Antarctic, Weddel Sea	EC open path	pack ice	-18.18 to -4.55
(Semiletov et al., 2007) & (Repina et al., 2007)	September 2005	Arctic, Shelf and shelf slope of the Laptev Sea	EC open path	near edge of the multi-year sea ice	-1.2 to 1.7

Publication	Date	Location	Method	Type of sea ice	Range of CO_2 flux [mmol m^{-2} d^{-1}]
(Heinesch et al., 2010)	Jan. - June 2009	Arctic, Barrow, Alaska, USA	EC closed path	land-fast sea ice	up to 51.8
(Nomura et al., 2010b)	Feb. - March 2006 & 2008	Okhotsk Sea coast of Hokkaido, Japan	Chamber	fast ice	-3.6 to 1.0
(Nomura et al., 2010a)	May 2008	Arctic, Chukchi Sea, off Barrow, Alaska	Chamber	fast ice	-1 to 0.7
(Miller et al., 2011b)	Jan. - May 2004	Arctic, Franklin Bay, Canada	EC open path	fast ice	daily average -60.48 to 74.3
(Papakyriakou and Miller, 2011)	May - June 2002	Arctic, McDougall Sound, Canadian Archipelago	EC open path	fast ice	-259.2 to 86.4
(Sejr et al., 2011)	March 2008	Arctic, Young Sound, Greenland	closed Chamber	growing ice	1.1
(Geilfus, 2011)	April 2009	Arctic, Barrow, Alaska, USA	Chamber	young, rapidly forming sea ice	4.2 to 9.9
(Geilfus et al., 2012b)	April - June 2008	Arctic, Amundsen Gulf, Beaufort Sea, Canada	Chamber	Drift and land-fast sea ice	-2.63 to 0.84

atmosphere. While further studies (see Table 3.1) added important data from different types of sea ice, none of these supported diurnal long term measurements as provided by measurements with eddy covariance. Data were limited only to a few measurements during the experiments. Thus, a possible diurnal cycle could not be observed and interpretations of the measurements could be misleading when it comes to quantification of fluxes above sea ice.

Therefore, the objective of this study was to: (1) Provide the first continuous CO_2 measurements over day and night with the chamber technique while maintaining the ambient pressure inside the chamber, (2) to investigate a potential diurnal effect on the CO_2 fluxes between atmosphere and ice due to heat transfer and permeability of sea ice and (3) to look for possible effects of snow cover on the CO_2 fluxes between atmosphere and ice.

3.2 Methods

3.2.1 Study area and background measurements

The study was performed from 10 March to 16 March 2010 on land fast sea ice in Kapisigdlit Kangerdluat, Southwest Greenland at N 64°26' and W 50°13' (Fig. 3.1). The sea ice thickness was 65 cm throughout the experiment. Air temperature and wind speed were measured with a sonic anemometer (Sonic USA-1, METEK, Germany) every 30 minutes. The sonic anemometer was installed on a mast 3 meter above the ice surface.

3.2.2 Longterm flux measurements

CO_2 fluxes were measured using the LI-COR LI-8100 automated soil CO_2 flux system (LI-COR, Inc., Lincoln, NE, USA). Continuous measurements (day and night over 7 days) were carried out with LI-COR long term chambers 8100-104 (Fig. 3.2) equipped with a pressure vent to minimize pressure pulses at chamber closing and to allow chamber pressure to track the ambient pressure

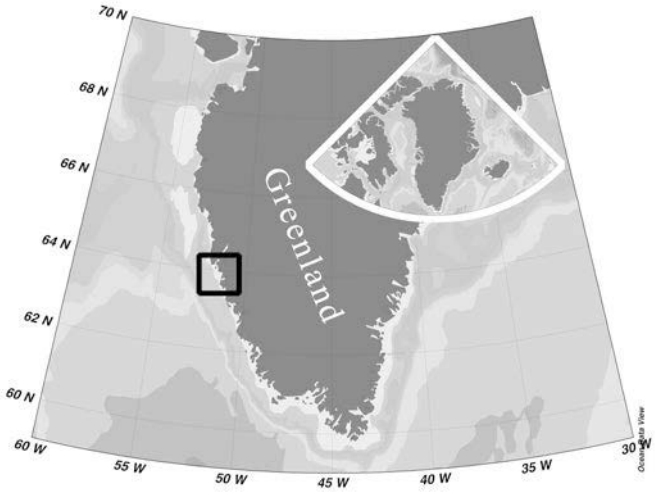

Figure 3.1: Location of sampling site during the Study in Kapisigdlit, Kangerdluat, Greenland

under calm and windy conditions (Xu et al., 2006). The air in the chamber was circulated with a pump within the LI-COR Multiplexer (LI-8150) at a flow rate of 2.1 L min^{-1}. Electricity was provided by a special 12V car battery. The non-dispersive infrared analyzer (LI-840) within the LI-8100 was calibrated by LI-COR Biosciences, Lincoln, Nebraska USA prior the experiment. The calibration error of the analyzer was -0.013 % $°C^{-1}$ at 370 ppm. The CO_2 zero drift was 0.022 ppm $°C^{-1}$ at 0 ppm.

At the beginning of the experiment one chamber (chamber 1) was put on the sea ice. A specially made metal toothed collar (height = 11 cm, diameter = 20 cm) was cut permanently 2-3 cm into the ice surface after the snow cover was removed. The long term chamber was carefully placed on the collar and subsequently the setup was checked carefully for leaks. Continuous measurements started 12 hours after installation. The CO_2 flux was measured for 140 hours twice every hour automatically by programming the LI-8100. Measurements were interrupted on two occasions due to bad weather conditions for a few hours only. During each measurement the chamber was closed for 8 min-

utes. In between the chamber was open for re-equilibration with the ambient air. During each measurement before the chamber was closed, the air inside the chamber tubings and the analyzer was purged to allow air in the LI-8100 to return to ambient conditions. After the chamber was closed a dead band of 30 seconds was applied to establish steady chamber mixing. The rate at which CO_2 diffuses into the air from the ice or snow interface or vice versa was determined by measuring the rate of increase/decrease of CO_2 within the chamber over a designated time interval. The slope of the increase or decrease was tested for statistical significance.

In order to determine the effect of the snow cover on the CO_2 fluxes between sea ice and atmosphere two additional chambers where installed on the ice. Chamber 2 was installed on the ice without removing the initial snow cover for the same time period as chamber 1. A third chamber was installed prior a heavy snow event. The site for Chamber 3 was also cleared from the initial snow cover before the precipitation event between 14 and 15 March. During the snow event we observed the snow cover on a regular basis by measuring the snow thickness in chamber 2 and 3 while chamber 1 was always cleared from the snow. This resulted in three categories of surface properties: (1) sea ice without snow cover; (2) sea ice with initial thin snow cover and fresh snow on top; and (3) sea ice with fresh snow on top.

3.2.3 Sea ice sampling

Sea ice temperatures were measured using a thermistor chain. The temperature probes were installed every 2 cm. Every two days four complete ice cores were obtained for bulk salinity and temperature measurements in the morning and in the afternoon. Ice cores for vertical temperature profiles were placed on a clean plastic foil and a digital thermometer probe (Testo 720, Germany) was inserted in predrilled holes at 4 cm vertical intervals in the ice. The second core was cut into sections of 4 cm and stored in plastic containers and brought

Figure 3.2: Longterm chamber 8100-104 on Subarctic sea ice, March 2010, Kapisigdlit, Kangerdluat, Greenland

to the laboratory on the ship (KISAQ). Samples were melted and bulk salinity was determined (Horner et al., 1992).

3.3 Results

3.3.1 Background measurements

During the 7 day experiment air temperatures ranged between -10.7 and 3.4°C, which included a warming phase at the beginning with daytime temperatures above +2°C, followed by a relative stable colder phase with an average temperature of -3°C. Finally from 15 to 16 March, temperatures dropped to almost -11 °C. The average wind speed was 2.77 m s^{-1} with a maximum on 10 March of 8 m s^{-1}. High wind speeds up to 6.7 m s^{-1} were also measured on 15 March. (Fig. 3.3). Ice temperatures ranged between -4.3 and -0.7°C and show a typical

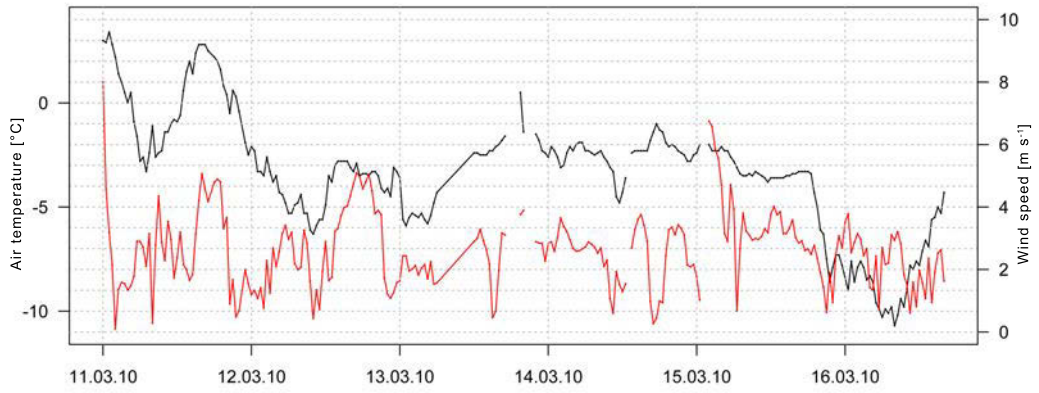

Figure 3.3: Air temperatures (black) and wind speed (red) from 10 March to 16 March 2010, Kapisigdlit, Kangerdluat, Greenland

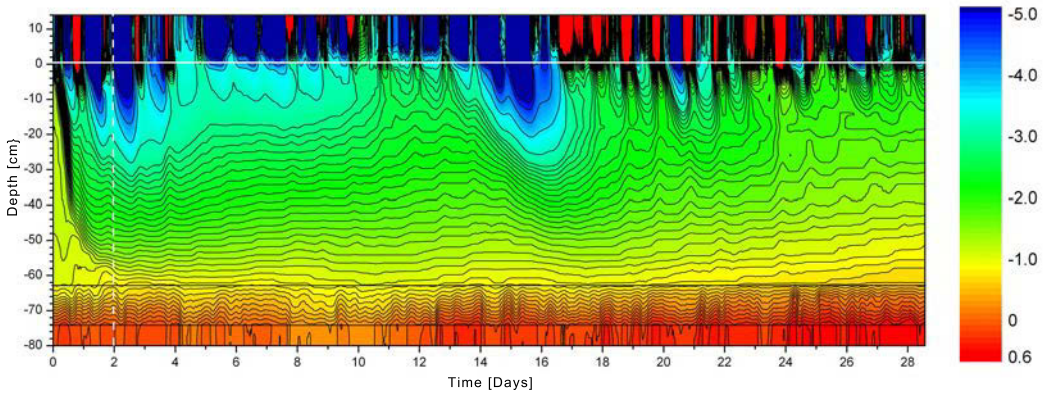

Figure 3.4: Sea ice temperatures [°C] from 10 March (Day 0) to 8 April 2010, Kapisigdlit, Kangerdluat, Greenland (Glud et al., unpublished data)

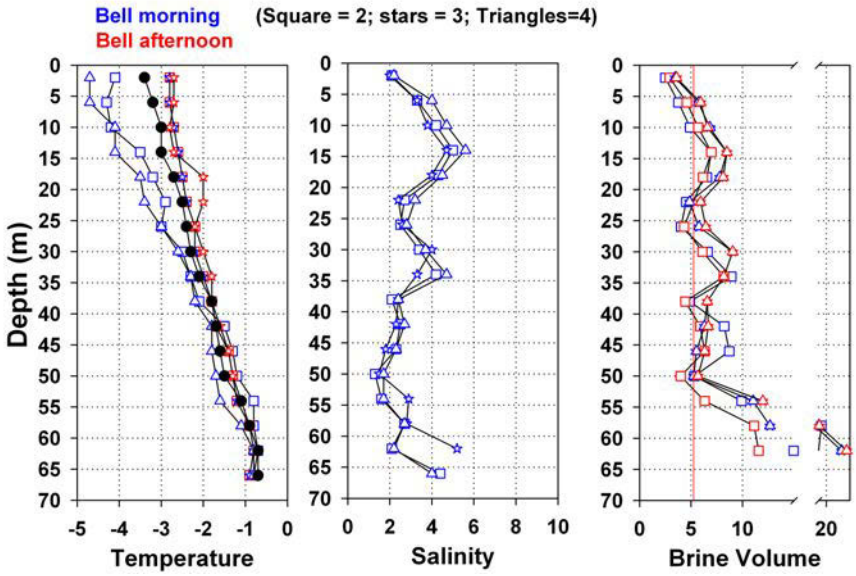

Figure 3.5: Sea ice temperature, bulk salinity and brine volume, calculated after Cox and Weeks (1986) and Leppäranta and Manninen (1988), March 2010, Kapisigdlit, Kangerdluat, Greenland

increase from the surface to the bottom of the ice (Fig. 3.4). Bulk salinity was low between 1.3 and 8.8. The bulk salinity profile was rather atypical. With low values at the top, indicating melting sea ice, bulk salinity increased in the underlying layer. However, a remarkable decrease of bulk salinity between 20 and 30 cm was observed. Brine volume followed bulk salinity but remained below the threshold permeability of liquids (Golden et al., 1998). Brine volume in sea ice layers between 10 and 20 cm and below 30 cm was always above 5% (Fig. 3.5). At the beginning of the study, a thin snow cover of 3 cm was present, which can be described as hard icy snow. Snow thickness increased by a few centimeters after a precipitation event between 14 and 15 March.

3.3.2 CO_2 fluxes above bare sea ice

Sea ice was always permeable for gases. Fluxes ranged between -1.5 and 9.5 mmol m^{-2} d^{-1}, where positive numbers refer to an efflux from the ice to

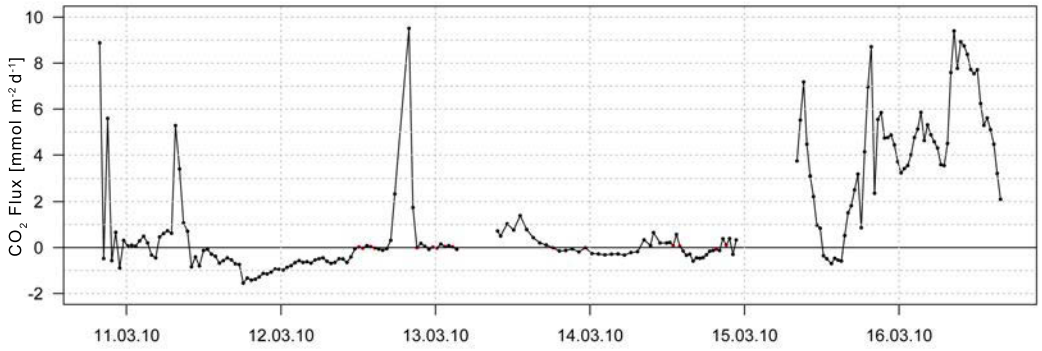

Figure 3.6: Flux of CO_2 between sea ice without any snow cover and the atmosphere in March 2010, Kapisigdlit, Kangerdluat, Greenland, red points indicate that the slope for this flux was not significant, positive numbers refer to a degassing of sea ice and negative numbers to an influx

the atmosphere and negative numbers show an influx (Fig. 3.6). Large efflux were observed at the beginning of the experiment, which inverted to an influx with an average of about 1 mmol m^{-2} d^{-1}. This was followed by a period of low fluxes, which were interrupted by a sudden degassing event at the end of 12 March. On 15 and 16 March fluxes increased again and remained high until the end of the experiment. A diurnal variation of the CO_2 fluxes could not be observed.

3.3.3 CO_2 fluxes above snow covered sea ice

Fluxes above snow covered sea ice ranged between -2.2 and 7.3 mmol m^{-2} d^{-1}. Snow thickness increased in chamber 2 after an event of snow precipitation, resulting in an additional layer of powder snow of 5 cm on top of the 3 cm thick layer of icy snow. Fluxes above snow covered snow ice were a bit lower than above sea ice without snow cover. However, fluxes showed the same pattern in time. Also the sudden degassing event on 12 March occurred but was not as pronounced as above bare sea ice.

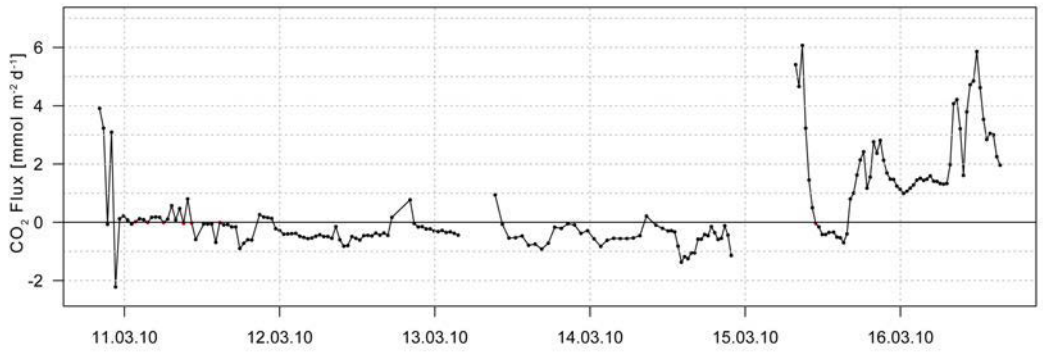

Figure 3.7: Flux of CO_2 between sea ice with initial thin snow cover and the atmosphere in March 2010, Kapisigdlit, Kangerdluat, Greenland, red points indicate that the slope for this flux was not significant, positive numbers refer to a degassing and negative numbers to an influx

Measurements after the event of snow precipitation above sea ice without snow cover, sea ice with initial icy snow cover plus fresh snow, and sea ice with fresh powder snow showed the same patterns for the CO_2 fluxes between sea ice and atmosphere. After initially high effluxes, values dropped to zero and partly negative fluxes during midday. Subsequently, fluxes increased again and stabilized during nighttime. During the morning, fluxes increased even more but decreased slowly towards the afternoon. Although the patterns were similar for ice with and without snow cover, the magnitude of the fluxes were different (Fig. 3.8). Highest fluxes were observed above sea ice without snow cover, followed by sea ice with a layer of fresh powder snow and lastly sea ice with different types of snow layers.

3.4 Disscussion

The flux of CO_2 between sea ice and atmosphere with different techniques such as eddy covariance (i.e. Zemmelink et al. (2006); Miller et al. (2011b)) and chamber (i.e. Semiletov et al. (2004); Delille (2006)) measurements have been

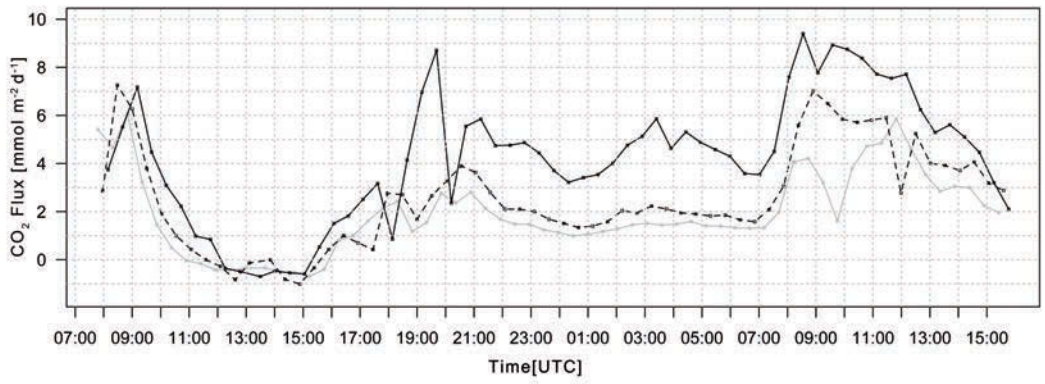

Figure 3.8: Flux of CO_2 between sea ice and atmosphere from 15 to 16 March 2010, Kapisigdlit, Kangerdluat, Greenland on different surfaces, black line = sea ice without snow cover, black dashed line = sea ice with fresh snow layer of 5 cm, grey line = sea ice with initial snow cover (3cm) plus fresh snow (5cm) on top, positive numbers refer to a degassing and negative numbers to an influx

repeatedly reported. The observed fluxes with the chamber method during this study were of the same order of magnitude as reported by Delille (2006) and Nomura et al. (2010b). Influx were similar to values measured by Nomura et al. (2010a) while the efflux represent, as also reported by Geilfus (2011), the highest values measured with the chamber method.

3.4.1 Sea ice properties

The observed salinity profiles (Fig. 3.5) do not reflect typical sea ice profiles (Petrich and Eicken, 2010). The decrease of bulk salinity in the layer around 25 cm potentially indicates an influence of fresh water which is transported from the water shed of the fjord by river discharge. Thus the brine volume in this layer decreased, but was always around the threshold of permeability for liquids in sea ice (Golden et al., 1998). Just below the sea ice - atmospheric boundary layer the brine volume was always below 5% during the study. At a depth of 6 cm permeability oscillated around the threshold of permeability

with higher values of brine volume during the afternoon when sea ice had warmed up during the day. Hence, fluxes between ice and atmosphere were most likely during this time. However, with values around the threshold of permeability fluxes were expected to be small. Though, one of the highest fluxes above sea ice were reported during the experiment. This coincides with findings of Papakyriakou and Miller (2011) and Miller et al. (2011b) who also reported fluxes during cold periods with small brine volumes, which suggests that the threshold of brine volume for permeability of gases in sea ice is lower than the calculated values for fluids (Golden et al., 1998). On the other hand it might be possible that processes within sea ice alone are potential sources of gas transfer between sea ice and atmosphere (Miller et al., 2011b).

3.4.2 Continuous flux measurements above bare sea ice

The fluxes at the beginning of the study occurred since ice temperature and hence brine volume was high enough (Golden et al., 1998) to allow fluxes from the ice to the atmosphere. In addition ice temperatures were below the freezing point of sea water and thus brine pCO_2 is assumed to be supersaturated with respect to atmospheric CO_2 and potentially the driving force of the fluxes (Delille et al., 2007; Miller et al., 2011a; Geilfus, 2011). With decreasing temperatures starting from the end of 11 March, fluxes shifted from efflux to an uptake within 24 hours. A phenomenon which was also observed by Papakyriakou and Miller (2011) applying the eddy covariance method. The reason for this uptake is assumed to originate from the increased solubility of gases due to lower ice temperatures. The sudden degassing on 12 March corresponds to a decrease in temperature. This might result from degassing due to freezing processes (Nomura et al., 2006; Geilfus, 2011). The almost cutoff of the fluxes after this event agree well with ice temperatures dropping below $-5°C$. However, even at those low temperatures fluxes were observed. This is also in agreement with Gosink et al. (1976) who show that gas fluxes through sea ice

are possible even at −15°C. As reported by Papakyriakou and Miller (2011) and Miller et al. (2011b) wind and ice temperatures are most likely linked with fluxes of CO_2 which is also shown in this study with the highest fluxes at the beginning and at the end of the experiment when wind speed was also high.

The observed link of wind speed and fluxes with the chambers indicates, that the pressure vent of the chambers enables the following of events of high wind speed during the measurements and corroborates the findings obtained with the eddy covariance method (Papakyriakou and Miller, 2011). Providing the first continuous measurements of day and night with the chamber method, this study showed, that single measurements could result in an incorrect estimates of the CO_2 flux between sea ice and atmosphere. The observed values showed, that single measurements during the day as usually conducted when using the chamber method could miss events such as the sudden degassing which occur i.e. only over a period of a few hours on 12 March. Also the differences in fluxes over several measurements during a couple of hours on 15 March could not be resolved without the diurnal (24 h) measurements. In addition continuous measurements enabled observations of periods where sea ice does not significantly exchange gases with the atmosphere. Following from the observation above, the continuous measured fluxes during this study confirmed the whole range from low and high values as reported in different studies (Delille, 2006; Nomura et al., 2006; Delille et al., 2007; Nomura et al., 2010b,a; Geilfus, 2011). Thus, the use of of long-term measurements with the chamber method provides the opportunity of a more accurate estimation of the fluxes of CO_2 between sea ice and atmosphere. However, a budget calculating for sea ice could not be provided, since the length of the study was to short and Subarctic sea ice is not representative for the ice covered oceans.

Though a diurnal effect of CO_2 fluxes could not be observed during the study, it might be possible to observe these when meteorological and ice parameters such as wind speed and ice temperature experience significant changes which affects properties such as brine volume and turbulent mixing during the

course of a day.

3.4.3 Influence of snow on fluxes of CO_2

Fluxes above sea ice where initial snow cover was removed were the highest during the study. Whereas fluxes above snow covered sea ice were lower (Fig. 3.7), which indicates the importance of snow cover and supports the findings of Nomura et al. (2010b). Though snow is permeable for gas transport (Zimov et al., 1993; Sommerfeld et al., 1993) it obviously reduces the amount of CO_2 which is able to penetrate through the medium. Nomura et al. (2010b) showed that CO_2 fluxes decreases with increasing snow depth and reach almost zero already at snow depth smaller than 10 cm. During this study this could only be partially verified, when fluxes decreased with increasing snow depth (Fig. 3.8) but were still high. Therefore fluxes of CO_2 are most likely influenced by a range of variables such as snow depth, wind speed, sea ice temperature and accordingly brine volume. Figure 3.8 shows clearly the effect of different types of sea ice cover. With more than 75 words for snow in Iñupiaq, the Inuit language spoken in northern Alaska (Sturm and Massom, 2010), showing the heterogeneity of types of snow cover, leads to the expectation that these different types will influence the fluxes in different ways. This is important since snow cover in Arctic and Antarctic are significantly different (Thomas and Dieckmann, 2010) and potentially leads to different fluxes above sea ice in both hemispheres.

Welker et al. (2000) describes higher CO_2 effluxes from Arctic dry and moist tundra ecosystems, due to deeper snow depth. In contrast Schindlbacher et al. (2007) showed fluxes through snow which, decreased with increasing snow thickness. However, the latter two studies were conducted above soils which were above freezing temperatures. Sea ice with it's subzero temperatures and influence of salinity is a different system and might not be comparable to ecosystems studied in Zimov et al. (1993); Sommerfeld et al. (1993); Welker

et al. (2000) and Schindlbacher et al. (2007). Thus a more detailed investigation of the effect of snow on the fluxes of CO_2 between sea ice and atmosphere, i.e. seasonality, is needed.

3.5 Conclusion

We examined the flux of CO_2 between Subarctic sea ice with and without snow cover and the atmosphere using for the first time long-term chamber measurements. The fluxes ranged between -2.2 and 9.5 mmol m^{-2} d^{-1}. We showed, that the long-term chambers are able to track pressure changes in the atmosphere during the measurements. Furthermore we showed that fluxes can shift within 24 hours from an efflux to an uptake. Thus showing that fluxes are highly variable on a diurnal cycle and continuous measurements are essential. However, a diurnal effect on the CO_2 fluxes could not be observed. We confirmed the range of fluxes previously reported by several studies in one experiment. Fluxes are influenced by several factors, such as wind speed, ice temperature and subsequently brine volume. A more important influence is most likely the occurrence of snow on top of sea ice. However, a more detailed study of the exact impact of snow cover is needed to allow a reliable estimation of the seasonal fluxes of CO_2 in the ice covered oceans.

Acknowledgements. The study received financial support from the Danish Agency for Science, Technology and Innovation, the Canada Excellence Research Chair (CERC) program. The study is a part of the Greenland Climate Research Center's activities, GCRC6507 (www.natur.gl).

Chapter 4

Surface based flux measurements and the evolution of CO_2 in Arctic sea ice, melt ponds, seawater, and atmosphere during winter - spring - summer transition

Fischer, M.[1], Brown, K.[2], Papakyriakou, T.[3], Tison, J.L.[4], Delille, B.[5], Mundy, C.J.[3], Haas, C.[6], Kaleschke, L.[7], Miller, L.[2], and Wolf-Gladrow, D.A.[1]: Surface based flux measurements and the evolution of CO_2 in Arctic sea ice, meltponds, seawater, and atmosphere during winter-spring-summer transition, Manuscript draft

[1]Alfred Wegener Institute for Polar and Marine Reserach, Bremerhaven, Germany

[2]Institute of Ocean Sciences, Fisheries and Oceans Canada, Sidney, British Columbia, Canada

[3]Centre for Earth Observation Science, Department of Environment and Geography, University of Manitoba, Winnipeg, Manitoba, Canada

[4]Glaciology Unit, Department of Earth and Environmental Science, Université Libre de Bruxelles, Belgium

[5]Unité d'Oceanographie Chimique, Astrophysics, Geophysics and Oceanography department, University of Liège, Belgium

[6]Depts. Earth & Atmospheric Sciences and Geophysics, University of Alberta, Edmonton, Alberta, Canada

[7]Institute of Oceanography, University of Hamburg, Germany

Abstract. Recent studies show that sea ice is a significant player in the carbon cycle of polar waters. It cannot longer be regarded as an impermeable barrier for the exchange of CO_2 between the ocean and the atmosphere. Yet, seasonal studies on the partial pressure of carbon dioxide (pCO_2) within sea ice and related air-ice CO_2 fluxes at the same location are rare. We examined the pCO_2 in water, land fast seasonal sea ice, and atmosphere and the related ice-atmosphere flux of CO_2 in Allen Bay, Canadian Arctic Archipelago from winter conditions into the melting season until sea ice break up. The pCO_2 was measured with in situ samplers. The air-ice exchange of CO_2 was examined by using continuous (24 h) long-term chamber measurements. High partial pressures of CO_2 of up to ≈ 3900 μatm were observed in the upper layer of sea ice at the beginning of the study. Sea ice was oversaturated in CO_2 until late in the melt season, leading to a net efflux (0.3 mmol m^{-2} d^{-1}) during May and June from the sea ice to the atmosphere. Fluxes of CO_2 between ice and atmosphere were observed during all seasons and ranged between -3.41 to 3.92 mmol m^{-2} d^{-1}. Measurements over snow-covered sea ice indicate that snow significantly influences the CO_2 flux. Efflux and influx during the melting season can occur at the same time when gas bubbles from the interior of sea ice become mobile and are subsequently released to the atmosphere while melt ponds efficiently take up CO_2 from the atmosphere.

4.1 Introduction

Polar oceans play a significant role in the global carbon cycle (Takahashi et al., 2009). The ice-covered seas in the Arctic in particular are subject to a dramatic change with respect to sea ice extension and thickness. Recent studies show the decrease in the CO_2 uptake capacity in an ice-free Arctic Ocean (Cai et al., 2010). At the same time the role of sea ice in the gas exchange between the atmosphere and the oceans is not yet fully understood (Fransson et al., 2011; Rysgaard et al., 2011; Loose et al., 2011a; Geilfus et al., 2012b). Fluxes of CO_2 between ocean, sea ice and the atmosphere are only beginning to be documented in sea-ice-covered regions (Papadimitriou et al., 2012, and references therein). Budgeting the carbon pathways in the polar oceans of both hemispheres in the range of Pg C a^{-1} reveals the importance of sea ice in the global carbon cycle (Rysgaard et al., 2011; Papadimitriou et al., 2012).

The role of the coastal oceans in the air-sea CO_2 gas exchange have been discussed from different points of view during the last decades (Bates and Mathis, 2009). More recent studies show the highly variable pattern of CO_2 fluxes in space and time (Cai and Dai, 2004; Borges et al., 2005; Chen and Borges, 2009). However, those studies only investigate the direct air-sea fluxes under ice-free conditions. Only a few investigations focused on ice-covered oceans in the Arctic dealing with the inorganic carbon cycle in sea ice and the underlying water column (Rysgaard et al., 2007, 2009), the direct air-ice CO_2 fluxes (Semiletov et al., 2004; Repina et al., 2007; Heinesch et al., 2010; Nomura et al., 2010a; Else et al., 2011; Papakyriakou and Miller, 2011), or combining both (Miller et al., 2011b; Geilfus et al., 2012b).

Measuring climate relevant gases in sea ice is inherently difficult. For carbon dioxide, most studies determine two out of the four measurable variables of the carbonate system. Usually total alkalinity (TA), dissolved inorganic carbon (DIC) or pH are measured in bulk sea ice (Rysgaard et al., 2007, 2009, 2012; Fransson et al., 2011; Geilfus et al., 2012b) or brine samples (Gleitz

et al., 1995; Papadimitriou et al., 2004; Delille, 2006; Papadimitriou et al., 2007; Delille et al., 2007; Papadimitriou et al., 2009; Nomura et al., 2010a; Papadimitriou et al., 2012) and used for the calculation of pCO_2 (Zeebe and Wolf-Gladrow, 2001). Delille (2006), Delille et al. (2007), and Geilfus et al. (2012b) were, to the best of our knowledge, the only ones to measure pCO_2 directly in sea ice brine. However, as pointed out by Papadimitriou et al. (2012), averaging out bulk samples (i.e. integration of brine over the whole depth of a sackhole) potentially yield inaccurate estimates of the carbonate system. Further, dissociation constants, which are available at present for the calculation of pCO_2, are only valid for a salinity up to 50 (Mehrbach et al., 1973; Dickson and Millero, 1987; Roy et al., 1993; Delille, 2006; Millero et al., 2006). However, sea ice brine values can be far above this threshold (Perovich and Richter-Menge, 1994). Though Delille (2006) showed that their validity might be stretched a bit beyond their estimated salinity range and calculations at lower brine salinities ($S_{brine} < 44$) as observed by Fransson et al. (2011) are possible, calculations at very low subzero temperatures and resulting high salinities ($S_{brine} > 50$) might lead in incorrect pCO_2 estimates. In addition calculations of pCO_2 using TA and DIC at high pCO_2 have been shown to result in inconsistencies in carbonate chemistry measurements (Hoppe et al., 2012). Therefore the direct measurement of pCO_2 should be preferred. Recently there have been new attempts of measuring CO_2 directly in sea ice in situ (Miller et al. 2011a,b, and Brown, K. et al. in prep.) or with a direct non-destructive sampling method (Geilfus et al., 2012a). While the latter provides high resolution measurements it is not suitable for observing sea ice CO_2 over a long period at the same location. At the same time the method of Miller et al. (2011b) was experimental, measuring very high pCO_2 values. Miller et al. (2011b) encourages further studies to confirm or contradict these findings and to improve the method and its sampling protocol. Since fluxes of CO_2 above sea ice are also observed during winter (Heinesch et al., 2010; Miller et al., 2011b), a long-term observation is needed to track the CO_2 in the

water, sea ice, and in the atmosphere from winter conditions into the melting season allowing to connect CO_2 gradients and resulting fluxes between the ice and the atmosphere.

Sea ice was (and in some cases still is) thought to impede fluxes of gases such as CO_2 between the ocean and the atmosphere (Gibson and Trull, 1999; Bates, 2006). In particular, when modelling the carbon cycle in polar regions, gas exchange between sea ice and the atmosphere is neglected (Sun and Matsumoto, 2010). Though Miyake and Matsuo (1963); Gosink et al. (1976), and Kelley and Gosink (1979) already considered sea ice as permeable for gases, measurements of fluxes of CO_2 between ice and atmosphere were only first conducted during the last decade (Semiletov et al., 2004; Delille, 2006). Two methods are currently applied for CO_2 flux measurements. For measuring fluxes over large areas the eddy covariance (EC) method is used (Zemmelink et al., 2006; Miller et al., 2011b; Papakyriakou and Miller, 2011). Another method entails the measuring of local fluxes with the chamber technique (Semiletov et al., 2004; Delille et al., 2007; Nomura et al., 2010b; Geilfus et al., 2012b). As pointed out by Geilfus (2011) EC and chamber technique are applied at different spatial and temporal scales. The values obtained from one method may not be quantitatively similar to the values derived from the other. However, to the best of our knowledge there is no published study comparing EC and chamber technique on sea ice in any comprehensive way. Moreover, measurements with chambers were only conducted as short-term single observations at different locations. In addition measurements above different surfaces (such as snow-covered ice versus bare ice) are still sparse. Only a few studies investigated the influence of the snow cover on the CO_2 flux between the atmosphere and sea ice using the chamber technique. While Nomura et al. (2010b) and Geilfus (2011) provide short-term measurements above snow-covered sea ice, Fischer et al. (unpublished, Chapter 3) investigated the flux of CO_2 above different types of surfaces with long-term (7 days) deployments of chambers. Though Geilfus (2011) measured CO_2 fluxes above sea ice over a period of two months,

there is, to the best of our knowledge, no published study providing long-term chamber measurements at one fixed location from Arctic winter until ice break up in summer, combining synchronous CO_2 measurements in the atmosphere, water, and sea ice.

The objective of this study was (1) to track pCO_2 variability in sea ice, in the atmosphere and in the water column during the winter-spring-summer transition until sea ice break up, (2) to investigate possible stratification of CO_2 in the "near-ice"-surface atmosphere, and (3) to investigate the CO_2 fluxes during the winter-spring-summer transition performing long-term continuous (24 hours) chamber measurements.

4.2 Methods

4.2.1 Study area

The field study was accomplished from end of April until 26 June 2011 under the umbrella of the Arctic-ICE (Arctic Ice-Covered Ecosystem in a Rapidly Changing Environment) program, located in Allen Bay and based out of the Polar Continental Shelf Program (PCSP) base, Nunavut, Canada. The location of the field site (74°43'N, 95°12'W) is highlighted in Figure 4.1. Comparing Figures 1c and 1d, demonstrates the relative consistency of the ice edge throughout the study and clearly shows the transition from snow-covered to melt pond-covered sea ice surface.

4.2.2 Atmospheric monitoring

An atmospheric monitoring system was deployed at 74°42.85'N, 95°11.98'W approximately 1 km west of the main base camp. Ice thickness was 1.58 m at the time of the installation. Snow thickness ranged between 4 and 15 cm in the vicinity of the tower over the sampling period. Equipment was powered by a battery bank, which was continually charged by a diesel generator

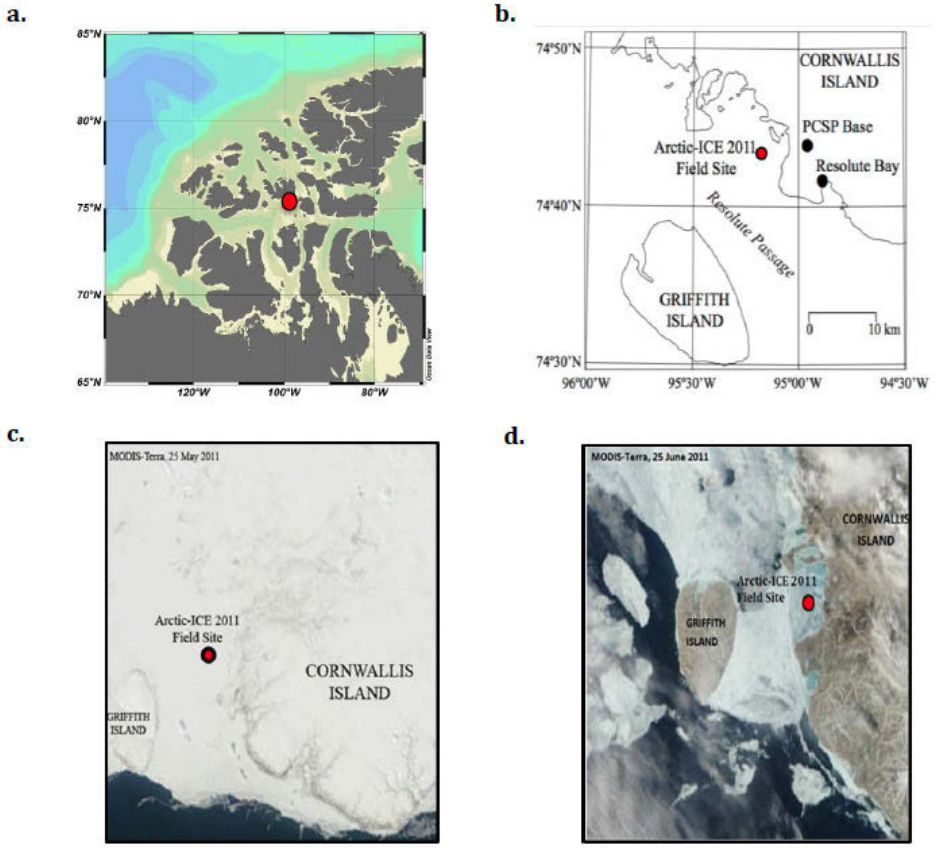

Figure 4.1: Map of the Arctic-ICE 2011 field study location (red dot: 74°43'N; 95°09'W) relative to (a) the Arctic, (b) the Canadian Arctic Archipelago, (c) the ice edge on 25 May, and (d) Allen Bay, the ice edge on 25 June. Images (c) and (d) were obtained from the MODIS-Terra satellite real time website, http://rapidfire.sci.gsfc. nasa.gov/realtime/

located on a pallet and protected by a wooden box at 74°42.876'N, 95°11.936'W 50 m in a N/NE direction from the meteorological tower. The position was chosen with regard to the dominant wind direction. The batteries and charger were located at an equidistant position between the generator and the tower. Wind speed and direction were measured with a wind monitor (Model 05103, ± 0.6 m $s^{-1}, \pm 3°$ deg, RMYoung, USA) at 4.65 m above the ice surface. Air temperature was measured at 4.20 m above the ice with a temperature/relative humidity probe (HMP45C212, ±0.1°C, Vasailla, Finland). Photosynthetic active radiation was measured at 4.50 m above the ice with a PAR sensor (PAR lite, Campbell Scientific, Canada).

4.2.3 Sea ice sampling

Full ice thickness cores (diameter = 9 cm) for temperature and bulk salinity were collected every fourth day using a Kovacs Mark II coring system. Temperature was measured at 5 cm intervals by drilling a 2 mm diameter hole to the centre of the core and inserting a temperature probe (Testo 720, ±0.2°C, Germany). A second core adjacent to the temperature core was cut into 10 cm sections and placed into Whirlpack® bags and transported back to the lab at PCSP base for melting. The salinity of each melt core was measured with a hand-held electric conductivity meter (Cond 330i, ±0.1, WTW, Germany) at room temperature. Brine volume was calculated according to Cox and Weeks (1986) and Leppäranta and Manninen (1988).

4.2.4 In situ pCO_2 measurements

Changes in the mixing ratio of CO_2, xCO_2 (in ppm), within the sea ice and water column were monitored over the course of the ice camp using in situ peeper gas samplers (Figure 4.3) adapted from Owens (2008); Miller et al. (2011a,b), and Brown et al. (in prep.). The peepers deployed during the Allen Bay camp were made from 10 cm of gas permeable Si tubing (3.8 cm inner

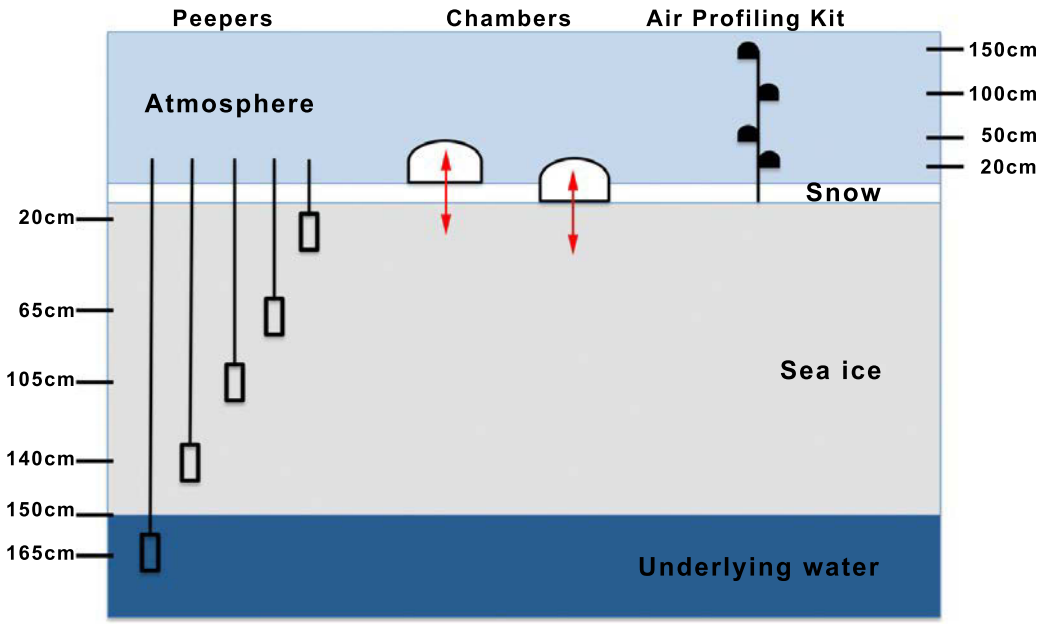

Figure 4.2: Sampling schema for the partial pressure in atmosphere, sea ice, brine, and water column and the CO_2 flux between ice and atmosphere

diameter, 0.16 cm wall) fitted around an aluminium coil for support. Each end was sealed with a 3.5 cm diameter Teflon foil lined rubber stopper. Ports to sample the air space content within the silicon tubing were created using two pieces of metal sampling tubing inserted through the top stopper. These pieces of tubing extended into the top (in-port) and bottom (out-port) of the peeper. To place the peepers, holes were drilled through the sea ice using a 2-inch auger with a power head. After slush and snow were removed, the peepers were lowered into the holes to the desired depth (Figure 4.2) and allowed to freeze into place for a period of 5 days. Two sets of peepers were deployed during the study. Peeper locations: Set 1 was stationed at 74°42.916'N, 95°11.93'W, and set 2 at 74°42.826'N, 95°11.919'W. Peeper set 1 was close to the long-term chambers and the atmospheric monitoring system. Peeper set 2 was close to the meteorological tower approximately 120 m away from peeper set 1. Each peeper array consisted of 5 peepers at various depth intervals, as shown in

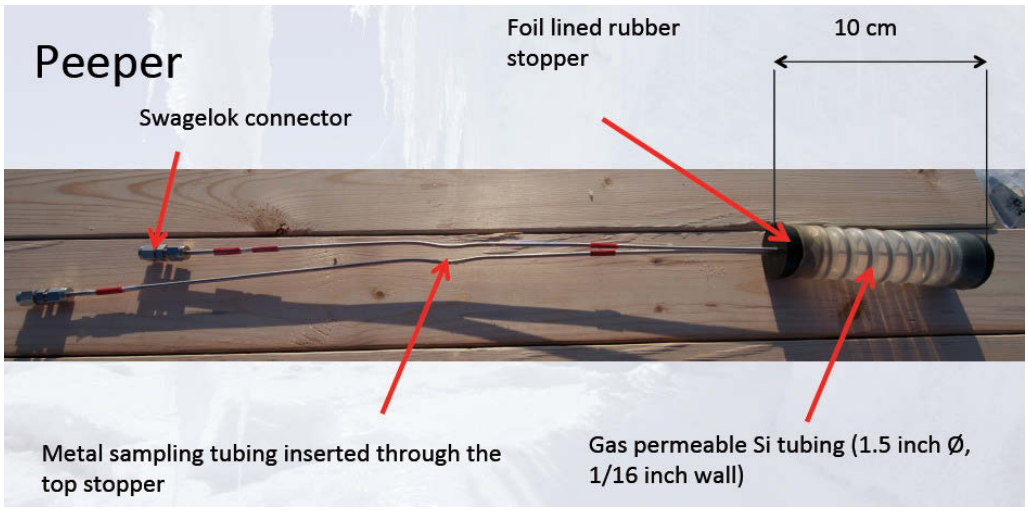

Figure 4.3: The peepers deployed during the Allen Bay camp were made from 10 cm of gas permeable Si Tubing (3.8 cm inner diameter, 0.16 cm wall) fitted around an aluminium coil for support. Each end was sealed with a 3.5 cm diameter Teflon foil lined rubber stopper. Ports to sample the air space content of the coil reinforced Si tubing were created using two pieces of metal sampling tubing inserted through the top stopper. These pieces of tubing extended into the top (in-port) and bottom (out-port) of the peeper (developed by K. Johnson (IOS) and O. Owens (UofM)).

Figure 4.2. Both peeper sets were sampled regularly throughout the duration of the field campaign. The xCO_2 in the peepers was measured every 2 days in the afternoon (local time) between 20:00 and 22:00 UTC using a Continuous Automated CO_2 Sampler (CACS) system equipped with a LI-820 NDIR gas analyzer (LI-COR Biosciences) and CR10X data logger (Campbell Scientific, USA). The CACS system was connected to the peepers using Teflon tubing and Swagelok connectors and air space within the tubing/peeper was cycled at a rate of 100 mL min^{-1}. Before the analyzer was connected with the peepers, the pump was switched off to avoid any pressure changes in the peeper. After the connection of the peepers the pump was switched on again and sampling was carried out over 4 minutes to account for the metal tubing air space and the peeper volume of gas from the peeper made it all the way through the detector. The CACS system was calibrated at the beginning (April 26), and then checked again (May 18). Calibrations utilized a 1968 ppm CO_2 span gas and N_2 zero gas, followed by running a 958 ppm CO_2 tank as a calibration check. The readings at zero were 0.5 ppm, 1968 ppm for the span gas, and 955 ppm for the calibration check. In the present study the value of the mixing ratio of CO_2 (xCO_2 in ppm) is considered to be equal to the value of the partial pressure of CO_2 (pCO_2 in μatm), since differences are small at atmospheric pressure.

On several occasions CO_2 in the water column was directly measured using an equilibrator (1 x 5.5 MiniModule, membrane contactors, Membrana, Germany) connected to an infrared analyzer (LI-820, LI-COR Biosciences). The water was pumped through the equilibrator for 15 minutes.

Plots with interpolations were compiled using Ocean Data View (Schlitzer, 2012).

4.2.5 Flux measurements

CO_2 fluxes were measured using the LI-8100A automated soil CO_2 flux system (LI-COR Biosciences, Lincoln, USA) with an analyzer control unit (Infrared Gas Analyzer) and the LI-8150-8 Multiplexer. Chamber measurements were made at 74°42.911'N, 095°11.933'W in conjunction with an air-profiling kit (LI-COR Biosciences, Lincoln, USA). Continuous flux measurements (from 9 May until 25 June 2011) were carried out with LICOR long-term chambers 8100-104 providing a pressure equilibrium between the air outside and inside the chamber even under windy conditions (Xu et al., 2006). Chambers were put on different surfaces. While chamber 1 was placed on sea ice without snow cover, chamber 2 and 3 where placed on sea ice with different snow depths. The sampling site of chamber 1 was influenced by melt pond formation at the end of the experiment. Initial snow cover for chamber 2 was 4 cm and varied during the sampling period between a maximum of 11 cm and a minimum of 0 cm during the melting phase. The sites of chamber 2 and 3 were not influence by melt pond formation. To carry out a measurement, a PVC collar (11 cm high) was pressed into the snow pack and/or cut into the ice surface using a specially made metal toothed collar. The PVC collar was wrapped into a white tape to minimize bias from heat transport to the ice due to the heating from solar radiation. For the third chamber a site with initial snow thickness of 31 cm was chosen adjacent to chambers one and two. A special collar (40 cm high) was pressed through the snow down to the ice surface. Measurements were conducted until 2nd June when snow depth decreased by several centimetres. Before the offset (height of the collar above the snow or ice interface) was recorded, the 20 cm diameter long-term chamber was carefully placed on the collar. The continuous measurement was started 12 hours after installation by programming the LI-8100A. The rate at which CO_2 diffuses into the air from the ice or snow interface or vice versa was determined by measuring the rate of increase/decrease of CO_2 within the chamber over a designated time interval.

The slope of the increase or decrease was tested for statistical significance. The time interval of each measurement was set to 15 minutes. Pre-purging and post-purging were both set to 2 minutes. A dead band of 30 seconds was applied. These options allowed approximately one measurement per chamber and hour over 7 weeks, resulting in more than 3500 single measurements over the course of the experiment.

In addition, an atmospheric monitoring system was set up with 4 sample devices at 20 cm, 50 cm, 100 cm, and 150 cm above the ice surface (Fig. 4.2). The atmospheric xCO_2 was measured at each height for 60 seconds with a dead band of 30 seconds to account for the tubing.

The LI-8100A was calibrated at in situ temperatures with N_2 zero gas and a 301.7 ppm CO_2 span gas. The CO_2 flux system was powered over two 12 V / 100 Ah sealed AGM (Absorbed Glass Mat) deep cycle batteries, which were charged with a 400 W Silentwind (Spreco Lda, Portugal) wind generator and a diesel generator as backup. The LI-8100A and the batteries were placed in a styrofoam box for protection against extreme cold air temperatures. To produce valid flux estimates, sensors within the chamber continually monitored temperature, barometric pressure, and moisture content, while a pressure vent at the top of the chamber maintained an equilibrium pressure between the inside of the chamber and the ambient air. The research site was visited daily. Chambers were checked for alignment and obstruction. Usually the site visit occurred shortly after 3 am and 2 pm (UTC) and personnel were onsite for approximately 3 hours. Periodic visits occurred during the rest of the day.

4.2.6 Melt pond sampling

Direct measurement of xCO_2 in melt ponds were conducted from 12 June until 22 June. Several melt ponds were sampled each day using the same equipment as for the water sampling.

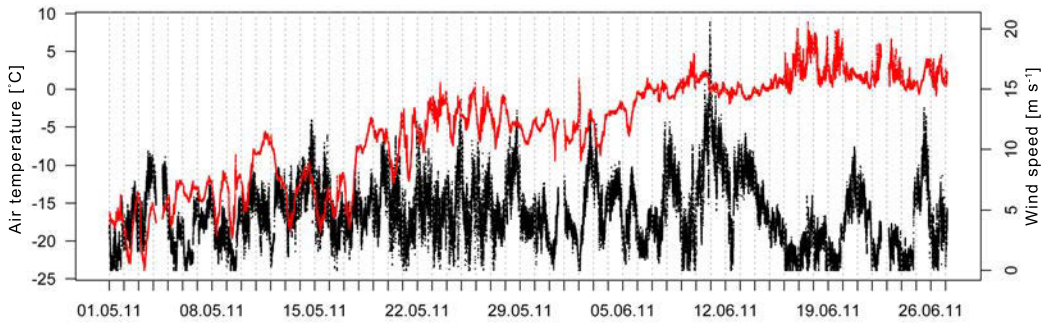

Figure 4.4: Air temperature (red) and wind speed (black) in May and June 2011 in Allen Bay, NU, Canada

4.2.7 Ice structure

One ice core was taken on May 1, 2011, for the analysis of vertical profiles of crystal texture and pore structure. Thick sections between 0.3 to 0.5 cm were cut with a band saw in the cold laboratory. The thick sections were then viewed through crossed polarizers and texture was visually interpreted and named following a scheme defined by Lange (1988). As May 1 was near the end of the ice growth season, the texture information obtained at different depths is thus considered to be representative of ice texture in the near vicinity and provides a detailed record of the growing conditions throughout the winter.

4.3 Results

4.3.1 Background measurements

The study site consisted of an apparently homogenous layer of land fast sea ice formed approximately in November 2010. Air temperature ranged from −25 °C to 9 °C (Fig. 4.4). Initial sea ice thickness at the beginning of the study in late April ranged between 150 and 160 cm. The texture analysis of the ice core drilled on May 1st showed alternating, 1 - 2 cm thick layers of columnar and granular ice in the upper 9 cm, indicative of potential rafting of

Table 4.1: Textural stratigraphy of an ice core taken on May 1, 2011, in Allen Bay, NU, Canada during Arctic-ICE 2011

Section top depth	Section bottom depth	Section width	Texture
0	1	1	Granular
1	4	3	Columnar
4	6	2	Granular
6	9	3	Columnar
9	59	50	Granular
59	64	5	Columnar
64	68	4	Mix
68	157	89	Columnar

nilas ice during initial sea ice growth (Table 4.1, Fig. 4.5). This was underlain by a 50 cm thick layer of slightly stratified granular ice, followed by two 5 and 4 cm thick distinct layers of columnar and mixed columnar/granular ice. These layers represent rapid ice growth with variable oceanic currents and mixing until the ice was 68 cm thick. Below, a continuous, 89 cm thick layer of undisturbed columnar ice with crystal length of more than 20 cm in some cases represents slow congelation ice growth under quite conditions for the majority of the winter leading into the study period. The bottom of this layer and the ice core was characterized by a 2 cm thick skeleton layer with dendritic crystals protruding into the water, indicative of active, slow ice growth at the time of sampling(Fig 4.5). Superimposed ice was not observed during the study.

At time when snow cover was present, snow depths varied from 4 to 30 cm. The snow cover was present until beginning of June.

The temperature of the sea ice was developing from cold winter sea ice (-14 °C), over a typically warming period, to porous melting (> -1.9 °C) sea ice (Fig. 4.6). Ice became isothermal at the beginning of June (-2 to -3 °C) rising to isothermal values above the freezing point of seawater during mid

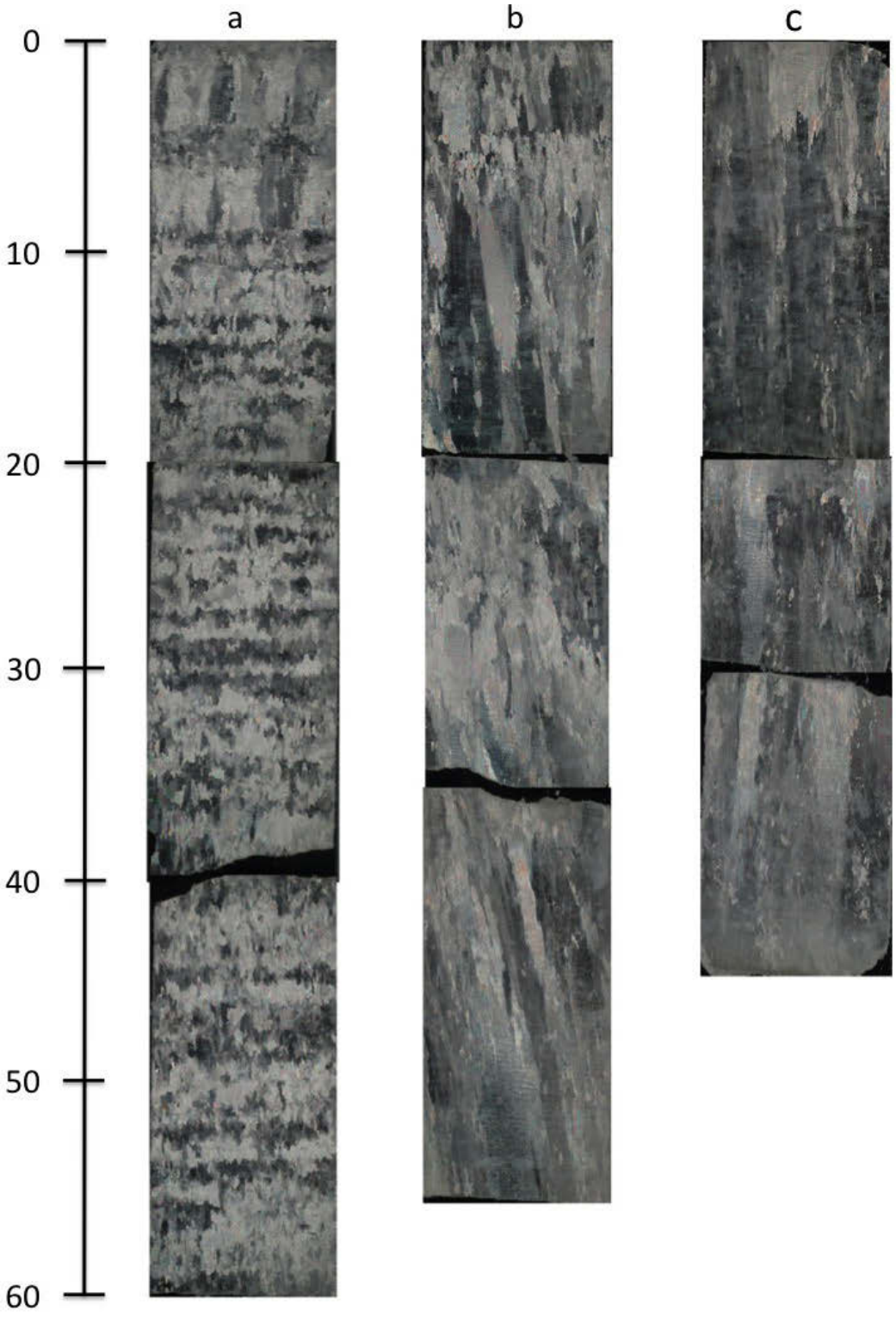

Figure 4.5: Thick sections of an ice core taken on May 1, 2011, in Allen Bay, NU, Canada during Arctic-ICE 2011. a) 0-60 cm, b) 60-114 cm, c) 114-157 cm. The scale is provided in cm.

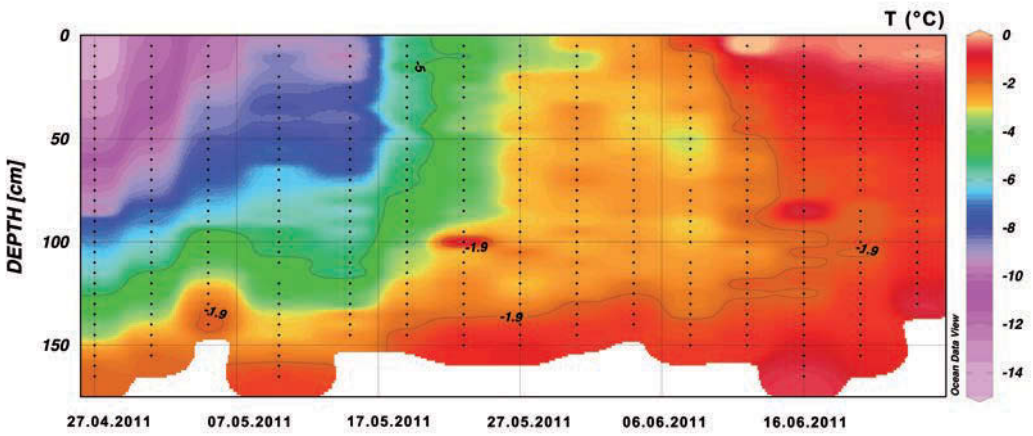

Figure 4.6: Contour plot of sea ice temperature in Arctic sea ice between April and June 2011 in Allen Bay, NU, Canada, contour line of freezing temperature of sea water

June. Bulk salinity during the winter period showed a typical "C-shaped" profile (Petrich and Eicken, 2010). After a reduction of bulk salinity during mid May in the top layer, it increased again at the end of May and beginning of June and subsequently reduced drastically towards the end of the study (Fig. 4.8), as typically observed in decaying sea ice. According to sea ice temperature and bulk salinity, brine volume reached the 5% permeability threshold in sea ice, at depths between 0 and 120 cm, around May 19 and increased up to 40% just before ice break up (Fig. 4.9). Melt ponds started to form on 10 June and were followed by a rapid sea ice melt resulting in a sea ice break up on 27 June due to strong offshore winds. Total sea ice thickness on 24 June was 120 cm. Wind speed varied between 0 and 21 m s^{-1} with average values of 4.4 m s^{-1} in May and 3.1 m s^{-1} in June. During May the wind direction was mainly from NW while in June it changed to North and East directions.

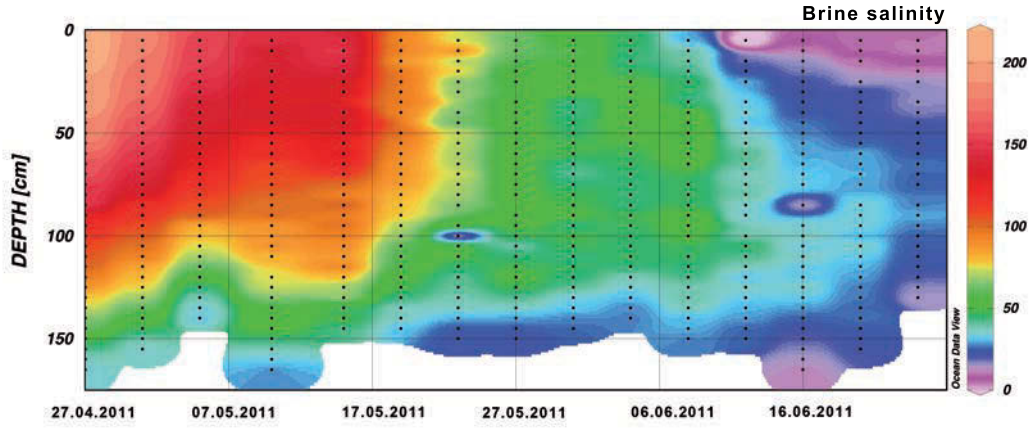

Figure 4.7: Contour plot of brine salinity in Arctic sea ice between April and June 2011 in Allen Bay, NU, Canada, calculated from sea ice temperature according to Petrich and Eicken (2010)

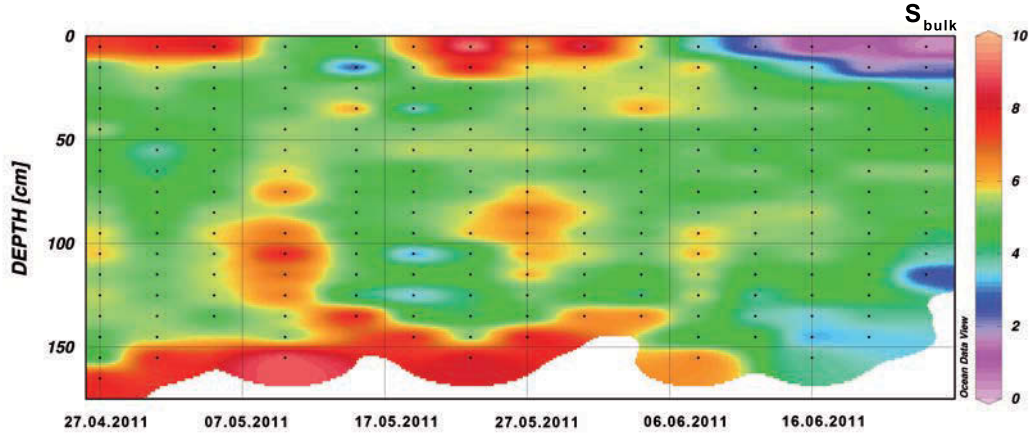

Figure 4.8: Contour plot of sea ice bulk salinity in Arctic sea ice between April and June 2011 in Allen Bay, NU, Canada

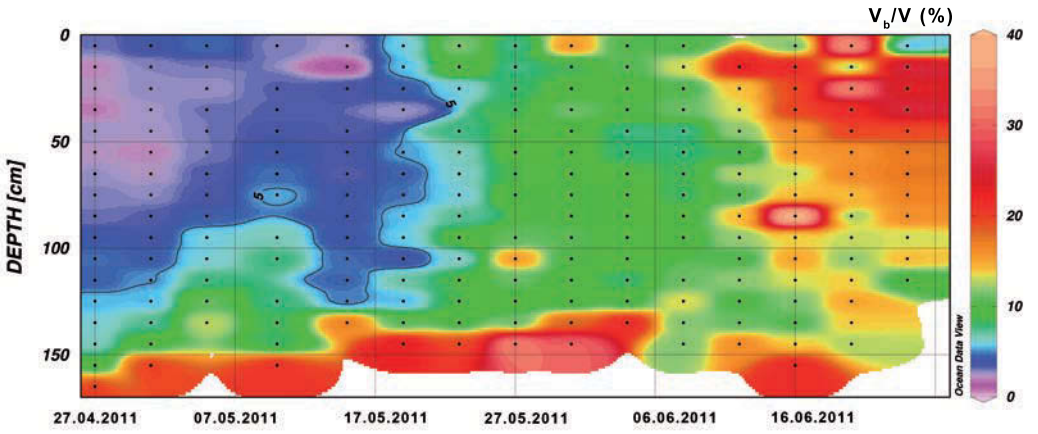

Figure 4.9: Contour plot of brine volume in Arctic sea ice between April and June 2011 in Allen Bay, NU, Canada, contour line of 5% threshold of brine volume for permeability of fluids, calculated after Cox and Weeks (1986) and Leppäranta and Manninen (1988)

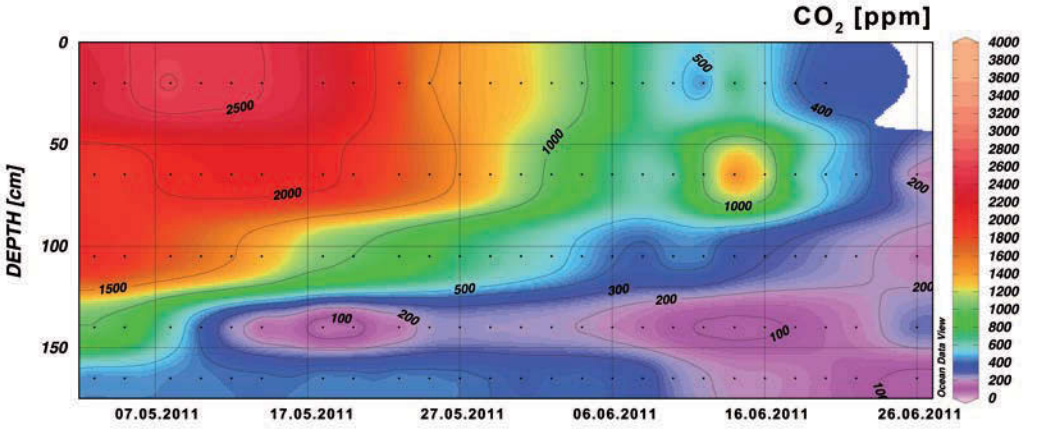

Figure 4.10: Contour plot of in situ xCO_2 at different depths in Arctic sea ice and the water column between May and June 2011 in Allen Bay, NU, Canada from peeper set 1, ice thickness at the beginning was 155 cm

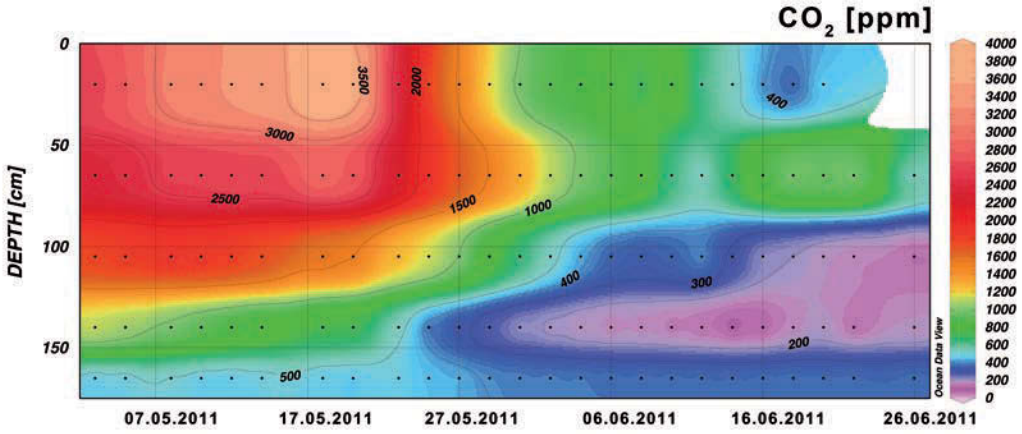

Figure 4.11: Contour plot of in situ xCO_2 at different depths in Arctic sea ice and the water column between May and June 2011 in Allen Bay, NU, Canada from peeper set 2, ice thickness at the beginning was 158 cm

4.3.2 In situ sea ice and water column CO_2

In situ values of CO_2 within the sea ice showed the same patterns for both peeper sets (Fig. 4.10 and 4.11). With high CO_2 values in winter sea ice in the upper layer reaching up to 3881 ppm, which persist until late May, and lower values, still over saturated with respect to atmospheric CO_2 values, in the bottom layer. Over the course of the study values of CO_2 were dropping throughout the ice column with a distinct decrease after May 23. At the sea ice-ocean interface measurements showed an undersaturation with respect to atmospheric CO_2 already in early spring, reaching values well below 200 ppm down to 2.7 ppm. These low numbers stretched to upper layers with increasing time leading to a pronounced undersaturation throughout the sea ice just before ice break up. Unexpected increase of CO_2 in both peeper sets at 65 cm occurred during mid of June. Although it was more pronounced in peeper set 1, the increase could also be observed in peeper set 2 over several days before values dropped again.

Direct measurements of CO_2 in the water column using the equilibrator

showed same values (± 5 μatm) as obtained from the peepers at 165 and 168 cm from the ice surface, respectively. This shows that both methods, peeper and direct measurements provide the same quality of data in the water column. CO_2 values of the water below the sea ice was slightly over saturated ($410 - 450$ μatm) and became soon undersaturated ($72 - 243$ μatm) with respect to atmospheric CO_2.

4.3.3 Atmospheric CO_2

Atmospheric CO_2 values ranged from 385 to 396 ppm. A stratification of the CO_2 in the atmospheric layer from 0 to 150 cm above the ice could not be observed. Values were homogeneous at the beginning of May and during periods in length of several days. The highest increase of the concentration occurred between May 16 and May 19 (Fig. 4.12) when values increased up to 396 ppm, while the lowest values were observed from June 8 onwards when concentrations decreased down to 385 ppm. Until the end of the study CO_2 values fluctuated between 385 and 392 ppm. Lower values were observed during high wind speed and higher values occurred during light wind and calm conditions, respectively.

4.3.4 CO_2 fluxes

Fluxes of CO_2 were measured over the whole period of the study. Fluxes ranged between -3.41 and $+3.92$ mmol m^{-2} d^{-1}, where positive numbers refer to a degassing from the ice to the atmosphere and negative numbers show an influx. Fluxes from early spring sea ice ($T_{\text{sea ice}} < -8$ °C) were low but existent with an average of 0.22 mmol m^{-2} d^{-1} (Fig. 4.13). Starting from the end of May 16 an increase of positive fluxes from the chamber site without any snow cover was observed. This increase lasted until May 18 with a maximum value of 2.08 mmol m^{-2} d^{-1}. This sharp increase was limited to a short period of time. The degassing period between May 17 and May 20 is corresponding to higher

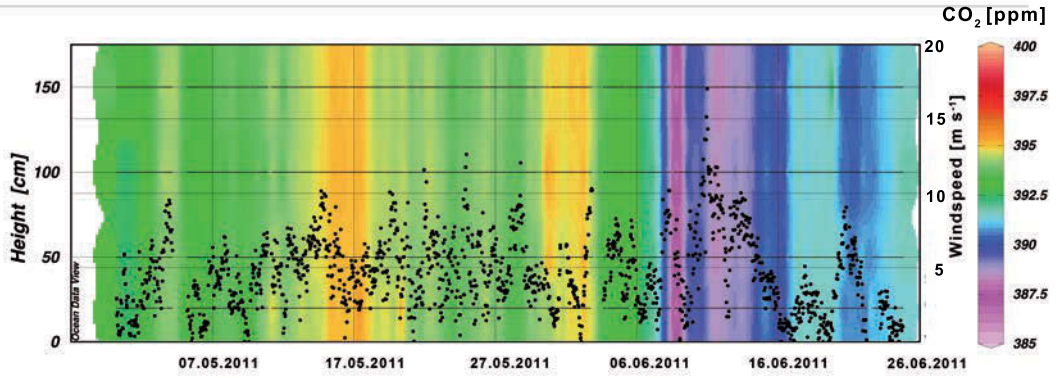

Figure 4.12: Contour plot of xCO_2 in the atmosphere above Arctic sea ice between April and June 2011 in Allen Bay, NU, Canada, measured at: 20 cm, 50 cm, 100 cm, and 150 cm and wind speed in m s^{-1} (black points).

winds on May 16, while brine volume was crossing the permeability threshold. Moreover these findings also correspond the higher atmospheric CO_2 values between May 16 and May 19. Between May 20 and June 2 fluxes reduced to an average of 0.07 mmol m^{-2} d^{-1} with many measurements showing no fluxes. However, an influx could be observed. Fluxes were alternating at low values between efflux and influx on a diurnal cycle. From June 4 fluxes started to increase with continuous efflux above 1 mmol m^{-2} d^{-1} (Fig. 4.13). During the last two weeks of the measurements CO_2 was mainly degassing from the ice with values up to 2.23 mmol m^{-2} d^{-1}. However, from June 18 onwards fluxes alternated with differences up to 5.67 mmol m^{-2} d^{-1} between minimum and maximum flux on a diurnal cycle. Influxes occurred during early afternoon while degassing was observed mainly in the morning.

The flux measurements of chamber 2 with initial thin snow cover showed similar patterns with very low to zero fluxes during the cold period when permeability was low and alternating fluxes at low values during a transition time from cold to isothermal sea ice. Although damped (compared to chamber 1), an higher efflux was observed during the period between May 17 and May

20. During the change from snow covered into white ice, fluxes increased at the beginning of June and reduced again during mid of June. Similar to chamber 1, larger fluxes in both directions were observed from mid of June onwards with an overweight of positive fluxes. The measurements of chamber 2 showed the highest values measured during the experiment. The alternating fluxes showed the same pattern as for chamber 1 with CO_2 degassing during the first half of the day and events of influx during the second half of the day.

Flux measurements of chamber 3 showed an influence of snow on the fluxes of CO_2. During the cold period fluxes were very low and at the detection limit. This is clearly seen by many statistically insignificant fluxes (red dots in Fig. 4.15). Starting with the beginning of the warming period, fluxes increased slightly to a low level. However, fluxes occurred in both directions from and towards the ice, while influx occurred mainly during the day and efflux was measured at the end of a day. With increasing temperatures and melting of snow, fluxes increased significantly with a maximum > 1 mmol m^{-2} d^{-1} at the end of this experiment, when measurements above snow had to be stopped due to snow melting.

A typical measurement sequence from which the flux was calculated is shown in Figure 4.16. Most of the measurements showed such a clear steady increase/decrease of CO_2 within the chamber over a designated time interval. However, some measurements, especially during the melting phase showed irregular variations of the CO_2 concentrations (Fig. 4.17 and 4.18). This might be due to degassing of bubbles from the interior of the sea ice during the flux measurements, leading to sudden peaks, which disappear within a short time frame due to a steady mixing within the monitoring system. The occurrence of bubbles and subsequent degassing from the interior of the ice was observed throughout the melting period.

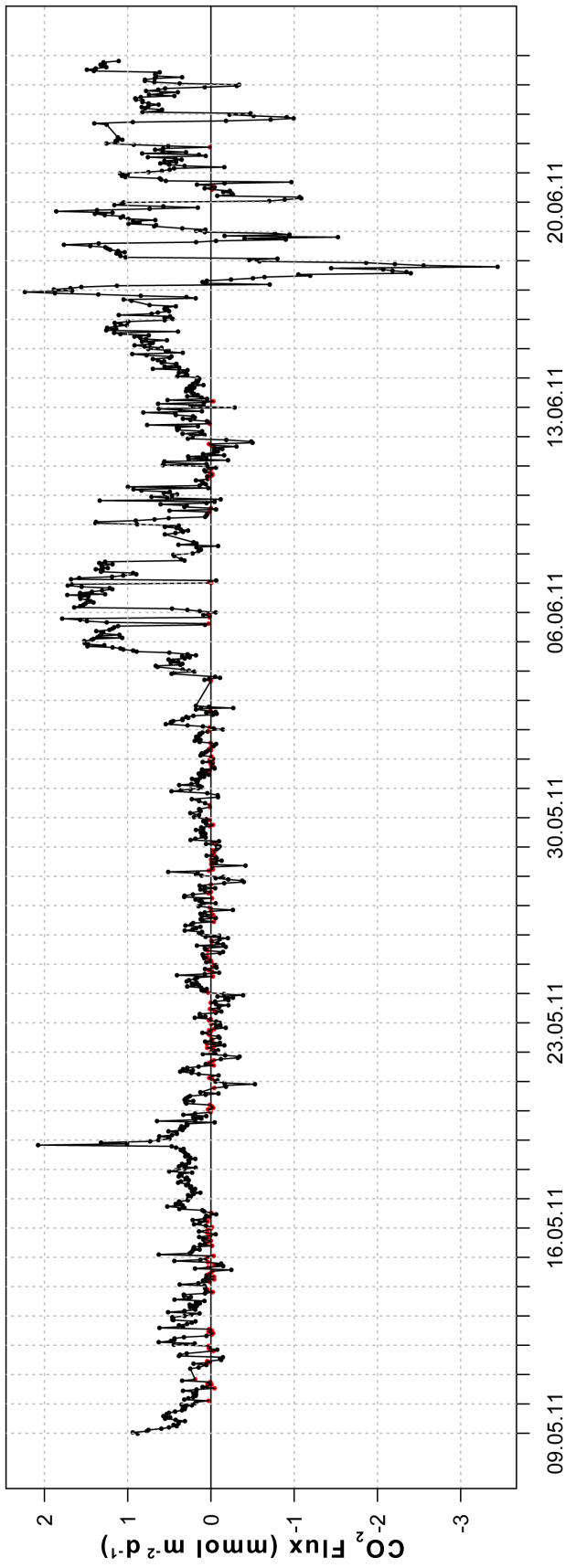

Figure 4.13: Flux of CO_2 between sea ice without any snow cover and the atmosphere between May and June 2011 in Allen Bay, NU, Canada, red points indicate that the slope for this flux was not significant, positive numbers refer to a degassing and negative numbers to an influx.

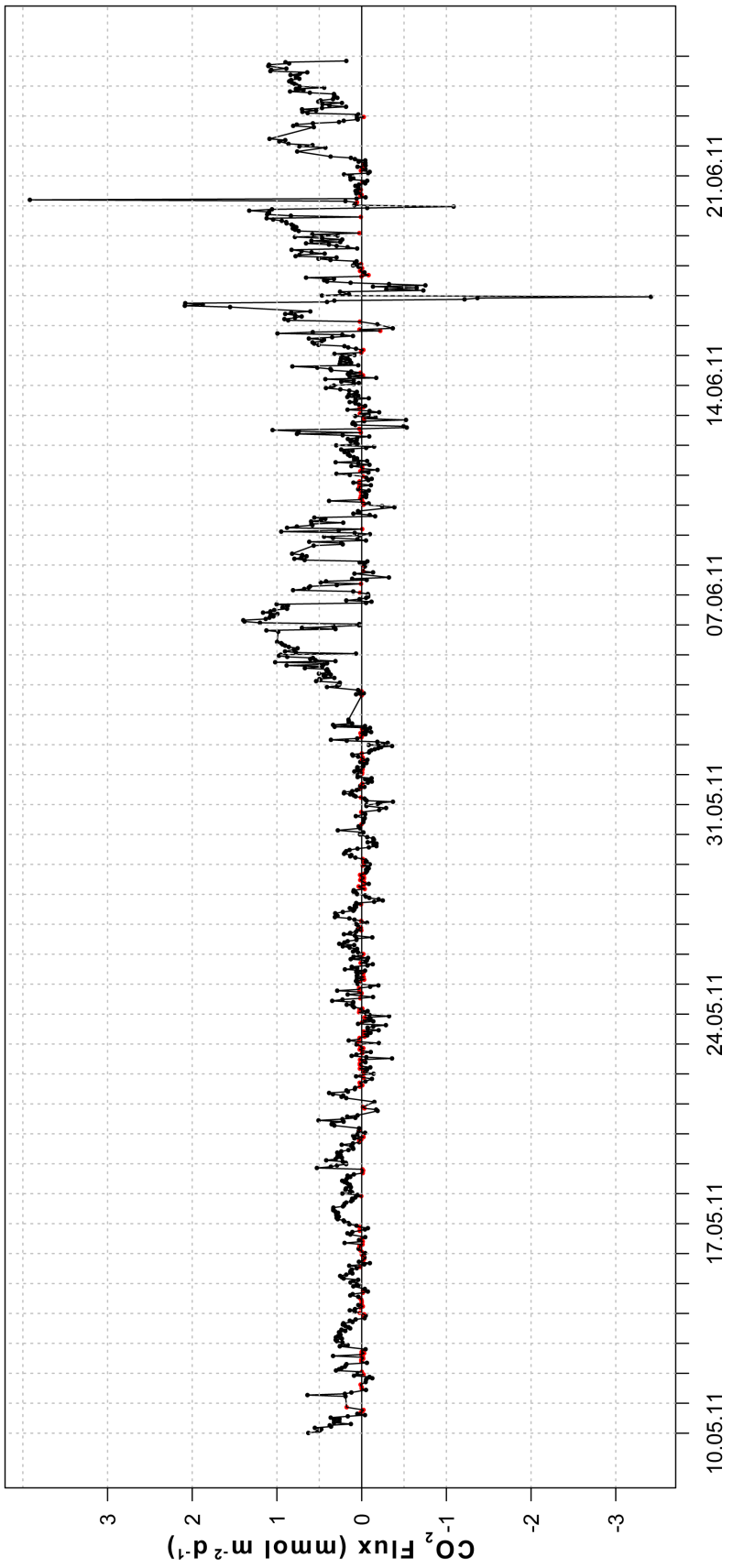

Figure 4.14: Flux of CO_2 between snow covered sea ice, which is turning into sea ice without snow cover, and the atmosphere between May and June 2011 in Allen Bay, NU, Canada, red points indicate that the slope for this flux was not significant, positive numbers refer to a degassing and negative numbers to an influx.

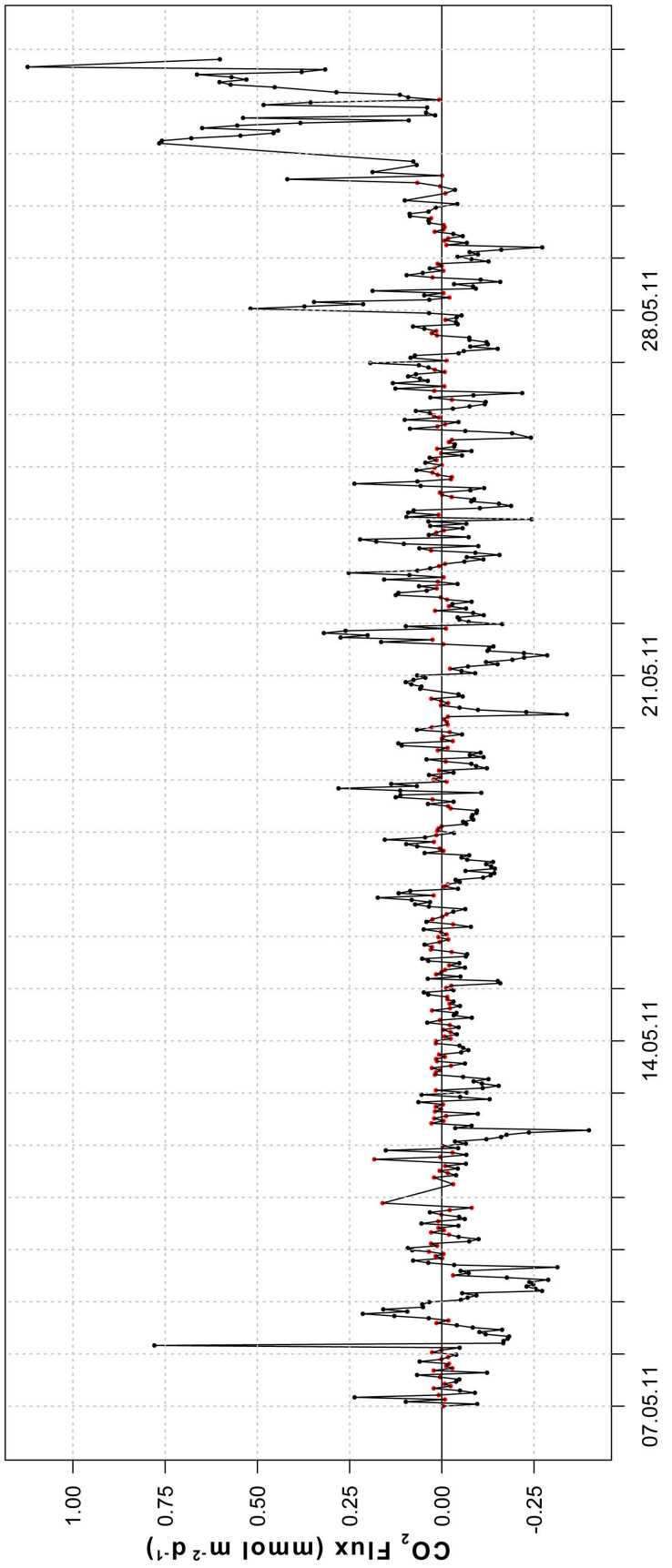

Figure 4.15: Flux of CO_2 between snow covered sea ice and the atmosphere between May and June 2011 in Allen Bay, NU, Canada, where initial snow thickness was 30 cm and the collar was pushed through the snow to the ice surface, red points indicate that the slope for this flux was not significant, positive numbers refer to a degassing and negative numbers to an influx.

4.3.5 Melt pond CO_2

Melt ponds were always undersaturated with respect to atmospheric CO_2, ranging between 37.4 and 365.5 ppm (Fig. 4.19). Values were dropping with continuous melting and a reduction of wind speed. CO_2 levels raised again with increasing wind velocity and dropped accordingly to them at the end of the measurements.

4.4 Discussion

4.4.1 CO_2 in sea ice and water column

CO_2 values in sea ice have been reported with indirect in situ (Geilfus et al., 2012a) and direct in situ measurements (Miller et al., 2011a,b). Our results are in the range of Miller et al. (2011a) and the morning sampling in Miller et al. (2011b). Compared to the afternoon measurements of (Miller et al., 2011b), this study reports values twice to three time less. Aside from possible natural variations these authors ascribe the extremely high pCO_2 values to a potential artificially produced vacuum due to the sampling procedure. Though no vacuum occurred in our peeper sets, our results are still recognizably higher than those reported by the sampling method of Geilfus et al. (2012a) or those obtained from direct brine pCO_2 measurements of Delille (2006), Delille et al. (2007) and Geilfus (2011). A possible reason of higher pCO_2 values in Arctic sea ice compared to Antarctic sea ice could be a higher bacterial activity and subsequently higher respiration and related CO_2 production within Arctic sea ice (Geilfus et al., 2012b). This is supported by values of dissolved organic carbon (DOC), which are 2 - 3 orders of magnitude higher in Arctic sea ice and therefore indicate a potentially higher bacterial activity (Geilfus et al., 2012b, and references therein). Moreover, our results most likely do not suffer from the bias as the values from (Miller et al., 2011b) since our pCO_2 values are in phase with fluxes, where sinks appear while measured pCO_2 is below

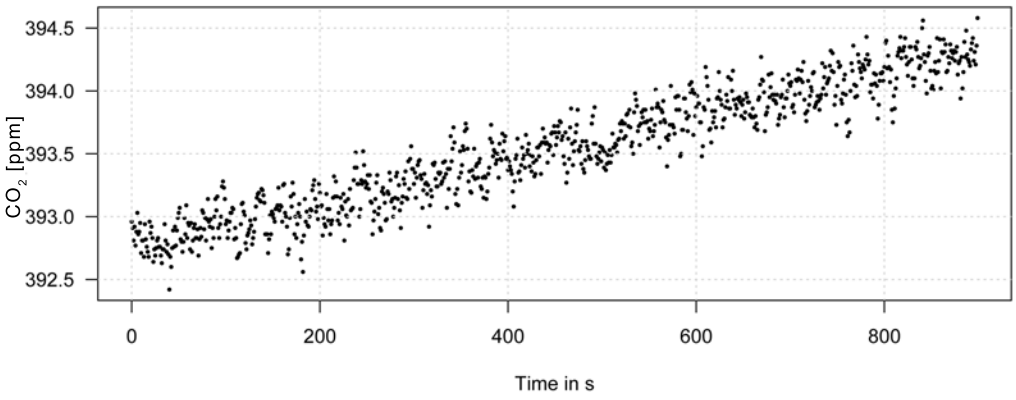

Figure 4.16: Single flux measurement of CO_2 between sea ice and the atmosphere end of June 2011 in Allen Bay, NU, Canada, showing continuous degassing of CO_2 from the ice

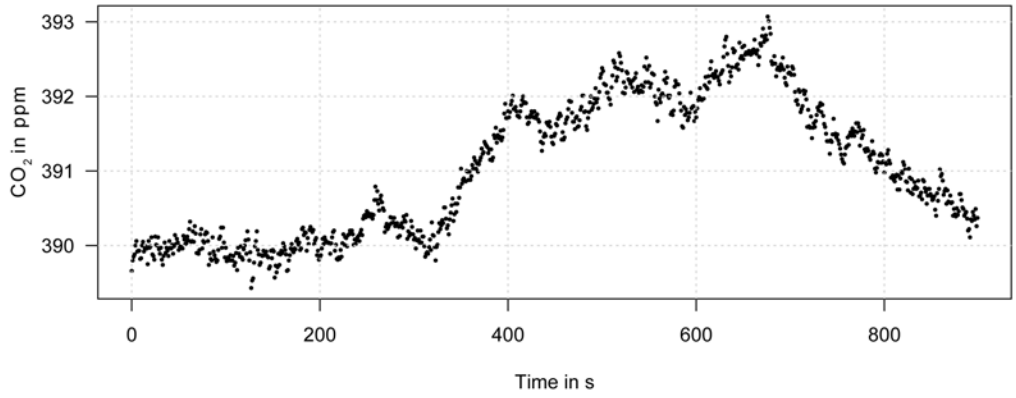

Figure 4.17: Single flux measurement of CO_2 between sea ice and the atmosphere end of June 2011 in Allen Bay, NU, Canada, showing overlapping of influx and efflux

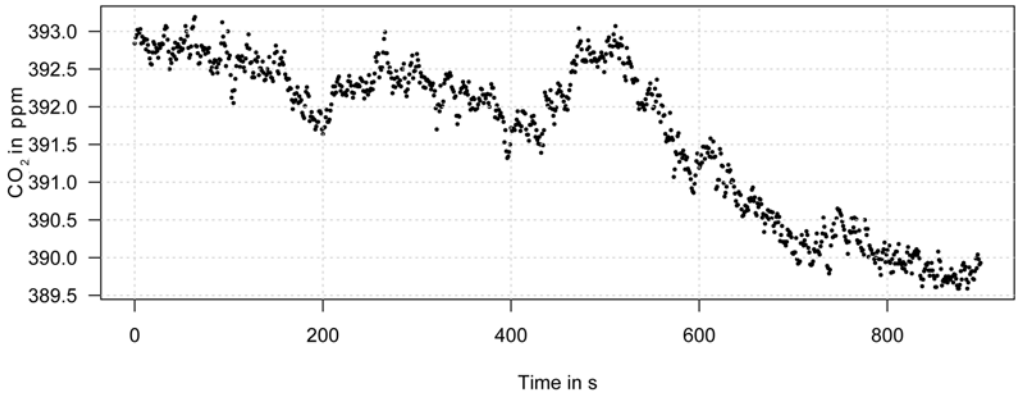

Figure 4.18: Single flux measurement of CO_2 between sea ice and the atmosphere end of June 2011 in Allen Bay, NU, Canada, showing overlapping of influx and efflux

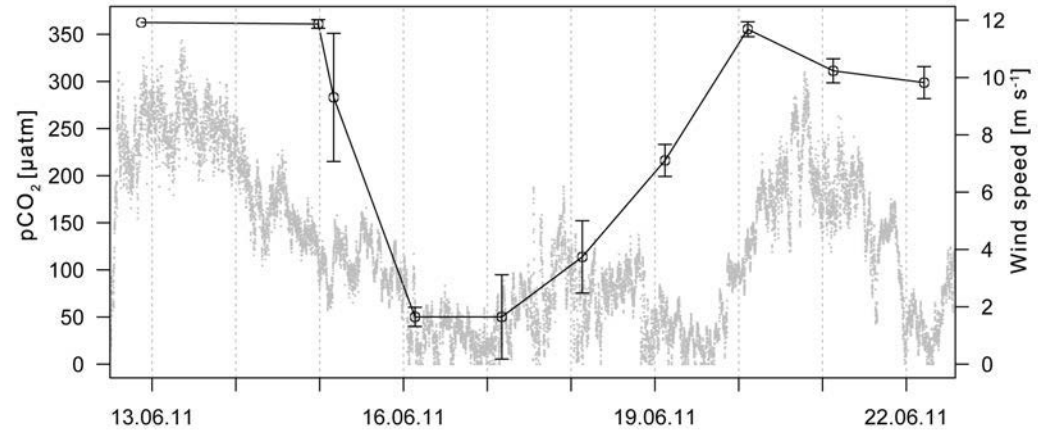

Figure 4.19: Temporal evolution of pCO_2 (black) in melt ponds and wind speed (grey) on Arctic sea ice in Allen Bay, NU, Canada

atmospheric values. Thus, our values and values as presented by Miller et al. (2011a) and Delille et al. (2007) are most likely in the right ballpark and that Arctic pCO_2 values are simply higher than the ones reported from Antarctica (compare Figure 4.20, Geilfus et al. (2012b).

However, another reason for the observed higher pCO_2 values might be due to the used sampling procedure as applied in Delille (2006), Delille et al. (2007), Geilfus et al. (2012b). Brine sampled with the sackhole method potentially accumulates from a large spatial surrounding including brine from lower layers containing a lower salinity and thus lower pCO_2 values. In addition the pCO_2 (for values above atmospheric pCO_2) in the brine might drop due to the exchange with the atmosphere in the sackholes. However, this would not explain the differences when compared to Geilfus et al. (2012a). Further, comparing the calculated theoretical CO_2 values (Fig. 4.20) with the observed values in this study, reveals inconsistencies. Neglecting the salinity range $S > 50$ in figure 4.20, since dissociation constants might not be valid above that threshold, it is clearly seen that measured values scatter around the theoretical curve, but often attaining values twice that of the theoretical values. The same is shown by Miller et al. (2011a), where calculated pCO_2 values in Figure 4 are also always higher than the measured ones. The CO_2 system in sea ice is driven by numerous factors as shown by Papadimitriou et al. (2012), which might explain the observed values. A possible explanation for the increased CO_2 concentration within sea ice could be the release of CO_2 to internal gas bubbles during sea ice growth in autumn and winter resulting in an increased internal CO_2 gradient (Tison et al., 2002; Papadimitriou et al., 2012). Thus, elevated CO_2 concentrations, measured during this study, might be explained with a combination of high partial pressure of CO_2 in sea ice brine (due to the salinity effect and precipitation of $CaCO_3$) and in addition by gas bubbles which are trapped within the sea ice.

Observed pCO_2 evolution in this sea ice study followed the previously described decrease with increasing temperatures (Papadimitriou et al., 2004;

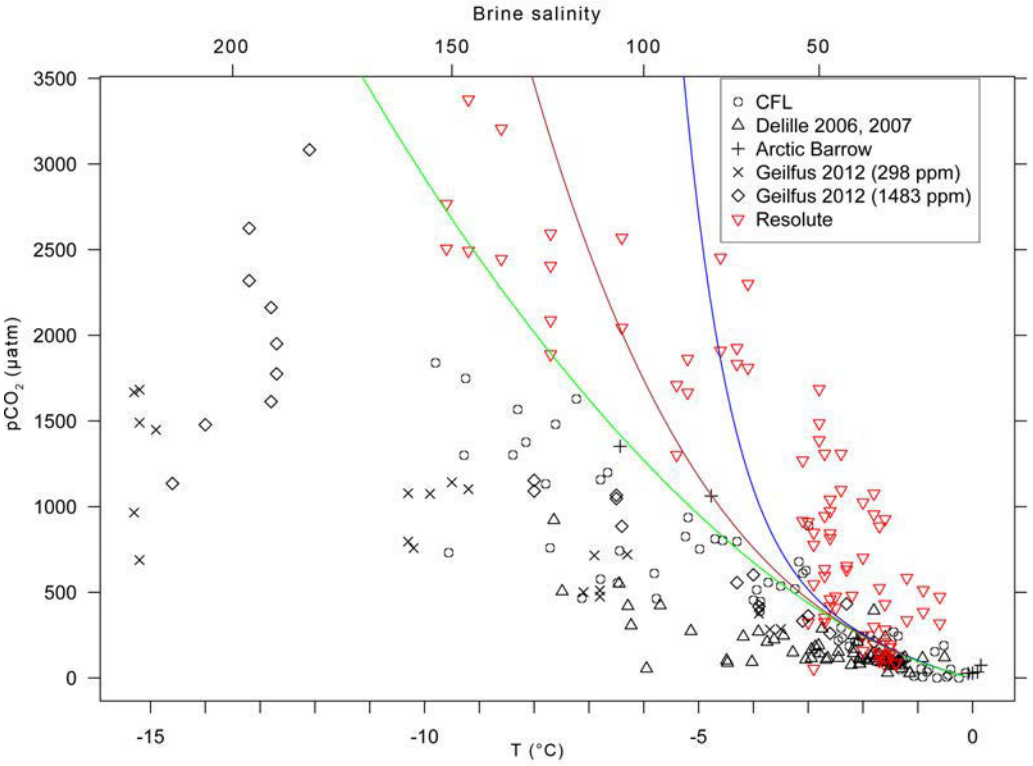

Figure 4.20: Comparison between pCO_2 measurements on bulk standard sea ice, peeper measurements, and in situ measurements of brine pCO_2 with calculated theoretical partial pressure of CO_2 in brine at different salinities/temperatures using CO2calc (Robbins et al., 2010) with dissociation constants of Mehrbach et al. (1973) = green, Roy et al. (1993) = brown, and Millero et al. (2006) = blue. Initial normalized ($S_i = 35$) values, $DIC_{35} = 2227.9$ μmol kg^{-1}, and $TA_{35} = 2417.8$ μmol kg^{-1} derived from relationships of DIC and TA with sea ice brine as presented for Arctic sea ice (Geilfus et al., 2012b). Influences of nutrients on TA and calcium carbonate precipitation were neglected. Brine salinity was calculated from sea ice temperature according to (Petrich and Eicken, 2010). Modified after (Geilfus et al., 2012a)

Delille, 2006; Geilfus, 2011) from winter into the melting season (Figure 4.10 and 4.11). Increasing temperature leads to a reduction of the salinity within the brine due to the dilution through melting ice crystals. Lower brine salinity results in an increased solubility of gases such as CO_2 and thus to a reduction of the partial pressure of CO_2 within the ice (Zeebe and Wolf-Gladrow, 2001). In addition precipitates of calcium carbonate within the ice might potentially dissolve and thereby consume CO_2 (Dieckmann et al., 2008, 2010; Fischer et al., 2013; Geilfus, 2011; Rysgaard et al., 2012). However, due to supersaturation of pCO_2 with respect to atmospheric values throughout the ice column and especially in the uppermost layer until late in the melt season we would expect degassing from the sea ice to the atmosphere. Thus, the melting and subsequent dilution of the sea ice brine will lead to a decrease of the pCO_2 values within the ice.

In contrast we observed an unexpected increase of CO_2 at a depth of 65 cm during mid of June in both peeper sets. The following rationale is proposed. Melt pond data of pCO_2 at that time showed values of around 350 μatm (Fig. 4.19). If this water drains downwards into the ice due to the hydrostatic head, having a low salinity, would face subzero temperature leading to a refreezing of the water (Eicken et al., 2002). Thus the partial pressure of CO_2 would increase again, because of an increase of brine salinity. This could explain the pCO_2 values which were measured in both peeper sets. Another reason could be bacterial respiration, since primary production within the ice is low at that time (Campbell et al., 2012), but this remains elusive.

Just before ice break up pCO_2 values throughout the ice column are undersaturated with respect to atmospheric values. This can be ascribed to dilution due to ice melting since no chl α concentration could be measured in sea ice at that period of time (Campbell et al., 2012). These conditions favour the uptake of CO_2 as proposed by Delille (2006) and Rysgaard et al. (2011).

Low pCO_2 values < 200 μatm in the lower layers of the ice and the water column are mainly driven by biological productivity when chl a concentrations

in sea ice increased up to 27.6 mg m^{-2} at the beginning of June (Campbell et al., 2012). Since chl a values sharply decreased after the storm event on 10 June, low values of CO_2 at the ice water interface can be ascribed mainly to inorganic processes, such as dissolution of $CaCO_3$ and dilution of brine and thus a reduction of salinity and pCO_2. The very low pCO_2 value of 2.7 μatm is consistent with findings of other studies. For example, taking values of Gleitz et al. (1995) with pH = 9.9, TA = 1775 μmol kg^{-1}, and S = 26.9 results in $pCO_2 < 1$ μatm.

4.4.2 Fluxes and implications for atmospheric CO_2

Highest atmospheric xCO_2 values were observed during the cold period (May). Similar to what Heinesch et al. (2010); Miller et al. (2011b) and Papakyriakou and Miller (2011) observed above winter or cold sea ice respectively, we also observed fluxes from the sea ice to the atmosphere during the early sampling period when sea ice surface temperatures ranged between -14 and -8 °C. This suggest that sea ice is most likely permeable for gases below the threshold of 5% brine volume, which is reported for liquids in sea ice (Golden et al., 1998).

Variations of atmospheric CO_2 in Arctic regions are observed in several studies, with maxima during winter and minima during summer periods (Skjelvan et al., 1999; Nagurnyi, 2008, 2010). Though several potential explanations are proposed, sea ice has been neglected or only considered as a minor player. However, (Alexkseev and Nagurnyi, 2007) primarily attribute annual variations of CO_2 in the Arctic to the influence of sea ice due to its seasonal cycle. Our observations are in accordance with those findings. Changes in CO_2 concentrations in the atmosphere can be ascribed to processes which occur on and in the ice.

Fluxes are low until mid June. Albeit, there are two exceptions showing higher fluxes. A first outburst occurs on about May 17, when liquid permeability in sea ice is re-established, which results in a degassing of CO_2 to

the atmosphere. The sudden degassing event in mid May was observed at different levels. The chamber measurements showed an efflux while the monitoring of the near-ice-surface atmosphere showed a corresponding increase of the atmospheric CO_2 concentration. Peeper measurements showed a high over saturation of CO_2 within the ice with respect to atmospheric values, resulting in a large gradient which would favour a degassing. At the same time, brine volume reached the permeability threshold (Golden et al., 1998; Pringle et al., 2009) leading to a release of CO_2 to the atmosphere, which is in good agreement with theory and results of other studies (Delille, 2006; Delille et al., 2007; Geilfus et al., 2012b). Carbon dioxide fluxes during winter may also be triggered by $CaCO_3$ precipitation at the surface of sea ice (Nedashkovsky and Shvetsova, 2010; Fischer et al., 2013). However, the degassing was rather limited to a short period of time. A second outburst, observed on June 6 and 7, can be ascribed to an increasing brine volume ($V_b > 10\%$) leading to a mobilization of bubbles, which then start to escape from the ice. Between June 6 and June 14 the 10% iso-brine volume curve (Fig. 4.9) progresses downwards in the ice, resulting in further bubble degassing from lower layers. The latter is supported by measurements as presented in Fig. 4.17, where degassing events of bubbles most likely resulted in short peaks which were then reduced due to steady mixing during a single measurement. In addition, efflux due to the release of gas bubbles may overlap influx (Figure 4.18).

From June 14, diurnal cycles of insulation and temperature (always above 0°C) result in flux cycles. Two main processes potentially drive the alternation of the fluxes. The effect might be triggered by algae and/or temperature. Algal communities have been reported in ice melt water in melt ponds (Mundy et al., 2011). Lee et al. (2012) report an average annual carbon production in sea ice melt ponds of 0.67 g C m^{-3} a^{-1}, which they translate into an annual carbon production of all melt ponds in the Arctic of $\approx$ 2.6 Tg C. Hence, CO_2 would be consumed by the algae when solar radiation is high.

Another possible explanation would be the temperature effect. Taking typ-

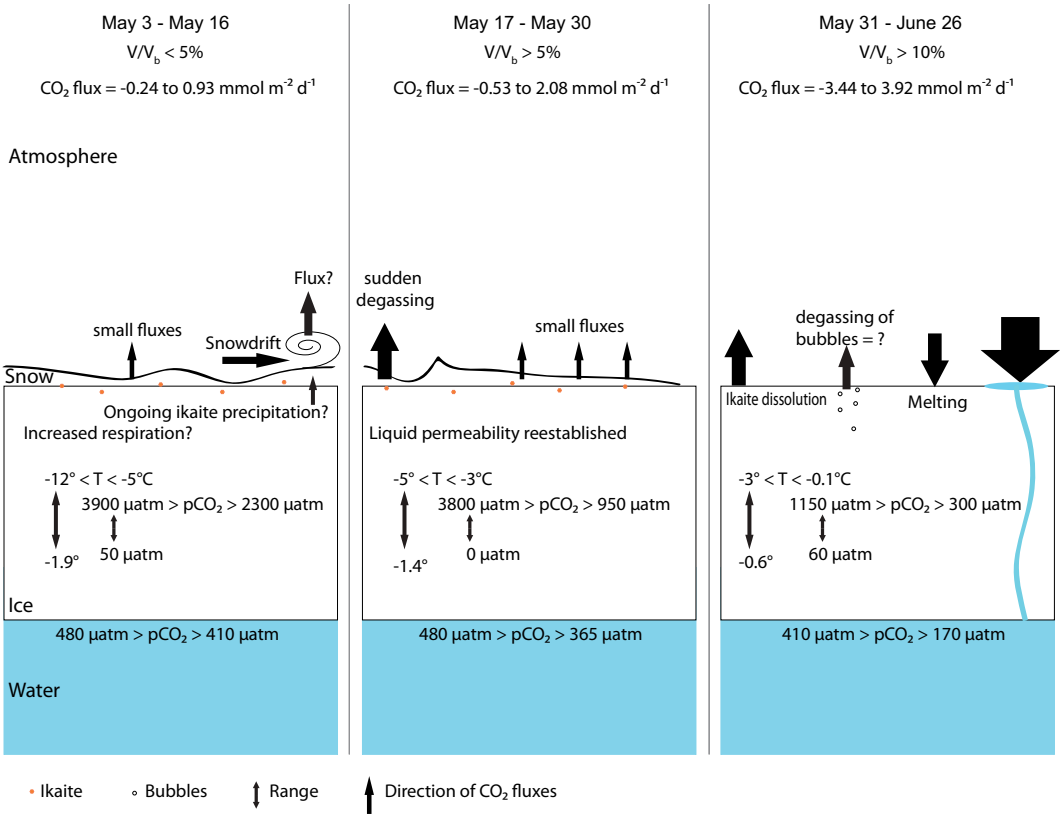

Figure 4.21: Summary of the measured parameters in sea ice and the water column and the resulting directions of fluxes of CO_2 during winter-spring-summer transition above Arctic sea ice, Allen Bay, NU, Canada

ical values of TA =2400 μmol, DIC 2260 μmol for sea ice at that time (Geilfus et al., 2012b) will result in different pCO_2 values at different temperatures. At T=2 °C, S=35, and using the dissociation constants of Mehrbach et al. (1973)), this would result in a pCO_2 of 392 μatm, at T=5 °C the pCO_2 would be at 449 μatm, and at T=0.1 °C would reduce to 359 μatm. This shows that the partial pressure alternates between over and undersaturation with respect to atmospheric values, which therefore likely explains the occurrence of efflux and influx on a diurnal cycle.

Solar radiation can be used as a proxy for primary production. One could hypothesize that with increasing photosynthetic active radiation (PAR) and

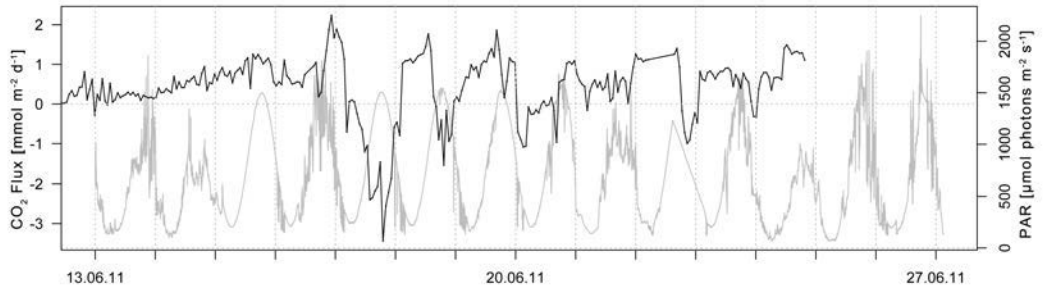

Figure 4.22: Photosynthetic active radiation (PAR, grey) and CO_2 fluxes (black) from mid June 2011 until ice break up on Arctic sea ice without any snow cover, Allen Bay, NU, Canada

subsequent increase in primary production, CO_2 values would decrease, resulting in an influx from the atmosphere to the ice. The influx observed between June 16 and June 20 corresponds to high PAR values (Fig. 4.22). Moreover, analysing PAR versus CO_2 fluxes (Fig. 4.23) confirms that highest influx values correspond to high values of solar radiation. However, influx during low light conditions and efflux during high light conditions were also observed, indicating that other processes may be responsible. Most likely, physical and biological driven processes act concurrently, thus overlapping or amplifying each other.

4.4.3 Effect of melt ponds

Measurements of chamber 1, when sampling site was influenced by melt pond formation, show fluxes 15 times less than reported by Semiletov et al. (2004) who measured an influx up to 51 mmol m^{-2} d^{-1} above melt ponds in the Arctic. However, a remarkable drop of atmospheric CO_2 by almost 10 ppm (Fig. 4.12) is observed at the time of formation of melt ponds. With accelerated melting, melt water, undersaturated with respect to atmospheric carbon dioxide, is effectively taking up atmospheric CO_2. Similar findings are also reported by Nedashkovsky and Shvetsova (2010). Especially melt ponds obviously play

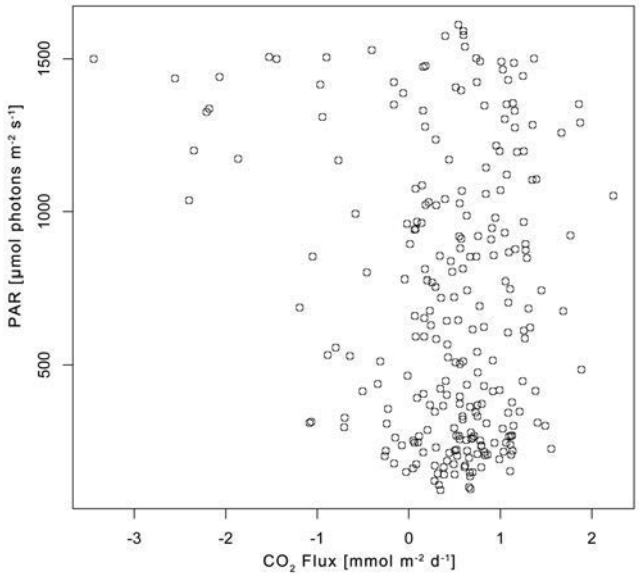

Figure 4.23: Photosynthetic active radiation vs. CO_2 fluxes from mid June 2011 until ice break up on Arctic sea ice without any snow cover, Allen Bay, NU, Canada

an important part in acting as an effective CO_2 sink. Melt ponds are continuously drained to the underlying water while at the same time refilled with fresh melt water low in CO_2. Shallow melt ponds quickly take up CO_2 due to turbulent mixing. Partial pressure of CO_2 in the melt ponds dropped down to approximately 50 μatm within two days when almost no wind was present which is consistent to values reported by Geilfus et al. (2012b). As soon as the wind picked up, CO_2 values again increased (Fig. 4.19). Thus, coupling of dilution due to melting and turbulent mixing due to wind leads to an effective CO_2 sink. This coincides with findings of (Alexkseev and Nagurnyi, 2007) who show that those fluctuations in sea ice regions are observed regularly in the Arctic. Further, Nagurnyi (2008) shows that the seasonal amplitude of CO_2 in the centre of the Arctic Ocean is almost twice as at the coastal monitoring stations, reaching up to 35 ppm, promoting sea ice as the driving factor.

However, a quantification of the possible uptake of CO_2 due to melt pond formation remains elusive since our observations cover only a period of 10 days and the occurrence of melt ponds stretches over several months from May to August while exhibiting different degrees of fractional and absolute melt pond coverage (Rösel and Kaleschke, 2012).

4.4.4 Effect of snow on CO_2 fluxes

Effects of snow on gas exchange between sea ice and the atmosphere have been reported by Nomura et al. (2010b); Geilfus (2011), and Fischer et al. (unpublished). Though, snow is porous and thus permeable for gases (Sommerfeld et al., 1993), it impairs the fluxes between sea ice and atmosphere (Fig. 4.14). However, as soon as snow melts and subsequently vanishes, sea ice is exposed with its bare surface to the atmosphere. Thus, an efflux occurs as long as sea ice is supersaturated in CO_2 with respect to atmospheric values. This effect is clearly represented in Fig. 4.15 where fluxes at the onset of melting become significantly larger than the fluxes observed during snow coverage. However, the question arises why Papakyriakou and Miller (2011) and Miller et al. (2011b) measured significant fluxes above snow-covered sea ice during the cold season using the eddy covariance method. Takagi et al. (2005) show that CO_2 is exchanged with the atmosphere through snow pack by wind-driven mass transfer. Also Colbeck (1989); Albert and Shultz (2002) and Heinesch et al. (2010) show that high winds ventilate the snow and may thus favour gas exchange with the atmosphere. Continuous snow drifts were also observed during our study, promoting the release of CO_2 which potentially was stored within the snow pack. Kelley et al. (1968) already suggested that the accumulated CO_2 within the snow canopy is more rapidly released under conditions of high wind speed. In addition, despite cold air temperatures, temperatures at the sea ice surface might be high enough to allow fluxes as snow isolates the sea ice surface from the cold air (Sturm and Massom, 2010).

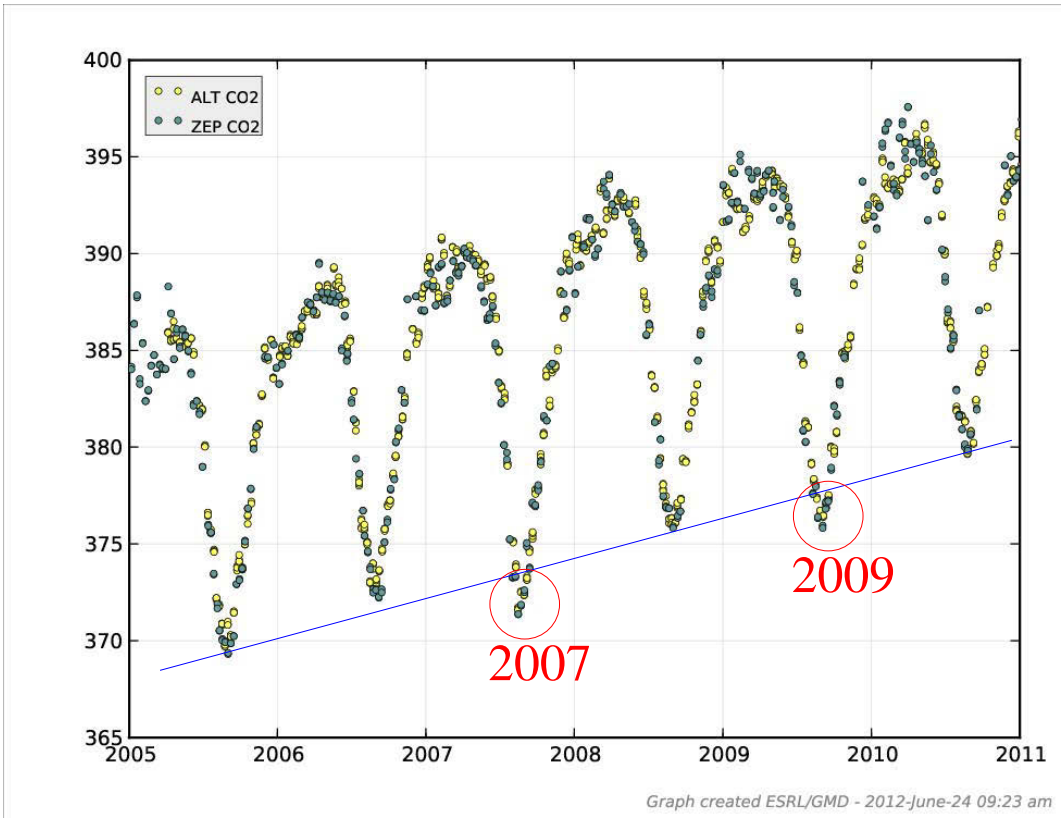

Figure 4.24: Atmospheric CO_2 values between 2005 and 2011 from observatories in Alert, NU, Canada and Ny-Alesund, Svalbard, Norway

Snow thickness itself is influencing the amount of fluxes (Fig. 4.14 and 4.15). Fluxes above a thick layer of snow being lower. Having only two chambers above different snow depths we could not fully unravel the role of snow cover with respect to fluxes of CO_2. Thus, we are still at a stage of uncertainty about the magnitude of air-ice CO_2 exchange above snow covered sea ice and further dedicated research on different surfaces as also proposed by Nomura et al. (2010a,b) is clearly needed.

4.4.5 Implications for Arctic carbon cycle

Fluxes of CO_2 above sea ice occur during all seasons (Delille, 2006; Else et al., 2011; Miller et al., 2011b; Papakyriakou and Miller, 2011; Geilfus et al., 2012b).

However, larger efflux most likely occurs as soon as ice becomes permeable. In addition influx of CO_2 occurs during the melting season when melt water and resulting melt ponds take up large amounts of CO_2 from the atmosphere, which is then transported through the ice boundary layer into the ocean. Biological productivity within sea ice is low during this part of the season (Campbell et al., 2012), which suggest that inorganic processes are the main drivers during this period. However, this might not hold true for the Antarctic and further studies in the Southern Hemisphere are urgently needed.

Melting of sea ice and subsequent occurrence of melt ponds potentially play an important role in the uptake of CO_2 by the ocean. The amplitudes of CO_2 in the years 2007 and 2011 were the highest in the last decade, with enhanced summer lows, (Fig.4.24), which correspond to exceptional melt pond occurrence in the years 2007 and 2011 on the Arctic sea ice (Rösel and Kaleschke, 2012). Very low atmospheric CO_2 values during summer might thus, in addition to primary production, occur due to the melting of sea ice (Rysgaard et al., 2011; Loose et al., 2011a). Further, the amplitude of variations of monthly mean CO_2 concentrations had a tendency to increase between 1994 - 2004 (Nagurnyi, 2008). At the same time the amount of seasonal sea ice has increased compared to multi year sea ice (Maslanik et al., 2007; Lindsay et al., 2008). Therefore, with an increased fraction of seasonal sea ice (Kwok et al., 2009) more CO_2 could be taken up due to the sea ice driven carbon pump (Delille, 2006; Rysgaard et al., 2007), thus resulting in a negative feedback in climate-associated changes in the global carbon cycle (Barber et al., 2012). However, if accelerated reduction of the total sea ice surface (Maslanik et al., 2007; Stroeve et al., 2011) continues, then the vanishing of sea ice in the long run would mean a reduced uptake capacity of the ocean, since the sea ice carbon pump is missing. It is yet not clear if, with sea ice loss, biological CO_2 draw down, due to increasing photosynthesis in Arctic surface waters, will be enhanced under ice-free conditions. Nishino et al. (2011) show that different regions such as the Beaufort Gyre will experience an inhibition of growth of

large-bodied phytoplankton due to nutrient limitation, while conversely other regions outside the Beaufort Gyre potentially experience an enhanced biological pump. Cai et al. (2010) show that in contrast to predicted elevated CO_2 uptake by the ocean due to primary production, potentially the Arctic will not become a CO_2 sink in the future. This demonstrates the importance of sea ice and its related biogeochemical (inorganic and organic) processes for the polar carbon cycle. Therefore, further studies on the polar carbon cycle, including sea ice and under ice-free conditions, are requested to fully assess this unique complex system.

4.5 Conclusion

This study examined the pCO_2 in water, sea ice, and atmosphere and the resulting fluxes between ice and atmosphere in the Canadian Arctic Archipelago from winter conditions into the melting season until sea ice break up. Fluxes of CO_2 between ice and atmosphere were observed during all seasons and ranged between -3.41 to 3.92 mmol m^{-2} d^{-1}. We show that snow is influencing the flux of CO_2 significantly. The presented findings support the thesis of the synchronicity between atmospheric CO_2 and the sea-ice seasonal cycle as described by Halloran (2012) and show the effective uptake of CO_2 from the atmosphere by melt pond formation.

High partial pressures in sea ice of up to ≈ 3900 μatm were observed in the upper layer. Sea ice is oversaturated in CO_2 until late in the melt season, leading to a net efflux during May and June from the sea ice to the atmosphere. We showed, that sea ice brine analyses alone are not sufficient to unravel the inorganic CO_2 cycle within sea ice and that frequency and quantity of gas bubbles within sea ice potentially play a crucial role. Thus, future studies have to take bubble formation within sea ice into account to fully asses the polar carbon cycle.

The presented observations refine the knowledge of the CO_2 flux across the

air-ice-ocean boundary layer from winter conditions until ice break up. To fully asses the CO_2 flux due to the sea ice driven carbon cycle, studies over the complete seasonal cycle of sea ice growth and decay are encouraged to provide an optimal data set.

Acknowledgements. This research was supported through funding from the Natural Sciences and Engineering Research Council of Canada (NCERC), Canada Research Chairs program (CRC), Polar Continental Shelf Program (PCSP) of Natural Resources Canada, the Centre for Earth Observation Sciences (CEOS) at the University of Manitoba and the Alfred Wegener Institute for Polar and Marine Research, Germany. We thank Gernot Nehrke for very useful comments that helped to crystallize our discussion. We thank Bruce Johnson for the support during the field work.

Chapter 5

Synthesis

The publications presented in this thesis deal with the polar carbon cycle. Investigations involved the study of $CaCO_3$ precipitation in Antarctic sea ice and the physical and biogeochemical environment, which potentially influences the precipitation of calcium carbonate. Longterm continuous (24 hours) CO_2 flux measurements over sea ice, using the chamber technique, were introduced for the first time and subsequently used in a follow-up project measuring synchronously ice-atmosphere CO_2 fluxes, atmospheric CO_2, and in situ pCO_2 in sea ice and the water column. Major findings are summarized below and will be elaborated in a broader context of the polar carbon cycle and its implication for the polar regions.

5.1 Major findings in the context of the polar carbon pump

5.1.1 Insignificant impact of $CaCO_3$ precipitation on the annual CO_2 flux?

Precipitation of $CaCO_3$ in sea ice is thought to drive significant CO_2 uptake by the ocean (Rysgaard et al., 2007, 2012). One mol of CO_2 is produced per mol

of precipitated $CaCO_3$. The publication in chapter 2 provides a first estimate of the possible contribution of calcium carbonate precipitation to the carbon cycle. The calculations showed that $CaCO_3$ formation in sea ice could potentially represent a contribution of between 0.1 and 9 Tg C a^{-1} to the carbon flux in the polar oceans in both hemispheres. This corresponds to only $\approx 5\%$ of the total carbon flux of the high-latitude oceans (Takahashi et al., 2009). However, the large heterogeneity observed in the distribution of ikaite makes such an estimate highly uncertain. Thus, at present it is not fully understood to which extent $CaCO_3$ precipitation contributes to the annual polar carbon flux. Moreover, the amount of CO_2 which is released to the atmosphere or to the underlying water column, respectively, due to the precipitation of $CaCO_3$ also remains elusive. If all of the CO_2, which is produced during the precipitation of $CaCO_3$, would be released to the atmosphere, since $CaCO_3$ most likely occurs only in the uppermost layers of sea ice, then the consumption of CO_2 during dissolution of the mineral during the melting phase (Rysgaard et al., 2012; Nomura et al., ress) would balance the efflux during precipitation. Thus $CaCO_3$ would not contribute to the polar carbon cycle. However, as soon as excess CO_2 due to calcium carbonate precipitation is rejected together with brine to the underlying column, then the mineral is potentially rendered an important role in the polar carbon cycle as proposed by (Rysgaard et al., 2007, 2012).

Rysgaard et al. (2011) and Geilfus (2011) assume a homogenous precipitation of $CaCO_3$ across the whole sea ice column. However, our data (Chapter 2) show that the precipitation of ikaite occurs predominantly in the uppermost layers. This coincides with findings of Munro et al. (2010) where stable carbon isotopic signatures in sea ice suggest that significant $CaCO_3$ precipitation occurs in the uppermost layers of ice. Thus, the calculations as presented in Rysgaard et al. (2011) might result in an overestimation of the fluxes of CO_2. Hence, it is difficult to fully assess the contribution of $CaCO_3$ to the polar carbon cycle.

Recent studies elaborated the influence of abiotic processes on the sea ice carbon cycle (Munro et al., 2010; Geilfus, 2011). Though it is still uncertain if CO_2 degassing, due to brine enrichment, or $CaCO_3$ precipitation is the dominant process leading to DIC depletion, Munro et al. (2010) and Geilfus (2011) consider CO_2 degassing as the only responsible process and $CaCO_3$ precipitation as a minor effect. This would suggest that $CaCO_3$ precipitation and dissolution during the annual cycle of sea ice growth and decay would not contribute significantly to the polar carbon pump.

5.1.2 Under estimated ice-atmosphere CO_2 flux?

The review of processes controlling the air-sea exchange of CO_2 during the cycle of sea ice growth and decay by Rysgaard et al. (2011) and Loose et al. (2011a) show the importance of the ice covered oceans in the global carbon cycle. Several processes are elaborated with a focus on abiotic processes, which are controlled by sea ice physics and geochemistry. Though sea ice-atmosphere fluxes of CO_2 are acknowledged in these reviews they are only considered as minor and negligible. Rysgaard et al. (2011) conclude that the largest flux of CO_2 is driven by brine drainage to the under-ice water, which is subsequently sequestered into deep water masses. Their calculations of the air-sea flux of CO_2 due to the sea ice carbon pump are based on values of TA and DIC of initial conditions of the surface oceanic water mass from which sea ice is formed and the sea ice itself. The fluxes of CO_2 from sea ice to the atmosphere are not incorporated. Although the rejection of DIC together with brine from growing sea ice is the dominant process of the sea ice carbon pump, the continuously measured ice-atmosphere fluxes (Chapter 3 and 4) revealed that they are significant and can therefore not be ignored. Hence, they have to be taken into account when it comes to budgeting of the sea ice carbon cycle.

Sea ice degasses during most of the seasonal cycle of sea ice growth and decay. In the previous chapter, fluxes during winter, spring, and summer con-

ditions are shown. Small fluxes were observed above cold sea ice ($T < -8°C$) consistent with observations over winter sea ice by Heinesch et al. (2010) and Miller et al. (2011b) using the eddy covariance technique. However, our measurements and those of Geilfus et al. (2012b) show that fluxes above very cold sea ice ($T < -11°C$) are most likely not significant. Fluxes from growing sea ice have been reported from natural and artificial sea ice, respectively (Nomura et al., 2006; Geilfus, 2011; Miller et al., 2011a). If we take the mean flux values of 0.7 mmol m^{-2} d^{-1} in Nomura et al. (2006) and 6.7 mmol m^{-2} d^{-1} of Geilfus (2011) respectively between ice and atmosphere in the Arctic, for an annual ice cover (first-year ice, assuming sea ice growth to occur only once) (Comiso, 2010) and integrating these values over one week, we would see a carbon flux between 0.4 to 3.9 Tg C during this period of sea ice growth. Geilfus (2011) reports fluxes of 0.01 Pg C by calculating the fluxes from DIC depletion. Since sea ice permeability will not be cut off immediately after the first layer of sea ice has formed, we can expect larger ice-atmosphere fluxes during sea ice growth. While fluxes in winter most likely are not significant, further degassing can be expected during spring as long as sea ice is supersaturated in CO_2 with respect to atmospheric values (Chapter 4). Miyake and Matsuo (1963) already suggested degassing of CO_2 from melting sea ice. Geilfus et al. (2012b) report fluxes above bare sea ice between 0.84 to -2.63 mmol m^{-2} d^{-1} during spring. They are in the same range as the values provided in chapter 4. Using the mean flux in May and June of 0.3 mmol m^{-2} d^{-1} (Chapter 4) and the annual first-year ice cover from Comiso (2010) results in an ice-atmosphere carbon flux of 1.5 Tg C during this period in the Arctic. However, Geilfus (2011) argued that efflux, measured with the chamber technique, could be underestimated by a factor of 4. Thus, the ice-atmosphere flux presented above may potentially be significantly higher. The calculated fluxes from DIC depletion (Geilfus, 2011) are between the range reported from eddy covariance and chamber technique. At this point the reason of the differences between both methods remain unclear. Although these methods measure at different temporal and spatial

scales, they should result in similar annual values. Hence, further evaluation of both methods is required to validate the measured fluxes. Continuous measurements in particular are needed to differentiate between single outbursts and continuous efflux or influx in order to assess a reliable budget of the CO_2 flux between sea ice and atmosphere.

Most of the sea ice in both hemispheres is covered with snow (Sturm and Massom, 2010). While there are good data sets of the Arctic snow cover, data is lacking from Antarctic sea ice. Flux measurements of CO_2 above snow are rare (Chapter 3, 4). Snow effectively influences the flux of gases between ice and atmosphere (Chapter 3 and references therein). Mostly fluxes of CO_2 are lower compared to measurements above bare sea ice. In contrast, Geilfus et al. (2012b) report higher fluxes above snow. Large influx is likely to occur, especially when snow is melting. Snow influences the sea ice in several ways i.e. by its insulative properties and as a source of freshwater to the ocean when it melts (Sturm and Massom, 2010). Insulating the sea ice surface from the atmosphere results in higher sea ice temperature and may therefore extend the time during which sea ice is permeable for gas transport. At this point it is not clear if this effect would lead to further degassing of CO_2 which might subsequently be stored in the snow layer. This is pure speculation but would be significant for the transport of CO_2 across ice and snow to the atmosphere. If this would be the case, then dislocation of snow (snow drift) due to strong winds might result in peaks of CO_2 release to the atmosphere and would explain efflux as observed by Heinesch et al. (2010). Thus, snow may be a crucial component in polar CO_2 atmosphere-ice-ocean interactions.

5.1.3 Potential significance of bubbles in sea ice

In chapter 4 the observation of bubbles and their degassing to the atmosphere is described. Although acknowledged by several authors (i.e. Thomas and Dieckmann 2010; Papadimitriou et al. 2012), bubble formation in sea ice has

received only little attention to date. Especially with regard to fluxes between ice and atmosphere this phenomenon has been largely ignored. Gas inclusions in sea ice resulting from biogeochemical processes were already suggested in the 1940's (Tsurikov, 1979, and references therein). Matsuo and Miyake (1966) were, to the best of my knowledge, the first to study the gas composition in sea ice in more detail. They analyzed pressure and gas composition of bubbles within sea ice. Killawee et al. (1998) analyzed the segregation of solutes and gases in artificial sea ice. They found very high CO_2 concentrations up to 63% within the bubbles. However the average CO_2 concentration was $2.69 \pm 0.45\%$, which is still significantly higher than in the atmosphere. The most recent study on gas content and composition in young sea ice has been conducted by Tison et al. (2002). They ascribe their high CO_2 concentrations found in artificial sea ice to the biases in their experimental settings. However, their range of total gas content values ($3.5 - 18$ ml STP kg^{-1}, STP = standard temperature and pressure = 0°C and 1.01325 bar) are comparable to the measurements of Matsuo and Miyake (1966) ($2.2 - 21.2$ ml STP kg^{-1}). Data on gas composition of bubbles in natural sea ice are scarce. Only a few are provided by Matsuo and Miyake (1966) with a range of CO_2 between 0.53 to 24.3% and by Bruns (1937) in Tsurikov (1979) with a range of CO_2 between 0.4 to 0.6%.

Though the values are only provided for Antarctic sea ice, they are assumed to be valid for Arctic sea ice in the following simple calculation. The volume of sea ice in both hemisphere is calculated with the seasonal ice cover in the Antarctic (Comiso, 2010) having an average thickness of 0.62 m (Worby et al., 2008) and the seasonal ice cover in the Arctic (Comiso and Nishio, 2008) having an average thickness of 1.06 m (Kwok et al., 2009) resulting in a volume of $9.9 * 10^{12}$ m^3 and $8.5 * 10^{12}$ m^3, respectively. With a sea ice density of 930 kg m^{-3} and the values of gas content and composition from Matsuo and Miyake (1966) and Killawee et al. (1998) this would result in a storage capacity of between 1 and 47 Tg C in the gas bubbles in sea ice at its maximum extent. However, the latter seems to be unrealistically high compared to the

numbers proposed by Rysgaard et al. (2011). If one would take the average CO_2 concentration of 2.69 % from Killawee et al. (1998), this would result in a range between 0.5 and 5.2 Tg C, which is stored in the seasonal ice cover in both hemisphere. Although these numbers are highly uncertain since they rely only on a few measurements, they show the potential significance of gas bubbles in sea ice. Thus, when budgeting the sea ice driven carbon pump, they have to be taken into account, if most of them would be released to the atmosphere during sea ice melt. However, further studies of the gas content and composition in natural sea ice during each stage of sea ice growth and decay, relating flux measurements, and on the fate of bubbles within sea ice during sea ice melt are urgently needed to fully asses their contribution to the sea ice carbon cycle.

5.1.4 Improved understanding of the sea ice carbon pump

Sea ice is a very active component in the polar carbon cycle. The findings described in the chapters and sections above strengthen the concept of the sea ice driven polar carbon pump at high latitudes and support its acceptance within the sea ice-biogeochemistry community (Delille et al., 2007; Delille, 2010; Rysgaard et al., 2011; Loose et al., 2011a; Miller et al., 2011b; Geilfus et al., 2012b; Papadimitriou et al., 2012). Further, they improve the state of knowledge of the carbon dynamics within sea ice. A consolidation of the conceptual models of seasonal carbon fluxes in ice-covered seas as presented by Delille (2010); Geilfus (2011), and Rysgaard et al. (2011) is provided in Figure 5.1. The findings from the chapters and sections above are incorporated in this schematic.

During sea ice formation in Autumn CO_2 is released to atmosphere (Else et al., 2011; Miller et al., 2011a) while at the same time DIC is rejected together with brine to the underlying water column (Miller et al., 2011a; Rysgaard et al., 2007). In addition $CaCO_3$ precipitates in frost flowers (Geilfus, 2011) and the

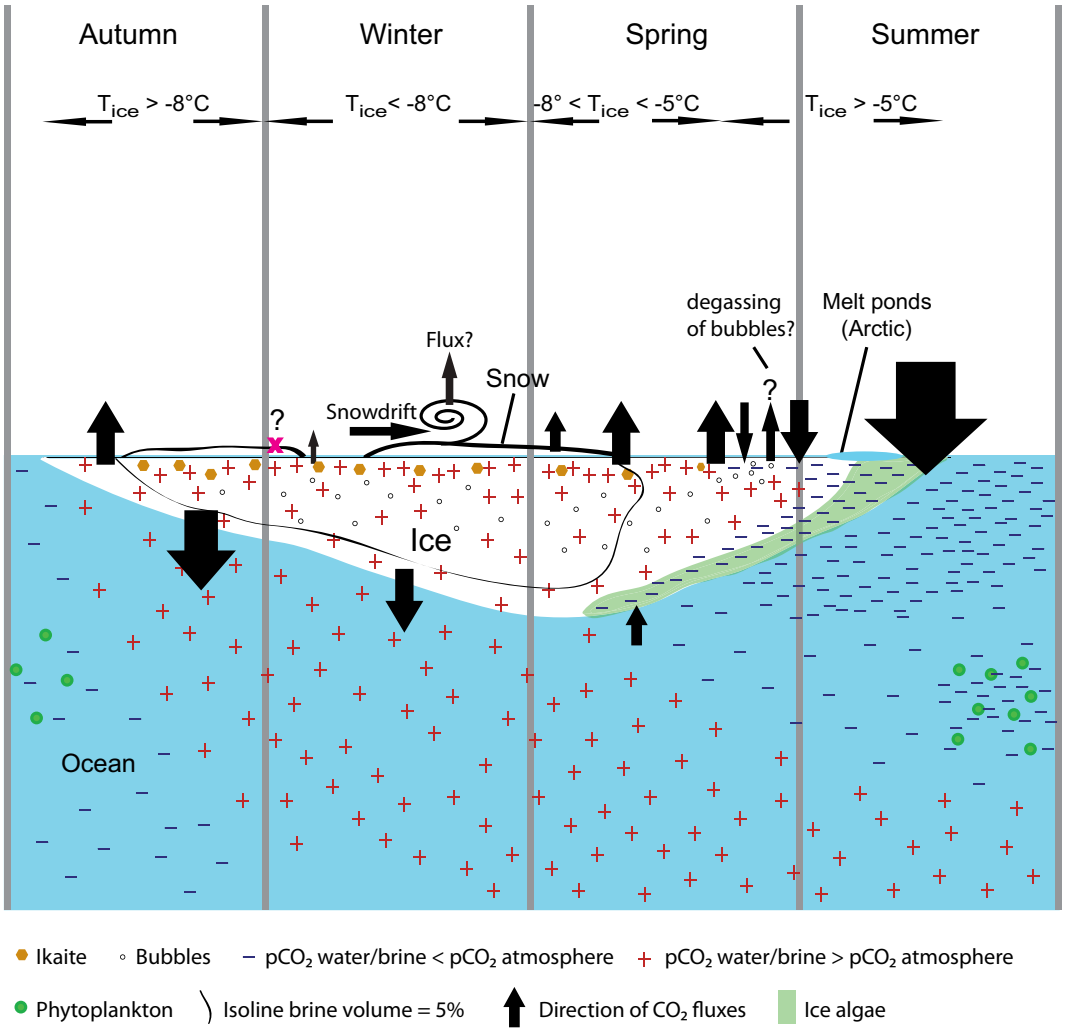

Figure 5.1: Illustration of the involved components of the sea ice carbon pump and relating carbon fluxes throughout the seasonal cycle. Modified after Delille (2010); Geilfus (2011); Rysgaard et al. (2011)

upper layers of sea ice (Fischer et al., 2013) releasing CO_2. However, it remains unclear if the CO_2 released during the formation of ikaite completely degasses to the atmosphere or partly contributes to the increase in pCO_2 within sea ice brine as proposed by Rysgaard et al. (2007). Further, it also remains elusive if $CaCO_3$ continues to precipitate during winter. Fluxes above winter sea ice as observed by Heinesch et al. (2010) and Miller et al. (2011b) might be an indicator for this process, since sea ice, reaching the threshold of permeability (Golden et al., 1998), is thought to impede gas fluxes from the interior. However, Geilfus (2011) and Miller et al. (2011b) report occasional fluxes of CO_2 above cold sea ice ($T_{ice} < 5°C$), especially during periods of high wind speed. Although this is pure speculation, it is plausible that snow isolates the sea ice surface from the cold air (Sturm and Massom, 2010) leading to temperatures still high enough to allow fluxes from the sea ice. Carbon dioxide might accumulate within the snow canopy (Kelley et al., 1968) and is subsequently released under conditions of high wind speed, which ventilates the snow (Colbeck 1989; Albert and Shultz 2002, and Chapter 4). Thus, the events of snow drift might favour the gas exchange across the ice-snow-atmosphere boundary layer. As spring arrives sea ice is still supersaturated in CO_2 with respect to atmospheric values. Observations as described in chapter 4 show that a sudden outburst may occur at this time of year as soon as the permeability of sea ice is re-established. Further degassing might be reduced due to the appearance of super imposed ice, which can effectively stop gas exchange between sea ice and atmosphere (Geilfus, 2011). The findings in chapter 4 show that sea ice does not rapidly turn from a source to a sink of CO_2. Different processes seem to overlay each other. Primary production in the bottom layer of sea ice consumes CO_2 leading to an undersaturation of CO_2 in the lower parts of the sea ice body (Rysgaard et al., 2011; Loose et al., 2011a). Sea ice may still release CO_2 to the atmosphere while at the same time melt pond formation and drainage reverse the flux of CO_2, resulting in an effective transport regime of the greenhouse gas from the atmosphere to the ocean. Increasing brine vol-

ume ($V_b > 10\%$) leads to a mobilization of bubbles, which then start to escape from the ice. Therefore efflux and influx may occur at the same time.

Measurements of pCO_2 in melt ponds (Chapter 4) and adjacent wind speed show that melt ponds effectively enhance the flux of CO_2 from the atmosphere to the ocean. If we take mean DIC and TA values of sea ice meltwater from Rysgaard et al. (2012), the low pCO_2 value of 50 μatm in the melt ponds, the wind speed from chapter 4, and using the dissociation constants for carbonic acid from Mehrbach et al. (1973) refitted by Dickson and Millero (1987), we would get an influx of up to -45.4 mmol m^{-2} d^{-1}. This value corresponds very well with fluxes reported by Semiletov et al. (2004) and Nomura et al. (2010a). For a simple calculation to asses the impact of melt ponds occurrence on the atmosphere-ice flux we use the mean melt pond area of $1.49 * 10^6$ km^2 as reported by Rösel and Kaleschke (2012), the low fluxes as reported by Geilfus et al. (2012b), the high fluxes as calculated above and reported by Semiletov et al. (2004), and integrate them over 6 weeks (see Rösel and Kaleschke (2012)). The result shows a potential influx between 2 Tg C and 34 Tg C during this period. This calculation is a first estimate and needs further refinement. However, it shows the potential significance of melt ponds in the sea ice carbon cycle. During summer, several processes i.e. dilution of the surface water through sea ice meltwater, primary production of sea ice algae, and pelagic primary production in the surface water lead to further reduction of surface water pCO_2, resulting in an enhanced air-sea flux of CO_2.

5.1.5 Negative feedback on climate-associated changes in the global carbon cycle?

The Fifth Assessment Report (AR5) of the IPCC is underway. It will most probably confirm the findings of the IPCC Report 2007 (IPCC, 2007) of a reduced sea ice cover in the Arctic. The transition towards a seasonally open Arctic Ocean is expected (Lindsay et al., 2008; Stroeve et al., 2011). The

question that arises is what impact has the retreat of the Arctic sea ice have on the polar carbon pump as described by Rysgaard et al. (2011); Loose et al. (2011a), and chapter 1?

Multi-year sea ice is disappearing (Stroeve et al., 2011) while at the same time an increase of the fraction as well as the absolute area of first-year ice is observed (Kwok et al., 2009). An increasing area of first year sea ice would mean a strengthening of the proposed carbon pump by Rysgaard et al. (2007), since a larger area would undergo the cycle of sea ice growth and decay. Moreover, recent studies show an increase of the melt season length by almost 20 days during the last 30 years (Markus et al., 2009). Having a longer period of continuous melt and more seasonal sea ice would lead to a higher carbon uptake capacity of the ocean due to the sea ice driven carbon pump during each seasonal cycle. Thus, these processes would result in a negative feedback in climate-associated changes in the global carbon cycle. With continuous vanishing of sea ice, this process will at some stage be reduced. Therefore the negative feedback is likely to occur only on short time scale, since the sea ice driven carbon pump is reduced with the decrease of the sea ice cover. As pointed out in chapter 4, it is yet not clear if the biological CO_2 draw down, due to increasing photosynthesis in Arctic surface waters, will be enhanced under ice-free conditions. Nishino et al. (2011) show that different regions such as the Beaufort Gyre will experience an inhibition in the growth of large-bodied phytoplankton due to nutrient limitation, while conversely other regions outside the Beaufort Gyre will potentially experience an enhanced biological carbon pump. Cai et al. (2010) show that in contrast to predicted elevated CO_2 uptake by the ocean due to primary production, most probably the Arctic will not become a CO_2 sink in the future.

At the same time, as pointed out in chapter 1, the Antarctic is experiencing an increase in the total sea ice cover. Thus, the sea ice driven carbon pump in the Southern Ocean will most likely not be affected as it is in the Arctic Ocean. An increasing sea ice cover might in fact enhance the carbon pump.

Since measurements of the CO_2 flux in the Antarctic are scarce, it remains elusive if the increased ice cover in the Antarctic would balance the reduction of the sea ice driven carbon pump in the Arctic.

5.2 Perspectives for future research

The research on processes of the sea ice driven carbon cycle and coupled interactions across the air-ice-ocean boundary layer is a young discipline (Papadimitriou et al., 2012). The data presented in this thesis have contributed to the understanding of the polar carbon cycle in general and the air-ice CO_2 flux and the $CaCO_3$ precipitation within sea ice in particular. However, more research is necessary to unravel the complete sea ice driven carbon cycle during sea ice growth and decay.

Flux measurements above growing and winter sea ice are of particular interest. There have only been a few winter expeditions up to present, resulting in a major gap in our knowledge. Though first attempts have been conducted, they are yet not sufficient for budgeting the carbon fluxes during these seasons, since they only provide data in the Arctic and are limited to single locations. Flux measurements above Antarctic sea ice with both, eddy covariance and chamber measurements are scarce during spring and summer. To the best of my knowledge there are no winter-time flux measurement above Antarctic sea ice and these are therefore strongly encouraged. Findings presented in this study and from Geilfus et al. (2012b) indicate that the sea ice driven carbon pump in the southern hemisphere, although similar to the Arctic, may yield different quantities.

Although extremely ambitious, an optimal data set would be the continuous measurement of all components involved in the sea ice driven carbon pump over the course of a complete cycle of sea ice growth and decay. This would include organic and inorganic components in sea ice and the water column, such as total alkalinity, dissolved inorganic carbon, partial pressure of CO_2, precipita-

tion of $CaCO_3$, primary production, dissolved and particulate organic carbon, dissolved organic matter, extracellular polymeric substances, bacterial abundance and dynamics (respiration), and the resulting fluxes of CO_2 across the atmosphere-ice-ocean boundary layer. Measurements of biogeochemical parameters within sea ice are inherently difficult and different approaches, such as bulk ice or direct brine measurements have been applied. However, none of these methods is appropriate to obtain data at the scale of the microenvironment of brine channels and pockets, since they average out the properties in the obtained samples. New approaches in measuring at these small spatial scales might advance the knowledge of the biogeochemistry within sea ice. A potential approach could be the adaptation of a rhizon in situ sampler used in pore water studies in aquatic sediments (Seeberg-Elverfeldt et al., 2005), although various challenges have to be mastered (i.e. freezing of the sampled brine within the rhizon).

The potential significance of bubble formation within sea ice for the ice-atmosphere gas flux has been shown in this thesis. Thus, further studies on gas content and composition in sea ice should be promoted. A possible study could consist of simultaneous measurements of ice-atmosphere fluxes using the LICOR Automated Soil Flux System (Chapter 3 and 4) and analyses of ice structure and gas inclusions (bubbles) using continuous full core X-ray micro-computed tomography during growth of artificial sea ice. Subsequently, gas inclusions within sea ice could be investigated with Raman spectroscopy as conducted in galcial ice (Weikusat et al., 2012).

Recent measurements of methane in sea ice brine (Damm et al., unpublished data) call for a closer look at other greenhouse gases and their flux across the air-ice-ocean boundary layer. In addition, up-scaling of the findings in this and other recent studies using remote sensing may provide new insights into the global significance of the sea ice driven carbon cycle.

5.3 Conclusion

The sea ice driven polar carbon pump is a uniquely complex system influenced by a concert of biogeochemical processes. The discoveries described in this thesis reflect progress in our understanding and enable improved estimates of the CO_2 flux which drives the sea ice carbon pump. Surface based continuous long-term (24 h) chamber measurements of the sea ice-atmosphere flux of CO_2 have been introduced, verifying the significance of CO_2 degassing from sea ice to the atmosphere. The observed fluxes range between -3.4 and 9.5 mmol m^{-2} d^{-1}. Sea ice is supersaturated in CO_2 which it subsequently releases to the atmosphere until late in the melt season before turning into a sink for CO_2. The average flux of CO_2 during the spring-summer transition above land fast sea ice is estimated to be 0.3 mmol m^{-2} d^{-1}. Based on observations and calculations in section 5.1.2 the efflux from Arctic sea ice to the atmosphere can be expected to result in an annual flux of several Tg C. Thus, fluxes of CO_2 between ice and atmosphere have to be taken into account when it comes to budgeting the sea ice driven carbon pump. The findings in this thesis indicate that snow most probably plays a crucial role in the air-ice exchange of CO_2. Fluxes above sea ice can shift from an efflux to an uptake within 24 hours, demonstrating that fluxes are highly variable on a diurnal basis and continuous measurements are essential.

The occurrence of melt ponds on Arctic sea ice plays a crucial role in the polar carbon cycle. Melt ponds are considered to be responsible for a potential carbon flux of up to 34 Tg C a^{-1} from the atmosphere into the ocean. In addition, the potential degassing of CO_2 due to the release of bubbles from within sea ice might contribute up to $\approx$ 5.2 Tg C to the annual carbon flux in the Arctic and Antarctic. Together these components play a significant role in the sea ice carbon cycle. However, further investigations are needed to validate these findings. In addition an advanced understanding of each subprocess in the sea ice driven carbon cycle and their translation into potential fluxes of

CO_2 is required for an improved budgeting of the polar carbon cycle. For example, conditions at the time of precipitation of ikaite within sea ice and its fate during sea ice melt have to be further investigated in general and for its significance for the carbon cycle in particular. Moreover, dissociation constants for carbonic acid need to be urgently extended to high salinities ($S > 50$) and subzero temperatures.

The investigation of the components of the sea ice driven carbon cycle over a complete seasonal cycle of sea ice growth and decay are encouraged to provide an optimal data set. However, a priority should be the examination of the biogeochemical processes and resulting fluxes of CO_2 across the air-ice-ocean boundary layer in the ice covered southern ocean. Accepted by the sea-ice-biogeochemical community, the concept of the sea ice driven carbon pump and the presented refinements in this thesis are at the forefront of polar research and needs further propagation outside the community to be incorporated, for example, in model calculations of the global carbon cycle.

Bibliography

Aagaard, K., Swift, J., and Carmack, E. (1985). Thermohaline circulation in the Arctic Mediterranean Seas. *Journal of Geophysical Research*, 90:4833 – 4846, doi:10.1029/JC090iC03p04833.

Albert, M. R. and Shultz, E. F. (2002). Snow and firn properties and air-snow transport processes at Summit, Greenland. *Atmospheric Environment*, 36:2789–2797, doi:10.1016/S1352-2310(02)00119-X.

Alexkseev, G. V. and Nagurnyi, A. P. (2007). Role of Sea Ice in the Formation of Annual Carbon Dioxide Cycle in the Arctic. *Doklady Earth Sciences*, 417A:1398 – 1401.

Anderson, L., Falck, E., Jones, E. P., Jutterström, S., and Swift, J. (2004). Enhanced uptake of atmospheric CO_2 during freezing of seawater: A field study in Storfjorden, Svalbard. *Journal of Geophysical Research*, 109:C06004, doi:10.1029/2003JC002120.

Anderson, L. G. and Jones, E. P. (1985). Measurement of total alkalinity, calcium, and sulfate in natural sea ice. *Journal of Geophysical Research*, 90:9194 – 9198.

Aslam, S., Underwood, G. J. C.and Kaartokallio, H., Norman, L., Autio, R., Fischer, M., Kuosa, H., Dieckmann, G. S., and Thomas, D. (2012). Dissolved extracellular polymeric substance (dEPS) dynamics and bacterial growth during sea ice formation in an ice tank study. *Polar Biology*, 35:661 – 676, doi:10.1007/s00300-011-1112-0.

Baldocchi, D. (2003). Assessing the eddy covariance technique for evaluating carbon dioxide exchange rates of ecosystems: past, present and future. *Global Change Biology*, 9:479 – 492.

Baldocchi, D., Hinks, B., and Meyers, T. (1988). Measuring Biosphere-Atmosphere Exchanges of Biologically Related Gases with Micrometeorological Methods. *Ecology*, 69:1331 – 1340.

Barber, D., Asplin, M., Papakyriakou, T., Miller, L., Else, B., Iacozza, J., Mundy, C., Gosselin, M., Asselin, N., Ferguson, S., Lukovich, J., Stern, G., Gaden, A., Pucko, M., Geilfus, N.-X., and Wang, F. (2012). Consequences of change and variability in sea ice on marine ecosystem and biogeochemical processes during the 2007-2008 Canadian International Polar Year program. *Climate Change*, 115:135 – 159, doi:10.1007/s10584-012-0482-9.

Bates, N. R. (2006). Air-sea CO_2 fluxes and the continental shelf pump of carbon in the Chukchi Sea adjacent to the Arctic Ocean. *Journal of Geophysical Research*, 111:C10013, doi:10.1029/2005JC003083.

Bates, N. R. and Mathis, J. T. (2009). The Arctic Ocean marine carbon cycle: evaluation of air-sea CO_2 exchanges, ocean acidification impacts and potential feedbacks. *Biogeosciences*, 6:2433 – 2459.

Berner, R., Westrich, J., Graber, R., Smitz, J., and Martens, C. (1978). Inhibition of aragonite precipitation from supersaturated seawater. *Amer. J. Sci.*, 278:816 – 837.

Bischoff, J. L., Fitzpatrick, J. A., and Rosenbauer, R. J. (1993). The Solubility and Stabilization of ikaite $CaCO_3 \cdot 6H_2O$ from 0° to 25°C: Environmental and Paleoclimatic Implications for Thinolite Tufa. *The Journal of Geology*, 101:21 – 33.

Borges, A. V., Delille, B., and Frankignoulle, M. (2005). Budgeting sinks and

sources of CO_2 in the coastal ocean: Diversity of ecosystem counts. *Geophys. Res. Lett.*, 32:L14601, doi:10.1029/2005GL023053.

Bowman, J. and Deming, J. (2010). Elevated bacterial abundance and exopolymers in saline frost flowers and implications for atmospheric chemistry and microbial dispersal. *Geophys. Res. Lett.*, 37:L13501.

Burba, G. and Anderson, D. (2007). *Introduction to the eddy covariance method: General Guidelines, and conventional workflow.* LI-COR Biosciences.

Cai, W.-J., Chen, L., Chen, B., Gao, Z., Lee, S. H., Chen, J., Pierrot, D., Sullivan, K., Wang, Y., Hu, X., Huang, W.-J., Zhang, Y., Xu, S., Murata, A., Grebmeier, J. M., Jones, E. P., and Zhang, H. (2010). Decrease in the CO_2 Uptake Capacity in an Ice-Free Arctic Ocean Basin. *Science*, 329:556 – 559, doi:10.1126/science.1189338.

Cai, W.-J. and Dai, M. (2004). Comment on "Enhanced Open Ocean Storage of CO_2 from Shelf Sea Pumping". *Science*, 306:1477, doi:10.1126/science.1102132.

Campbell, K., Mundy, C., Barber, D., and Gosselin, M. (2012). Time series measurements of ice algae biomass using transmitted irradiance and assessment of influential physical variables over the spring melt period. *Journal of Marine Systems.* submitted.

Chen, C.-T. A. and Borges, A. V. (2009). Reconciling opposing views on carbon cycling in the coastal ocean: Continental shelves as sinks and near-shore ecosystems as sources of atmospheric CO2. *Deep Sea Research Part II: Topical Studies in Oceanography*, 56:578 – 590, doi:10.1016/j.dsr2.2009.01.001.

Colbeck, S. (1989). Air movement in snow due to windpumping. *Journal of Glaciology*, 35:209 – 213.

Comiso, J. C. (2010). Large-scale Characteristics and Variability of the Global Sea Ice Cover. In Thomas, D. N. and Dieckmann, G. S., editors, *Sea Ice: An introduction to its physics, chemistry, biology and geology*. Blackwell, Oxford.

Comiso, J. C. and Nishio, F. (2008). Trends in the sea ice cover using enhanced and compatible AMSR-E, SSM/I, and SMMR data. *Journal of Geophysical Research*, 113:C02S07, doi:10.1029/2007JC004257.

Cox, G. and Weeks, W. (1986). Changes in the salinity and porosity of sea-ice samples during shipping and storage. *Journal of Glaciology*, 32:371 – 375 371 – 375.

Delille, B. (2006). *Inorganic carbon dynamics and air-ice-sea CO_2 fluxes in the open and coastal waters of the Southern Ocean*. PhD thesis, Université de Liège, Liège.

Delille, B. (2010). Sea-ice CO_2 dynamics and related air-sea CO_2 fluxes. *SOLAS News*, 11:7.

Delille, B., Jourdain, B., Borges, A. V., Tison, J.-L., and Delille, D. (2007). Biogas CO_2, O_2, dimethylsulfide dynamics in spring Antarctic fast ice. *Limnol. Oceanogr*, 52(4):1367 – 1379.

Dickens, B. and Brown, W. B. (1970). The Crystal Structure of Calcium Carbonate Hexahydrate at $\sim$ - 120°. *Inorganic Chemistry*, 9(3):480 – 486.

Dickson, A. G. and Millero, F. J. (1987). A comparison of the equilibrium constants for the dissociation of carbonic acid in seawater media. *Deep-Sea Research*, 34(10):1733 – 1743.

Dieckmann, G. and Hellmer, H. (2010). The Importance of Sea Ice: An Overview. In Thomas, D. N. and Dieckmann, G. S., editors, *Sea Ice: An introduction to its physics, chemistry, biology and geology*. Blackwell, Oxford.

Dieckmann, G. S., Nehrke, G., Papadimitriou, S., Göttlicher, J., Steininger, R., Kennedy, H., Wolf-Gladrow, D., and Thomas, D. N. (2008). Calcium carbonate as ikaite crystals in Antarctic sea ice. *Geophys. Res. Lett.*, 35:L08501, doi:10.1029/2008GL033540.

Dieckmann, G. S., Nehrke, G., Uhlig, C., Göttlicher, J., Gerland, S., Granskog, M. A., and Thomas, D. N. (2010). Brief communication: ikaite $CaCO_3$*$6H_2O$ discovered in Arctic sea ice. *The Cryosphere*.

Eicken, H. (2003). From the Microscopic, to the Macroscopic, to the Regional Scale: Growth, Microstructure and Properties of Sea Ice. In Thomas, D. N. and Dieckmann, G. S., editors, *Sea Ice: An introduction to its physics, chemistry, biology and geology*, chapter 2, pages 22–81. Blackwell.

Eicken, H., Gradinger, R. Salganek, M., Shirasawa, K., Perovich, D., and Leppäranta, M., editors (2010). *Field Techniques for Sea-Ice Research*. University of Alaska Press, Fairbanks, USA.

Eicken, H., Krouse, H., Kadko, D., and Perovich, D. K. (2002). Tracer studies of pathways and rates of meltwater transport through Arctic summer sea ice. *Journal of Geophysical Research*, 107:8046, doi:10.1029/2000JC000583.

Else, B. G. T., Papakyriakou, T. N., Galley, R. J., Drennan, W. M., Miller, L. A., and Thomas, H. (2011). Wintertime CO_2 fluxes in an Arctic polynya using eddycovariance: Evidence for enhanced air-sea gas transfer during ice formation. *Journal of Geophysical Research*, 116:C00G03, doi:10.1029/2010JC006760.

Emerson, S. and Hedges, J. (2008). *Chemical Oceanography and the Marine Carbon*. Cambridge University Press, Cambridge, United Kingdom and New York, NY, USA.

Etheridge, D., Steele, L., Langenfelds, R., Francey, R., Barnola, J.-M., and Morgan, V. (1996). Natural and anthropogenic changes in atmospheric CO_2

over the last 1000 years from air in Antarctic ice and firn. *Journal of Geophysical Research*, 101:4115 – 4128, doi:10.1029/95JD03410.

Feistel, R. (2008). A Gibbs function for seawater thermodynamics for −6 to 80°C and salinity up to 120 g kg^{-1}. *Deep Sea Research Part I*, 55:1639 – 1671.

Fischer, M., Thomas, D., Krell, A., Nehrke, G., Göttlicher, J., Norman, L., Riaux-Gobin, C., and Dieckmann, G. S. (2013). Quantification of ikaite in Antarctic sea ice. *Antarctic Science*, doi:10.1017/S0954102012001150.

Fransson, A., Chierici, M., Yager, P. L., and Smith Jr., W. O. (2011). Antarctic sea ice carbon dioxide system and controls. *Journal of Geophysical Research*, 116:C12035, doi:10.1029/2010JC006844.

Geiger, R., Aron, R., and Todhunter, P. (2009). *The Climate Near the Ground*. Rowman and Littlefield Publishers, Inc., Lanham, USA.

Geilfus, N.-X. (2011). *Inorganic carbon dynamics in coastal arctic sea ice and related air-ice CO_2 exchanges*. PhD thesis, Université de Liège.

Geilfus, N.-X., Delille, B., Verbeke, V., and Tison, J. L. (2012a). Instruments and Methods: Towards a method for high vertical resolution measurements of the partial pressure of CO_2 within bulk sea ice. *Journal of Glaciology*, 58:287 – 300, doi:10.3189/2012JoG11J071.

Geilfus, N.-X., Garnat, G., Papakyriakou, T., Tison, J. L., Else, B., Thomas, H., Shadwick, E., and Delille, B. (2012b). Dynamics of pCO_2 and related air-ice CO_2 fluxes in the Arctic coastal zone (Amundsen Gulf, Beaufort Sea). *Journal of Geophysical Research*, 117:C00G10, doi:10.1029/2011JC007118.

Gibson, J. and Trull, T. (1999). Annual cycle of fCO_2 under sea-ice and in open water in Prydz Bay, East Antarctica. *Marine Chemistry*, 66:187 – 200.

Gitterman, K. E. (1937). *Thermal analysis of seawater*, volume 287. USACREL, Hanover, New Hampshire.

Gleitz, M., Rutgers v.d. Loeff, M., Thomas, D. N., Dieckmann, G. S., and Millero, F. (1995). Comparison of summer and winter inorganic carbon, oxygen and nutrient concentrations in Antarctic sea ice brine. *Marine Chemistry*, 51:81 – 91.

Golden, K., Ackley, S. F., and Lytle, V. (1998). The Percolation Phase Transition in Sea Ice. *Science*, 282:2238 – 2241, doi:10.1126/science.282.5397.2238.

Golden, K., Eicken, H., Heaton, L., Miner, J., Pringle, D., and Zhu, J. (2007). Thermal evolution of permeability and microstructure in sea ice. *Geophys. Res. Lett.*, 34:L16501, doi:10.1029/2007GL030447.

Gosink, T., Pearson, J. G., and Kelley, J. J. (1976). Gas movement through sea ice. *Nature*, 263:41 – 42.

Hales, B., van Geen, A., and Takahashi, T. (2004). High-frequency measurement of seawater chemistry: Flow-injection analysis of macronutrients. *Limnol. Oceanogr.: Methods*, 2:91 – 101.

Halloran, P. (2012). Does atmospheric CO_2 seasonality play an important role in governing the air-sea flux of CO_2? *Biogeosciences*, 9:2311 – 2323, doi:10.5194/bg-9-2311-2012.

Hanson, H. and Koroleff, F. (1983). Determination of nutrients. In Grasshoff, K., Ehrhardt, M., and Kremling, K., editors, *Methods of Seawater analysis*, pages 159 – 228. Wiley-VCH, Weinheim.

Heinesch, B., Tison, J. L., Carnat, G., Eicken, H., Geilfus, N.-X., Goosens, T., Papakyriakou, T., Yernaux, M., and Delille, B. (2010). Micrometeorological survey of air-sea ice CO_2 fluxes in arctic coastal waters. In *EGU Genral Assembly, 2 - 7 May, 2010, Vienna, Austria.*

Holland, M. and Bitz, C. (2003). Polar amplification of climate change in coupled models. *Climate Dynamics*, 21:221 – 232, doi:10.1007/s00382-003-0332-6.

Hoppe, C. J. M., Langer, G., Rokitta, D., Wolf-Gladrow, D., and Rost, B. (2012). Implications of observed inconsistencies in carbonate chemistry measurements for ocean acidfication studies. *Biogeosciences*, 9:2401 – 2405.

Horner, R., Ackley, S. F., Dieckmann, G. S., Gulliksen, Hoshiai, T., Legendre, L., Melnikov, I. A., Reeburgh, W. S., Spindler, M., and Sullivan, C. W. (1992). Ecology of sea ice biota. *Polar Biology*, 12:417 – 427.

IPCC (2007). *Climate Change 2007: The Physical Science Basis. Contribution of Working Group I to the Fourth Assessment Report of the Intergovernmental Panel on Climate Change [Solomon, S., D. Qin, M. Manning, Z. Chen, M. Marquis, K.B. Averyt, M. Tignor and H.L. Miller (eds.)].* Cambridge University Press, Cambridge, United Kingdom and New York, NY, USA.

Jones, E. P. and Coote, A. R. (1981). Oceanic CO_2 Produced by the Precipitation of $CaCO_3$ From Brines in Sea Ice. *Journal of Geophysical Research*, 86:11,041 – 11,043.

Kandianis, M., Fouke, B., Johnson, J., and Inskeep, W. (2008). Microbial biomass: A catalyst for $CaCO_3$ precipitation in advection-dominated transport regimes. *Geological Society of America Bulletin*, 120:442 – 450.

Kelley, J. J. and Gosink, T. (1979). *Gases in Sea Ice 1975 - 1979.* Final Rep. N000 14-76C-0331. Univ. of Alaska, Fairbanks.

Kelley, J. J., Weaver, D. J., and Smith, B. (1968). The Variation of Carbon Dioxide Under the Snow in the Arctic. *Ecology*, 49:358 – 361.

Killawee, J. A., Fairchild, I. J., Tison, J.-L., Janssens, L., and Lorrain, R. (1998). Segregation of solutes and gases in experimental freezing of di-

lute solutions: Implications for natural glacial systems. *Geochimica et Cosmochimica Acta*, 62(23/24):3637 – 3655.

Kroon, H. (1993). Determination of nitrogen in water: comparison of continuous flow method with on-line UV digestion with the original Kjedahl method. *Anal. Chim. Acta*, 276:287 – 293.

Kwok, R., Cunningham, G., Wensnahan, M., Rigor, I., Zwally, H., and Yi, D. (2009). Thinning and volume loss of the Arctic Ocean sea ice cover: 2003-2008. *Journal of Geophysical Research*, 114:C07005, doi:10.1029/2009JC005312.

Lange, M. (1988). Basic properties of Antarctic sea ice as revealed by texture analysis of ice cores. *Annals of Glaciology*, 10:95 – 101.

Lee, S. H., Stockwell, D., Joo, H., Son, Y., Kang, C., and Whitledge, T. (2012). Phytoplankton production from melting ponds on Arctic sea ice. *Journal of Geophysical Research*, 117:C04030, doi:10.1029/2011JC007717.

Leppäranta, M. and Manninen, T. . (1988). *The brine and gas content of sea ice with attention to low salinities and high temperatures.* Finnish Institute of Marine Research internal report.

Lindsay, R., Zhang, J., Schweiger, A., Steele, M., and Stern, H. (2008). Arctic Sea Ice Retreat in 2007 Follows Thinning Trend. *Journal of Climate*, 22:165 – 176, doi:10.1175/2008JCLI2521.1.

Liu, J., Curry, J., and Hu, Y. (2004). Recent Arctic sea ice variability: connections to the arctic oscillation and the ENSO. *Geophys. Res. Lett.*, 31:L09211.

Loose, B., McGillis, W., Schlosser, P., Perovich, D. K., and Takahashi, T. (2009). Effects of freezing, growth, and ice cover on gas transport processes in laboratory seawater experiments. *Geophys. Res. Lett.*, 36:L05603, doi:10.1029/2008GL036318.

Loose, B., Miller, L., Elliott, S., and Papakyriakou, T. (2011a). Sea ice biogeochemistry and material transport across the frozen interface. *Oceanography*, 24(3):202 – 218, doi:10.5670/oceanog.2011.72.

Loose, B., Schlosser, P., Perovich, D. K., Ringelberg, D., Ho, D., Takahashi, T., Richter-Menge, J. A., Reynolds, C., Mcgillis, W., and Tison, J. L. (2011b). Gas diffusion through columnar laboratory sea ice: implications for mixed-layer ventilation of CO_2 in the seasonal ice zone. *Tellus*, 63B:23 – 39, doi:10.1111/j.1600-0889.2010.00506.x.

Marion, G. M. (2001). Carbonate mineral solubility at low temperatures in the Na-K-Mg-Ca-H-Cl-SO_4-OH-HCO_3-CO_3-CO_2-H_2O system. *Geochimica et Cosmochimica Acta*, 65(12):1883 – 1896.

Markus, T., Stroeve, J., and Miller, J. (2009). Recent changes in Arctic sea ice melt onset, and melt season length. *Journal of Geophysical Research*, 114:C12024, doi:10.1029/2009JC005436.

Maslanik, J., Fowler, C., Stroeve, J., Drobot, S., Zwally, J., Yi, D., and Emery, W. (2007). A younger, thinner Arctic ice cover: Increased potential for rapid, extensive sea-ice loss. *Geophys. Res. Lett.*, 34:L24501.

Matsuo, S. and Miyake, Y. (1966). Gas Composition in Ice Samples from Antarctica. *Journal of Geophysical Research*, 71:5235 – 5241.

Mehrbach, C., Culberson, C., Hawley, J., and Pytkowicz, R. (1973). Measurement of the apparent dissociation constants of carbonic acrid in seawater at atmospheric pressure. *Limnol. Oceanogr.*, 18:897 – 907.

Meiners, K., Norman, L.and Granskog, M. A., Krell, A., Heil, P., and Thomas, D. N. (2011). Physico-ecobiogeochemistry of East Antarctic pack ice during the winter-spring transition. *Deep-Sea Research II*, 58:1172 – 1181, doi:10.1016/j.dsr2.2010.10.033.

Midttun, L. (1985). Formation of dense bottom water in the Barents Sea. *Deep Sea Research*, 32:1233 – 1241.

Miller, L., Garnat, G., Else, B., Sutherland, N., and Papakyriakou, T. (2011a). Carbonate system evolution at the Arctic Ocean surface during autumn freeze-up. *Journal of Geophysical Research*, 116:C00G04, doi:10.1029/2011JC007143.

Miller, L., Papakyriakou, T., Collins, E., Deming, J., Ehn, J., Macdonald, R., Mucci, A., Owens, O., Raudsepp, M., and Sutherland, N. (2011b). Carbon dynamics in sea ice: A winter flux time series. *Journal of Geophysical Research*, 116:C02028, doi:10.1029/2009JC006058.

Millero, F. J., Graham, T. B., Huang, F., Bustos-Serrano, H., and Pierrot, D. (2006). Dissociation constants of carbonic acid in seawater as a function of salinity and temperature. *Marine Chemistry*, 100:80 – 94.

Miyake, Y. and Matsuo, S. (1963). A Role of Sea Ice and Sea Water in the Antarctic on the Carbon Dioxide Cycle in the Atmosphere. *Papers in Meteorology and Geophysics*, 14:120 – 125.

Mundy, C., Gosselin, M., Ehn, J., Belizle, C., Poulin, M., Alou, E., Roy, S., Hop, H., Lessard, S., Papakyriakou, T., Barber, D., and Stewart, J. (2011). Characteristics of two distinct high-light acclimated algal communities during advanced stages of sea ice melt. *Polar Biology*, 34:1869 – 1886, doi:10.1007/s00300-011-0998-x.

Munro, D., Dunbar, R., Mucciarone, D., Arrigo, K. R., and Long, M. (2010). Stable isotope composition of dissolved inorganic carbon and particulate organic carbon in sea ice from the Ross Sea, Antarctica. *Journal of Geophysical Research*, 115:C09005, doi:10.1029/2009JC005661.

Nagurnyi, A. P. (2008). On the Role of the Arctic Sea ice in Seasonal Vari-

ability of Carbon Dioxide Concentration in Northern Latitudes. *Russian Meteorology and Hyrdology*, 33:43 – 47, doi:10.3103/S106837390801007X.

Nagurnyi, A. P. (2010). Analysis of Measurement Data on Carbon Dioxide Concentration in the Near-ice Surface Atmosphere at North Pole-35 Drifting Ice Station (2007-2008). *Ru*, 35:619 – 623.

Nansen, F. (1906). *Northern Waters: Captain Roald Amundsen's oceanographic observations in the Arctic Seas in 1901*. In commission by Jacob Dybwad, Christiania.

Nedashkovsky, A., Khvedynich, S., and Petrovsky, T. (2009). Alkalinity of Sea Ice in the High-Latitudinal Arctic According to the Surveys Performed at North Pole Drifting Station 34 and Characterization of the Role of the Arctic Ice in the CO_2 Exchange. *Marine Chemistry*, 49:61 – 69.

Nedashkovsky, A. and Shvetsova, M. (2010). Total inorganic carbon in sea ice. *Oceanology*, 50:861–868, doi:10.1134/S0001437010060056.

Nishino, S., Kikuchi, T., Yamamoto-Kawai, M., Kawaguchi, Y., Hirawake, T., and Itoh, M. (2011). Enhancement/reduction of biological pump depends on ocean circulation in the sea-ice reduction regions of the Arctic Ocean. *Jounral of Oceanography*, 67:305 – 314, doi:10.1007/s10872-011-0030-7.

Nomura, D., Assmy, P., Nehrke, G., Granskog, M., Fischer, M., Dieckmann, G.S. Fransson, A., Hu, Y., and Schnetger, B. (in press). Characterization of ikaite ($CaCO_3$*$6H_2O$) crystals in first-year Arctic sea ice north of Svalbard. *Annals of Glaciology*.

Nomura, D., Eicken, H., Gradinger, R., and Shirasawa, K. (2010a). Rapid physically driven inversion of the air-sea ice CO_2 flux in the seasonal land fast ice off Barrow, Alaska after onset of surface melt. *Continental Shelf Research*, 30:1998 – 2004, doi:10.1016/j.csr.2010.09.014.

Nomura, D., Yoshikawa-Inoue, H., and Toyota, T. (2006). The effect of sea-ice growth on air-sea CO_2 flux in a tank experiment. *Tellus*, 58b:418 – 426, doi:10.1111/j.1600-0889.2006.00204.x.

Nomura, D., Yoshikawa-Inoue, H., Toyota, T., and Shirasawa, K. (2010b). Effects of snow, snowmelting and refreezing processes on air-sea-ice CO_2 flux. *Journal of Glaciology*, 56(196):262 – 270.

Norman, L., Thomas, D. N., Stedmon, C. A., Granskog, M. A., Papadimitriou, S., Krapp, R. H., Meiners, K. M., Lannuzel, D., van der Merwe, P., and Dieckmann, G. S. (2011). The characteristics of dissolved organic matter (DOM) and chromophoric dissolved organic matter (CDOM) in Antarctic sea ice. *Deep Sea Research Part II*, 58:1075 – 1091, doi:10.1016/j.dsr2.2010.10.030.

Oechel, W., Vourlitis, G., Brooks, S., Crawford, T., and Dumas, E. (1998). Intercomparison among chamber, tower, and aircraft net CO_2 and energy fluxes measured during the Arctic System Science Land-Atmosphere-Ice Interactions (ARCSS-LAII) Flux Study. *Journal of Geophysical Research*, 103:28993 – 29003.

Owens, O. C. (2008). Wintertime measurements of pCO_2 in Arctic Landfast Sea Ice. Master's thesis, University of Manitoba.

Papadimitriou, S., Kennedy, H., Kattner, G., Dieckmann, G. S., and Thomas, D. N. (2004). Experimental evidence for carbonate precipitation and CO_2 degassing during sea ice formation. *Geochimica et Cosmochimica Acta*, 68(8):1749 – 1761, doi:10.1016/j.gca.2003.07.004.

Papadimitriou, S., Kennedy, H., Norman, L., Kennedy, D. P., Dieckmann, G. S., and Thomas, D. N. (2012). The effect of biological activity, $CaCO_3$ mineral dynamics, and CO_2 degassing in the inorganic carbon cycle in sea

ice in late winter-early spring in the Weddell Sea, Antarctica. *Journal of Geophysical Research*, 117:C08011, doi:10.1029/2012JC008058.

Papadimitriou, S., Thomas, D., Kennedy, H., Kuosa, H., and Dieckmann, G. S. (2009). Inorganic carbon removal and isotopic enrichment in Antarctic sea ice gap layers during early austral summer. *Marine Ecology Progress Series*, 386:15 – 27.

Papadimitriou, S., Thomas, D. N., Kennedy, H., Haas, C., Kuosa, H., Krell, A., and Dieckmann, G. S. (2007). Biogeochemical composition of natural sea ice brines from the Weddell Sea during early austral summer. *Limnol. Oceanogr*, 52(5):1809 – 1823.

Papakyriakou, T. and Miller, L. (2011). Springtime CO_2 exchange over seasonal sea ice in the Canadian Arctic Archipelago. *Annals of Glaciology*, 52(57).

Perovich, D. K. and Richter-Menge, J. A. (1994). Surface characteristics of lead ice. *Journal of Geophysical Research*, 99:16,341 – 16,350.

Petrich, C. and Eicken, H. (2010). Growth, Structure, and Properties of Sea Ice. In Thomas, D. N. and Dieckmann, G. S., editors, *Sea Ice*, chapter 2, pages 23 – 77. Wiley-Blackwell Publishing, Oxford.

Pringle, D., Miner, J., Eicken, H., and Golden, K. (2009). Pore space percolation in sea ice single crystals. *Journal of Geophysical Research*, 114:C12017, doi:10.1029/2008JC005145.

Qian, J. and Mopper, K. (1996). An automated, high performance, high temperature combustion dissolved organic carbon analyzer. *Anal. Chem.*, 68:3090 – 3097.

Rankin, A. M. and Wolff, E. W. (2002). Frost flowers: Implications for tropospheric chemistry and ice core interpretation. *Journal of Geophysical Research*, 107:4683, doi:10.1029/2002JD002492.

Repina, I., Semiletov, I., and Smirnov, A. (2007). Eddy correlation measurements of air-sea CO_2 fluxes in the Laptev Sea in the summer period. *Doklady Earth Sciences*, 413:452–456, doi:10.1134/S1028334X07030300.

Robbins, L. L., Hansen, M. E., Kleypass, J. A., and Meylan, S. C. (2010). *CO2calc - A user-friendly seawater carbon calculator for Windows, Max OS X, and iOS (iPhone): U.S. Geological Survey Open-File Report 2010*, volume 1280. U.S. Geological Survey.

Rösel, A. and Kaleschke, L. (2012). Exceptional melt pond occurrence in the years 2007 and 2011 on the Arctic sea ice revealed from MODIS satellite data. *Journal of Geophysical Research*, 117:C05018, doi:10.1029/2011JC007869.

Rothrock, D., Yu, Y., and Maykut, G. (1999). Thinning of Arctic sea-ice cover. *Geophys. Res. Lett.*, 26:3469 – 3472.

Roy, R. N., Roy, L. N., Vogel, K. M., Porter-Moore, C., Pearson, T., Good, C. E., Millero, F. J., and Campbell, D. M. (1993). The dissociation constants of carbonic acid in seawater at salinities 5 to 45 and temperatures 0 to 45°C. *Marine Chemistry*, 44:249 – 267.

Rudels, B., Muench, R., Gunn, J., Schauer, U., and Friedrich, H. (2000). Evolution of the Arctic Ocean boundary current north of the Siberian shelves. *Journal of Marine Systems*, 25:77 – 99, doi:10.1016/S0924-7963(00)00009-9.

Rysgaard, S., Bendtsen, J., Delille, B., Dieckmann, G. S., Glud, R. N., Kennedy, H., Mortensen, J., Papadimitriou, S., Thomas, D. N., and Tison, J. L. (2011). Sea ice contribution to the air-sea CO_2 exchange in the Arctic and Southern Oceans. *Tellus B.*, 63:823 – 830, doi:10.1111/j.1600-0889.2011.00571.x.

Rysgaard, S., Bendtsen, J., Pedersen, L. T., Ramløv, H., and Glud, R. N. (2009). Increased CO_2 uptake due to sea ice growth and de-

cay in the Nordic Seas. *Journal of Geophysical Research*, 114:C09011, doi:10.1029/2008JC005088.

Rysgaard, S., Glud, R., Lennert, K., Cooper, M., Halden, N., Leakey, R. J. G., Hawthorne, F. C., and Barber, D. (2012). Ikaite crystals in melting sea ice - implications for pCO_2 and pH levels in Arctic surface waters. *The Cryosphere*, 6:901 – 908, doi:10.5194/tc-6-901-2012.

Rysgaard, S., Glud, R. N., Sejr, M. K., Bendtsen, J., and Christensen, P. B. (2007). Inorganic carbon transport during sea ice growth and decay: A carbon pump in polar seas. *Journal of Geophysical Research*, 112:C03016, doi:10.1029/2006JC003572.

Sabine, C., Feely, R., Gruber, N., Key, R. M., Lee, K., Bullister, J., Wanninkhof, R., Wong, C., Wallace, D. W., Tilbrook, B., Miller, J. ad Peng, T., Koyzr, A., Ono, T., and Rios, A. (2004). The Oceanic Sink for Anthropogenic CO_2. *Science*, 305:367 – 371, doi:10.1126/science.1097403.

Sala, M., Delmonte, B., Frezzotti, M., Proposito, M., Scarchilli, C., Maggi, V., Artioli, G., M, D., Marino, F., Ricci, P., and De Giudici, G. (2008). Evidence of calcium carbonates in coastal (Talos Dome and Ross Sea area) East Antarctica snow and firn: Environmental and climatic implications. *Earth Planet. Sci. Lett.*, 271(1):43 – 52, doi:10.1016/j.epsl.2008.03.045.

Sander, R., Burrows, J., and Kaleschke, L. (2006). Carbonate precipitation in brine - a potential trigger for tropospheric ozone depletion events. *Atmos. Chem. Phys.*, 6:4653 – 4658.

Sander, R. and Morin, S. (2010). Introducing the bromide/alkalinity ratio for a follow-up discussion on "Precipitation of salts in freezing seawater and ozone depletion events: a status report", by Morin et. al., published in Atmos. Chem. Phys., 8, 7317-7324, 2008. *Atmos. Chem. Phys.*, 10:7655 – 7658.

Sarma, D. (2009). *Geostatistics with Applications in Earth Sciences*. Springer, Heidelberg, 2nd edition.

Sarmiento, J. L. and Gruber, N. (2006). *Ocean biogeochemical dynamics*. Princeton University Press, Princeton, New Jersey, USA.

Schindlbacher, A., Zechmeister-Boltenstern, S., Glatzel, G., and Jandl, R. (2007). Winter soil respiration from an Austrian mountain forest. *Agricultural and Forest Meteorology*, 146:205 – 215, doi:10.1016/j.agrformet.2007.06.001.

Schlitzer, R. (2012). Ocean Data View. http://odv.awi.de.

Seeberg-Elverfeldt, J., Schlüter, M., Feseker, T., and Kölling, M. (2005). Rhizon sampling of porewaters near the sediment-water interface of aquatic systems. *Limnology and Oceanography: Methods*, 3:361 – 371.

Sejr, M. K., Krause-Jensen, D., Rysgaard, S., Sørensen, L., Christensen, P. B., and Glud, R. (2011). Air-sea flux of CO_2 in arctic coastal waters influenced by glacial melt water and sea ice. *Tellus B*, 63(5):815–822, doi:10.1111/j.1600-0889.2011.00540.x.

Semiletov, I., Makshtas, A., and Aksofu, S.-I. (2004). Atmospheric CO_2 balance: The role of Arctic sea ice. *Geophys. Res. Lett.*, 31:L05121.

Semiletov, I. P., Pipko, I. I., Repina, I., and Shakhova, N. E. (2007). Carbonate chemistry dynamics and carbon dioxide fluxes across the atmosphere-ice-water interfaces in the Arctic Ocean: Pacific sector of the Arctic. *Journal of Marine Systems*, 66:204 – 226.

Sigman, D., Hain, M., and Haug, G. (2010). The polar ocean and glacial cycles in atmospheric CO_2 concentration. *nature*, 466:47 – 55, doi:doi:10.1038/nature09149.

Skjelvan, I., Johannessen, T., and Miller, L. (1999). Interannual variability of fCO_2 in the Greenland and Norwegian Seas. *Tellus*, 51B:477 – 489.

Sommerfeld, R., Mosier, A., and Musselman, R. (1993). CO_2, CH_4 and N_2O flux through a Wyoming snowpack and implications for global budgets. *Nature*, 361:140 – 142.

Stroeve, J., Serreze, M., Holland, M., Kay, J., Malanik, J., and Barrett, A. (2011). The Arctic's rapidly shrinking sea ice cover: a research synthesis. *Climatic Change*, 110:1005–1027, doi:10.1007/s10584-011-0101-1.

Sturm, M. and Massom, R. (2010). Snow and Sea Ice. In Thomas, D. N. and Dieckmann, G. S., editors, *Sea Ice: An introduction to its physics, chemistry, biology and geology*. Blackwell, Oxford, 2nd edition.

Sun, X. and Matsumoto, K. (2010). Effects of sea ice on atmospheric pCO_2: A revised view and implications for glacial and future climates. *Journal of Geophysical Research*, 115:G02015.

Sundquist, E. (1993). The Global Carbon Dioxide Budget. *Science*, 259:934 – 941.

Takagi, K., Nomura, M., Ashiya, D., Takahashi, H., Sasa, K., Fujinuma, Y., Shibata, H., Akibayashi, Y., and Koike, T. (2005). Dynamic carbon dioxide exchange through snowpack by wind-driven mass transfer in a conifer-broadleaf mixed forest in northernmost Japan. *Global Biogeochemical Cycles*, 19:GB2012, doi:10.1029/2004GB002272.

Takahashi, T., Sutherland, S., Wanninkhof, R., Sweeney, C., Feely, R., Chipman, D. W., Hales, B., Friederich, G., Chavez, F., Sabine, C., Watson, A., Bakker, D., Schuster, U., Metzl, N., Yoshikawa-Inoue, H., Ishii, M., Midorikawa, T., Nojiri, Y., Körtzinger, A., Steinhoffm, T., Hoppema, M., Olafsson, J., Arnarson, T., Tilbrook, B., Johannessen, T., Olsen, A., Bellerby,

R., Wong, C., Delille, B., Bates, N., and de Baar, H. (2009). Climatological mean and decadal change in surface ocean pCO_2, and net sea-air CO_2 flux over the global oceans. *Deep-Sea Research*, 56:554 – 577, doi:10.1016/j.dsr2.2008.12.009.

Thomas, D., Papadimitriou, S., and Michel, C. (2010a). Biogeochemistry of Sea Ice. In Thomas, D. N. and Dieckmann, G. S., editors, *Sea Ice: An introduction to its physics, chemistry, biology and geology*. Blackwell, Oxford.

Thomas, D. N. and Dieckmann, G. S. (2010). *Sea Ice, 2nd edition*. Wiley-Blackwell Publishing, Oxford.

Thomas, D. N., Kattner, G., Engbrodt, R., Giannelli, V., Kennedy, H., Haas, C., and Dieckmann, G. S. (2001). Dissolved organic matter in Antarctic sea ice. *Annals of Glaciology*, 33:297 – 303.

Thomas, D. N., Lara, R. J., Schnack-Schiel, S. B., Nöthig, E. M., Dieckmann, G. S., Kattner, G., and Mizdalski, E. (1998). Biological soup within decaying summer sea ice in the Amundsen Sea, Antarctica. In *Antarctic Sea Ice Biological Processes, Interactions and Variability*, Antarctic Research Series 73, pages 161 – 171. American Geophysical Union.

Thomas, D. N., Papadimitriou, S., and Michel, C. (2010b). Biogeochemistry of sea ice. In Thomas, D. N. and Dieckmann, G. S., editors, *Sea Ice. An introduction to its physics, chemistry, biology and geology*. Blackwell Publishing.

Thoning, K., Kitzis, D., and Crotwell, A. (2012). Atmospheric Carbon Dioxide Dry Air Mole Fractions from quasi-continuous measurements at Barrow, Alaska; Mauna Loa, Hawaii; American Samoa; and South Pole, 1973-2011, Version: 2012-05-07.

Timco, G. and Frederking, R. (1996). A review of sea ice density. *Cold Regions Science and Technology*, 24:1 – 6.

Tison, J. L., Haas, C., Gowing, M. M., Sleewaegen, S., and Bernard, A. (2002). Tank study of physico-chemical controls on gas content and composition during growth of young sea ice. *Journal of Glaciology*, 48:177 – 191.

Tsurikov, V. (1979). The formation and composition of the gas content of sea ice. *Journal of Glaciology*, 22(86):67 – 81.

Turner, J., Comiso, J. C., Marshall, G., Lachlan-Cope, T., Bracegirdle, T., Maksym, T., Meredith, M., Wang, Z., and Orr, A. (2009). Non-annular atmospheric circulation change induced by stratospheric ozone depletion and its role in the recent increase of Antarctic sea ice extent. *Geophys. Res. Lett.*, 36:L008502, doi:10.1029/2009GL037524.

Turner, J., Maksym, T., Phillips, T. Marshall, G., and Meredith, M. (2012). The impact of changes in sea ice advance on the large winter warming on the western Antarctic Peninsula. *International Journal of Climatology*, page in press, doi:10.1002/joc.3474.

Weikusat, C., Freitag, J., and Kipfstuhl, S. (2012). Raman spectroscopy of gaseous inclusions in EDML ice core: First results - microbubbles. *Journal of Glaciology*, 58:761 – 766.

Welker, J., Fahnestock, J., and Jones, M. (2000). Annual CO_2 flux in dry and moist Arctic Tundra: Field responses to increases in summer temperatures and winter snowdepth. *Climate Change*, 44:139 – 150.

Wettlaufer, J. S. and Worster, M. G. (1995). Dynamics of premelted films: Frost heave in a capillary. *Physical Review E*, 51:4679 – 4689.

Worby, A. P., Geiger, A., Paget, M., van Woert, M., Ackley, S. F., and DeLiberty, T. (2008). Thickness distribution of Antarctic sea ice. *Journal of Geophysical Research*, 113:C05S92, doi:10.1029/2007JC004254.

Worby, A. P., Steer, A., Lieser, J. L., Heil, P., Yi, D., Markus, T., Allison, I., Massom, R., Galin, N., and Zwally, J. (2011). Regional-scale sea-ice and

snow thickness distributions from in situ and satellite measurements over East Antarctica during SIPEX 2007. *Deep Sea Research Part II*, 58:1125 – 1136.

Xu, L., Furtaw, M. D., Madsen, R. A., Garcia, R. L., Anderson, D. J., and McDermitt, D. K. (2006). On maintaining pressure equilibrium between a soil CO_2 flux chamber and the ambient air. *Journal of Geophysical Research*, 111:D08S10, doi:10.1029/2005JD006435.

Zeebe, R. E. and Wolf-Gladrow, D. (2001). *CO_2 in seawater: equilibrium, kinetics, isotopes*, volume 65 of *Elsevier Oceanography Series*. Elsevier Science B.V., first edition.

Zemmelink, H. J., Delille, B., Tison, J. L., J., H. E., Houghton, L., and Dacey, J. W. H. (2006). CO_2 deposition over the multi-year ice of the western Weddell Sea. *Geophysical Research Letters*, 33, doi:10.1029/2006GL026320.

Zimov, S., Semiletov, I., Daviodov, S., Voropaev, Y., Prosyannikov, S., Wong, C., and Chan, Y.-H. (1993). Wintertime CO_2 Emmision from Soils of Northeastern Siberia. *Arctic*, 46:197 – 204.

Zullig, J. J. and Morse, J. W. (1988). Interaction of organic acids with carbonate mineral surfaces in seawater and related solutions: I. Fatty acid adsorption. *Geochimica et Cosmochimica Acta*, 52:1667 – 1678.

de Jong, E., Redmann, R., and Ripley, E. (1979). A Comparison of Methods to Measure Soil Respiration. *Soil Science*, 127:300 – 307.

Årthun, M., Ingvaldsen, R., Smedsrud, L., and Schrum, C. (2011). Dense water formation and circulation in the Barents Sea. *Deep Sea Research Part I*, 58:801 – 817.

Appendix A

Appendix

A.1 Characterization of ikaite ($CaCO_3 \cdot 6H_2O$) crystals in first-year Arctic sea ice north of Svalbard

This manuscript is in press in Annals of Glaciology, 54 (62) - Seasonal snow and ice.

Characterization of ikaite ($CaCO_3 \cdot 6H_2O$) crystals in first-year Arctic sea ice north of Svalbard

Daiki NOMURA [1, 2, 3] *, Philipp ASSMY [1], Gernot NEHRKE [4], Mats A. GRANSKOG [1], Michael FISCHER [4], Gerhard S. DIECKMANN [4], Agneta FRANSSON [1], Yubin HU [4], Bernhard SCHNETGER [5]

1. Norwegian Polar Institute, Fram Centre, NO-9296 Tromsø, Norway.

2. Japan Society for the Promotion of Science (JSPS), 6 Ichiban-cho, Chiyoda, Tokyo 102-8471, Japan.

3. Institute of Institute of Low Temperature Science, Hokkaido University, Kita-19, Nishi-8, Kita-ku, Sapporo, Hokkaido 060-0819, Japan.

4. Alfred Wegener Institute for Polar and Marine Research, Am Handelshafen 12, D-27570 Bremerhaven, Germany.

5. Institute for Chemistry and Biology of the Marine Environment, Carl-von-Ossietzky-Str. 9-11, D-26111 Oldenburg, Germany.

*Corresponding author; Daiki Nomura, e-mail; daiki.nomura@npolar.no, Tel.: + 47 77 75 06 42.

ABSTRACT. We identified ikaite crystals ($CaCO_3 \cdot 6H_2O$) and examined their shape and size distribution from first-year Arctic pack ice, overlying snow and slush layers during the spring melt-onset north of Svalbard. Additional measurements of total alkalinity (TA) were made on melted snow and sea ice samples. Ikaite crystals were mainly found in the bottom of the snow pack, in slush and the surface layers of the sea ice where temperature was generally lower and salinity higher than in the ice below. Image analysis showed that ikaite crystals were characterized by a roughly elliptical shape and a maximum caliper diameter of 201.0 ± 115.9 µm (*n*=918). Since the ice melting season had already started ikaite crystals may already have begun to dissolve which might explain the lack of a relationship between ikaite crystal size and sea ice parameters (temperature, salinity, and thickness of snow and ice). Comparisons of salinity and TA profiles for melted-ice samples suggest that the precipitation/dissolution of ikaite crystals occurred at the top of the sea ice and the bottom of snow pack during the ice formation/melting processes.

INTRODUCTION

Ikaite ($CaCO_3 \cdot 6H_2O$) is a hydrated calcium carbonate polymorph that is generally found at cold and saline conditions (e.g. Pauly, 1963). The precipitation of calcium carbonate during the formation of polar sea ice was controversially discussed for decades but has only recently been shown to really occur (Dieckmann and others, 2008 and references cited therein). Dieckmann and co-workers were the first who reported the occurrence of ikaite in Antarctic sea ice (Dieckmann and others, 2008) and shortly later in Arctic sea ice (Dieckmann and others, 2010). Low-temperature and high-salinity conditions during seawater freezing and brine formation in sea ice lead to supersaturation for ikaite and subsequent precipitation of ikaite crystals in sea ice brine.

So far little is known about the fate of ikaite if the sea ice starts to melt. Two scenarios are possible. During the sea ice melt season, increase in ice temperature and decrease in brine salinity could induce dissolution of ikaite crystals. Alternatively, ikaite crystals could be rejected from the melting ice to the underlying water column which could affect the carbonate chemistry in underlying seawater (Fransson and others, 2011). The precipitation/dissolution of ikaite crystals in sea ice could be an important contributor to the atmosphere–sea ice–ocean carbon cycle in polar seas throughout the sea ice formation/melting processes (Rysgaard and others, 2007).

The quantification of ikaite in sea ice was examined so far by measuring the weight of the ikaite crystals (Dieckmann and others, 2008), by measuring the calcium concentration after dissolution of ikaite crystals (Fischer and others, 2012) and by analyzing the carbonate system in melted ice/brine samples (Rysgaard and others, 2007; Fransson and others, 2011; Geilfus and others, 2012). Dieckmann and others (2008, 2010) described the typical morphology of ikaite crystals and based

part of the phase identification on morphological grounds. However, so far, a detailed morphometric characterization of ikaite crystals found in polar sea ice is lacking.

In this study, we examined the shape and size distribution of ikaite crystals in Arctic first-year sea ice based on image analysis. A detailed characterization of crystal shape and size will provide important information needed to identify the environmental conditions and history of leading to the formation/dissolution of ikaite crystals in polar sea ice. Additionally, total alkalinity (TA) was used as a simple indicator to quantify precipitation/dissolution.

MATERIALS AND METHODS

Sea ice field observations were carried out at 8 sea ice stations on first-year Arctic pack ice at the spring melt-onset north of Svalbard from 27 April to 11 May 2011 (Fig. 1; Table 1) during the Norwegian Polar Institute's Centre for Ice, Climate and Ecosystems (ICE) cruise in 2011 on R/V *Lance*.

Snow and slush samples were collected using a clean polycarbonate shovel and transferred into polyethylene zip-lock bags. Snow and slush temperature was measured using a needle-type temperature sensor (Testo 110 NTC, Brandt Instruments, Inc., USA).

Sea ice samples were collected using an ice corer with an inner diameter of 9 cm (Mark II coring system, KOVACS Enterprises, Inc., USA). Immediately after sea ice collection, ice temperature was measured by inserting a needle-type temperature sensor in holes drilled at 5-10 cm interval into the core. Thereafter, a second ice core for ikaite crystals was collected within 10 cm of the temperature core and cut into 5–10 cm thick sections with a stainless steel saw and the ice sections placed into polyethylene zip-lock bags. At St. 21, a third core for measurements of ice algal pigments and phosphate concentrations was collected within 10 cm of the ikaite core and cut into 3–20 cm thick sections, transferred into polyethylene zip-lock bags and stored dark in a large cooler box.

Brine samples from sea ice were obtained at St. 21 using the sack hole method (e.g. Gleitz and others, 1995). Sack holes were made using an ice corer as described for ice coring above. A 25–50 cm deep hole in the sea ice was covered with a 5 cm-thick urethane lid to reduce heat and gas transfer across the brine/atmosphere interface. After the brine accumulated at the bottom of the hole over a period of approximately 10–15 min, the brine was sampled with a

diaphragm pump (EWP-01, As One Corporation, Japan), and collected into a 100-mL polypropylene bottle (I-Boy, As One Corporation, Japan) for measurement of salinity, and a 120-mL amber glass vial (Maruemu Co. Ltd, Japan) for measurement of TA. Brine temperature was measured in situ after the sampling of brine by the same sensor as described for ice cores above.

A detailed account of ikaite sample treatment can be found in Dieckmann and others (2008). Briefly, once back onboard, snow, slush and sea ice samples were immediately transferred into a refrigerator (+4 °C) for melting. The melting process was checked regularly. During the final melt phase, samples were swirled until the last bits and pieces of ice had melted. This ensured that the sample remains at a temperature of about 0 °C during the whole melting process of 2–3 days. The melted ice samples were transferred from polyethylene zip-lock bags into 1000 mL Nalgene polycarbonate containers (Thermo Fisher Scientific, USA). In order to examine the presence/absence of the ikaite crystals in the samples, the meltwater was stirred in the container to induce a vortex. Ikaite crystals, if present, accumulated in the centre of the container and could be detected by eye. When present the ikaite crystals were sampled with a pipette and filtered over 0.4 µm polycarbonate filters (Millipore, USA) under low vacuum, not exceeding 200 mbar. The filter was placed into a 2 ml Nalgene cryovial (Thermo Fisher Scientific, USA) with 75% cold Ethanol and then stored at –80 °C. Photographs of ikaite crystals were taken with a stereomicroscope (Model M205C, Leica Microsystems, Germany) prior to filtration.

For TA measurements, the supernatant of the remaining melted snow, slush and sea ice samples was transferred to a 120-mL amber glass vial.

Once on board, sea ice samples for ice algal pigment and phosphate were transferred into light-proof ice core boxes and thawed at +4 °C. After thawing, meltwater was filtered onto Whatman GF/F glass-fiber filters under low vacuum.

For ice algal pigment, filters were placed in a 2 ml Nalgene cryovial (Thermo Fisher Scientific, USA), shock-frozen in liquid nitrogen and then stored at –80 °C. For phosphate measurements, the filtered water was transferred into double rinsed 50-mL polypropylene tube (VWR, Germany) and then stored at –20 °C until analysis.

The salinity of the brine and melted snow, slush and sea ice were measured with a conductivity sensor (Cond 315i, WTW, Germany). The TA of the brine and melted snow and sea ice were measured with a titration system (TitroLine alpha plus, SI Analytics GmbH, Germany). The TA measurements were calibrated using an in-house standard (North-Sea water collected of shore Helgoland) traceable to the Certified Reference Material (Batch 111) (Scripps Institution of Oceanography, USA). Ice algal and phytoplankton photosynthetic pigments (Chlorophyll *a*) were measured according to Hoffmann and others (2006) by high-performance liquid chromatography (HPLC) with a Waters 600 controller (Waters Corporation, USA).

Phosphate concentrations were determined with an auto-analyzer system (Quaatro, SEAL Analytical, Ltd., UK, method Q-031-04 Rev.2), according to the Joint Global Ocean Flux Study (JGOFS) spectrophotometric method (JGOFS, 1994). The analyzer was calibrated from 0-3 µmol L^{-1} with standard reference materials for nutrient analysis (CertiPUR, Merck, Germany) and checked with spiked low nutrient seawater (LNSW) provided by OSIL, UK.

Phase identification for the ikaite crystal was done by means of a WITec alpha 300 R (WITec GmbH, Germany) confocal Raman microscope. Ikaite crystals stored in a freezer (–20 °C) were transferred to a glass Petri dish in the cold room (+4 °C) and immediately set to the microscope to keep cool during the investigation (within 2–3 minutes). Some photographs of the ikaite crystals were also taken under the stereomicroscope (SteREO Discovery. V12, Carl Zeiss Microscopy Co., Ltd., Germany).

The image analysis program ImageJ (software version 1.45s, Wayne Rasband, National Institutes of Health, USA; http://rsb.info.nih.gov/ij) was used to investigate the shape and size of the ikaite crystals from micrographs (Fig. 2). The surface area (S), perimeter (P), and maximum/minimum caliper diameters (d_{max}/d_{min}) for each crystal were determined. The diameter of a circle that has the same area: $d_S = (4S/\pi)^{1/2}$, and the same perimeter: $d_P = P/\pi$ as the crystal were calculated. Relationships between d_S and d_P are measures of deformation of the crystals, and have previously been used in a sea ice floe study (e.g. Toyota and others, 2006).

RESULTS

Air temperature ranged from –12.8 °C to +0.3 °C during the sampling time (Table 1). Air temperatures measured continuously at 30 second intervals during the study period (27 April to 11 May) over the R/V *Lance* indicated that the mean air temperature was –5.3±4.4 °C.

A slush layer had developed at the snow–sea ice interface at Sts. 20, 27a and 27b (Table 1). Snow accumulation over sea ice leads to the formation of a slush layer below sea level (Haas and others, 2001). In this study, slush was generally observed at stations with high-snow depth/low-ice thickness (Table 1).

Snow and slush depth ranged from 1.0 cm to 39.0 cm for all station and 3.0 cm to 10.0 cm for Sts. 20, 27a and 27b, respectively (Table 1). Ice thickness ranged from 31.0 cm to 125.0 cm, with the notable exception of >500.0 cm at St. 1 (multi-year ice or rafted ice). Generally, slush was observed at stations with high-snow depth/low-ice thickness (Table 1).

Mean temperature ranged from –5.3 °C to –0.4 °C for snow, –2.8 °C to –1.5 °C for slush (–3.9 °C for brine), and –4.2 °C to –0.8 °C for sea ice (Table 2). For sea ice, temperatures at the top of the core were generally lower than those at the middle and bottom of the core.

Mean salinity ranged from 0 to 6.0 for snow, 20.2 to 23.4 for slush layers and 0 to 7.1 for sea ice (Table 2). In general, slush salinity was higher than snow and sea ice salinity. Extremely high salinity (78.3) was measured for the brine samples at St. 21 (Table 2).

Phase identification of collected crystals with a confocal Raman microscope

confirmed that the crystals found during the cruise were indeed ikaite. The general appearance of ikaite crystals is illustrated for the slush sample collected at St. 20 (Fig. 2a). Similar images of ikaite crystals were obtained from other stations.

During the study period, a total of 96 samples of melted snow (n=13), slush (n=5) and sea ice (n=78) were checked for the presence of ikaite crystals. We found ikaite crystals in 32 samples (1/3 of all samples). The majority of ikaite findings were associated with sea ice (n=26) as compared to snow (n=4) and slush (n=2). Highest number of crystals were found in the samples from the bottom of snow, slush layers at the ice-snow interface (e.g. Fig. 2a) and the top most part of sea ice, while only small amounts were discovered in the remaining samples, especially in the downcore samples crystals were practically absent.

Temperature and salinity deviated widely and no clear relationship between the two for presence/absence of the ikaite crystals (Fig. 3). The average temperature of samples containing ikaite crystals and those lacking crystals was very similar with -2.2±1.1 and -2.4±1.2 °C respectively (Fig. 3). The average salinity was 7.0±5.3 for samples with crystals and 4.9±6.1 for samples without. These results indicate that there was no significant difference between presence and absence of the ikaite crystals relative to temperature and salinity at the time of sampling.

Mean and median of d_{max} ranged from 112.4 μm to 375.7 μm and 108.3 μm to 381.0 μm between stations (Table 3). For all crystals (n=918), mean and median of d_{max} were 201.0 μm and 171.4 μm, respectively (Table 3 and Fig. 4). The mode of the size distribution for d_{max} was 125.0 μm (Fig. 4). Relationships between d_{max} (mean) and parameters (ice and air temperature, salinity and thickness of snow and ice) indicated that there were no relationships (r=0.5, p=0.3 for ice temperature; r=0.4, p=0.5 for air temperature; r=0.3, p=0.6 for salinity; r=0, p=0.9 for ice thickness; r=0, p=0.8 for snow thickness).

The slope of the relationship between d_s and d_p and d_{min} and d_{max} for all crystals (n=918) of 1.14 and 1.65 respectively (Fig. 5) represents the deformation ratio in the former and the aspect ratio in the latter.

Bulk ice/snow TA tended to decrease with depth, from 1238.9 μmol L^{-1} at the bottom of snow, to 305.7 μmol L^{-1} at the bottom of the sea ice (Fig. 6). For the upper parts of the snow, bulk TA was almost zero (12.8 μmol L^{-1}). Bulk ice/snow salinity also tended to decrease with depth, from 18.0 at the bottom of snow, to 4.0 at the bottom of the sea ice. For the upper parts of the snow, salinity was zero. Bulk ice/snow TA and salinity profiles showed very similar trends except for the bottom of snow and top 25 cm of sea ice (Fig. 6).

Bulk ice/snow TA was normalized to a salinity of 5.4, the mean value of bulk ice/snow salinity. The normalized-TA (n-TA) was constant (410.3±10.0 μmol L^{-1}) for the middle and the bottom parts of the sea ice while it deviated more than 39 μmol L^{-1} from the mean values (410.3 μmol L^{-1}) for the bottom of snow and top 25 cm of sea ice.

Chlorophyll *a* concentrations at St. 21 were lower than 0.3 μg L^{-1} throughout the core, except for the bottom 3 cm (5.8 μg L^{-1}). Phosphate concentrations were lower than 0.12 mol L^{-1} throughout the core.

For the middle and the bottom parts of the sea ice and upper parts of the snow, bulk ice/snow TA and salinity were highly correlated (r=0.99, p<0.0001; Fig. 7a). Data points for the bottom of the snow and the top of the sea ice deviated from this regression line (Fig. 7a). Brine TA was considerably higher with 4440.3±132.5 μmol L^{-1} and located below the regression line (Fig. 7b).

DISCUSSION AND CONCLUSION

Comparison of the images taken of the ikaite crystals in this study with those from previous studies in the Antarctic sea ice (Dieckmann and others, 2008; Fischer and others, 2012) and Arctic sea ice (Dieckmann and others, 2010) indicates that they share a similar morphology.

Generally, cold and saline conditions favor the precipitation of ikaite crystals in the natural environment (e.g. Omelon and others, 2001). Lowest temperatures are generally measured at the top of the sea ice cover, closest to the cold atmosphere, leading to the formation of the highest brine salinity through the sea ice. Therefore, ikaite crystals were most frequently found at the top of sea ice (Dieckmann and others, 2008, 2010; Fischer and others, 2012). Additionally, the slush layer formation observed during the study period supplied seawater to the top of the sea ice, and likely enabled ikaite precipitation in the slush and snow-sea ice when temperature decreases. On the other hand, for the warm sea ice, seawater supply to the top of sea ice leads to the undersaturation for ikaite due to a dilution effect. Therefore, ikaite crystals tend to dissolve.

Temperature and salinity relationships showed no significant difference between samples with and without ikaite crystals. During the sampling period, snow and sea ice temperatures were relatively high and it is reasonable to assume that ikaite crystals tend to dissolve during the spring melt-onset. Relationships between temperature and salinity measured during the study period therefore did not reflect the physical-chemical conditions which prevailed when the precipitation of ikaite occurred. This is one of the reasons why we did not detect significant differences in temperature and salinity conditions for samples with and without ikaite crystals (Fig. 3). Our results suggest that knowledge about the sea ice growth history, particularly low temperatures during the freezing season, will be important to

360 elucidate the conditions for ikaite formation because brine salinity is strongly
361 driven by brine temperature in the brine (e.g. Eicken, 2003), which in turn will
362 determine precipitation.
363
364 Most ikaite crystals were roughly elliptical to elongate in shape (Fig. 2 and 5). A
365 previous study (Dieckmann and others 2008) has pointed out that the shape of the
366 ikaite crystals varied from almost idiomorphic to xenomorphic, and some were
367 apparently constrained by the dimensions of the brine channel network. The size
368 range for the ikaite crystals obtained in this study (36–812 μm), is consistent with
369 that for Antarctic sea ice (<5–600 μm; Dieckmann and others, 2008). Although
370 crystal size was not quoted, light micrographs of ikaite crystals in Arctic sea ice
371 (Fig. 2 in Dieckmann and others, 2010) showed a similar size range as obtained in
372 this study. At the saline spring discharge, much larger sizes of ikaite crystals (up to
373 5000 μm) were observed (Omelon and others, 2001) although the water quality
374 and environmental conditions were much different to those of sea ice. Therefore,
375 as was the case with the shape of the ikaite crystals (e.g. Dieckmann and others,
376 2008), the size of the crystals in sea ice systems might also be restricted by the size
377 of the brine channel and pockets.
378
379 Comparison TA and salinity profiles suggests that the precipitation/dissolution of
380 the ikaite crystals occurred at the bottom of snow, the top parts of the sea ice and
381 brine, where ikaite crystals were found. Additionally, deviations of n-TA for the
382 bottom of snow and the top parts of the sea ice from the mean values for the
383 middle and the bottom parts of the sea ice also suggest the
384 precipitation/dissolution of the ikaite crystals at the bottom of snow and the top
385 parts of the sea ice. During the precipitation of calcium carbonate, TA decreases
386 (Zeebe and Wolf-Gladrow, 2001). Therefore, TA and salinity relationships can be
387 useful indicators for the precipitation/dissolution of ikaite crystals: the precipitation
388 of ikaite crystals leads to a decrease in the TA:S ratio (n-TA) (data points would be
389 below the regression line given in Fig. 7). Although the dissolution of ikaite crystals

390 leads to an increase in the TA:S ratio (n-TA), the dissolution of all ikaite crystals
391 previously formed in a given depth of sea ice would compensate changes in
392 alkalinity (data points would stay on the regression line given in Fig. 7). However,
393 one data point above the regression line (Fig. 7a), suggests excess dissolution of
394 ikaite crystals transferred from adjacent parts of the sea ice. The well developed
395 brine channel network during the spring melt-onset could facilitate ikaite
396 transport.
397
398 Biological activity also alters TA in addition to the precipitation/dissolution of
399 $CaCO_3$ (Zeebe and Wolf-Gladrow, 2001). Largest deviations in TA and salinity
400 were observed at low chlorophyll *a* concentrations at the surface of sea ice while
401 TA and salinity were not deviated at high chlorophyll *a* concentrations measured
402 in the bottom 3 cm of the core. These results suggest that the effect of biological
403 activity on TA was minor for the sea ice system in this study.
404
405 Relationships between TA and salinity were used to quantify ikaite concentrations
406 in sea ice and snow. Deviation of TA from the regression line was used as a
407 measure for the amount of ikaite crystals in sea ice and snow. We have calculated
408 ikaite concentrations at the bottom of snow and the top of sea ice, except for the
409 one data point from the top of sea ice, where the plot was above the regression
410 line. Ikaite concentrations (expressed as mg-ikaite $L^{-1}$of melted samples) ranged
411 between 5.6–11.3 mg L^{-1}. Our values fall within the range reported by previous
412 studies (0–19.4 mg L^{-1}: Dieckmann and others, 2008 and 0.01–126 mg L^{-1}: Fischer
413 and others, 2012) from Antarctic sea ice. Maximum values were higher than those
414 reported in this study.
415
416 The variation in ikaite concentrations reported so far for polar sea-ice can be
417 explained by different scenarios. Since the ice melting season had already started,
418 when this study was conducted, ikaite crystals may already have begun to dissolve
419 which might explain the lack of a relationship between ikaite crystal size and sea

ice parameters (temperature, salinity, and thickness of snow and ice). It is also possible that differences in ikaite concentration are related to differences in the seawater (brine) composition. It has been reported that high concentrations of phosphate favors the precipitation of ikaite (Bischoff and others, 1993). In this study, phosphate concentrations were almost zero (<0.1 μmol L^{-1}) at the top parts of sea ice. However, sea ice growth history especially ice temperature can be expected to be the most important driving force behind ikaite precipitation (dissolution) in sea-ice. Without knowing this parameter exactly over time the reasons why ikaite concentrations reported so far (this study, Dieckmann and others, 2008; Fischer and others, 2012) differ, is difficult to answer. For a solid quantification of ikaite formation in polar sea ice, investigations are need in which the temperature (and other physico-chemical parameter) are determined from the beginning of ice formation until the time of sampling.

ACKNOWLEDGEMENTS

We would like to express heartfelt thanks to the crew of *Lance,* Dr. N. Koc, Dr. H. Hop, Dr. A. Sundfjord, Dr. M. Lenau and all members of the ICE11-3 cruise for their support in conducting the field work. We thank Ms. J. Hölscher for the support in TA analyses. This work was supported by the Centre for Ice, Climate and Ecosystems (ICE) at the Norwegian Polar Institute and the Fram Centre. G.N. and G.D. have been supported by the DFG by grant NE 1564/1-1 (SPP 1158).

REFERENCES

Bischoff J.L., J.A. Fitzpatrick and R.J. Rosenbauer. 1993. The solubility and stabilization of ikaite ($CaCO_3 \cdot 6H_2O$) from 0° to 25°C: Environmental and paleoclimatic implications for thinolite tufa. *J. Geol.*, **101**, 21–33.

Dieckmann, G.S., G. Nehrke, S. Papadimitriou, J. Göttlicher, R. Steininger, H. Kennedy, D. Wolf-Gladrow and D.N. Thomas. 2008. Calcium carbonate as ikaite crystals in Antarctic sea ice. *Geophys. Res. Lett.*, **35**, L08501, doi:10.1029/2008GL033540.

Dieckmann, G.S., G. Nehrke, C. Uhlig, J. Göttlicher, S. Gerland, M.A. Granskog and D.N. Thomas. 2010. Brief Communication: Ikaite ($CaCO_3 \cdot 6H_2O$) discovered in Arctic sea ice. *The Cryosphere*, **4**, 227–230.

Eicken, H. 2003. From the microscopic, to the Microscopic, to the regional scale: Growth, microstructure and properties of sea ice. In *Sea Ice-an introduction to its physics, chemistry, biology and geology* (ed. D.N. Thomas and G.S. Dieckmann).

480 Blackwell Science, Oxford, 22–81.
481
482 Fischer, M., D.N. Thomas, A. Krell, G. Nehrke, J. Göttlicher, L. Norman, C.
483 Riaux-Gobin and G.S. Dieckmann. 2012. Quantification of ikaite in Antarctic sea
484 ice. *The Cryosphere Discuss*., **6**, 505–530.
485
486 Fransson, A., M. Chierici, P.L. Yager and W.O. Smith Jr. 2011. Antarctic sea ice
487 carbon dioxide system and controls. *J. Geophys. Res*., 116, C12035,
488 doi:10.1029/2010JC006844.
489
490 JGOFS. 1994. Protocols for the Joint Global Ocean Flux Study core measurements.
491 *International JGOFS Report Series*, **19**, 174 pp.
492
493 Geilfus, N.-X., G. Carnat, T. Papakyriakou, J.-L. Tison, B. Else, H. Thomas, E.
494 Shadwick and B. Delille. 2012. Dynamics of pCO_2 and related air-ice CO_2 fluxes
495 in the Arctic coastal zone (Amundsen Gulf, Beaufort Sea), *J. Geophys. Res*., **117**,
496 C00G10, doi:10.1029/2011JC007118.
497
498 Gleitz, M., M.R. Vonderlo, D.N. Tomas, G.S. Dieckmann, F.J. Millero. 1995.
499 Comparison of summer and winter inorganic carbon, oxygen and nutrient
500 concentrations in Antarctic sea ice brine. *Mar. Chem*., **51**, 81–89.
501
502 Haas, C., D.N. Thomas and J. Bareiss. 2001. Surface properties and processes of
503 perennial Antarctic sea ice in summer. *J. Glaciol*., **47**, 159, 613–625.
504
505 Hoffmann, L., I. Peeken, K. Lochte, P. Assmy, M. Veldhuis. 2006. Different
506 reactions of Southern Ocean phytoplankton size classes to iron fertilization. *Limnol.*
507 *Oceanogr*., **51**, 3, 1217–1229.
508

509 Omelon, C.R., W.H. Pollard and G.M. Marion. Seasonal formation of ikaite
510 ($CaCO_3 \cdot 6H_2O$) in saline spring discharge at Expedition Fiord, Canadian High
511 Arctic: Assessing conditional constraints for natural crystal growth. *Geochim.*
512 *Cosmochim. Acta*, **65**, 1429–1437.
513
514 Pauly, H. 1963. "Ikaite" a new mineral from Greenland. *Arctic,* **16**: 263–264.
515
516 Rysgaard, S., R.N. Glud, M.K. Sejr, J. Bendtsen and P.B. Christensen. 2007.
517 Inorganic carbon transport during sea ice growth and decay: A carbon pump in
518 polar seas. *J. Geophys. Res.*, **112**, C03016, doi:10.1029/2006JC003572.
519
520 Toyota, T., S. Takatsuji and M. Nakayama. 2006. Characteristics of sea ice floe
521 size distribution in the seasonal ice zone. *Geophys. Res. Lett.,* **33**, L02616,
522 doi:10.1029/2005GL024556.
523
524 Zeebe, R. and D. Wolf-Gladrow. 2001. *CO_2 in Seawater: Equilibrium, Kinetics,*
525 *Isotopes*. Elsevier Oceanography Series, **65**.
526
527
528
529
530
531
532
533
534
535
536
537
538

539

540 **FIGURE CAPTIONS**

541

542 Fig. 1. Location map of the sampling area north of Svalbard.

543

544 Fig. 2. Photographic image of ikaite crystals in slush (a). Due to the overlap of
545 ikaite crystals (a), ImageJ software could not extract each crystal. Therefore, each
546 crystal was outlined by visually drawing a red line around its perimeter (b) and
547 moved to eliminate the overlap between crystals (c). Then, each crystal was
548 colored red and extracted according to its brightness using ImageJ. Note that
549 crystals touching the edge of the image were excluded from the analysis.

550

551 Fig. 3. Relationships between temperature and salinity for melted snow, slush and
552 sea ice samples. Symbols were shown for presence and absence of ikaite crystals.
553 Black and gray lines indicate the mean value for presence and absence of ikaite
554 crystals, respectively.

555

556 Fig. 4. Size distribution of d_{max} for all of ikaite crystals (n=918) examined in this
557 study.

558

559 Fig. 5. Relationships between (a) d_S and d_P, and (b) d_{max} and d_{min}. d_S and d_P indicate
560 the diameters based on the area and perimeter, respectively. d_{max} and d_{min} indicate
561 maximum and minimum caliper diameters, respectively.

562

563 Fig. 6. Depth profiles for the bulk ice/snow TA (blue) and salinity (red) in snow and
564 sea ice at St. 21.

565

566 Fig. 7. Plots of (a) TA and salinity for snow and sea ice at St. 21, and (b) addition of
567 brine data to (a). Dotted red line represents the regression of data points from the
568 middle and the bottom of the sea ice and the top of the snow (blue circles).

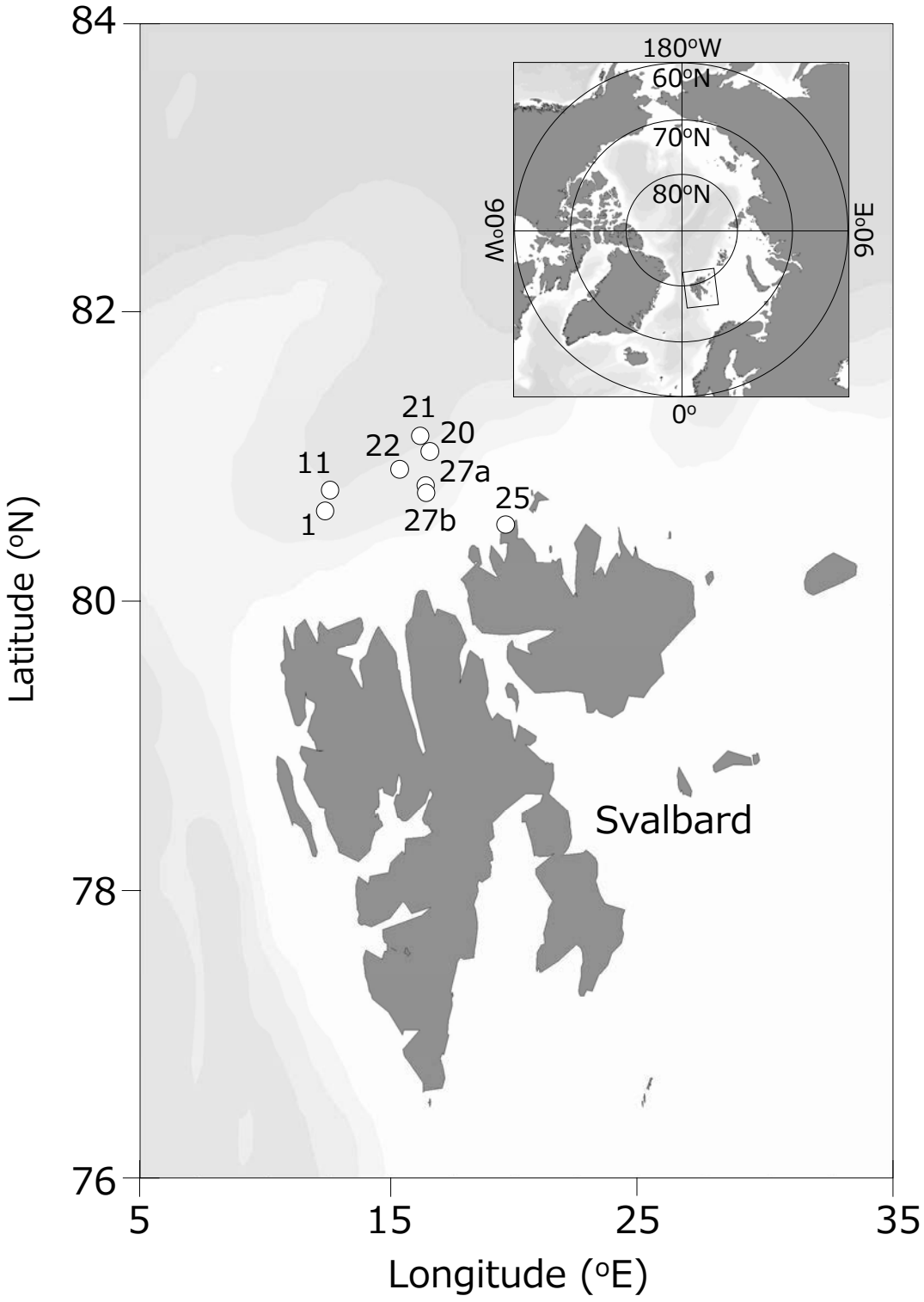

Figure 1, Nomura et al.

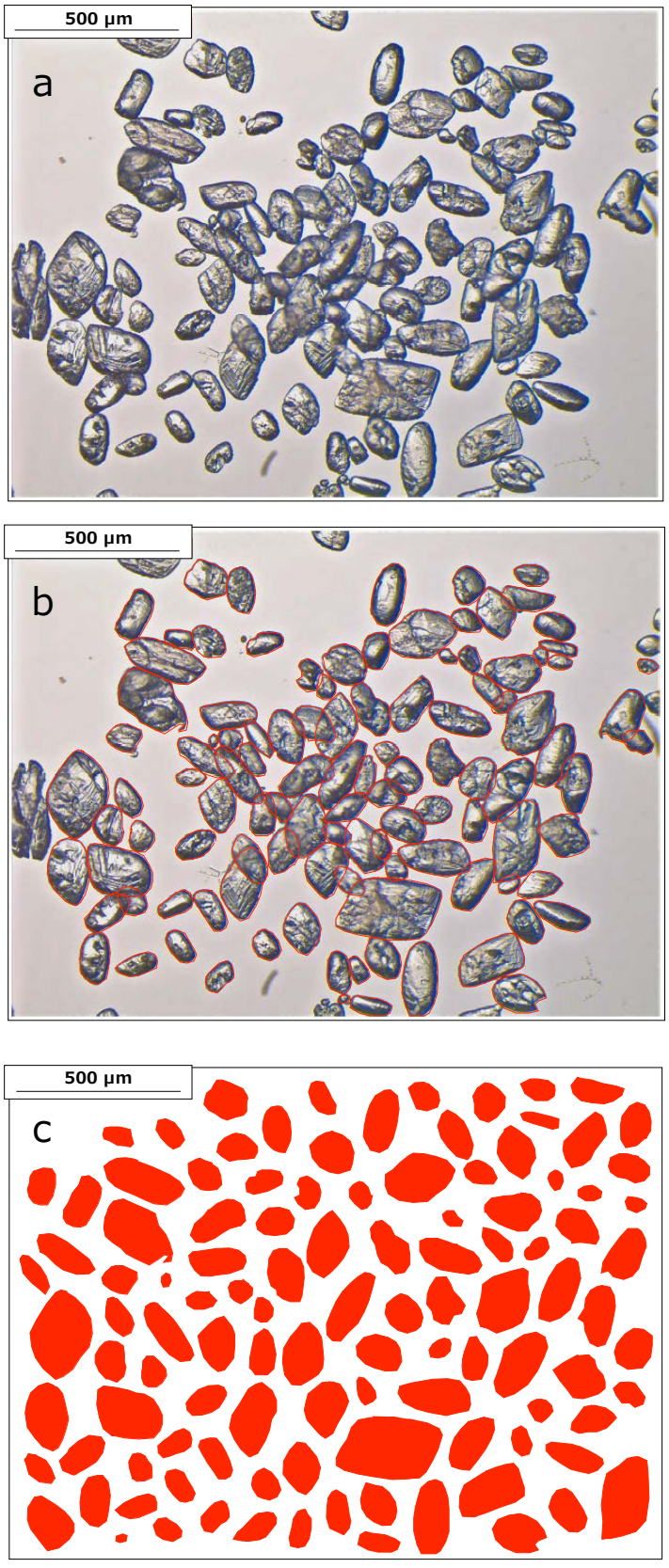

Figure 2, Nomura et al.

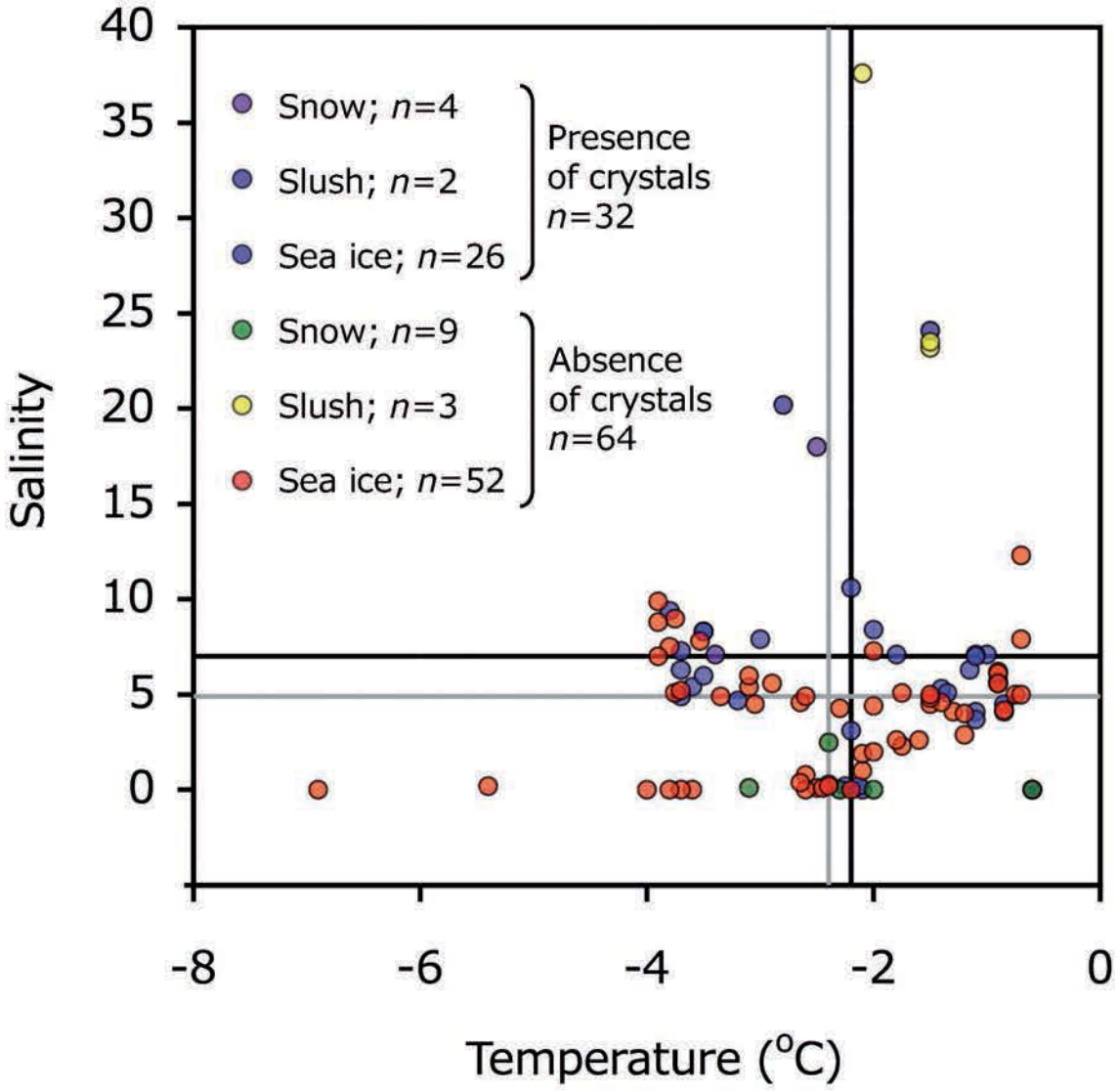

Figure 3, Nomura et al.

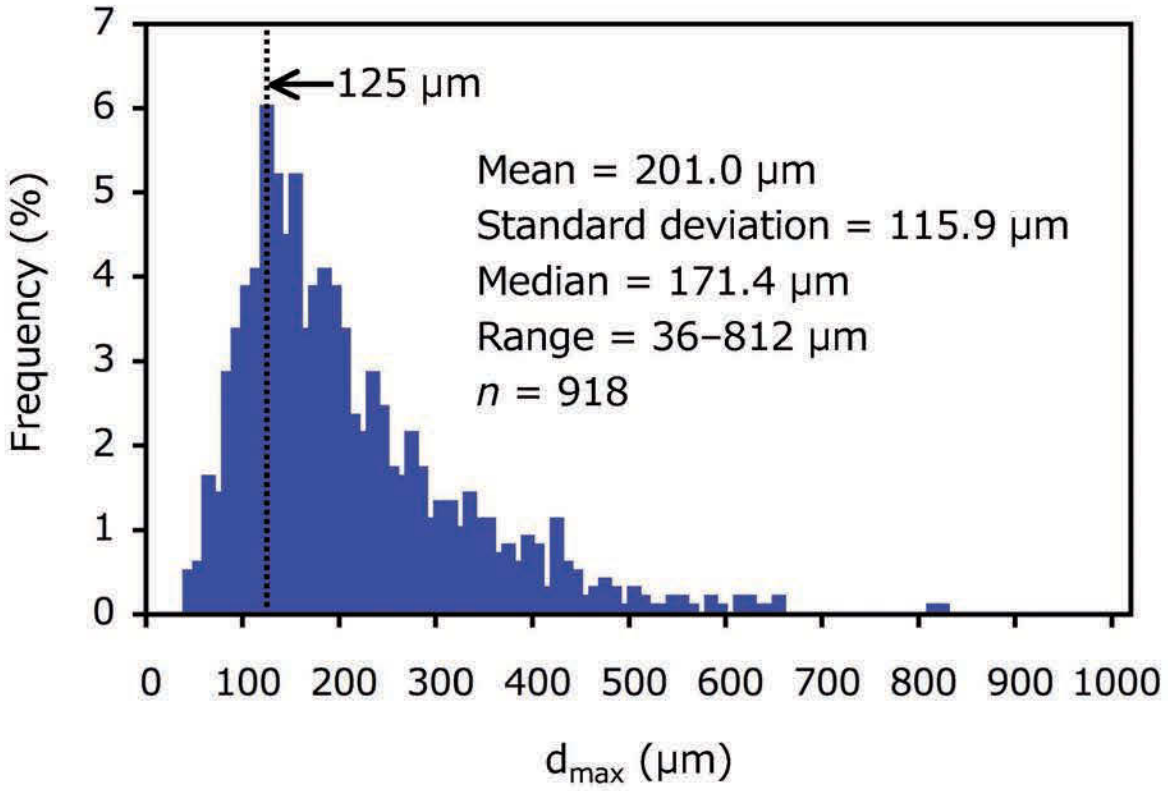

Figure 4, Nomura et al.

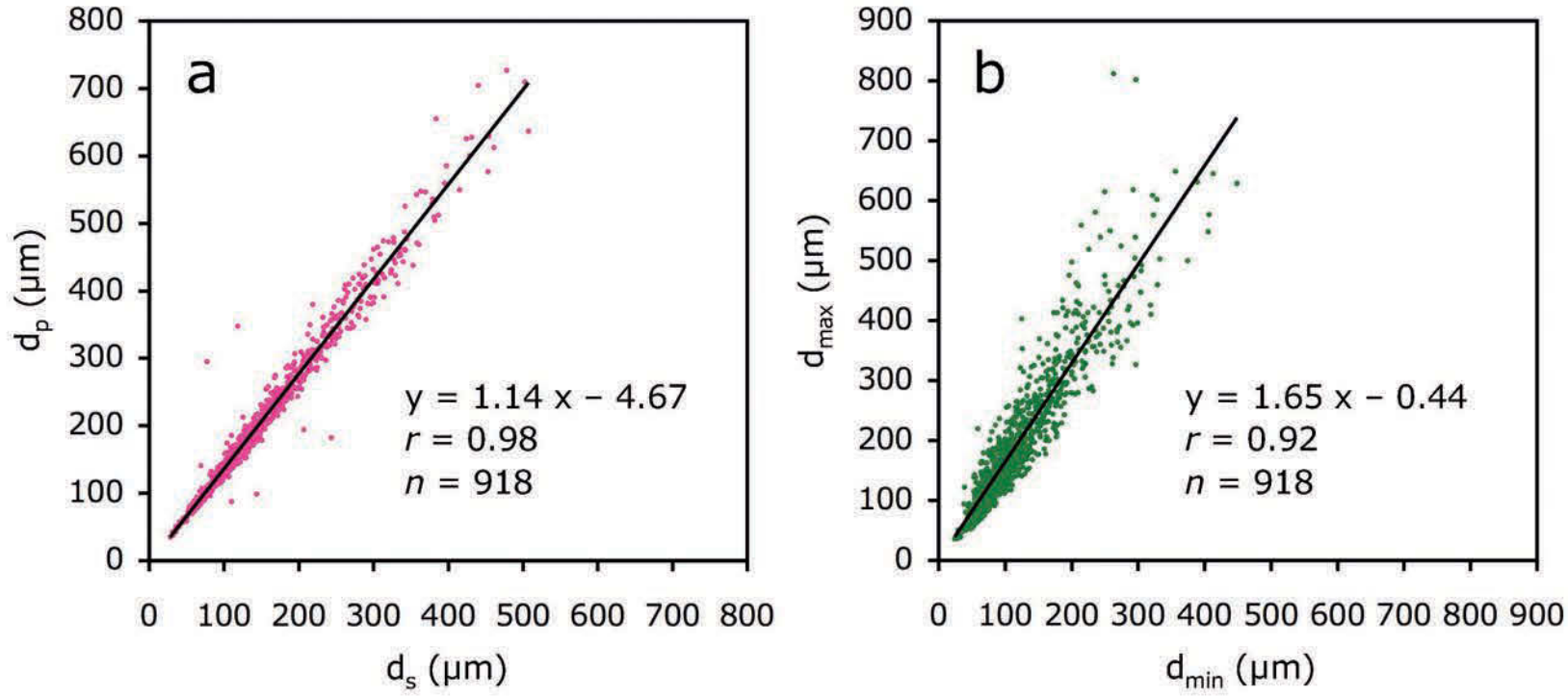

Figure 5, Nomura et al.

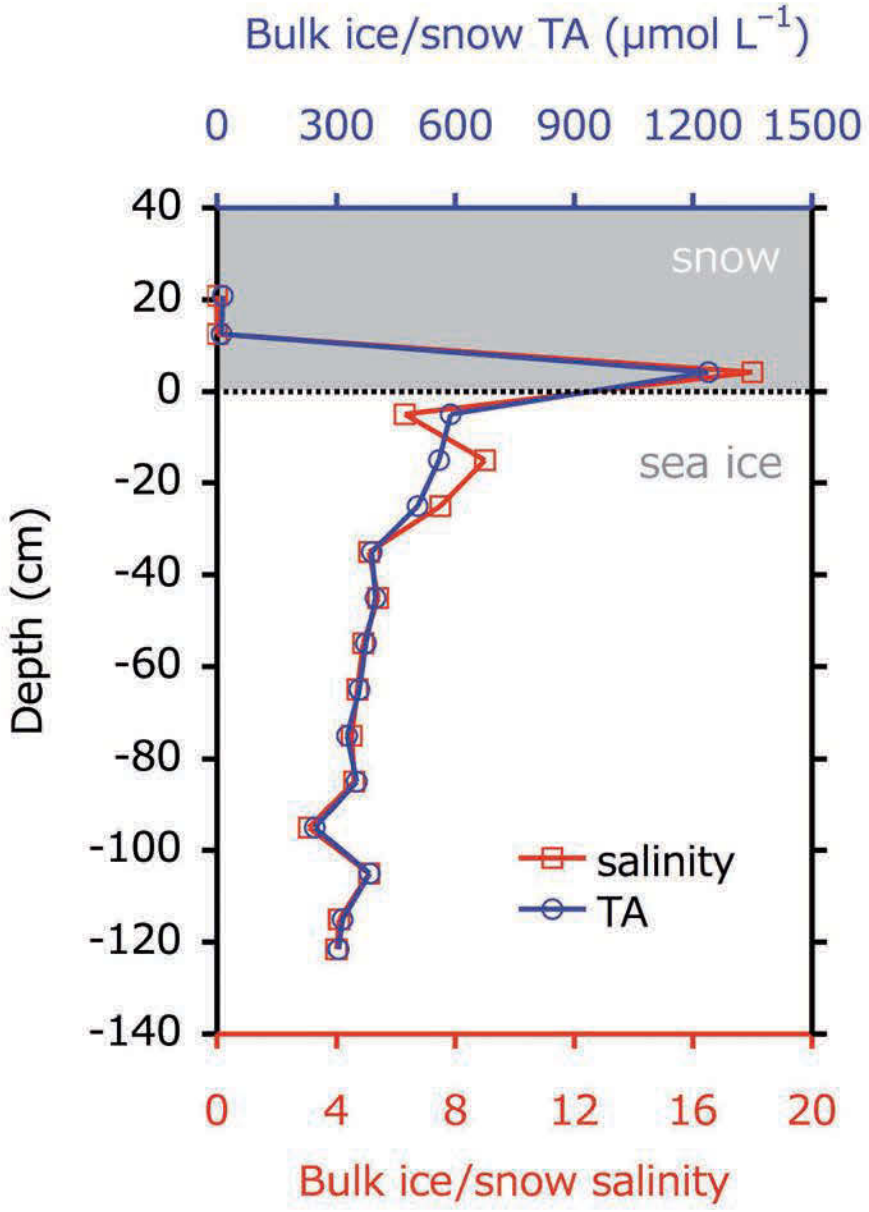

Figure 6, Nomura et al.

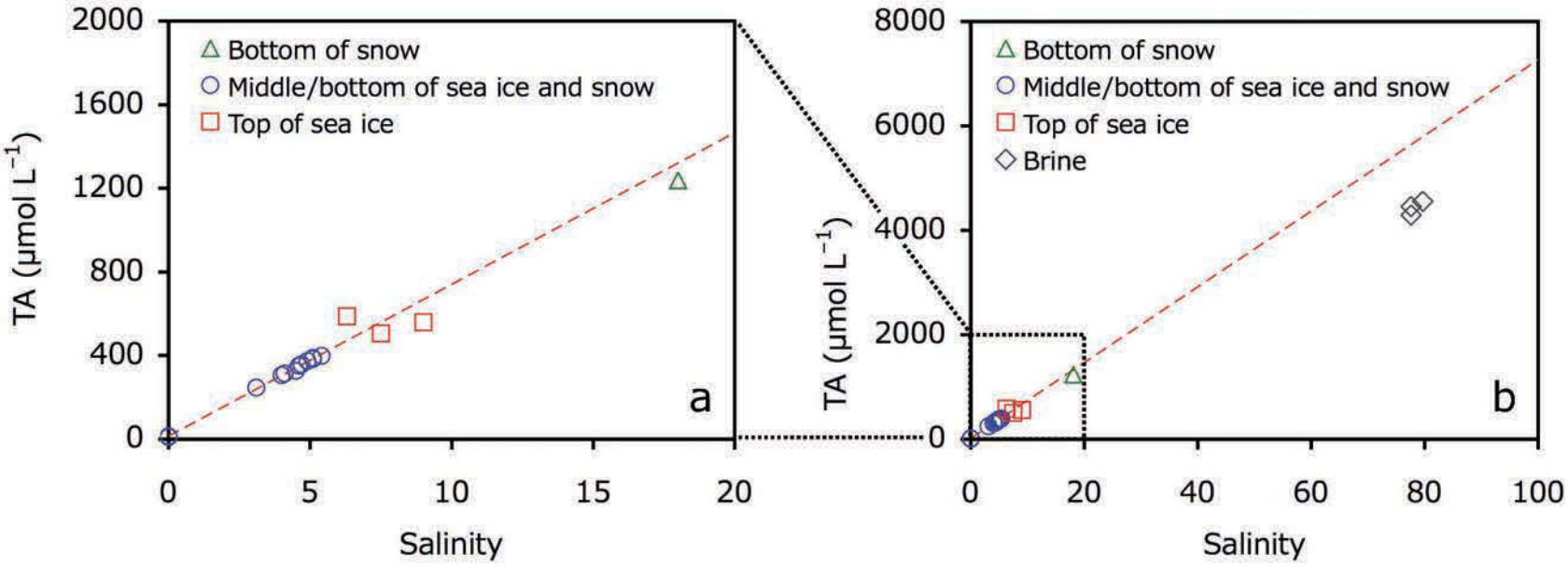

Figure 7, Nomura et al.

Table 1. Sampling date, time (UTC), location, air temperature (ºC), snow and slush depths (cm) and ice thickness (cm) at stations.

Station	Date of 2011	Time	Location	Air temperature	Snow depth	Slush depth	Ice thickness
1	27 April	14:23	80º38′49″N, 12º16′27″E	-3.5	33.5	no slush	>500
11	29 April	09:00	80º47′38″N, 12º26′05″E	-0.7	5.0	no slush	88.0
20	02 May	10:30	81º03′09″N, 16º27′00″E	+0.3	19.6	7.0	58.0
21	03 May	11:00	81º09′43″N, 16º02′41″E	-6.5	25.0	no slush	125.0
22	06 May	10:00	80º55′47″N, 15º16′44″E	-0.9	30.0	no slush	119.0
25	08 May	08:30	80º32′46″N, 19º27′07″E	-1.9	3.3	no slush	85.0
27a	10 May	14:00	80º49′04″N, 16º17′36″E	-12.8	39.0	3.0	124.0
27b	11 May	09:00	80º48′01″N, 16º17′27″E	-10.5	1.0	10.0	31.0

Table 2. Mean (range) temperature and salinity for sampled snow, slush (brine) and sea ice.

Station	Temperature			Salinity		
	Snow °C	Slush °C	Sea ice °C	Snow	Slush	Sea ice
1	−3.0 (−5.1 to −1.7)	no slush	−4.2 (−4.7 to −3.6)	0.0 (0.0 to 0.0)	no slush	0.0 (0.0 to 0.0) [1]
11	−1.2 (−2.5 to +0.1)	no slush	−2.3 (−3.5 to −1.0)	0.0 (0.0 to 0.0)	no slush	6.5 (5.2 to 8.3)
20	−0.5 (−1.5 to ±0.0)	−2.8 (−2.8 to −2.8)	−1.6 (−2.0 to −0.9)	1.3 (0.0 to 2.5)	20.2 [2]	7.1 (4.1 to 10.6)
21	−2.2 (−3.2 to −1.9)	−3.9 (−3.9 to −3.8) [3]	−2.9 (−4.1 to −1.1)	6.0 (0.0 to 18.0)	78.3 (77.6 to 79.6) [3]	5.3 (3.1 to 9.0)
22	−2.4 (−3.4 to −0.1)	no slush	−2.9 (−3.9 to −1.5)	2.4 (0.0 to 7.1)	no slush	5.8 (4.3 to 8.8)
25	−0.4 (−0.6 to −0.1)	no slush	−1.0 (−1.5 to −0.7)	0.0 [1]	no slush	6.4 (3.7 to 12.3)
27a	−5.3 (−8.9 to −2.4)	−2.1 [2]	−2.1 (−2.7 to −1.2)	0.1 (0.0 to 0.2)	37.6 [2]	1.4 (0.1 to 2.9)
27b	−3.3 [2]	−1.5 (−1.5 to −1.5)	−0.8 (−0.9 to −0.6)	no data	23.4 (23.2 to 23.5)	5.3 (4.1 to 7.0)

1. Only top 15 cm of sea ice
2. Only one data
3. Brine (no slush)

Table 3. Mean, standard deviation (SD) and median for d_{max} (μm) of ikaite crystals.

Sample name	Station	Sample type	Sample position	Number of crystals	d_{max}		
					Mean	SD	Median
#03	20	Sea ice	Top 7 cm	168	200.7	86.4	181.2
#09	20	Slush	–	111	150.9	56.4	143.5
#10	20	Sea ice	Top 10 cm	132	213.6	130.0	122.6
#16	21	Snow	Bottom 9 cm	76	375.7	153.7	381.0
#17	21	Sea ice	Top 10 cm	177	112.4	44.1	108.3
#29	22	Snow	Bottom 10 cm	210	218.0	94.5	199.2
#35	27b	Sea ice	Top 5 cm	44	265.0	80.8	263.5
All of crystals	–	–	–	918	201.0	115.9	171.4

A.2 Dissolved extracellular polymeric substances (dEPS) dynamics and bacterial growth during sea ice formation in an ice tank study

This manuscript is published in Polar Biology (2012), 35:661 - 676.

Polar Biol (2012) 35:661–676
DOI 10.1007/s00300-011-1112-0

ORIGINAL PAPER

Dissolved extracellular polymeric substances (dEPS) dynamics and bacterial growth during sea ice formation in an ice tank study

Shazia N. Aslam · Graham J. C. Underwood · Hermanni Kaartokallio · Louiza Norman · Riitta Autio · Michael Fischer · Harri Kuosa · Gerhard S. Dieckmann · David N. Thomas

Received: 1 July 2011 / Revised: 19 September 2011 / Accepted: 7 October 2011 / Published online: 26 November 2011

Abstract Extracellular polymeric substances (EPS) are known to help microorganisms to survive under extreme conditions in sea ice. High concentrations of EPS are reported in sea ice from both poles; however, production and dynamics of EPS during sea ice formation have been little studied to date. This investigation followed the production and partitioning of existing and newly formed dissolved organic matter (DOM) including dissolved carbohydrates (dCHO), dissolved uronic acids (dUA) and dissolved EPS (dEPS), along with bacterial abundances during early stages of ice formation. Sea ice was formed from North Sea water with (A) ambient DOM (NSW) and (B) with additional algal-derived DOM (ADOM) in a 6d experiment in replicated mesocosms. In ADOM seawater, total bacterial numbers (TBN) increased throughout the experiment, whereas bacterial growth occurred for 5d only in the NSW seawater. TBN progressively decreased within developing sea ice but with a 2-fold greater decline in NSW compared to ADOM ice. There were significant increases in the concentrations of dCHO in ice. Percentage contribution of dEPS was highest (63%) in the colder, uppermost parts in ADOM ice suggesting the development of a cold-adapted community, producing dEPS possibly for cryoprotection and/or protection from high salinity brines. We conclude that in the early stages of ice formation, allochthonous organic matter was incorporated from parent seawater into sea ice and that once ice formation had established, there were significant changes in the concentrations and composition of dissolved organic carbon pool, resulting mainly from the production of autochthonous DOM by the bacteria.

Keywords Sea ice · Extracellular polymeric substances · Frost flowers · Bacteria · Dissolved carbohydrate · Dissolved organic matter · EPS

Electronic supplementary material The online version of this article (doi:10.1007/s00300-011-1112-0) contains supplementary material, which is available to authorized users.

S. N. Aslam (✉) · G. J. C. Underwood
Department of Biological Sciences, University of Essex, Wivenhoe Park, Colchester, Essex CO4 3SQ, UK
e-mail: shaziaa@essex.ac.uk

H. Kaartokallio · R. Autio · D. N. Thomas
Finnish Environment Institute (SYKE), Marine Research Centre, P.O. Box 140, 00251 Helsinki, Finland

L. Norman · D. N. Thomas
Ocean Sciences, College of Natural Science, Bangor University, Menai Bridge, Anglesey LL59 5AB, UK

M. Fischer · G. S. Dieckmann
Alfred Wegener Institute for Polar and Marine Research, Am Handelshafen 12, 27570 Bremerhaven, Germany

H. Kuosa
Tvärminne Zoological Station, University of Helsinki, Helsinki, Finland

Introduction

During sea ice formation, inorganic and organic (both dissolved and particulate) constituents become concentrated in the brines present in ice channels and pores, the volume of which is primarily dependent on temperature (Petrich and Eicken 2010). Organisms entrained into ice also undergo very different chemical and physical constraints during the phase shift from open water to a semi-solid system where water and gas exchange can be limited (Mock and Thomas 2005). The microbial community composition in sea ice at early stages of ice formation reflects that of the parent seawater, but as the ice ages, there is shift in population and

dominance of species leading towards the establishment of a psychrophilic community (Caron and Gast 2010; Collins et al. 2010; Deming 2010). Bacterial abundances and algae can be tightly coupled in young ice (Stewart and Fritsen 2004), although this relationship is not always so clear (reviewed by Brierley and Thomas 2002).

Studies have revealed that despite losses of dissolved organic matter (DOM) from consolidating sea ice due to brine drainage into the underlying water, there are generally significantly higher DOM concentrations in sea ice compared to seawater (Thomas et al. 2001; Dumont et al. 2009; Juhl et al. 2011; Norman et al. 2011). Within the ice, the distribution of DOM is unpredictable and dissolved organic carbon and nitrogen (DOC and DON) concentrations usually demonstrate a heterogeneous distribution (van der Merwe et al. 2009; Underwood et al. 2010).

A significant proportion of organic matter in sea ice can be present in the form of extracellular polymeric substances (EPS), predominantly polysaccharides containing uronic acids, sulphated sugars and some proteins (Hoagland et al. 1993; McConville et al. 1999; Meiners et al. 2003; Krembs et al. 2011), released by both bacteria and algae (Mancuso Nichols et al. 2005; Krembs and Deming 2008; Collins et al. 2010). EPS exist along a continuum of solubility, from dissolved to particulate states, that depends on both physical and chemical conditions, with EPS contributing up to 60% to particulate organic carbon (POC) and up to 99% to DOC (Herborg et al. 2001; Thomas et al. 2001; Riedel et al. 2006; Dumont et al. 2009; Underwood et al. 2010). Like DOC and DON, dissolved EPS (dEPS) concentrations in sea ice have a heterogeneous distribution pattern within ice core profiles, while particulate EPS (pEPS) are predominantly found in biomass-rich horizons in the ice (Krembs et al. 2002; Volkman and Tanoue 2002; Meiners et al. 2003; Dumont et al. 2009; van der Merwe et al. 2009; Krembs et al. 2011). EPS can modify the ice environment by changing ice microstructures, therefore increasing the sea ice habitability (Krembs and Deming 2008; Ewert and Deming 2011; Krembs et al. 2011). Presence of high concentrations of complex EPS (both particulate and dissolved forms) in sea ice is thought to be due to EPS playing an important role for sea ice microbial communities by providing buffer zones and cryo-protection against salinity and low temperatures (Bowman and Deming 2010; Underwood et al. 2010; Krembs et al. 2011). Both dEPS and pEPS may also be serving as important carbon sources in sea ice (Mock and Thomas 2005) as higher rates of bacterial activity have been reported to be associated with high molecular weight DOC fractions in other environments (Tranvik 1990). Similarly, pEPS are also reported as hot spots of microbial activity in sea ice (Meiners et al. 2008). However, it is likely that not all bacteria present can utilise all EPS types, as has been shown in estuarine sediments (Hofmann et al. 2009).

Both experimental and field studies have suggested that initial distribution of inorganic and organic matter in sea ice follows patterns of conservative enrichment (Clarke and Ackley 1984; Cota et al. 1987; Garrison et al. 1990) and that as the ice ages, microbial communities influence the subsequent distribution of DOM in sea ice (Stedmon et al. 2007). However, to understand the fate of organic matter in growing sea ice, systematic studies are needed. Giannelli et al. (2001) performed a mesocosm study to investigate the partitioning of DOM in young sea ice. Partitioning of inorganic nutrients and dissolved organic matter into brines, seawater and sea ice fractions were measured, but this study did not try to link DOM with microbial biomass and/or activity within the experimental systems. To the best of our knowledge, there have been no other detailed environmentally controlled sea ice tank studies that make simultaneous measurements of organic matter and bacterial dynamics during ice formation. The objective of the work presented here was to refine the experimental approach used by Giannelli et al. (2001) and to investigate the partitioning of organic matter, and changes in the dynamics and composition of dEPS during the early stages of ice growth in relation to bacteria numbers in ice and the underlying water. Furthermore, the addition of a complex algal-derived DOM source was included in the experimental matrix both to follow the partitioning of this additional organic carbon (both dissolved and particulate) and its effect on bacterial growth in the early stages of ice formation.

Materials and methods

General methods

The experiments were conducted between 30 September and 9 October 2009 at the HSVA environment test basin, Hamburg, Germany (http://www.hsva.de). Experimental polyethylene (PE) bags (total 18) supported by a floating frame were arranged in a random block design within the main test basin (Fig. 1a). On 30 September, each bag was filled with 1.2 m^3 of unfiltered seawater from the North Sea, and the temperature of the air was set to approximately 0°C to cool the water. The 21 m^3 of surface seawater had been pumped onto a ship close to the island of Helgoland (54°11′N, 7°55′E), transferred to a cleaned (food quality) road tanker and delivered to the experimental facility within 24 h of initial collection. The temperature of the seawater on collection was 13 ± 1°C. This temperature was maintained ±1°C during the transport to the test basin.

Each experimental bag was equipped with a PVC tubing in one corner (fixed on the floating frame) to allow for

Fig. 1 **a** Experimental mesocosms in environmental test basin of HSVA, **b** Frost flowers on surface of one of the mesocosms on day 6. The surface area of each mesocosm was 1 m^2

water pressure equilibration during ice growth and to ensure that the ice was always in contact with the underlying water. These tubes were cleared of ice every day and also served as a portal for sampling under-ice water once an ice cover had developed. A simple circulation pump was set up, and continually running, in each of the experimental bags to ensure that mixing of the water was complete at all stages of the experiment.

On 2 October, 900 ml of a concentrated solution of algal-derived organic matter (ADOM) was added to 9 bags, which are referred to as the ADOM series, while remaining 9 bags filled with North Sea water were used as controls and are referred as NSW. The ADOM additive was produced as follows: Frozen paste of the freshwater green alga *Chlorella vulgaris* (supplied by Varicon Aqua Ltd, U.K.) was melted in synthetic seawater of a salinity of 34 (1 kg paste melted in 1 l seawater). The resulting suspension was sonicated in 500 ml batches with a Branson 450 Digital Sonifier (Branson Ultrasonics Corporation, Danbury, CT, USA). Samples were sonicated in a seawater/ice bath so that sample temperature did not rise above 0°C. The resulting suspensions were pooled, centrifuged at 12,235*g* in a Beckmann Coulter centrifuge using a J-LITE® JLA-8.1000 Rotor (Fixed Angle, Aluminum, 6 × 1,000 ml) and the supernatant was frozen at −18°C until used in Hamburg. This solution was pink in colour, presumably due to the chlorophyll breakdown products as described by Engel et al. (1991) and Hortensteiner et al. (2000). The dissolved organic carbon (DOC) concentration of this material was 550 mmol l^{-1}. Experimental set-up was designed to prevent autotrophic growth. The room was in darkness except during sampling periods (2–3 h per day) when the light levels were very low.

Initial samples (d0) were taken on the 2 October after >24 h of mixing of the water and ADOM. Freezing of the water in the mesocosms was then initiated by decreasing the air temperature to −13°C (±2°C), and spraying a fine mist of Milli-Q water over the surface of the mesocosms to provide surface ice nucleation points (Giannelli et al. 2001). This temperature was maintained throughout the experiment.

The seawater was sampled from all mesocosms on d0 and d3; afterwards, underlying water was sampled along with ice in randomly chosen mesocosms on days 4, 5 and 6 in each of the two treatment series. Brines were collected on days 5 and 6 only, and once brines and ice were sampled from bags, no further sampling was done from those bags.

The seawater was sampled through the PVC pressure release tube. Firstly, ice (when present) was removed and then the water in the tube was sampled using 50 ml plastic syringes and small-bore Teflon tubes. At each sampling time, the temperature of the water was measured.

Ice was sampled by sawing ice cores from the ice sheet and sectioning the cores immediately (less than 1 min). The ice cores were floated until sectioning, minimising brine drainage from the skeletal layer. Ice temperatures, at 4 cm depth intervals, were measured on representative ice cores. The ice cores were melted at room temperature overnight in 5 l acid-washed PE drums. The melting was carefully monitored, and the temperature of the melt water did not rise above 0°C.

Brines were collected following sackhole drilling to a depth of 6 cm, using a Cherepanov ice ring of 20 cm diameter. Brine drained into the core rim left when the corer and core shavings were removed, but the partial core was left in place (see discussion by Papadimitriou et al. 2007). This approach enabled a minimum surface area of brine to come into contact with the air. Even so, due to the cold air and ice temperatures, only small volumes (<200 ml in 30 min) of brine were collected in each sackhole. Consequently, brines collected from several sackholes within each mesocosm had to be pooled to generate sample volumes necessary for subsequent analyses. Prior to sampling, the temperature of the brine was measured in each of the sackholes. The sackholes were drilled as far away from the location of ice core sampling as possible, so as not to compromise the samples.

Frost flowers developed on the surface of all of the mesocosms (NSW and ADOM, Fig. 1b) from day 2 onwards. On days 5 and 6, these were sampled by carefully scraping the frost flowers into acid-washed 1 l PE containers, using the rim of the container as the "scraper" and ensuring that the frost flowers fell straight into the container, thereby minimising contamination issues. The frost flowers were melted at room temperature (<1 h) and again the melt water did not rise above 0°C.

It has been shown that bacteria are capable of surviving short-term salinity reductions associated with direct melting without losing their viability (Helmke and Weyland 1995); therefore, ice cores were melted without the addition of seawater to avoid any potential dilution of samples and addition of allochthonous DOM or bacteria. Samples for determining major inorganic nutrients (nitrate, nitrite, phosphate and silicate), dissolved organic nitrogen (DON), dissolved organic carbon (DOC), dissolved carbohydrates (dCHO), dissolved uronic acids (dUA) and ethanol solubility-based fractionated dEPS were collected from seawater, melted ice, sackhole brine and melted frost flowers within 2 h, after filtering through pre-combusted (400°C for 2 h) Whatmann GF/F filters (20–500 ml). The filtrates were stored at −20°C until analysis. Salinity measurements were made on aliquots of these samples prior to freezing.

Temperature and salinity measurements

All ice (in the gradient across the ice), brine, frost flowers (base of frost flowers) and water temperatures were measured with a calibrated Testo 110 thermometer. Salinities of water, brines and melted ice were measured at laboratory temperature (17–22°C) using a SEMAT Cond 315i/SET salinometer with WTW Tetracon 325 probe.

Bacterial abundance and oxygen measurements

Samples for bacterial abundance determination were fixed with 0.2 μm filtered electron microscopy-grade glutaraldehyde (final concentration of 0.5%) and stored at 4°C. Cells were stained with SYBR Green I (Molecular Probes) at a final dilution of 1:10,000 for at least 10 min in the dark and analysed with an LSR II flow cytometer (BD Biosciences) using a 488 nm laser (essentially after Gasol et al. 1999) within 30 min of staining. CountBright beads (Molecular Probes) were added to each sample to calculate the volume of sample used in counting. Bacterial data were typically acquired until 50,000 events were recorded, and cell populations of high and low DNA bacteria identified from bivariate plots of green fluorescence vs. SSC (side scatter) using FACS Diva software (BD Biosciences). Cell abundance in cells ml^{-1} was calculated from sample flow rates and number of events recorded.

Dissolved oxygen concentrations of water samples (50 ml samples) were measured by Winkler titration with photometric end-point detection (HydroBios GmbH).

Organic carbon (POC and DOC) analyses

DOC was analysed by high temperature combustion on an MQ1000 TOC analyser (Qian and Mopper 1996), see Papadimitriou et al. (2007) and Norman et al. (2011) for further details. For POC measurements, samples (filters) were treated with 2N HCL to remove inorganic carbon if present and were kept overnight in the fume cupboard to dry. POC was measured on Shimadzu Solid Sample Module (SSM 5000A) linked with Shimadzu TOC-VCSH Analyser. TOC (total organic carbon) was calculated by adding DOC and POC together.

Carbohydrate analysis

Samples (in duplicate) were dialysed at room temperature for 8–15 h, depending on salinity, through 8 kDa dialysis tubing (VWR, USA) against Milli-Q water to a final salinity <1. The desalted samples were freeze-dried and stored at −20°C until further analysis. Subsequently, the samples were re-dissolved in 4 ml Milli-Q water (into four aliquots of 1 ml each). One aliquot was used for carbohydrate analysis (total dissolved carbohydrate dCHO), and other three were used for ethanol precipitation of dEPS. Carbohydrate concentrations in dissolved form (dCHO) and in dEPS (ethanol solubility-based EPS fractions) were determined by a modified method of Dubois et al. (1956) as described in Underwood et al. (2010). Glucose was used as a standard and so the carbohydrate concentrations are reported as glucose-carbon-equivalents. Uronic acids (dUA) concentrations in each fraction were determined by standard carbazole assay (Bitter and Muir 1962; Bellinger et al. 2005). Glucuronic acid was used as a standard, and all uronic acids are therefore expressed as glucuronic-carbon-equivalents. Fractions were calculated both as concentrations (μmol l^{-1} C) and as percentages of the total dissolved carbohydrate recovered.

EPS components with different solubility were precipitated with 30, 50 and 70% (v/v) ethanol overnight at 4°C. The precipitates for each were recovered by centrifugation (3,500*g*, 15 min), air-dried and re-dissolved in Milli-Q water (0.65 ml). These precipitated dEPS fractions were named as EPS-30, EPS-50 and EPS-70 (precipitated with 30, 50 and 70% ethanol, respectively). The terms EPS-30, EPS-50 and EPS-70 refer to the concentrations (μmol l^{-1} C) of highly complex, complex and less complex dEPS fractions and were used when carbohydrate concentration of each dEPS fractions were considered.

The term dCHO describes total dissolved carbohydrates (≥8 kDa) concentration (μmol l^{-1} C), which measures the carbohydrate concentrations of both dEPS (EPS-30 + EPS-50 + EPS-70) and the non-EPS (which did not precipitate with any ethanol) carbohydrate fractions. The terms $\%CHO_{0–30}$ (highly complex EPS), $\%CHO_{30–50}$ (complex EPS), $\%CHO_{50–70}$ (less complex EPS) and $\%CHO_{70–100}$ (non-EPS) refer to the percentage contribution of dEPS and non-EPS carbohydrate fractions relative to the total dissolved carbohydrate (dCHO) concentration and were calculated as described by Underwood et al. (2010) (Online Resource 1).

Inorganic nutrients and DON analyses

Major dissolved inorganic nutrients (nitrate, nitrite, phosphate and silicate) were analysed by standard colorimetric methodology (Grasshoff et al. 1983) as adapted for flow injection analysis (FIA) on a LACHAT Instruments QuickChem 8000 autoanalyser (Hales et al. 2004). Dissolved ammonium was determined by fluorimetric method of Holmes et al. (1999) using a Hitachi F2000 fluorescence spectrophotometer. DON was determined by the subtraction of nitrate and ammonium from the total dissolved nitrogen (TDN) analysed using online peroxodisulfate oxidation coupled with ultraviolet radiation at pH 9.0 and 100°C (Kroon 1993).

All measurements [for both inorganic (nitrate, nitrite, phosphate and silicate) and organic components (DOC, POC, dCHO, dUA and dEPS)] were obtained on all ice sections of each ice core collected for both NSW and ADOM series, but where the term 'bulk ice' is used it refers to average values of all ice sections of ice cores collected on that particular day for each of the NSW and ADOM mesocosms. In order to minimise the effect of dilutions or concentrations occurring during sea ice formation, all data (except when used for discussion of the data set) presented here were normalised to the starting seawater salinity of 33. All statistical analyses except permutational multivariate analysis of variance (PERMANOVA) analysis were conducted on SPSS® 18.0. PERMANOVA for EPS profiles were carried out in Primer 6, data were analysed using Euclidean Distance similarity measures. Significant differences between NSW and ADOM samples were calculated by *t* test. Significant differences between sample types were determined using analysis of variance (ANOVA, with Tukey post hoc tests). Normality of all groups of samples was checked, but the assumption of normality could not be rejected in any case. Standard error (SE) was used as measure of variability for all. Pearson's correlation analysis was used to investigate relationships between different variables. All statistically significant differences quoted are at $P \leq 0.05$.

Results

Temperature, salinity and inorganic nutrients

By the final sampling day (d6), the average ice thickness was 12 cm ± 0.4 (±SE) having grown at a rate of 1.8 cm d^{-1} (±0.1). Water temperatures before ice formation on the first sampling day ranged from 0.3 to 0.7°C, but once ice cover was established (d4); under ice water temperatures remained stable at −1.8 to −1.9°C. Average ice salinities decreased from d4 to d6 in both NSW (12–10.8) and ADOM (13–10.7) series with highest salinities always occurring in the bottom ice sections (Online Resource 2). Brine temperatures decreased from a range of −3.1 to −5.1°C when first measured (on d5) to a range of −5.3 to −6.0°C on the final day (d6). Over the same time interval, brine salinities increased from 71.2–81.2 (d5) to 85.4–90.4 (d6).

At the start of experiment (d0), concentrations of both phosphate and ammonium were significantly higher ($t_{16} = 14.7$ and 9.8 for NH_4^+ and PO_4^{3-}, respectively both at $P < 0.001$) in ADOM seawater in comparison with NSW seawater (Fig. 2). Higher concentrations of phosphate (4–15-fold) and ammonium (2–19-fold) were present in all samples collected from ADOM mesocosms compared to the NSW series, with phosphate and ammonium concentrations varying little in the NSW samples but with decreases in phosphate and increases in ammonium concentrations in the ADOM series over time (Fig. 2).

Variations in the initial concentrations (c.f. d0) of nitrate, nitrite and silicate in the seawater were measured between individual mesocosms, but were not significantly different between the NSW and ADOM series (Fig. 2). Frost flowers had significantly higher concentrations of both nitrite and nitrate (at $P < 0.01$) than the underlying seawater (87- and 11-fold, respectively), sea ice (32- and 3-fold, respectively) and brines (53- and 11-fold, respectively) in both NSW and ADOM series.

Bacterial abundance and dissolved oxygen

Direct microscopic observation found no evidence of significant numbers of autotrophic protists (diatoms or flagellates). Abundances of both flagellates (278.1 ± 22.4 cells ml^{-1}) and ice algae (800 ± 188.6 cells ml^{-1}) were very low in the parent seawater (NSW at d0), and afterwards, the abundance of these taxa decreased progressively during the experiment, especially in the case of ice algae when only empty theca or broken cells were encountered after d3 (Online Resource 3).

The total bacterial numbers (TBN) were significantly ($P < 0.01$) higher in ADOM bags in comparison with NSW treatments, in all samples (seawater, sea ice, brines and frost

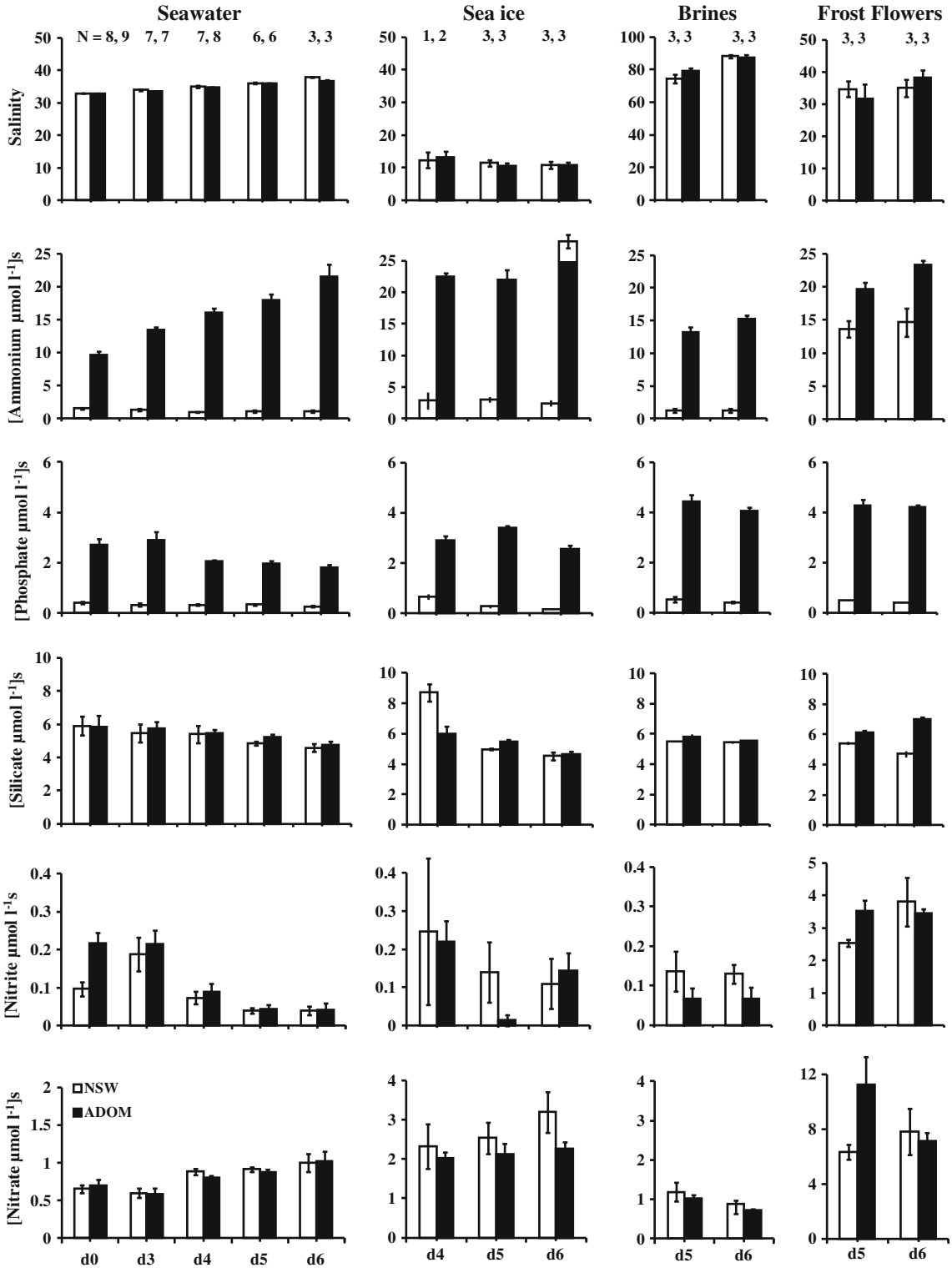

Fig. 2 Salinities and inorganic nutrients (normalised to salinity 33) in seawater, bulk sea ice, brines and frost flowers during experimental ice formation. The numbers (*N*) on the top of the *bars* represent sample number collected on that sampling day. No sampling was done on d1 and d2 (3rd and 4th Oct)

flowers; Fig. 3a–d). In ADOM seawater, TBN were still increasing after 6 days and the ratios of high-DNA/low-DNA bacteria doubled (2.7–6.6) during the last two sampling days (Online Resource 4). In NSW seawater, TBN (both high-DNA and low-DNA bacteria) declined after d5 (Fig. 3a). In both ADOM and NSW seawaters, TBN were negatively

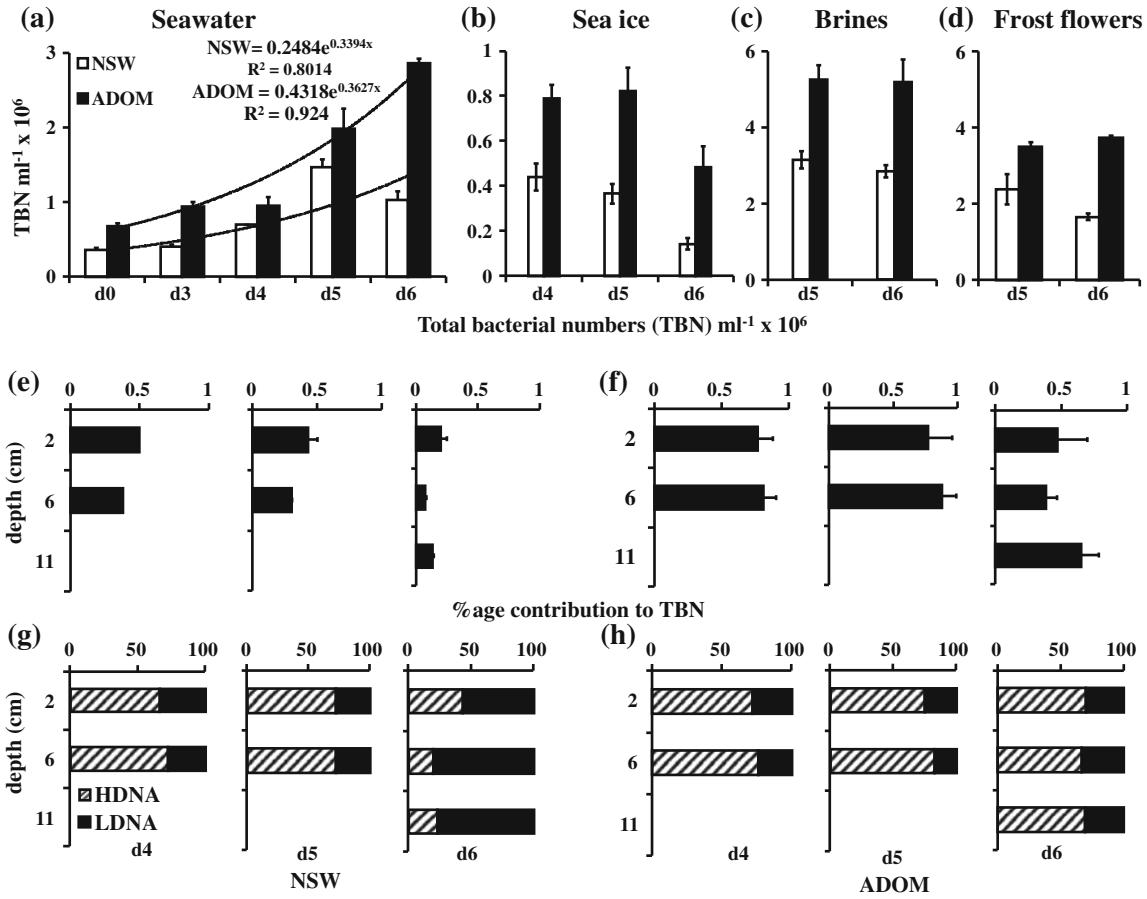

Fig. 3 Total bacterial numbers (TBN) in **a** seawater, **b** bulk sea ice, **c** brines and **d** frost flowers samples on each sampling day. Total bacterial numbers (TBN) along the vertical length of young sea ice (during growth from 0 to 14 cm thickness over sampling days) in **e** NSW and **f** ADOM mesocosms. Percentage contributions of high-DNA and low-DNA bacteria to TBN in **g** NSW and **h** ADOM ice. Except for ice cores collected on d4 ($N = 1$ and 2 for NSW and ADOM, respectively), N (number of samples) was ≥ 3 for all sample types collected from both NSW and ADOM mesocosm on each day

correlated with temperature ($r = 0.56$, $n = 23$ and $r = 0.56$, $n = 24$ at $P < 0.01$ NSW and ADOM seawater, respectively) and positively correlated with salinity ($r = 0.68$, $n = 23$ and $r = 0.91$, $n = 23$ at $P < 0.01$ NSW and ADOM seawater, respectively). In seawater, TBN in both series were also correlated with NO_2 and NO_3 concentration (Online Resource 5).

In bulk ice, TBN significantly (at $P < 0.05$) decreased with decreasing temperatures (Online Resource 2) over the sampling period (Fig. 3b), but this decrease in TBN was greater (2-fold higher) in NSW ice than ADOM ice. On the first ice sampling day (d4), high-DNA bacterial numbers (3.0×10^5 and 5.8×10^5 cells ml^{-1} for NSW and ADOM, respectively) were significantly higher than low-DNA bacterial numbers (1.4×10^5 and 2.0×10^5 cells ml^{-1} for NSW and ADOM, respectively) in both cases, but on d6, there was 6-fold decrease in high-DNA bacterial numbers compared to low-DNA (9.5×10^4 cells ml^{-1}) in NSW ice, as a result the ratio of high-DNA/low-DNA decreased to 0.5. In ADOM sea ice, high-DNA/low-DNA ratios were still high (2.2) on the last sampling day (Online Resource 4).

TBN distribution in the depth layers of growing sea ice was also measured (Fig. 3e–h). In NSW sea ice, TBN were higher in surface ice (5×10^5 cells ml^{-1}), compared to lower sections (3.8×10^5 cells ml^{-1}) on d4 (Fig. 3e), whereas in ADOM sea ice, TBN were homogenously distributed (7.7×10^5 and 8×10^5 cells ml^{-1} for top and bottom ice sections, respectively) throughout the ice (Fig. 3f). The distribution pattern of TBN remained almost the same throughout the experiment in the NSW sea ice, i.e., highest cell numbers in surface ice (Fig. 3e), whereas in ADOM ice, there was a decrease in TBN in the surface sections of the ice on d6 (Fig. 3f).

There were no significant differences in dissolved O_2 concentrations in the seawater in NSW (291 ± 2 µmol l^{-1}) and ADOM (287 ± 2 µmol l^{-1}) mesocosms at the start of the experiment (Online Resource 3). Over the course of the experiment, the O_2 concentrations increased in the under-ice water by 55.9 ± 2 µmol l^{-1} in NSW bags, whereas in ADOM seawater, O_2 concentrations decreased by 17 ± 5 µmol l^{-1} (Online Resource 6).

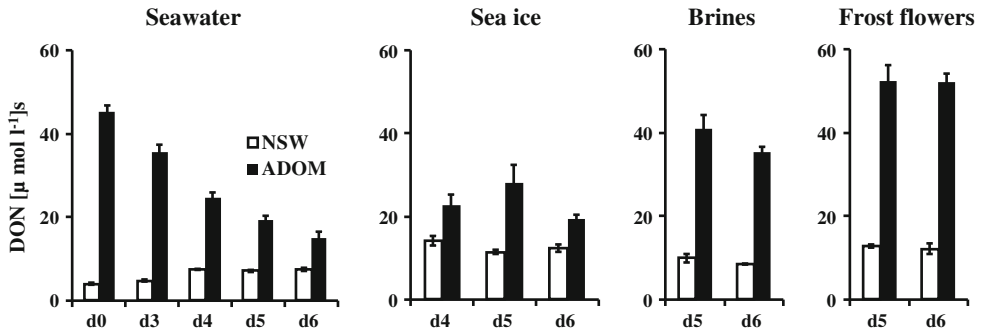

Fig. 4 Salinity-normalised (normalised to salinity 33) dissolved organic nitrogen (DON) in seawater, bulk sea ice, brines and frost flowers samples on each sampling day. Except for ice cores collected on d4 ($N = 1$ and 2 for NSW and ADOM, respectively), N (number of samples) was ≥3 for all sample types collected from both NSW and ADOM mesocosm on each day

Dissolved organic nitrogen (DON) and organic carbon (DOC and POC)

DON was significantly ($t_{12} = 40.8$ at $P < 0.01$) elevated at the start of the experiment (d0) in ADOM, compared to NSW mesocosms (Fig. 4). DON concentrations in the NSW mesocosms increased significantly (at $P < 0.01$) in the seawater by 4.0 ± 0.7 µmol l^{-1}, but changed little in the ice, brine and frost flowers over sampling period. In contrast, DON concentrations in seawater, bulk ice and brines decreased significantly (by 27.7 ± 0.4, 4.6 ± 1.0 and 5.6 ± 4.0 µmol l^{-1} for seawater, bulk ice and brine, respectively) in the ADOM mesocosms.

DOC constituted the major organic carbon fraction (74–85% of TOC) in the seawater and brine samples, whereas in frost flowers, DOC contributed only 48 and 36% of the TOC in NSW and ADOM samples, respectively. In comparison with NSW mesocosms, DOC and POC concentrations were significantly higher ($P < 0.01$) in all ADOM mesocosms at the start of the experiment (d0). Highest DOC levels (at $P < 0.01$) were measured in frost flowers (298.4 ± 12.9 and 520.2 ± 32.5 µmol l^{-1} from NSW and ADOM series, respectively) (Fig. 5a). For bulk ice samples, DOC concentrations decreased significantly (at $P < 0.05$) by 198 ± 21.2 and 161 ± 21.3 µmol l^{-1} in NSW and ADOM mesocosms, respectively, over the sampling period (Fig. 5a). There were also decreases in brine DOC concentrations from both NSW (decrease by 36.9 ± 6.9 µmol l^{-1}) and ADOM (decrease by 45.2 ± 3.6 µmol l^{-1}) series over the whole experiment (Fig. 5a). With these changes in DOC concentrations (except for brines), the ratios of DOC/DON also changed significantly in all groups of samples over the sampling period (Table 1).

POC concentrations were elevated in all samples taken from ADOM mesocosms with POC concentrations being higher ($t_{12} = 3.5$ at $P < 0.01$) in initial seawater (d0) by a factor of 2 (Fig. 5a).

Similar to the patterns showed by DOC, there was little variation in POC concentration in NSW seawater (5.1 ± 4.5 µmol l^{-1}), while there was a significant ($F_{4, 22} = 3.1$ at $P < 0.05$) increase in POC concentration (17.7 ± 12 µmol l^{-1}) in the ADOM water samples (Fig. 5a). POC concentrations increased by 31 ± 20.4 µmol l^{-1} in the ADOM ice, whereas there was a significant ($F_{2, 16} = 16.3$ at $P < 0.001$) decrease of 87 ± 6.4 µmol l^{-1} in the bulk ice from NSW mesocosms (Fig. 5a). In contrast to bulk ice, POC concentrations decreased in brines from both NSW (by 16.3 ± 3 µmol l^{-1}) and ADOM (by 34.5 ± 7 µmol l^{-1}) mesocosm (Fig. 5a).

Dissolved carbohydrates (dCHO and dUA) and different size fraction of dEPS

dCHO concentrations measured in seawater, brines and frost flowers were significantly higher in the ADOM mesocosms ($t = 5.0$–7.2 at $P < 0.05$). Highest concentrations of dCHO (at $P < 0.001$) were measured in bulk sea ice in comparison with all other sample types (Fig. 5b). Increases in dCHO concentrations were observed in bulk ice from both NSW (by 22.6 ± 3 µmol l^{-1}) and ADOM (by 37.0 ± 3.9 µmol l^{-1}) mesocosms (Fig. 5b). dCHO concentrations were correlated with temperature (negative for sea ice, but positive for brines and seawater) and salinity (negative for all samples types) in all samples collected from NSW tanks, whereas no such relationship was observed in samples taken from ADOM mesocosms (Table 2).

Dissolved uronic acids (dUA) concentrations were also significantly higher (at $P < 0.05$) in ADOM samples compared to NSW for all types of samples (Fig. 5b). Except for bulk ice from the NSW mesocosms, there was a gradual increase in dUA concentrations over the sampling period for all groups of samples (Fig. 5b). In seawater, the dUA contribution to dCHO increased significantly (at $P < 0.01$) up to 100% (for both NSW and ADOM) over the sampling period. In bulk ice, the dUA contribution to dCHO increased up to 83% in ADOM mesocosms, whereas in NSW treatments, it was reduced from 59 to 38% (Fig. 5b). In brines, there was also a significant ($P < 0.001$) increase

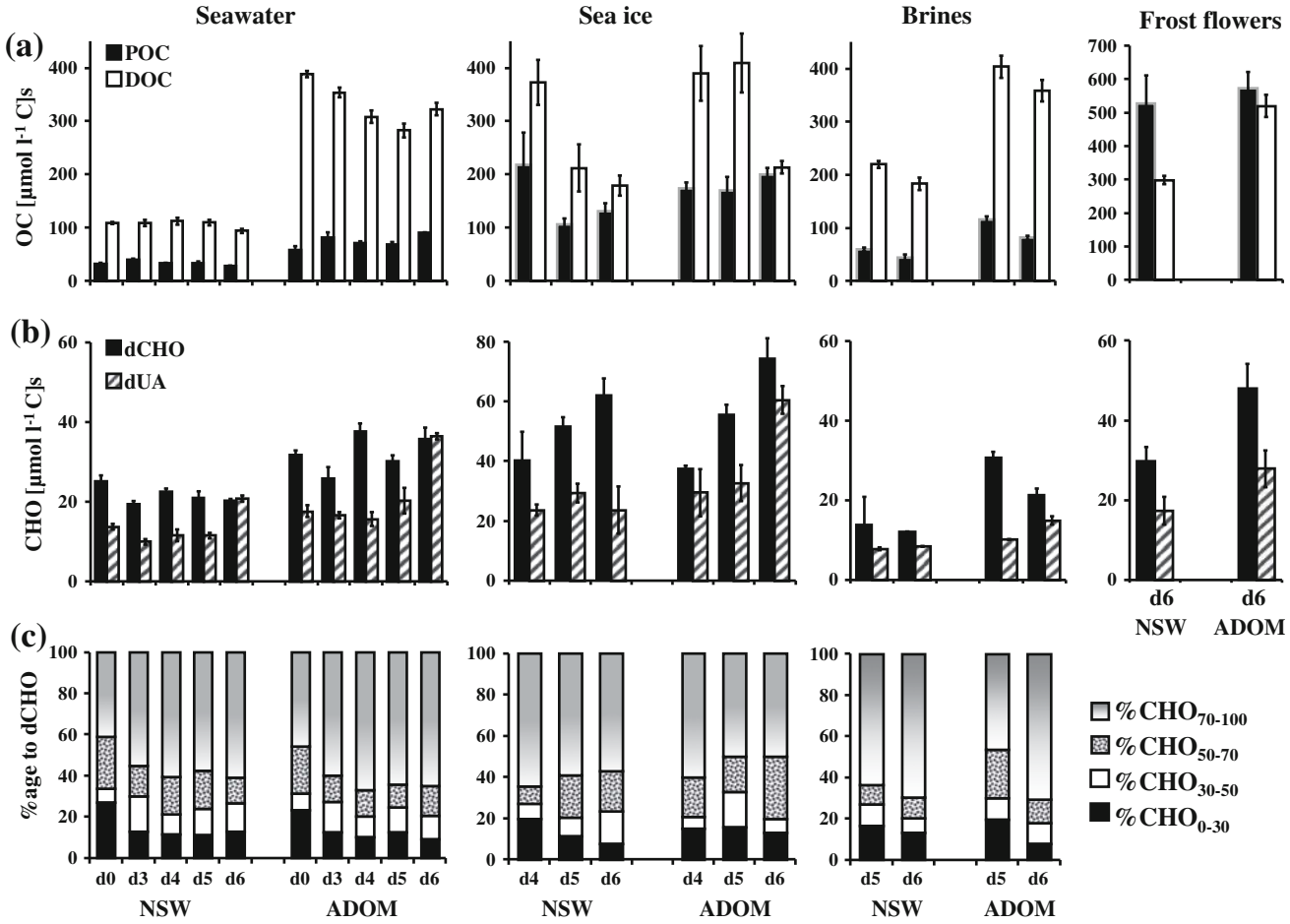

Fig. 5 Salinity-normalised (normalised to salinity 33) **a** organic carbon (POC and DOC), **b** carbohydrate (dCHO, dEPS and dUA) and **c** dEPS ($\%CHO_{0–30}$, $\%CHO_{50–30}$, $\%CHO_{70–50}$ and $\%CHO_{70–100}$) profile in seawater, bulk ice, brines and frost flowers. *Bars* on the left side of each graph represent concentrations in NSW samples, and bars on the right side are concentrations in ADOM mesocosms. Except for ice cores collected on d4 ($N = 1$ and 2 for NSW and ADOM, respectively), N (number of samples) was ≥ 3 for all sample types collected from both NSW and ADOM mesocosm on each day

Table 1 DOC/DON ratios of all groups of samples from sea ice generated in a 6d mesocosm experiment using North Sea water (NSW) and North Sea water enriched with additional algal-derived DOM (ADOM)

Sampling day	Seawater		Sea ice		Brines		Frost flowers	
	NSW	ADOM	NSW	ADOM	NSW	ADOM	NSW	ADOM
d0	27.9	9.0						
d3	23.1	10.0						
d4	15.1	12.5	27.5	17.7				
d5	15.3	12.6	18.0	15.0	22.2	9.8	14.2	10.8
d6	12.6	18.84	14.2	11.9	21.8	10.1	25.5	9.98

in dUA concentrations (34–69% to dCHO) over the sampling period in both NSW and ADOM mesocosms (Fig. 5b), whereas dUA contribution to dCHO was 57% (on day 6) in both NSW and ADOM frost flowers (Fig. 5b).

A significant proportion (>50%) of the dissolved carbohydrate present was composed of dEPS ($\%CHO_{0–30} + \%CHO_{30–50} + \%CHO_{50–70}$) in both NSW and ADOM seawater at the start of the experiment (d0), but dEPS levels decreased (from 59 to 39% and 54 to 33% in NSW and ADOM, respectively), and non-EPS ($\%CHO_{70–100}$) fraction increased (from 41 to 61% and 45 to 67% in NSW and ADOM, respectively) in both NSW and ADOM seawater over the sampling period (Fig. 5c).

Initially (d4), non-EPS carbohydrates ($\%CHO_{70–100}$) were proportionally abundant in bulk ice dCHO from both NSW (64%) and ADOM (60%) mesocosms. By d6, the

Table 2 Correlation between organic carbon (POC and DOC), dissolved carbohydrates (dCHO and dUA), dEPS fractions (EPS-30, EPS-50 and EPS-70), salinity and temperature in seawater, sea ice and brines

Variables	NSW							ADOM						
	DOC	POC	dCHO	EPS-30	EPS-50	EPS-70	dUA	DOC	POC	dCHO	EPS-30	EPS-50	EPS-70	dUA
Seawater														
Temperature	0.169 (29)	−0.181 (29	**0.631**** (29)	**0.877**** (29)	0.663 (29)	0.766 (29)	0.185 (28)	**0.691**** (27)	−0.505 (26)	0.066 (27)	**0.783**** (27)	**0.546**** (27)	**0.719**** (27)	−0.189 (26)
Salinity	−0.310 (31)	−0.309 (28)	**−0.414*** (29)	**−0.600**** (29)	**−0.522**** (29)	**−0.544*** (29)	0.374 (29)	**−0.749**** (33)	0.315 (26)	0.147 (27)	**−0.506**** (26)	**−0.424** (27)	**−0.463** (27)	**−0.574**** (26)
DOC		0.339 (28)	0.148 (29)	0.268 (29)	0.121 (29)	0.218 (29)	0.218 (29)		−0.206 (26)	−0.110 (27)	**0.557**** (27)	**0.527**** (27)	**0.576**** (27)	−0.077 (26)
POC			−0.270 (28)	−0.358 (28)	−0.325 (28)	−0.295 (28)	**−0.546**** (28)			−0.013 (26)	−0.558 (26)	**−0.468*** (26)	0.329 (26)	0.195 (25)
dCHO				**0.711**** (29)	**0.736**** (29)	**0.848**** (29)	0.07 (28)				0.288 (27)	**0.433*** (27)	**0.560*** (27)	0.166 (27)
TBN	−0.004 (23)	−0.100 (23)	0.354 (23)	**−0.430*** (23)	**−0.457*** (23)	**−0.479*** (23)	0.116 (23)	**−0.494*** (21)	**0.458*** (21)	0.103 (21)	**−0.439*** (21)	−0.409 (21)	−0.376 (21)	**0.858**** (20)
Bulk ice														
Temperature	−0.428 (16)	0.255 (15)	**−0.536*** (16)	0.227 (16)	−0.213 (16)	−0.336 (16)	0.174 (14)	0.221 (17)	−0.142 (18)	0.155 (18)	0.103 (18)	0.04 (18)	0.375 (18)	−0.028 (16)
Salinity	−0.072 (14)	0.066 (15)	**−0.739**** (16)	0.233 (16)	−0.322 (16)	−0.388 (16)	−0.102 (14)	0.246 (18)	−0.205 (18)	−0.302 (18)	−0.255 (18)	−0.452 (18)	−0.055 (18)	−0.231 (16)
DOC		**0.669**** (15)	0.113 (16)	0.183 (16)	0.044 (16)	0.202 (16)	−0.095 (14)		−0.266 (17)	−0.403 (17)	−0.397 (17)	−0.248 (17)	0.295 (17)	**−0.622*** (16)
POC			−0.45 (15)	0.105 (15)	0.351 (15)	−0.058 (16)	−0.078 (13)			0.168 (18)	−0.249 (18)	0.227 (18)	0.302 (18)	0.156 (16)
dCHO				−0.372 (16)	**0.563*** (16)	0.604 (16)	0.277 (14)				0.246 (18)	0.303 (18)	**0.608**** (18)	**0.739**** (16)
TBN	**0.635**** (16)	0.313 (15)	−0.256 (16)	0.342 (16)	−0.146 (16)	−0.367 (16)	−0.044 (14)	0.275 (16)	0.076 (18)	−0.400 (18)	−0.270 (18)	0.07 (18)	0.106 (18)	−0.301 (16)
Brines														
Temperature	**0.894*** (6)	0.593 (6)	**0.893*** (5)	**0.938*** (5)	**0.940*** (5)	0.981 (5)	−0.686 (5)	0.221 (6)	0.543 (6)	0.607 (6)	0.677 (6)	0.680 (6)	0.558 (6)	−0.553 (6)
DOC		0.625 (6)	0.815 (5)	**0.952*** (5)	0.809 (5)	0.880 (5)	−0.738 (5)		0.419 (6)	0.657 (6)	0.614 (6)	0.640 (6)	0.662 (6)	−0.639 (6)
Salinity	**−0.829*** (6)	−0.748 (6)	**−0.978**** (5)	**−0.906*** **(5)**	**−0.996**** (6)	**−0.910*** (6)	**0.829*** (6)	−0.560 (6)	−0.756 (6)	**−0.879*** (6)	**−0.896*** (6)	**−0.917*** (6)	**−0.892*** (6)	**−0.728*** (6)
POC			0.832 (5)	0.549 (5)	0.691 (5)	0.640 (5)	−0.732 (5)			**0.824*** (6)	**0.906*** (6)	**0.933**** (6)	**0.906*** (6)	**−0.92**** (6)
dCHO				0.873 (5)	**0.975**** (5)	0.866 (5)	−0.945 (5)				**0.979**** (6)	**0.935**** (6)	**0.951**** (6)	−0.786 (6)
TBN	−0.394 (7)	0.443 (6)	0.192 (5)	−0.102 (5)	0.018 (5)	0.241 (5)	0.205 (5)	−0.472 (6)	0.233 (6)	0.063 (6)	0.062 (6)	−0.047 (6)	0.006 (6)	−0.001 (6)

Values in bold are significant at $P < 0.05$* or < 0.01**

proportion of dEPS increased to almost parity with non-EPS fractions in both cases (Fig. 5c). In NSW sea ice, the percentage contribution of highly complex dEPS fraction ($\%CHO_{0-30}$) decreased to half (20–10%), whereas less complex EPS fraction ($\%CHO_{50-70}$) showed a significant increase (8–22%) on d5 (Fig. 5c). In general, there was an increase in dEPS contribution to dCHO over sampling period in both NSW and ADOM bulk ice, but these dEPS were mainly the less complex fractions ($\%CHO_{30-50}$ and $\%CHO_{50-70}$). Both dEPS ($\%CHO_{0-30}$, $\%CHO_{30-50}$ and $\%CHO_{50-70}$) and non-EPS ($\%CHO_{70-100}$) carbohydrate fractions did not show any significant temporal variation in NSW brines, whereas in ADOM brines contribution of highly complex EPS ($\%CHO_{0-30}$) decreased (3-fold) significantly and less complex EPS ($\%CHO_{50-70}$) and non-EPS ($\%CHO_{70-100}$) increased. Concentrations of dEPS fractions, in particular highly complex EPS (EPS-30) were significantly correlated with temperature and salinity in both seawater and brines (Table 2). Highly complex EPS (EPS-30) fraction was also negatively correlated with TBN in seawater (Table 2). In general, dEPS fractions (especially EPS-70) were correlated with dCHO for all sample types collected from NSW and ADOM mesocosms (Table 2).

Partitioning of POC, DOC, dCHO and dEPS within different depth layers of sea ice

Complete ice vertical sections (top to bottom) from each sampling day were analysed to study the partitioning of organic carbon (both DOC and POC), dissolved carbohydrates (dCHO and dUA) and ethanol solubility-based dEPS fractions in the growing sea ice (Fig. 6a–c). Except for ADOM sea ice on d5, DOC and POC showed identical distribution patterns in the ice. Initially (d4), dCHO concentrations were higher in surface ice sections in both series (Fig. 6b) and no significant changes were observed in NSW ice afterwards, while highest dCHO concentrations were measured in the middle ice sections in the ADOM ice on final sampling day (d6). The highest dUA concentrations were measured in bottom ice sections for both NSW (36 ± 13.6 µmol l^{-1}) and ADOM (62.1 ± 12 µmol l^{-1}) samples on the final sampling day. A 3-way PERMANOVA

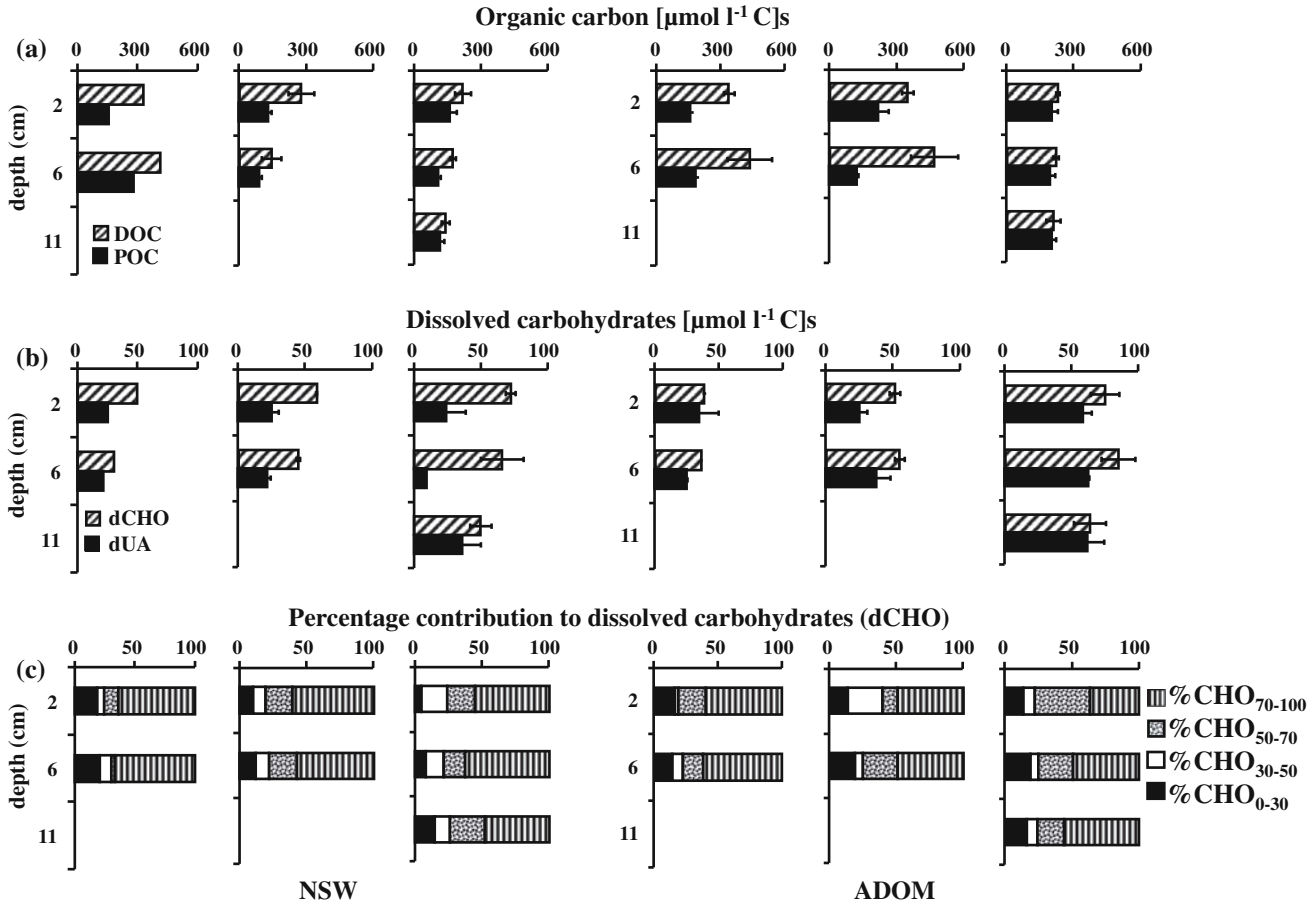

Fig. 6 Vertical profile of salinity-normalised (normalised to salinity 33) **a** organic carbon (POC and DOC), **b** carbohydrates (dCHO and dUA) and **c** dEPS profile in ice cores collected on each sampling day. Except for d4 ($N = 1$ and 2 for NSW and ADOM, respectively on d4), 3 ice cores were collected on each sampling day for both NSW and ADOM series and average of 3 ice cores was used for all graphs

analysis revealed that the profile of dEPS fractions in sea ice underwent significant changes over the sampling period ($F_{2,\ 26} = 3.2$ at $P < 0.05$) in both NSW and ADOM ($F_{1,\ 26} = 3.7$ at $P < 0.05$) treatments (Online Resource 5). SIMPER (Percentage similarities) revealed that these changes in dEPS profile were mainly due to increase in less complex EPS ($\%CHO_{50–70}$) and decrease in non-EPS ($\%CHO_{70–100}$) fractions in both NSW and ADOM series.

Physicochemical effects of changing salinity on the partitioning of organic carbon (DOC and POC) and carbohydrates (dCHO, dUA and dEPS fractions) in growing sea ice were also studied by plotting the salinity-normalised data against changing salinity over the sampling period (c.f. Gleitz et al. 1995). Partitioning of all the parameters studied deviated from the expected physical conservative concentration due to freezing (Online Resource 7). Overall (except for frost flowers from ADOM series), DOC concentrations declined below the levels expected due to physical concentration, while POC, dCHO, dUA and EPS-70 were enriched in both NSW and ADOM series (ESM_7).

Discussion

Bacterial abundance and activity

The aim of this experiment was to follow the partitioning of different organic carbon fractions together with the abundances of bacteria incorporated during the early stages of sea ice formation, using both unmodified seawater and seawater with a substantially enhanced DOC loading. The natural bacterial population in the water from the North Sea (which does not experience any extensive winter freezing) was able to grow in seawater at freezing point and were also presumably active in the newly formed sea ice as indicated by constant ratios of high-DNA/low-DNA bacteria with average temperatures of −7.5°C, particularly when additional organic substrates were added (ADOM treatment). This result is not surprising since in seasonally ice-covered non-polar seas (e.g. Baltic, Caspian Seas), ice forms over parent water that had reached the temperatures as high as +20°C during summer, yet psychrophilic ice communities emerge from that parent water (Kaartokallio et al. 2005, 2008). Although the North Sea does not have a direct history of ice, presumably, there are psychrophilic or psychrotolerant members in the bacterial communities that thrive in cold water during the winter months.

Decreases in bacterial abundance during the initial phases of ice formation in a natural sea ice system have been reported by Kaartokallio (2004) and have been considered to be a result of a gradual community shift towards an ice-adapted bacterial community (Collins et al. 2010; Deming 2010). Such a shift may be a possible explanation for observed decrease in ice bacterial abundances in the end of the experiment. Underlying seawater oxygen concentrations decreased significantly in ADOM bags, indicating high bacterial respiration rate (exceeding inputs of O_2 due to overlying ice formation). In NSW, increases in seawater O_2 concentrations, probably due to sea ice degassing and brine drainage, exceeded any decreases due to bacterial respiration.

Temperature and substrate concentrations were suggested by Pomeroy and Wiebe (2001) to act as interactive limiting factors for bacterial growth in cold environments, with abundant substrate compensating for cold temperature to a certain extent. This concept seems to be corroborated by our results, as substrate addition led to increased bacterial abundance as well as higher fractions of metabolically active, high-DNA bacteria in the bacterial population in the ADOM water. The increases in TBN in seawater were coupled to increases in NH_4^+ (due to the active metabolism of DON) and decreases in DOC concentration (Arrigo et al. 1995; Gleitz et al. 1995; Kattner et al. 2004), strongly indicating that the ADOM served as substrate and fuelled the growth of microbial assemblages in seawater (Junge et al. 2002; Brinkmeyer et al. 2003).

Negative correlation between TBN and temperature could be due to the temporal development of an ice-adapted bacterial community with the cooling of water. TBN were elevated in the ADOM treatments, with overall highest bacterial numbers present in the ADOM brines. These results reflect the spatial partitioning of cells into the brine channels (Junge et al. 2001), which in general occupy 8–10% of ice volume depending on temperature (Petrich and Eicken 2010). Bacterial abundance was lower in the forming ice than underlying seawater, with evidence of the establishment of heterotrophic bacterial community in the bottom ice segments (Deming 2010). There were gradual decreases in POC and DOC concentrations and changing characteristics of the EPS, along with highest TBN being recorded in bottom ice sections in the ADOM series. Greatest biological activity in bottom layers of ice is due to the close proximity to seawater, high rates of nutrient exchange with the underlying seawater, warmest temperatures and lowest fluctuations in salinity, making this zone a favourable habitat for microbial growth (Horner et al. 1992). Biological activity in bottom layers of ice is usually largely associated with ice algae and other protists (Arrigo et al. 2010), but probably because the experimental system was kept in darkness (as part of the experimental design), there was no evidence of any ice algae or protists growth in sea ice or seawater.

Partitioning and transformation of organic carbon

DOC concentration decreased with a subsequent increase in POC concentration in ADOM seawater, and these changes

in organic carbon were a result of increase in bacterial biomass, as indicated by the significant correlations of TBN with organic carbon (negative correlation with DOC and positive correlation with POC). An opposite trend was observed in samples collected from NSW mesocosms where a decrease was observed in both DOC and POC levels over the sampling period, which is indicative of decline in net heterotrophy (Deming 2010).

Dissolved carbohydrate (dCHO) concentrations were higher in sea ice than in the other types of samples, including brines and frost flowers, indicating that dCHO were retained in sea ice as described by other studies (Ewert and Deming 2011; Juhl et al. 2011). A major proportion of the dCHO was composed of acidic sugars (uronic acids), similar to field samples of Antarctic sea ice (Underwood et al. 2010). Dissolved uronic acid (dUA) concentrations showed large increases during the experiment, contributing up to 100% of the dCHO in seawater in both NSW and ADOM series. dUA are a major constituent of bacterial extracellular polysaccharides (Sutherland 1990), and production of uronic acids has also been reported to increase with increasing cold conditions (Mancuso Nichols et al. 2005). Hence, increases in uronic acid concentrations in this study could be evidence of bacterial adaptation to survive under extreme temperature condition in sea ice by the production of uronic acid-rich EPS. Our data support the hypothesis that developing microbial populations in the ice matrix utilised available DOM and produced new, chemically different DOM (Riedel et al. 2007). This interpretation is supported by the strong coupling of TBN with dUA concentrations in ADOM seawater and especially in the bottom ice layers where dUA concentrations increased up to 95% of the total dCHO pool. Changes in the DOM profiles observed in this study are related purely with bacterial activity as there was no evidence of either ice algal growth generating primary productivity or a sufficiently dense flagellate population whose grazing could control bacterial growth or create significant organic carbon transfer from bacteria to flagellates.

It is possible to fractionally precipitate a charged polymer (e.g. DNA and polysaccharides) based on its degree of polymerisation (complexity) by controlling the polarity of the solvent. A highly complex polymer precipitates in solvent at low polarity, while less complex polymers require high solvent polarity for precipitation. Hence, highly complex EPS are less soluble in a polar solvent (ethanol used for this study) and will precipitate with low concentration of solvent (30% ethanol in this case) in comparison with less complex EPS, which require high concentration of solvent (70% ethanol in this case) for precipitation (Aspinall 1982; Underwood et al. 2004, 2010). Sea ice bacteria are known to produce EPS (Mancuso Nichols et al. 2005), and such production is evident from the increases in dCHO and the significant increases in the proportions of dEPS (and decreases in $\%CHO_{70\text{-}100}$) in the bulk ice samples. In addition to production by bacterial communities, the increased dEPS concentration in sea ice could also be linked with cell lysis as TBN progressively decreased in growing sea ice. As a result of cell lysis, both intracellular and extracellular polysaccharide might have added to the dEPS pool in growing sea ice.

Higher concentrations of dEPS were measured in colder ice (surface ice sections). This increased production of dEPS in colder ice can be interpreted as an effort of psychrophilic bacteria to maintain a buffered environment to protect them against extreme salinity and temperature (Krembs and Deming 2008; Bowman and Deming 2010; Underwood et al. 2010; Ewert and Deming 2011; Krembs et al. 2011). Complex EPS do not easily drain into brine samples (Krembs et al. 2002; Underwood et al. 2010); hence, the brine samples contained predominantly $\%CHO_{70\text{–}100}$ and also DOM < 8 kD in size. This latter material was excluded from the carbohydrates (measurements during the course of study due to the necessary dialysis step (Underwood et al. 2010), which explains the low EPS and CHO concentrations measured in the brines, despite high DOC concentrations.

Frost flowers

Frost flowers developed on the surface of the developing sea ice, as is common on actively forming cold ice (Rankin et al. 2002; Kaleschke et al. 2004; Shaw et al. 2010). Frost flowers are formed by the upward transport of brine from the ice interior towards the surface (Style and Worster 2009) with subsequent evaporation of water. TBN in frost flowers were in the same order of magnitude as in the brines, but were several fold higher than in the bulk ice mainly because bacteria present in brines were concentrated into frost flowers as described by Bowman and Deming (2010). Upward transportation of nutrients from within sea ice to frost flowers was evident given the higher concentrations of NH_4^+, NO_3^- and NO_2^- measured in top ice sections. High nitrate and nitrite levels would have some implications to aerosol release from ice surfaces or melting sea ice (Shaw et al. 2010) as the formation of bromine nitrates can substantially modify the availability of reactive bromine (Piot and von Glasow 2007).

In frost flowers, both DOC (up to 3-fold) and POC (up to 18-fold) were elevated in comparison with seawater, sea ice and brines. These elevated levels of organic carbon and very high TBN were as recorded for frost flowers by Bowman and Deming (2010). Cell lysis is a non-probable source for the observed elevated DOC concentrations as all bacterial carbon present in frost flowers equals approximately 6–8 μmol C l^{-1} (calculated with a conservative

estimate of 35–40 fg C cell^{-1}), which is approximately 50–65 times lower than measured DOC concentrations (Fukuda et al. 1998). It would appear that the physical supply of organic and inorganic nutrients to frost flowers establishes them as potential sites of significant biogeochemical activity.

Conclusions

The addition of biolabile DOM in the ADOM treatment stimulated bacteria, supporting the view that bacteria in sea ice systems can be either limited or co-limited (Pomeroy and Wiebe 2001; Kuosa and Kaartokallio 2006) by the availability of biolabile organic substrate. In the early stages of ice formation, allochthonous organic carbon (DOC and POC) was incorporated from parent seawater into sea ice. Once ice formation was established, there were significant changes in the concentrations of organic carbon and the production of autochothonous DOM. This DOM appeared to be produced by a cold-adapted bacterial community that became established in sea ice (indicated by the production of dUA and dCHO) as well as the degradation of the NSW and algal-derived DOM (as indicated by the inorganic nutrient dynamics). Addition of algal-derived DOM continued to fuel the bacterial communities in ADOM seawater; as a result, bacterial communities were able to thrive in comparison with NSW treatment where bacterial growth declined after the first 5d. In ADOM sea ice, the complexity of dEPS produced by the bacteria was clearly linked with low temperature and high salinity since the highest concentrations and greatest contribution of the most complex fractions of dEPS were in the coldest and most saline surface ice sections. These results suggest that a psychrophilic community was established in growing sea ice possibly structured differently than the community in NSW that produced high concentrations of complex dEPS, suggesting that EPS play important roles of buffering and cryo-protection for microorganisms against harsh environmental conditions (low temperature and high salinity) in sea ice.

Acknowledgments The work described in this report was supported by the European Community's Sixth Framework Programme through the grant to the budget of the Integrated Infrastructure Initiative HYDRALAB III, Contract no. 022441(RII3) and U.K. Natural Environment Research Council (NE/E016251/1). The authors would like to thank the Hamburg Ship Model Basin (HSVA), especially Kalle Evers and the ice tank crew, for the hospitality, technical and scientific support and the professional execution of the test programme in the Research Infrastructure ARCTECLAB. We are indebted to Naomi Thomas for the unenviable task of producing the ADOM additive and her support in nutrient and DOM analyses. Erika Allhusen provided essential support for the setting up and successful execution of the experiment. We thank Dr Ben Green for PRIMER analysis. We are very grateful to 3 anonymous reviewers for their detailed and highly constructive suggestions on an earlier draft of the manuscript.

References

Arrigo KR, Dieckmann G, Gosselin M, Robinson DH, Fritsen CH, Sullivan CW (1995) High resolution study of the platelet ice ecosystem in McMurdo Sound, Antarctica: biomass, nutrient, and production profiles within a dense microalgal bloom. Mar Ecol Prog Ser 127:255–268. doi:10.3354/meps127255

Arrigo KR, Mock T, Lizotte MP (2010) Primary producers in sea ice. In: Thomas DN, Dieckmann GS (eds) Sea ice, 2nd edn. Blackwell, Oxford, pp 283–325

Aspinall GO (1982) The polysaccharides, vol 1. Academic Press, New York

Bellinger BJ, Abdullahi AS, Gretz MR, Underwood GJC (2005) Biofilm polymers: relationship between carbohydrate biopolymers from estuarine mudflats and unialgal cultures of benthic diatoms. Aquat Microb Ecol 38:169–180

Bitter T, Muir HM (1962) A modified uronic acid carbazole reaction. Anal Biochem 4:330–334. doi:10.1016/0003-2697(62)90095-7

Bowman JS, Deming JW (2010) Elevated bacterial abundance and exopolymers in saline frost flowers and implications for atmospheric chemistry and microbial dispersal. Geophys Res Lett 37:L13501. doi:10.1029/2010GL043020

Brierley AS, Thomas DN (2002) Ecology of Southern Ocean pack ice. Adv Mar Biol 43:171–276. doi:10.1016/S0065-2881(02)43005-2

Brinkmeyer R, Knittel K, Jürgens J, Weyland H, Amann R, Helmke E (2003) Diversity and structure of bacterial communities in Arctic versus Antarctic pack ice. Appl Environ Microbiol 69:6610–6619. doi:10.1128/AEM.69.11.6610-6619.2003

Caron DA, Gast RJ (2010) Heterotrophic protists associated with sea ice. In: Thomas DN, Dieckmann GS (eds) Sea ice, 2nd edn. Blackwell, Oxford, pp 327–356

Clarke DB, Ackley SF (1984) Sea ice structure and biological activity in the Antarctic marginal ice zone. J Geophys Res 89:2087–2095

Collins RE, Rocap G, Deming JW (2010) Persistence of bacterial and archaeal communities in sea ice through an Arctic winter. Environ Microbiol 12:1828–1841

Cota GF, Prinsenberg SJ, Bennett EB, Loder JW, Lewis MR, Anning JL, Watson NHF, Harris LR (1987) Nutrient fluxes during extended blooms of arctic ice algae. J Geophys Res 92:1951–1962. doi:10.1029/JC092iC02p01951

Deming JW (2010) Sea ice bacteria and viruses. In: Thomas DN, Dieckmann GS (eds) Sea ice, 2nd edn. Blackwell, Oxford, pp 247–282

Dubois M, Gilles KA, Hamilton JK, Rebers PA, Smith F (1956) Colorimetric method for determination of sugars and related substances. Anal Chem 28:350–356

Dumont I, Schoemann V, Lannuzel D, Chou L, Tison JL, Becquevort S (2009) Distribution and characterization of dissolved and particulate organic matter in Antarctic pack ice. Polar Biol 32:733–750

Engel N, Jenny TA, Mooser V, Gossauer A (1991) Chlorophyll catabolism in *Chlorella protothecoides*—isolation and structure elucidation of a red bilin derivative. FEBS Lett 293:131–133

Ewert MEM, Deming JW (2011) Selective retention in saline ice of extracellular polysaccharides produced by the cold-adapted marine bacterium *Colwellia psychrerythraea* strain 34H. Ann Glaciol 52:111–117

Fukuda R, Ogawa H, Nagata T, Koike I (1998) Direct determination of carbon and nitrogen contents of natural bacterial assemblages in marine environments. Appl Environ Microbiol 64:3352–3358

Garrison DL, Close AR, Gordon LI (1990) Nutrient concentrations in Antarctic pack ice during the austral winter. In: Ackley SF, Weeks WF (eds) Sea ice properties and processes. Proceedings of W. F. weeks sea ice symposium, CRREL, Monograph 90–91, pp 35–40

Gasol JM, Zweifel UL, Peters F, Fuhrman JA, Hagstrom A (1999) Significance of size and nucleic acid content heterogeneity as measured by flow cytometry in natural planktonic bacteria. Appl Environ Microbiol 65:4475–4483

Giannelli V, Thomas DN, Haas C, Kattner G, Kennedy H, Dieckmann GS (2001) Behaviour of dissolved organic matter and inorganic nutrients during experimental sea ice formation. Ann Glaciol 33:317–321. doi:10.3189/172756401781818572

Gleitz M, von der loeff MR, Thomas DN, Dieckmann GS, Millero FJ (1995) Comparison of summer and winter inorganic carbon, oxygen and nutrient concentrations in antarctic sea-ice brine. Mar Chem 51:81–91

Grasshoff K, Ehrhardt M, Kremling K (1983) Methods of seawater analysis. Verlag Chemie, Weinheim

Hales B, van Geen A, Takahashi T (2004) High-frequency measurement of seawater chemistry: flow-injection analysis of macronutrients. Limnol Oceanogr Meth 2:91–101

Helmke E, Weyland H (1995) Bacteria in sea-ice and underlying water of the eastern Weddell Sea in midwinter. Mar Ecol Prog Ser 117:269–287

Herborg LM, Thomas DN, Kennedy H, Haas C, Dieckmann GS (2001) Dissolved carbohydrates in Antarctic sea ice. Antarct Sci 13:119–125

Hoagland KD, Rosowski JR, Gretz MR, Roemer SC (1993) Diatom extracellular polymeric substances—function, fine-structure, chemistry, and physiology. J Phycol 29:537–566

Hofmann T, Hanlon ARM, Taylor JD, Ball AS, Osborn AM, Underwood GJC (2009) Dynamics and compositional changes in extracellular carbohydrates in estuarine sediments during degradation. Mar Ecol Prog Ser 379:45–58

Holmes RM, Aminot A, Kerouel R, Hooker BA, Peterson BJ (1999) A simple and precise method for measuring ammonium in marine and freshwater ecosystems. Can J Fish Aquat Sci 56:1801–1808. doi:10.1139/cjfas-56-10-1801

Horner R, Ackley SF, Dieckmann GS, Gulliksen B, Hoshiai T, Legendre L, Melnikov IA, Reeburgh WS, Spindler M, Sullivan CW (1992) Ecology of sea ice biota. Polar Biol 12:417–427

Hortensteiner S, Chinner J, Matile P, Thomas H, Donnison IS (2000) Chlorophyll breakdown in *Chlorella protothecoides*: characterization of degreening and cloning of degreening-related genes. Plant Mol Biol 42:439–450

Juhl AR, Krembs C, Meiners KM (2011) Seasonal development and differential retention of ice algae and other organic fractions in first-year Arctic sea ice. Mar Ecol Prog Ser 436:1–16. doi:10.3354/meps09277

Junge K, Krembs C, Deming J, Stierle A, Eicken H (2001) A microscopic approach to investigate bacteria under in situ conditions in sea-ice samples. Ann Glaciol 33:304–310. doi:10.3189/172756401781818275

Junge K, Imhoff F, Staley T, Deming JW (2002) Phylogenetic diversity of numerically important arctic sea-ice bacteria cultured at subzero temperature. Microb Ecol 43:315–328

Kaartokallio H (2004) Food web components, and physical and chemical properties of Baltic Sea ice. Mar Ecol Prog Ser 273:49–63

Kaartokallio H, Laamanen M, Sivonen K (2005) Responses of Baltic Sea ice and open-water natural bacterial communities to salinity change. Appl Environ Microbiol 71:4364–4371

Kaartokallio H, Tuomainen J, Kuosa H, Kuparinen J, Martikainen PJ, Servomaa K (2008) Succession of sea-ice bacterial communities in the Baltic Sea fast ice. Polar Biol 31:783–793

Kaleschke L, Richter A, Burrows J, Afe O, Heygster G, Notholt J, Rankin AM, Roscoe HK, Hollwedel J, Wagner T, Jacobi HW (2004) Frost flowers on sea ice as a source of sea salt and their influence on tropospheric halogen chemistry. Geophys Res Lett 31:L16114. doi:10.1029/2004GL020655

Kattner G, Thomas DN, Haas C, Kennedy H, Dieckmann GS (2004) Surface ice and gap layers in Antarctic sea ice: highly productive habitats. Mar Ecol Prog Ser 277:1–12

Krembs C, Deming JW (2008) The role of exopolymers in microbial adaptation to sea-ice. In: Margesin R, Schinner F, Marx J-C, Gerday C (eds) Psychrophiles: from biodiversity to biotechnology. Springer, Berlin, pp 247–264

Krembs C, Eicken H, Junge K, Deming JW (2002) High concentrations of exopolymeric substances in Arctic winter sea ice: implications for the polar ocean carbon cycle and cryoprotection of diatoms. Deep Sea Res I 49:2163–2181

Krembs C, Eicken H, Deming JW (2011) Exopolymer alteration of physical properties of sea ice and implications for ice habitability and biogeochemistry in a warmer Arctic. Proc Natl Acad Sci USA 108:3653–3658

Kroon H (1993) Determination of nitrogen in water—comparison of a continuous-flow method with online UV digestion with the original kjeldahl method. Anal Chim Acta 276:287–293

Kuosa H, Kaartokallio H (2006) Experimental evidence on nutrient and substrate limitation of Baltic Sea sea-ice algae and bacteria. Hydrobiologia 554:1–10

Mancuso Nichols C, Bowman JP, Guezennec J (2005) Effects of incubation temperature on growth and production of exopolysaccharides by an Antarctic sea ice bacterium grown in batch culture. Appl Environ Microbiol 71:3519–3523

McConville MJ, Wetherbee R, Bacic A (1999) Subcellular location and composition of the wall and secreted extracellular sulphated polysaccharides/proteoglycans of the diatom Stauroneis amphioxys Gregory. Protoplasma 206:188–200

Meiners K, Gradinger R, Fehling J, Civitarese G, Spindler M (2003) Vertical distribution of exopolymer particles in sea ice of the Fram Strait (Arctic) during autumn. Mar Ecol Prog Ser 248:1–13

Meiners K, Krembs C, Gradinger R (2008) Exopolymer particles: microbial hotspots of enhanced bacterial activity in Arctic fast ice (Chukchi Sea). Aquat Microb Ecol 52:195–207

Mock T, Thomas DN (2005) Recent advances in sea-ice microbiology. Environ Microbiol 7:605–619

Norman L, Thomas DN, Stedmon CA, Granskog MA, Papadimitriou S, Krapp RH, Meiners KM, Lannuzel D, van der Merwe P, Dieckmann GS (2011) The characteristics of dissolved organic matter (DOM) and chromophoric dissolved organic matter (CDOM) in Antarctic sea ice. Deep Sea Res II 58:1075–1091

Papadimitriou S, Thomas DN, Kennedy H, Haas C, Kuosa H, Krell A, Dieckmann GS (2007) Biogeochemical composition of natural sea ice brines from the Weddell Sea during early austral summer. Limnol Oceanogr 52:1809–1823

Petrich C, Eicken H (2010) Growth, structure and properties of sea ice. In: Thomas DN, Dieckmann GS (eds) Sea ice, 2nd edn. Blackwell, Oxford, pp 23–77

Piot M, von Glasow R (2007) The potential importance of frost flowers, recycling on snow, and open leads for ozone depletion events. Atmos Chem Phys Discuss 7:4521–4595. doi:10.5194/acpd-7-4521-2007

Pomeroy LR, Wiebe WJ (2001) Temperature and substrates as interactive limiting factors for marine heterotrophic bacteria. Aquat Microb Ecol 23:187–204

Qian JG, Mopper K (1996) Automated high performance, high-temperature combustion total organic carbon analyzer. Anal Chem 68:3090–3097

Rankin AM, Wolff EW, Martin S (2002) Frost flowers: implications for tropospheric chemistry and ice core interpretation. J Geophys Res 107:4683. doi:10.1029/20021JD002492

Riedel A, Michel C, Gosselin M (2006) Seasonal study of sea-ice exopolymeric substances on the Mackenzie shelf: implications

for transport of sea-ice bacteria and algae. Aquat Microb Ecol 45:195–206

Riedel A, Michel C, Gosselin M, Leblanc B (2007) Enrichment of nutrients, exopolymeric substances and microorganisms in newly formed sea ice on the Mackenzie shelf. Mar Ecol Prog Ser 342:55–67

Shaw PM, Russell LM, Jefferson A, Quinn PK (2010) Arctic organic aerosol measurements show particles from mixed combustion in spring haze and from frost flowers in winter. Geophys Res Lett 37:L10803. doi:10.1029/2010GL042831

Stedmon CA, Thomas DN, Granskog M, Kaartokallio H, Papadimitriou S, Kuosa H (2007) Characteristics of dissolved organic matter in Baltic coastal sea ice: Allochthonous or autochthonous origins? Environ Sci Technol 41:7273–7279

Stewart FJ, Fritsen CH (2004) Bacteria–algae relationships in Antarctic sea ice. Antarct Sci 16:143–156

Style RW, Worster MG (2009) Frost flower formation on sea ice and lake ice. Geophys Res Lett 36:L11501. doi:10.1029/2009GL037304

Sutherland IW (1990) Biotechnology of microbial exopolysaccharides. Cambridge University Press, Cambridge

Thomas DN, Kattner G, Engbrodt R, Giannelli V, Kennedy H, Haas C, Dieckmann GS (2001) Dissolved organic matter in Antarctic sea ice. Ann Glaciol 33:297–303. doi:10.3189/172756401781818338

Tranvik LJ (1990) Bacterioplankton growth on fractions of dissolved organic-carbon of different molecular-weights from humic and clear waters. Appl Environ Microbiol 56:1672–1677

Underwood GJC, Boulcott M, Raines CA, Waldron K (2004) Environmental effects on exopolymer production by marine benthic diatoms: dynamics, changes in composition, and pathways of production. J Phycol 40:293–304

Underwood GJC, Fietz S, Papadimitriou S, Thomas DN, Dieckmann GS (2010) Distribution and composition of dissolved extracellular polymeric substances (EPS) in Antarctic sea ice. Mar Ecol Prog Ser 404:1–19

van der Merwe P, Lannuzel D, Nichols CAM, Meiners K, Heil P, Norman L, Thomas DN, Bowie AR (2009) Biogeochemical observations during the winter-spring transition in East Antarctic sea ice: evidence of iron and exopolysaccharide controls. Mar Chem 115:163–175

Volkman JK, Tanoue E (2002) Chemical and biological studies of particulate organic matter in the ocean. J Oceanogr 58:265–279. doi:10.1023/A:1015809708632

List of Figures

List of Tables

Michael Fischer
Brandtstr. 36
28215 Bremen
michael.fischer@awi.de

Bremen, den 07.01.2013

Erklärung gemäß §6 (5) PromO (vom 14. März 2007)

Hiermit erkläre ich, dass ich die vorliegende Doktorarbeit mit dem Titel:

Sea ice and the air-sea exchange of CO_2

1. ohne unerlaubte fremde Hilfe angefertigt habe,
2. keine anderen als die von mir angegebenen Quellen und Hilfsmittel benutzt habe,
3. die den benutzten Werken wörtlich oder inhaltlich entnommenen Stellen als solche kenntlich gemacht habe.

Ebenfalls erkläre ich hiermit eidesstattlich, dass es sich bei den von mir abgegebenen Arbeiten um 3 identische Exemplare handelt.

.....
(Michael Fischer)